

Doctoral Dissertation

博士論文

**Spatiotemporal characteristics of
slow earthquakes in subduction zones
around Japan**

(日本周辺の沈み込み帯における
スロー地震の時空間特性の研究)

A Dissertation Submitted for Degree of Doctor of Philosophy

December 2021

Department of Earth and Planetary Science,
Graduate School of Science, The University of Tokyo

令和3年12月 博士(理学) 申請

東京大学大学院理学系研究科地球惑星科学専攻

Satoru Baba

馬場 慧

Abstract

Slow earthquakes, observed on plate boundaries in subduction zones or strike-slip faults, have longer and more various characteristic durations than regular earthquakes. Although there are many previous studies of slow earthquakes, the data and methods vary by area and there are few studies analyzing slow earthquakes around Japan comprehensively. Hence, comparison of slow earthquake activity in various regions and discussion of the factors which control the spatiotemporal variations in slow earthquake activity is difficult. To reveal the factors which affect slow earthquake activity based on physical models, simulations, or structural studies, I first detected very low frequency earthquakes (VLFs), which is a type of slow earthquakes and observed in 0.02–0.05 Hz, as a representative of slow earthquakes around Japan in a uniform method and quantified the spatiotemporal variations in VLFs on a regional scale. This is the first study which quantified spatiotemporal distribution of VLF activity around Japanese islands by evaluating the moment-density release rate and the swarm ratio.

I detected VLFs by the matched-filter technique by using synthetic waveforms as templates. I used continuous seismograms of F-net broadband seismometers. I calculated cross-correlation coefficients (CCs) between the synthetic template and F-net seismograms and detected events with the station- and component-averaged CCs exceeding the threshold set as nine times the median absolute deviation. After that, I estimated the seismic moment of each VLF and evaluated the spatiotemporal variation in the moment-density release rate of VLFs. As a result, the heterogeneity of spatial distribution of VLFs is much stronger in the shallower part than in the deeper part. The moment-density release rate of shallow VLFs off the Cape Muroto and off the Kii Peninsula is negatively correlated with interplate coupling derived from the distribution of the slip-deficit rate. This suggests that VLFs tend to be less active near the strongly coupled zones. The negative correlation suggests that the interplate coupling is weak in Hyuga-nada, where the moment-density release rate of VLFs is large. Furthermore, VLFs tend to be active in low seismic velocity anomalies which can be caused by fluids. Thus, fluids can potentially promote VLF activity.

Temporal variations in VLF activities are categorized into three patterns: activation after a large earthquake, quiescence after a large earthquake, and repetition of swarm activities and quiescence. Inside a large coseismic slip area of the 2011 Tohoku earthquake (Mw 9.0), the VLF activity was low thereafter, whereas, outside the area,

VLFE activity increased after the 2011 Tohoku earthquake probably caused by their afterslip. VLFE activity is related to interplate coupling and afterslip of large earthquakes, thus VLFE activity can be an indicator of stress state on the plate boundary. To quantify the characteristics of repetition of swarm activities and quiescence of VLFE activity, I estimated swarm ratios of VLFES and median intervals of two successive swarms. Swarm ratios of shallow VLFE activity are generally larger than those of deep VLFE activity. The intervals of swarms in shallow VLFES are very various from 8 months to 4 years. Based on simulation or structural previous studies, the difference in intervals of shallow VLFE swarms may be related to the spatial variations in the effective normal stress on the plate boundary. The variation in VLFE activity is larger in the shallower part than in the deeper part both spatially and temporally.

The moment-density release rate of VLFES in Hyuga-nada, off the Pacific coast of Kyushu Island, is especially larger than other slow earthquake regions. In addition, the relationship between VLFE activity and the subducted Kyushu-Palau Ridge can be discussed in Hyuga-nada. Therefore, I conducted a detailed analysis of slow earthquake activity in Hyuga-nada to reveal the factor which controls the spatial variation in slow earthquake activity on a local scale. I estimated the energy rates of tremors by using the seismograms of temporary ocean bottom seismometers in Hyuga-nada. I also evaluated the moment rates of VLFES using F-net seismograms. Generally, energy rates of tremors and moment rates of VLFES are larger outside the subducted Kyushu-Palau Ridge than inside the ridge, although there is an area with larger events in the updip part of the inside of the subducted ridge in 2015. Total moments of VLFES are larger in the south of the subducted ridge, where interplate coupling is expected to be weaker inferred from the slip rate of repeating earthquakes. Although interplate coupling in Hyuga-nada is generally weaker than other slow earthquake regions, the correlation between interplate coupling and VLFE activity is also found on the local scale in Hyuga-nada.

Tremors and VLFES start migrating in the south of the ridge with large energy rates and moment rates along the strike direction and decelerate after entering the area where the Kyushu-Palau Ridge is subducted. Based on a model by Newtonian rheology, the south and inside of the ridge are considered as strong and weak patch areas, respectively. There is a low velocity anomaly around the strong patch area. According to the physical and observation models, the low velocity anomaly can exist in the overriding plate. The dehydrated fluids can go into the overriding plate; therefore, the pore pressure

on the plate boundary can be lower. Thus, the effective normal stress on the plate boundary can be higher and the strength of the patches is stronger in the south of the subducted ridge. If a circular crack model is assumed, the stress drop of VLFs is approximately four times larger in the south (strong patch) than inside (weak patch) the subducted ridge. The approximately four times difference in stress drop between strong and weak patches in Hyuga-nada is sufficient to cause the parabolic migration pattern, which is explained by the effect of Newtonian rheology in the ductile background. Although the interplate coupling inferred from repeating earthquake activity is stronger, the strength of the patches is inferred to be weaker inside the ridge than in the south of the ridge. Inside the subducted ridge, the portion of the accumulated stress released by regular interplate earthquakes adjacent to slow earthquakes may be large. On the other hand, most of the accumulated stress is released by slow earthquakes in the south of the ridge, where the interplate coupling is weaker and the strength of the slow earthquake patches is suggested to be stronger. This study revealed the spatial variation in sizes of tremors and VLFs in Hyuga-nada. The heterogeneity of stress drop suggested by the difference in the magnitude of VLFs can control the migration pattern of slow earthquakes based on a physical model. This study suggested the variation in the style of stress release on the plate boundary inside and in the south of the subducted ridge.

Contents

Abstract	1
1. Introduction	6
1.1. Slow earthquakes	6
1.2. Slow earthquakes around Japan	9
1.3. Purpose of this study	15
2. Regional spatiotemporal characteristics of VLFE activities around Japan	17
2.1. Purpose of this chapter	17
2.2. Data and method	19
2.2.1. Data	19
2.2.2. Detection of VLFEs	19
2.2.3. Estimation of seismic moments of VLFEs	25
2.3. Spatial characteristics of VLFE activities	27
2.3.1. Correlation between the VLFE activity and interplate coupling	31
2.3.2. Correlation between the VLFE activity and seismic velocity structure	35
2.3.3. Characteristics of areas with slow earthquake activity	36
2.4. Temporal characteristics of VLFE activities	38
2.4.1. Activation and quiescence after a large earthquake	44
2.4.2. Swarm activities of VLFEs	49
2.5. Summary of this chapter	62

3. Spatial characteristics of slow earthquakes in Hyuga-nada	
on a local scale	64
3.1. Introduction	64
3.1.1. Tectonic setting in Hyuga-nada	64
3.1.2. Purpose of this chapter	67
3.2. Data and method	69
3.2.1. Seismic energy rates of tremors	69
3.2.2. Seismic moment rates of VLFs	78
3.3. Results	81
3.4. Discussion	85
3.4.1. Relationship between slow and repeating earthquakes	
in Hyuga-nada.....	85
3.4.2. Distribution of frictional properties inferred from	
physical models	87
3.4.3. Scaled energy of shallow slow earthquakes in Hyuga-nada	
compared with other slow earthquake regions	103
3.5. Summary of this chapter	108
3.6. Extension of discussion in Hyuga-nada to other slow	
earthquake regions around Japan	110
4. Conclusions	112
5. Future works	115
Acknowledgments	116
Appendix	118
References	135

1. Introduction

1.1. Slow earthquakes

Slow earthquakes have longer characteristic durations than regular earthquakes with the same magnitudes (e.g., Ide et al., 2007). After Obara (2002) first discovered tectonic tremors along the Nankai Trough by investigating the multi-traces of seismograms of Hi-net, operated by the National Research Institute for Earth Science and Disaster Resilience (NIED; Aoi et al., 2020; Okada et al., 2004), various types of slow earthquakes have been observed in areas surrounding seismogenic zones along strike-slip faults (e.g., Nadeau & Dolenc, 2005) or on the plate boundaries of subduction zones in the world (e.g., Beroza & Ide, 2011; Obara & Kato, 2016) (Figure 1.1).

Slow earthquakes are classified into several types based on frequencies, i.e., (1) low frequency earthquakes (LFEs) (e.g., Katsumata & Kamaya, 2003) and tectonic tremors (e.g., Obara, 2002) observed in 2–8 Hz, (2) very low frequency earthquakes (VLFs) observed in 0.02–0.05 Hz (e.g., Obara & Ito, 2005), and (3) slow slip events (SSEs) observed as crustal deformations with characteristic durations of several days to several years (e.g., Dragert et al., 2001; Hirose et al., 1999). Previous studies confirmed that the hypocenters and focal mechanisms of slow earthquakes are consistent with shear slip along the plate boundaries (e.g., Ito et al., 2007; 2009).

Obara & Kato (2016) summarized the relationships between slow and megathrust earthquakes, which have similar thrust-type fault mechanisms and occur in neighboring areas on the plate boundary: (1) slow and megathrust earthquakes have similar occurrence styles, such as repetitive nature, (2) slow earthquakes can reflect stress accumulation on the plate boundary because slow earthquakes are sensitive to stress changes of the seismogenic zones, and (3) stress transferred by slow earthquakes can increase the possibility of megathrust earthquakes, such as the 2011 Tohoku earthquake in Japan (Ito et al., 2013; Kato et al., 2012) and the 2014 Iquique earthquake in Chile (Kato & Nakagawa, 2014; Ruiz et al., 2014). In addition, the activation of slow earthquakes after a large earthquake was reported (e.g., Asano et al., 2008; Matsuzawa et al., 2015). These previous studies suggest that the research of slow earthquakes can provide us with new insight into megathrust earthquakes and stress state on the plate boundaries in the subduction zones.

Tremors and VLFs are often spatiotemporally correlated (e.g., Ghosh et al., 2015; Ito et al., 2007). Although the seismograms in the frequency range between tremors

and VLFs are affected by microseism noises (e.g., Hasselmann, 1963), slow earthquake signals in the frequency range of microseisms were detected when the microseism noises were quiet (Kaneko et al., 2018) or by stacking seismograms when LFEs occurred (Masuda et al., 2020). The results of these studies suggest that the slow earthquake is a broadband phenomenon; therefore, tremors, LFEs, and VLFs are considered as parts of the same broadband slow earthquakes and are observed in different frequency ranges (Figure 1.2; e.g., Ide, 2008; Ide & Maury, 2018).

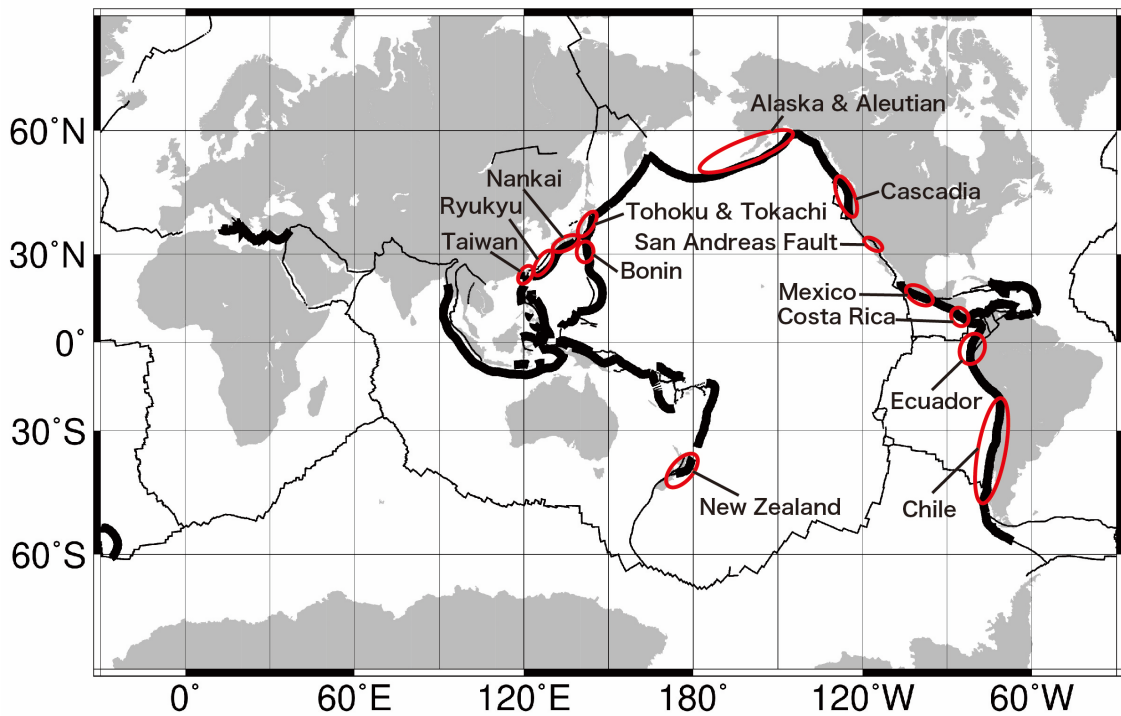


Figure. 1.1. Distribution of slow earthquakes in the world (Obara, 2020). Black lines indicate the plate boundaries (Coffin et al., 1998). Bold black lines represent the subduction zones.

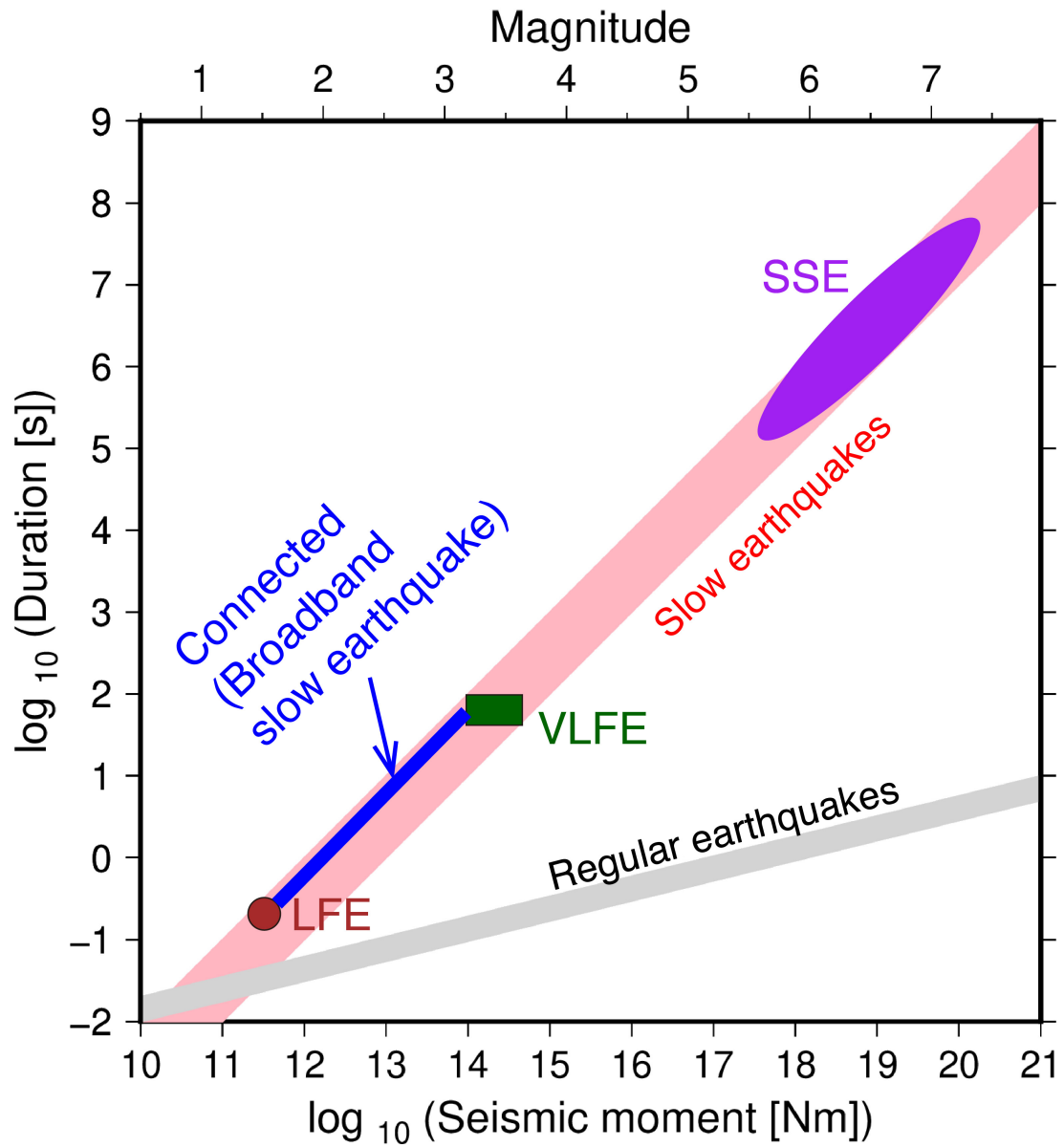


Figure 1.2. The relationship between characteristic durations and seismic moments of regular and slow earthquakes (rewrite of Ide et al. (2007) based on Kaneko et al., (2018) and Masuda et al. (2020)).

1.2. Slow earthquakes around Japan

The Philippine Sea Plate and Pacific Plate are subducting beneath the island arc around Japan (Figure 1.3). The characteristics of the two subducting plates completely differ. The Philippine Sea Plate subducting in the Nankai Trough is young and warm in southwest Japan, whereas the Pacific Plate subducting in the Japan and Kuril Trenches is old and cold in northeast Japan (e.g., Syracuse et al., 2010). The plate convergence rates of these plates also differ, 4–5 cm/year and 8–9 cm/year in the Nankai Trough and in the Japan and Kuril trenches, respectively (DeMets et al., 1994). Despite these differences, both subduction zones have repeatedly experienced megathrust earthquakes. Recent megathrust earthquakes are 1944 Tonankai (moment magnitude, M_w 8.0; e.g., Kikuchi et al., 2003) and 1946 Nankai earthquakes (M_w 8.4; e.g., Tanioka & Satake, 2001) along the Nankai Trough, and 2003 Tokachi-Okii (Mw 8.0; e.g., Yagi, 2004) and 2011 Tohoku earthquakes (M_w 9.0; e.g., Iinuma et al., 2012) along the Japan and Kuril Trenches.

Slow earthquakes are classified into deep slow earthquakes, which occur in the deeper extensions of seismogenic zones, and shallow slow earthquakes, which occur in offshore regions near the trench axis. Along the Nankai Trough, slow earthquakes occur in both the shallower and deeper extensions of the seismogenic zone; therefore, the distributions of slow earthquakes are separated from the seismogenic zone along the dip direction (Figure 1.3b). The distribution of deep slow earthquakes has been extensively investigated using nationwide inland seismic and geodetic networks (e.g., Maeda & Obara, 2009; Nishimura et al., 2013). Deep episodic tremor and slips (ETSs; e.g., Rogers & Dragert, 2003), spatiotemporal correlation of tremors, VLFs, and short-term SSEs (duration of ~ 1 week and recurrence interval of ~ 6 months), are observed at depths of 30–45 km (e.g., Hirose & Obara, 2005; Ito et al., 2007). Deep tremor activity has the heterogeneity of energy along the strike direction (e.g., Annoura et al., 2016; Kano, Kato et al., 2018), which is possibly related to the distribution of fluid (e.g., Nakajima & Hasegawa, 2016). Between the ETS and seismogenic zone along the dip direction, long-term SSEs with durations of one to several years are observed in Shikoku, off Kyushu (Takagi et al., 2016, 2019), in the Kii Channel, in Tokai (Ozawa, 2017), and in the east of Kii Peninsula (Kobayashi & Tsuyuki, 2019).

Shallow slow earthquakes along the Nankai Trough have been investigated using both onshore (e.g., Asano et al., 2008, 2015; Obara & Ito, 2005; Takemura, Matsuzawa, et al., 2019) and offshore seismic records (e.g., Nakano et al., 2018; Sugioka

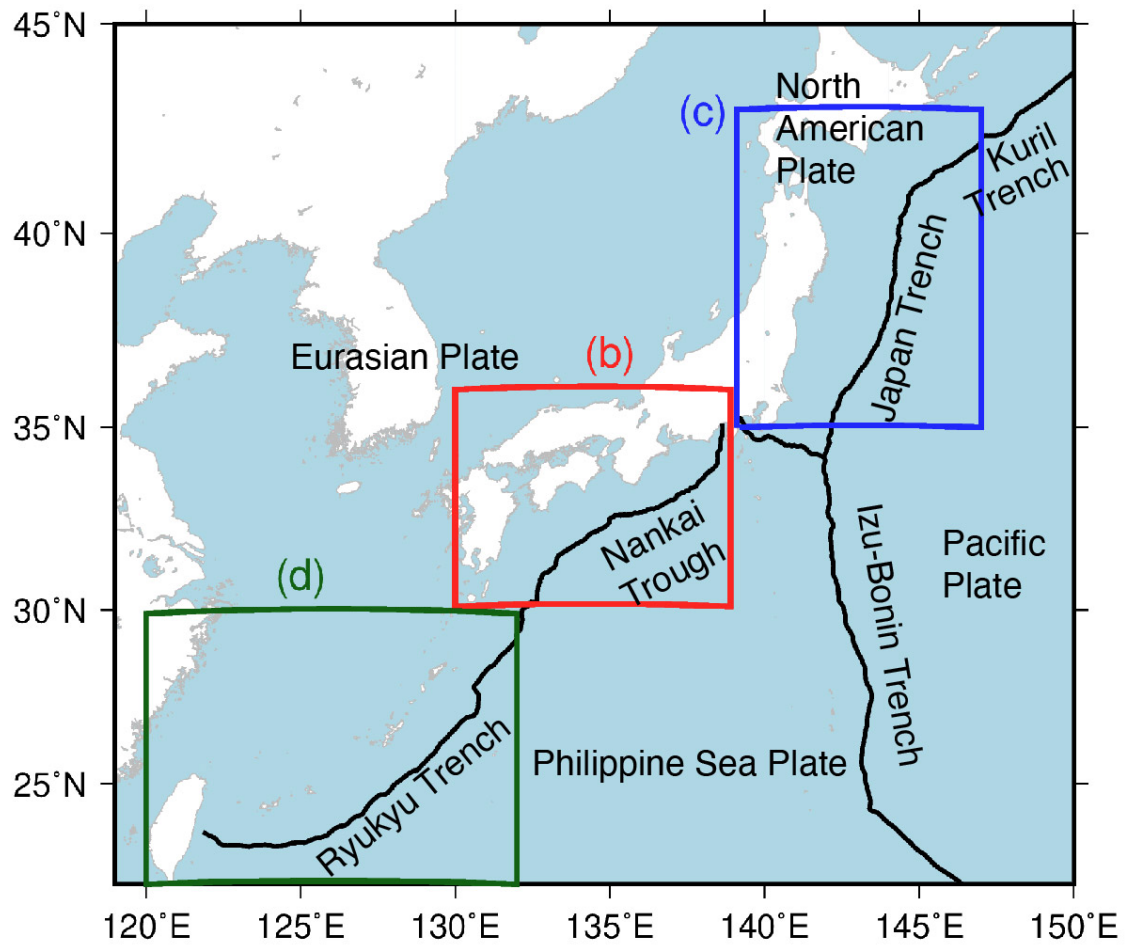
et al., 2012; Yamashita et al., 2015; 2021). The observation of shallow slow earthquakes has been developed by the deployment of an offshore seismic network, Dense Oceanfloor Network system for Earthquakes and Tsunamis (e.g., Kaneko et al., 2018; Nakano et al., 2018). Recently, shallow SSEs were detected by the investigation of offshore observations of borehole pore fluid pressure changes (Araki et al., 2017) or geodetic data (Yokota & Ishikawa, 2020). These studies revealed the simultaneous occurrences of shallow tremors, VLFs, and SSEs, which are similar to deep ETS. Takemura, Matsuzawa, et al. (2019) also suggested that shallow slow earthquakes are activated by high pore fluid pressure in regions surrounding strongly locked zones.

Along the Japan and Kuril Trenches, slow earthquakes have been observed off the Pacific coasts of Tohoku and Tokachi regions. Asano et al. (2008) and Matsuzawa et al. (2015) detected VLFs off Tokachi and Tohoku regions by using an onland network, respectively. They found the activations of VLFs off Tokachi after the 2003 Tokachi-Oki earthquake and off Tohoku after the 2011 Tohoku earthquake, respectively. In recent studies, tremors were located comprehensively by using an offshore seismic network, Seafloor Observation Network for Earthquakes and Tsunamis along the Japan Trench (e.g., Nishikawa et al., 2019; Tanaka et al., 2019). These studies suggest that the distribution of tremors and large coseismic slip area of the 2011 Tohoku earthquake are separated along the strike direction (Figure 1.3c).

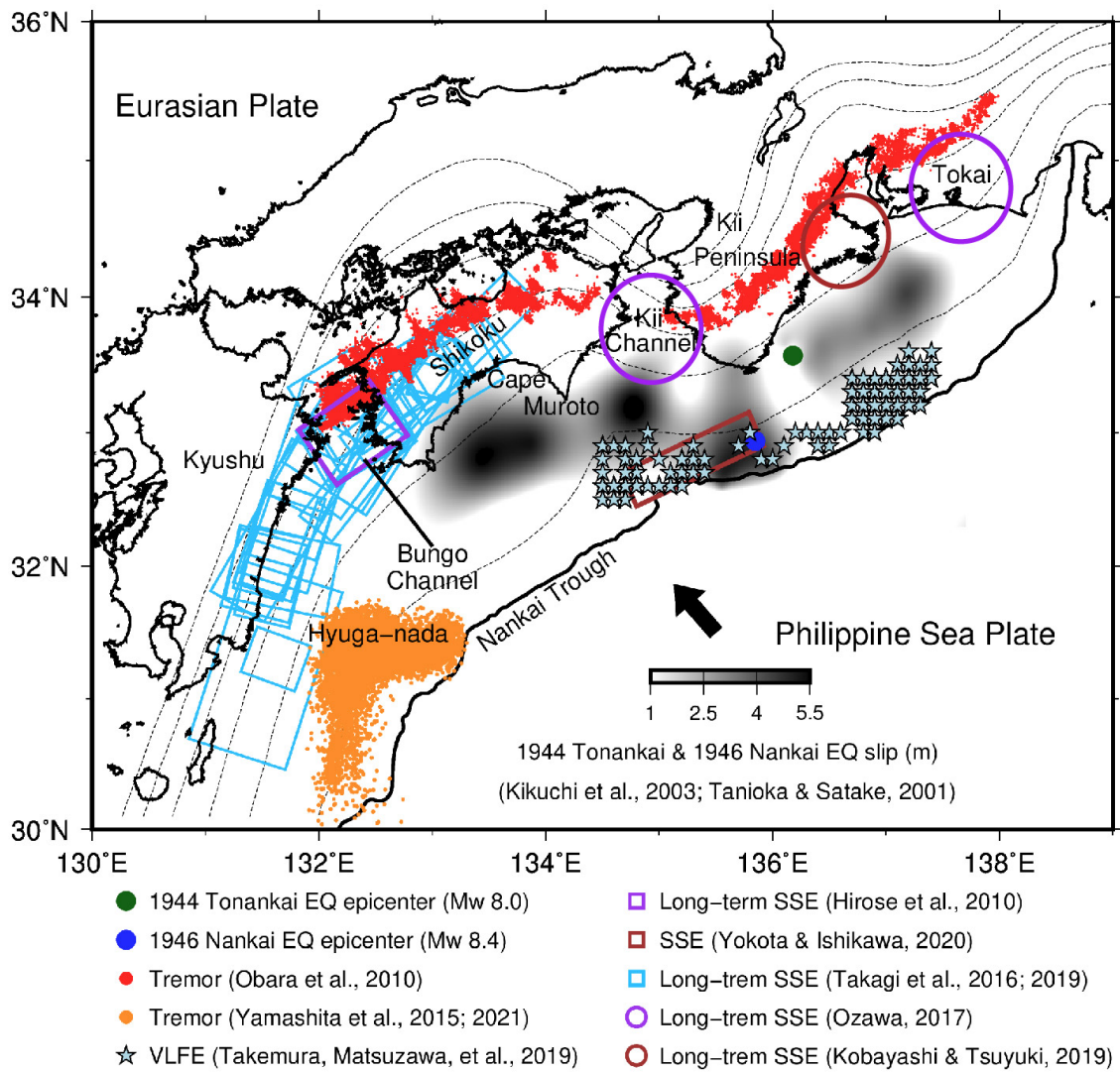
Slow earthquakes have been observed also along the Ryukyu Trench, south of the Nankai Trough (Figure 1.3d). VLFs and LFs are spatiotemporally correlated (Nakamura, 2017; Nakamura & Sunagawa, 2015) and are modulated by SSEs which occur biannually (Heki & Kataoka, 2008; Tu & Heki, 2017). Recently, the occurrence of SSEs was also suggested along the Izu-Bonin Trench, south of the Japan Trench (Arisa & Heki, 2017; Fukao et al., 2021).

Despite many observations, the tectonic condition where slow earthquakes are active and the factor of the variation in slow earthquakes are not clarified well. To reveal them, it is necessary to quantify the spatiotemporal variation in slow earthquake activity around Japan comprehensively.

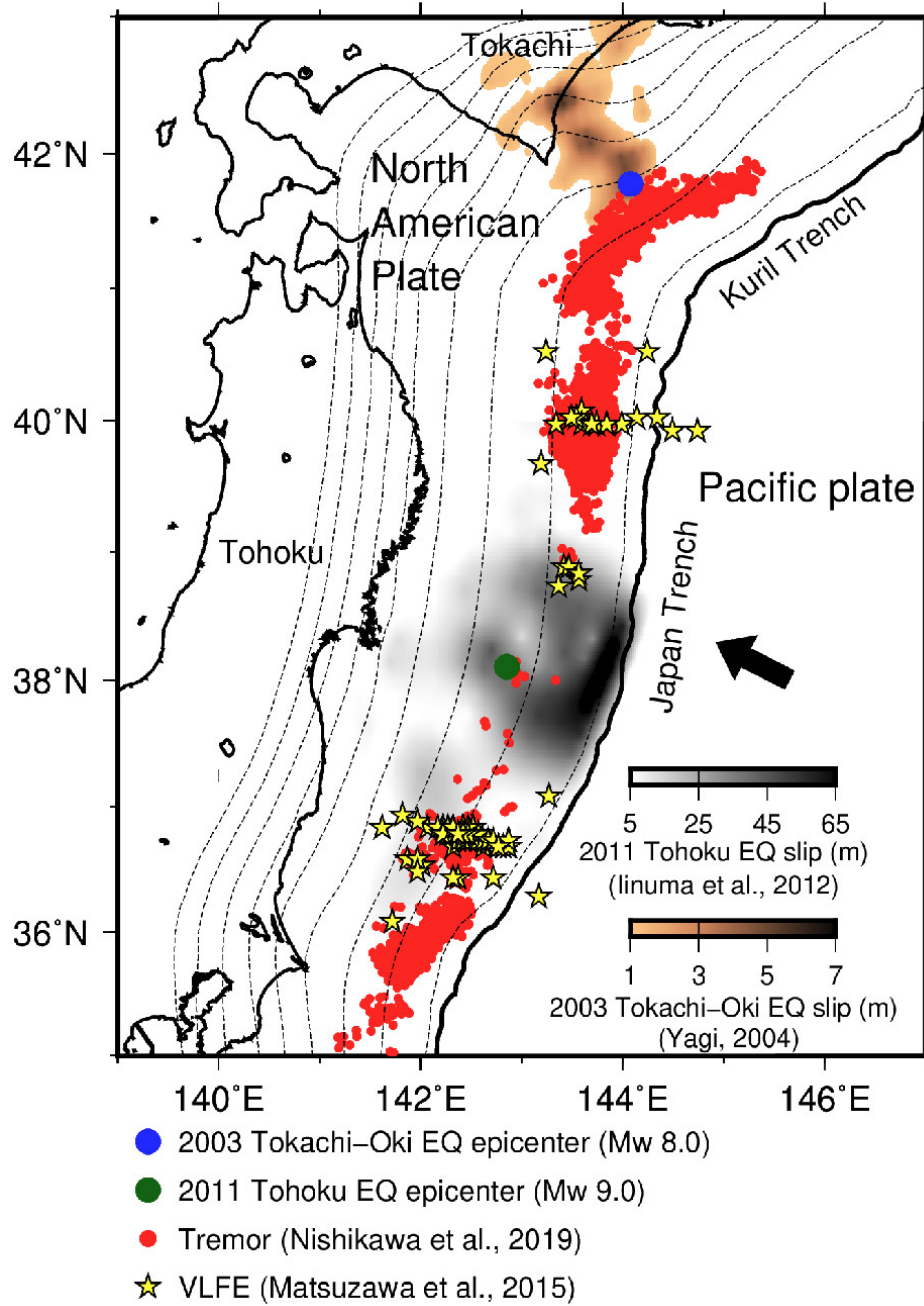
(a) Map of Japan



(b) Along the Nankai Trough in southwest Japan



(c) Along the Japan and Kuril Trenches
in northeast Japan



(d) Along the Ryukyu Trench

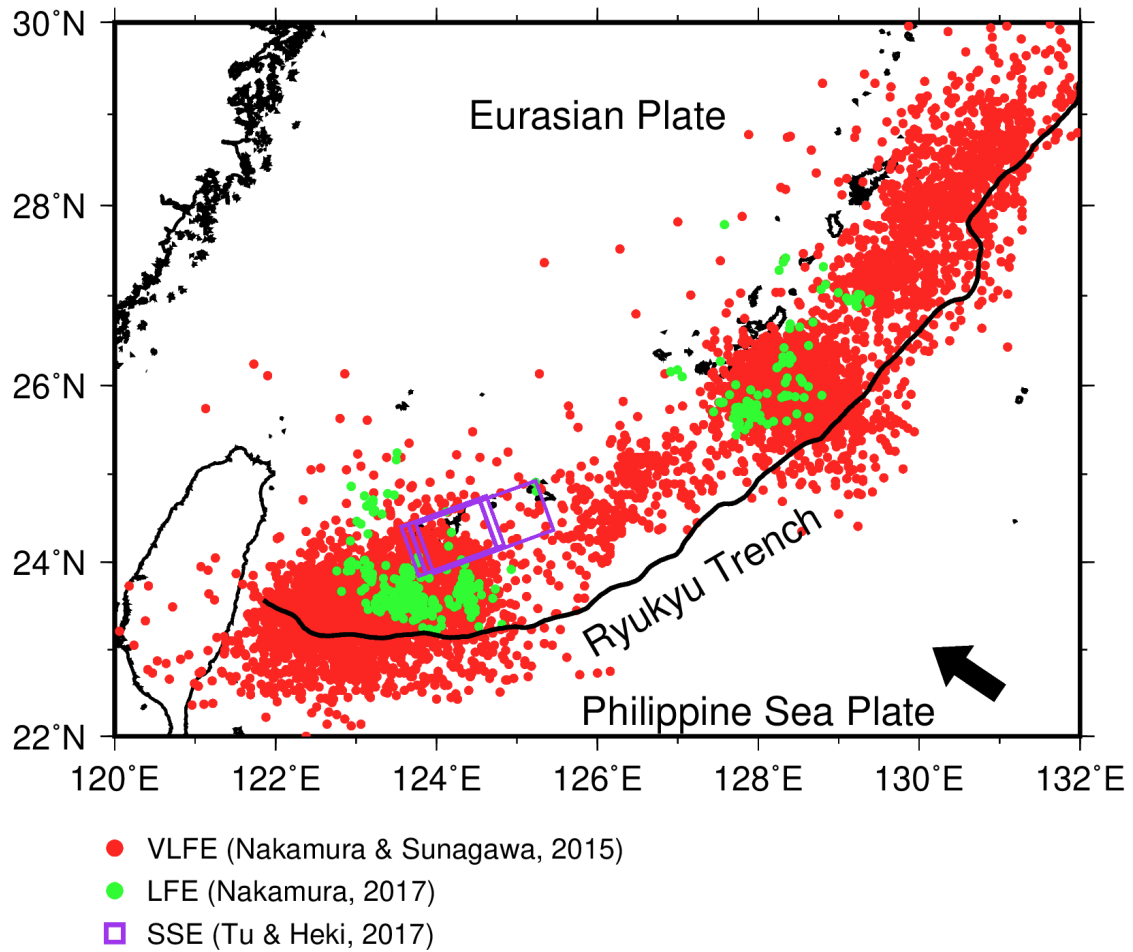


Figure 1.3. (a) Distribution of plates and trenches around Japan. (b-d) Slow and megathrust earthquakes based on previous studies (b) along the Nankai Trough in southwest Japan, (c) along the Japan and Kuril Trenches in northeast Japan, and (d) along the Ryukyu Trench. Dashed contours indicate the isodepths of the top of (b) the Philippine Sea plate (Koketsu et al., 2012) and (c) the Pacific plate with a 10-km interval (along the Japan Trench: Nakajima and Hasegawa, 2006; Nakajima et al., 2009; along the Kuril Trench: Kita et al., 2010). The black arrows in Figures 1.3b and 1.3d indicate the convergence direction of the Philippine Sea Plate, which subducts below the Eurasian Plate. The black arrow in Figure 1.3c represents the convergence direction of the Pacific Plate, which subducts underneath the North American Plate. The black lines represent trench axes.

1.3. Purpose of this study

The contents of this study are shown in Figure 1.4. The purpose of this study is to reveal the factors which control the spatiotemporal variations in slow earthquake activity on the plate boundary. For this purpose, I investigate the spatiotemporal characteristics of VLFE activity around Japan in Chapter 2. Although various types of slow earthquakes are observed, analysis areas, data (onland or offshore), and methods vary by studies. There are previous studies that detected tremors and compare their activity in the world (Ide, 2012; Idehara et al., 2014). However, there are few studies that analyzed deep and shallow slow earthquakes around Japan comprehensively by the same dataset and nearly uniform quality. In addition, the recurrence interval of shallow slow earthquake activity is several years. However, few studies analyzed slow earthquakes stably in a decade-scale period. Although the comparison of slow earthquake activities in various regions is necessary, it is difficult to compare the results in various areas analyzed by different data or methods because the detection capability or the resolution is different. Thus, the factors of slow earthquake activity have not been discussed well.

I, therefore, detect VLFES as a representative of slow earthquakes and quantify the spatiotemporal characteristics of VLFE activity around Japan. This is the first study that quantified spatiotemporal variation in VLFE activities in entire regions along the Nankai Trough and Japan and Kuril Trenches by the same data and a uniform method based on moment-density release rate and the swarm ratio. By the constructed VLFE catalog with uniform quality, I compare spatiotemporal characteristics of VLFE activity in various regions around Japan on a regional scale. This comparison enables me to discuss the factors which control the spatiotemporal variations in slow earthquake activity based on physical models, simulations, or structural studies.

As a result of Chapter 2, Hyuga-nada, off the Pacific coast of Kyushu Island, is a characteristic slow earthquake region, where slow earthquakes are the most active. In Chapter 3, I analyze VLFES and tremors in Hyuga-nada at a higher resolution and discuss the factors of spatial variations in slow earthquake activity.

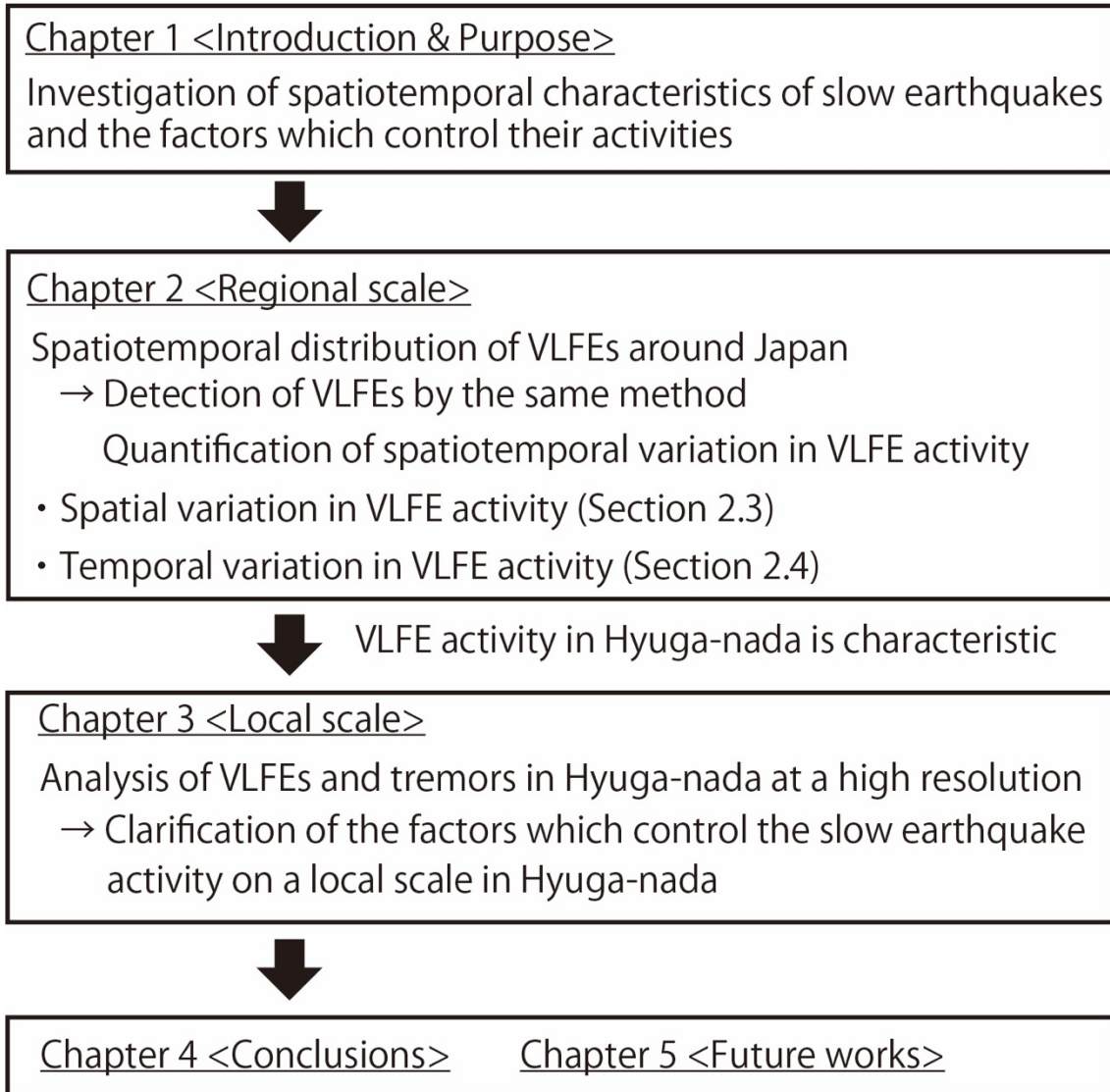


Figure 1.4. Flowchart of this study.

2. Regional spatiotemporal characteristics of VLFE activities around Japan

2.1. Purpose of this chapter

Slow earthquakes are heterogeneously distributed on the plate boundary (e.g., Obara & Kato, 2016). The spatiotemporal variation in their activity can reflect the heterogeneity of frictional conditions or the release of accumulated stress on the plate boundary, which can describe a host of different physical properties. Investigations of slow earthquake activities in subduction zones can provide new insights into the frictional conditions or stress accumulation on the plate boundary.

The relationship between SSE and VLFE activity has been discussed in previous studies. If the shear stress loaded by surrounding SSE increases on the stronger coupled patches of VLFES on the slip fault, these patches rupture (Ito et al., 2007). Thus, VLFE activity has been hypothesized to reflect the spatiotemporal evolution of SSEs. In addition, tremors and VLFES are considered as parts of the same broadband slow earthquakes and are observed in different frequency ranges (e.g., Ide & Maury, 2018; Kaneko et al., 2018; Masuda et al., 2020). Hence, the spatiotemporal variation in slow earthquakes can be revealed by investigating the spatiotemporal distribution of VLFES as a representative of slow earthquakes.

To compare VLFE activities across Japan, I comprehensively detected VLFES around Japan using the matched-filter technique. Offshore VLFES can be detected by an onland seismic record due to the effective propagation of surface waves (Figure 2.1) (e.g., Furumura et al., 2008; Takemura, Kubo, et al., 2019); therefore, both offshore and inland VLFES can be detected using the same dataset on land. A broadband seismic network, Full Range Seismograph Network of Japan (F-net), covered Japanese islands with nearly equal intervals. In addition, the observation period of F-net is longer than that of offshore networks. Since the analysis using F-net can make a VLFE catalog with a nearly unified quality in a decade-scale period, I detected VLFES by using F-net seismograms.

Based on the constructed catalog, I quantify the spatiotemporal distribution of VLFE activity by estimating the moment-density release rate and swarm ratio. I discuss the characteristics of regions with slow earthquake activity from geodetic and geophysical viewpoints. The shear stress is accumulated much mainly near the locked zone on the plate boundary as a result of plate subduction. In addition, the presence of pore fluid, which decreases the seismic velocity, can change the frictional conditions of the plate

boundary. Therefore, the comparisons of the VLFE activity with the slip-deficit rate and seismic velocity structure provide insights into the areas where slow earthquakes occur.

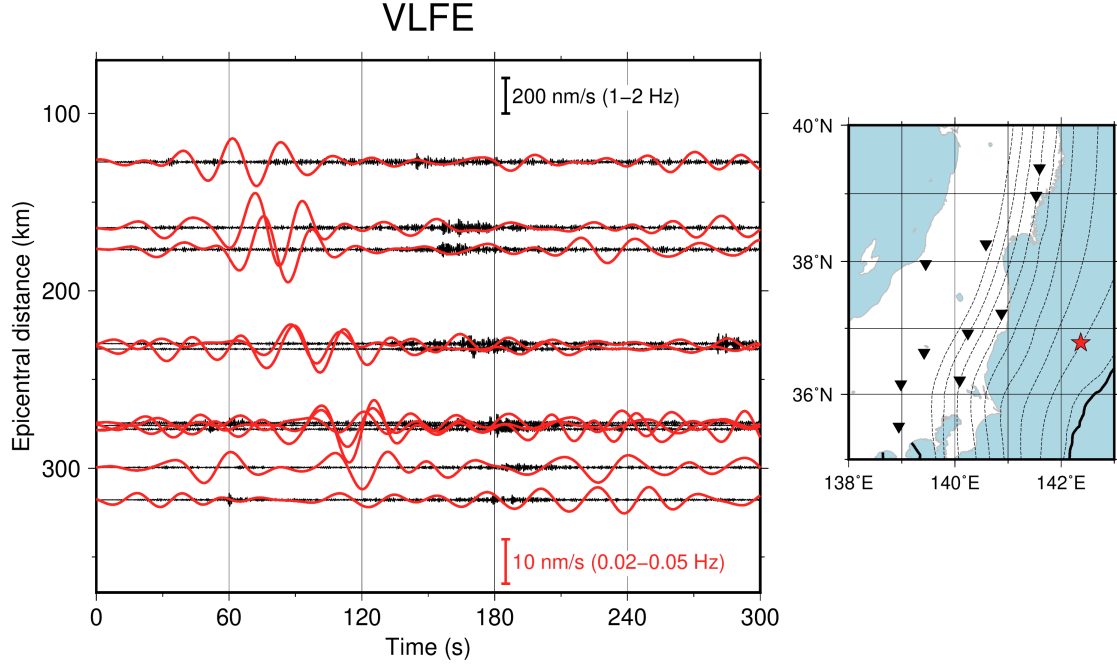


Figure 2.1. (a) Typical example of seismograms of a VLFE at 142.019°E, 36.534°N detected by Matsuzawa et al. (2015). Vertical components at 10 F-net stations are shown in the map. The observed waveforms are placed in epicentral distance order. The VLFE was detected at 4:39:31 JST on 5 March 2011. Red and black lines are seismograms after band-pass filtered in 0.02-0.05 Hz and 1-2 Hz, respectively. The epicenter of the VLFE is indicated by a red star in the map. The dashed lines indicate the isodepth contours of the top of the Pacific plate (Nakajima and Hasegawa, 2006). The black lines indicate the Japan Trench. The inverted triangles show the locations of the F-net stations.

2.2. Data and method

2.2.1. Data

I used continuous seismograms of F-net broadband seismometers (Aoi et al., 2020; Okada et al., 2004) from January 2003 to June 2021 after removing instrumental responses and resampling at one sample per second. A bandpass filter with a frequency range of 0.02–0.05 Hz was applied to all seismograms to enhance VLFE signals of seismic stations (e.g., Ghosh et al., 2015; Ito et al., 2009) and to avoid frequency band of microseism (e.g., Hasselmann, 1963; Kaneko et al., 2018).

2.2.2. Detection of VLFEs

I assumed 196 virtual source grids in intervals of 0.3° along the Nankai Trough and 123 virtual source grids in intervals of 0.4° along the Japan and Kuril Trenches (Figure 2.2). I used these grid intervals because the location uncertainty of VLFEs with M_w of 3–4, which is the typical size of VLFEs, is 0.3 – 0.4° in previous studies (Southwest Japan: Takemura, Noda, et al., 2019, Northeast Japan: Matsuzawa et al., 2015). The depths of virtual sources were fixed on the plate boundary of Japan Integrated Velocity Structure Model (JIVSM; Koketsu et al., 2012). In each virtual source, I detected VLFEs by using the matched-filter technique (e.g., Baba et al., 2018; Hutchison & Ghosh, 2019; Shelly et al., 2007). I used synthetic waveforms as templates in this study because the source locations of templates could be set at arbitrary points, and synthetic waveforms were noise-free. I computed three-component synthetic waveforms for the ten stations closest to each virtual source grid using an open-source seismic wave propagation code (OpenSWPC; Maeda et al., 2017). The OpenSWPC solves equations of motions in a viscoelastic medium based on staggered grid finite-difference method. I computed waveforms in a three-dimensional (3-D) velocity structure model of the JIVSM (Koketsu et al., 2012). The model was discretized by intervals of 0.2 km in space and 0.01 s in time. As a source time function, the Küpper wavelet with a duration of 10 s and M_w of 4.0 was used. The focal mechanisms were assumed to be consistent with the plate motion model, NUVEL-1A (DeMets et al., 1994), and the geometry of the plate boundary (along the Japan Trench: Nakajima & Hasegawa., 2006; Nakajima et al., 2009; along the Kuril Trench: Kita et al., 2010; along the Nankai Trough: JIVSM). To contain two signal cycles within a distance range of ~ 100 km, the time window of each template was defined as 140 s along the Nankai Trough and 150 s along the Japan and Kuril Trenches.

I then calculated cross-correlation coefficients (CCs) between the filtered synthetic template waveforms and F-net seismograms every 1 s. I selected events with the station- and component-averaged CCs exceeding the threshold defined as nine times the median absolute deviation (MAD) of the distributions at each grid. Generally, the threshold of $9 \times \text{MAD}$ is set in the range of 0.3–0.35. If the distribution is Gaussian case, $9 \times \text{MAD}$ is 6.1 times the standard deviation (Figure 2.3). The probability of exceeding $9 \times \text{MAD}$ for a normally distributed random variable is $\sim 6.4 \times 10^{-10}$ (Shelly et al., 2007). Figure 2.4 demonstrates waveforms at a detection across the network. As the VLFE waveform often contains multiple cycles, one event can be counted two or three times. When the interval between two events was smaller than 100 s, I only counted the event whose averaged CC was higher to avoid counting that event as multiple events. In the cases of large magnitude events, one event can be detected in neighboring multiple virtual sources simultaneously. When the averaged CCs exceeded the threshold at multiple virtual sources simultaneously, I only counted the one with the highest CC.

In the detection by the matched-filter technique, considerable false detections can be caused by other signals, such as local regular earthquakes or teleseismic earthquakes. False detections by local regular earthquakes along the Nankai Trough were removed using the catalog of the Japan Meteorological Agency (JMA). Along the Japan and Kuril Trenches, to exclude regional regular earthquakes, I calculated the maximum amplitudes of the nearest F-net station on the vertical components (1–2 Hz and 0.02–0.05 Hz) for each event, because some false detections by regular earthquakes were remained after the 2011 Tohoku earthquake by using the catalog of the JMA. Most of the events with amplitudes >160 nm/s in 1–2 Hz can be falsely detected due to local regular earthquakes. Therefore, I discarded the events with maximum amplitudes >160 nm/s in 1–2 Hz at the nearest F-net station.

In addition, I removed the events detected between the *P*-wave arrivals of teleseismic events whose M_w were more than 4.5 listed in the catalog of the United States Geological Survey and 600 s after the *S*-wave arrivals. Even after removing teleseismic events from the catalog, considerable false detections remained. I discarded these false detections by using a methodology of Baba et al. (2018). Although event amplitudes and CCs generally have a positive correlation (Figure 2.5), events with high amplitudes and low averaged CCs still exist. They are considered to be false detections and are mainly caused by teleseismic events whose M_w are small and are not listed in the USGS

earthquake catalog. Therefore, I did not count events with average CCs below 0.4 and relative amplitudes to templates higher than 0.2 or average CCs below 0.38 and relative amplitudes to templates higher than 0.1, except for Hyuga-nada along the Nankai Trough. In the Hyuga-nada region (south of 32°N in the study area), the events had average CCs below 0.4 and relative amplitudes to templates higher than 0.8. Along the Japan Trench, I did not count events with average CCs below 0.35 and relative amplitudes to templates higher than 0.2 or average CCs below 0.3 and relative amplitudes to templates higher than 0.1, except for the off Tokachi region. Off Tokachi (north of 40.2°N in the study area), the events had average CCs below 0.35 and relative amplitudes to templates higher than 0.5. I established different thresholds based on areas because typical VLFE amplitudes are different by area.

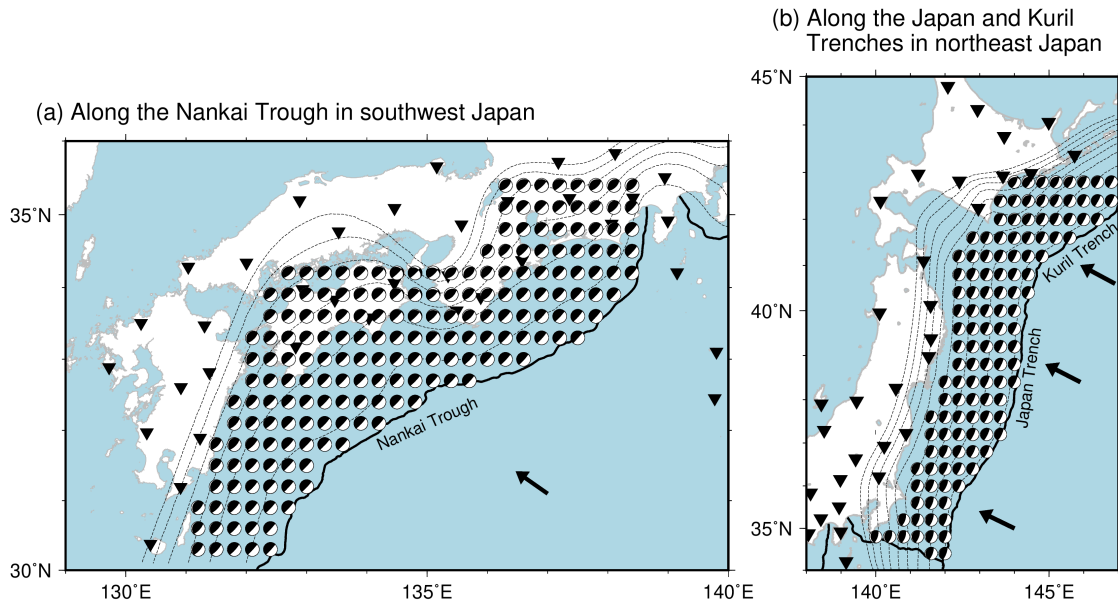


Figure 2.2. Virtual source grids analyzed in this study. Beach balls show the locations and focal mechanisms of virtual sources. Black inverted triangles show the locations of F-net stations. Black arrows and dashed contours are the same as displayed in Figure 1.3.

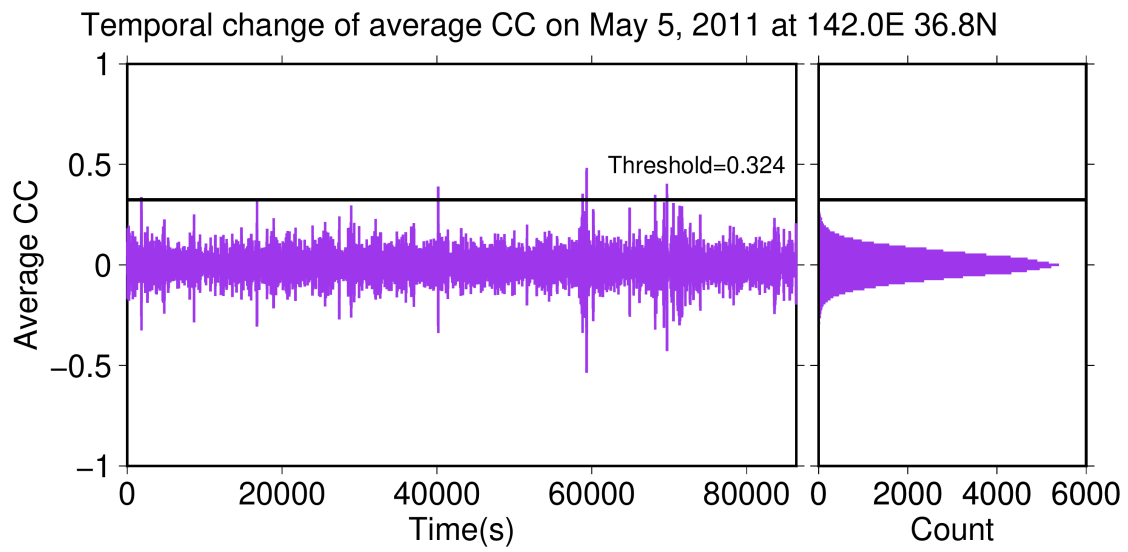


Figure 2.3. Temporal change of averaged CCs and histogram of averaged CCs at 142.0°E, 36.8°N on May 5, 2011. The horizontal line represents the detection threshold.

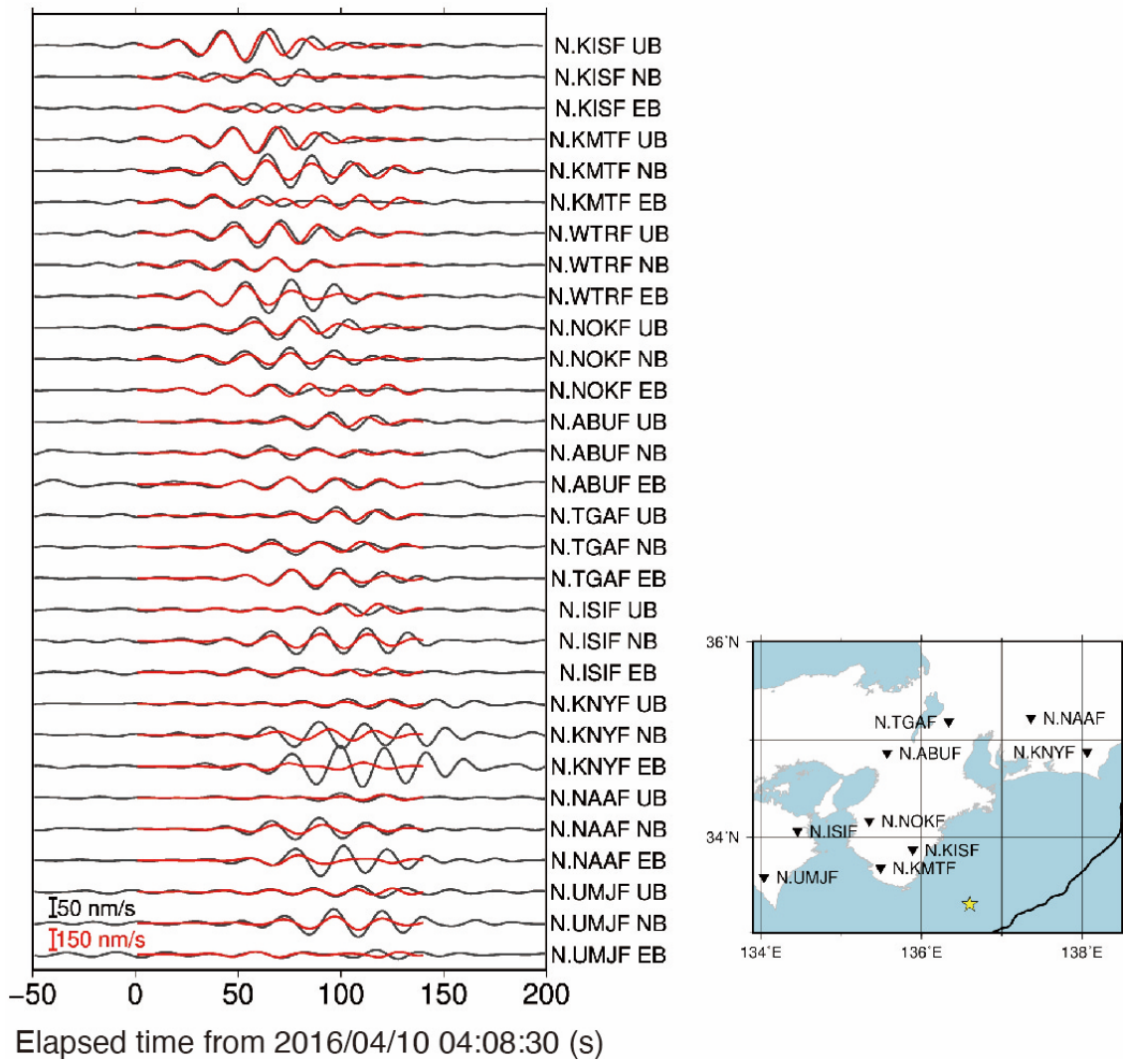


Figure 2.4. Example template with waveforms (red lines) from the virtual source grid located at 136.6°E and 33.3°N; F-net seismograms (gray lines) are from the event with origin time of 04:08:30 JST (UT+9), April 10, 2016. Templates and F-net seismograms are filtered in a frequency range of 0.02–0.05 Hz. The location of the virtual source grid and F-net stations are shown by a yellow star and black inverted triangles in the map, respectively.

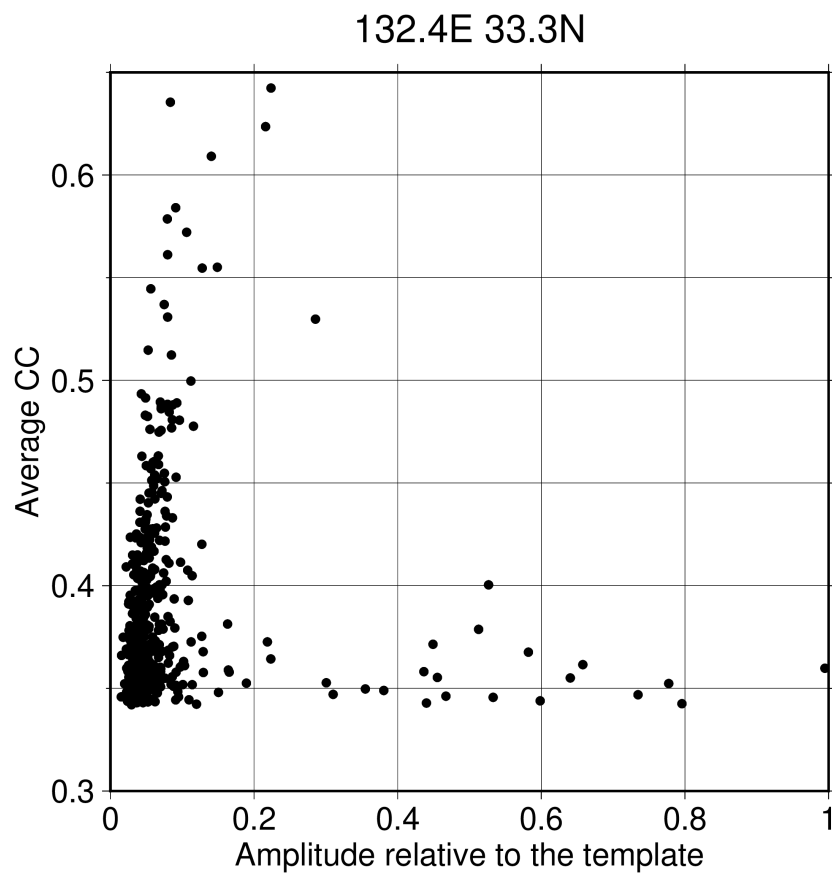


Figure 2.5. The relationship between averaged CCs and amplitudes of events relative to the templates detected at 132.4°E and 33.3°N.

2.2.3. Estimation of seismic moments of VLFs

I calculated the relative amplitude of an event to synthetic waveforms. The source duration of VLFs is longer than that of regular earthquakes; therefore, the estimated moments can change based on the source durations of synthetic waveforms. Then, I searched the source duration of each VLF in the range of 10–50 s by the same method of Yabe, Baba, et al. (2021). I calculated averaged CCs between synthetic and observed waveforms and adopted the source duration whose averaged CC is the highest in the grid search.

After that, I calculated the relative amplitude of an event to the synthetic waveform with the determined source duration (c):

$$c = \frac{\sum_{ij} \int g_{ij}(t) f_{ij}(t) dt}{\sum_{ij} \int g_{ij}(t)^2 dt} \quad (2.1)$$

where, $f_i(t)$ and $g_i(t)$ are the observed waveform and synthetic template waveform at the i -th station and j -th component, respectively. The relative amplitude c was calculated to minimize the variance reduction between the synthetic template waveform and the observed waveform (Yabe, Baba, et al., 2021). The moment of each event (M_o^{event}) was estimated from the amplitude of the event relative to the template:

$$M_o^{event} = c M_o^{syn} \quad (2.2)$$

where, M_o^{syn} is the moment of the synthetic waveforms of M_w 4.0. Subsequently, I estimated the VLF magnitude (M^{event}) using the following relationship between moment magnitude and seismic moment (e.g., Hanks & Kanamori, 1979):

$$M^{event} = \frac{\log_{10} M_o^{event} - 9.1}{1.5}. \quad (2.3)$$

When I estimated the seismic moments of VLFs, I excluded the virtual source grids in which most events were falsely detected mainly due to teleseismic events remaining after the removal process described in Section 2.2.2. The number of detected events in most of excluded source grids was below 35 and 20 along the Nankai Trough and along the Japan and Kuril Trenches, respectively. False detections were examined by checking the detected event waveforms visually. When the waveforms from all F-net stations were plotted, VLF signals are seen in approximately 10 F-net stations near the virtual source (Figure A1a). The events for which the signals appeared at almost

simultaneously at many F-net stations could have been falsely detected due to a teleseismic event (Figure A1b). Particularly, although many events were detected near the coast of Kyushu or off the coast of northern Hokkaido, most of them were remained false detections that remained. These false detections were probably caused by a small number of closely located stations and poor station coverage along the azimuth directions. I, therefore, excluded the grids of these areas.

The cumulative moment of each grid was calculated using the sum of seismic moments of all VLFs detected in the grid. The moment-density release rate at each grid is estimated by the cumulative moment divided by the analysis period and the area of the grid. It represents VLFE activity rate at each grid. I evaluated the errors of the cumulative moment of each grid by using the nonparametric bootstrap method (e.g., Tichelaar & Ruff, 1989). First, 500 bootstrap samples were prepared for each grid. A bootstrap sample was generated from the original events. If n events were detected at a grid, a bootstrap sample consisted of random n events including duplicates. Subsequently, cumulative moments were calculated by the sum of the moments of n events. Finally, I estimated the standard deviations of the 500 random samples.

2.3. Spatial characteristics of VLFE activities

VLFEs along the Nankai Trough are distributed at depths of 30–40 km (deep VLFEs) and 5–10 km (shallow VLFEs; Figures 2.6a and A2a). Depths of shallow VLFEs along the Nankai Trough are shallower than VLFEs in northeastern Japan (10–30 km; Figures 2.6b and A2b). The different source depths of VLFEs in these subduction zones may be related to the difference of the temperature distribution (Harris et al., 2013; Kimura et al., 2012), however, the relationship is unclear. I classified deep VLFE activity along the Nankai Trough into four regions (i.e. western Shikoku, eastern Shikoku, Kii Peninsula, and, Tokai), shallow VLFE activity along the Nankai Trough into four regions (i.e. Hyuga-nada, off Cape Muroto, off the southern Kii, and off the southeastern Kii), and VLFE activity along the Japan and Kuril Trenches into six regions (i.e. off Tokachi, off Aomori, off Iwate, off Miyagi, off Fukushima, off Ibaraki) according to their spatiotemporal characteristics.

The moment-density release rate of deep VLFEs and their spatial variation are smaller than those of shallow VLFEs (Figure 2.6). The distribution of deep VLFE activity is belt-like, while that of shallow VLFE activity is more spot-like. The along-strike spatial pattern of deep VLFE activities is generally consistent with the distribution of energy released by deep tremors (Annoura et al., 2016). On the other hand, shallow VLFE activity shows a strong spatial heterogeneity along the Nankai Trough (Figure 2.6). The largest moment-density release rate was observed in the Hyuga-nada region in which earthquakes with $M_w > 8$ have not been recorded. On the other hand, moment-density release rate in Nankai (i.e. off Cape Muroto, off the southern Kii, and off the southeastern Kii), where large earthquakes with $M_w \geq 8$ have occurred, is smaller than that in Hyuga-nada.

The M_w distribution of VLFEs represents that the maximum M_w range of VLFEs in Hyuga-nada is larger than that in other regions (Figure 2.7; Table 2.1). The maximum M_w range of deep VLFEs and VLFEs off Tohoku (i.e., off Iwate, off Miyagi, off Fukushima, and off Ibaraki) is smaller than that in other regions, that is, VLFEs with M_w of larger than 4.0 are rare. In Nankai and off Tokachi and Aomori, the maximum M_w is 4.2–4.3. In Hyuga-nada, the completeness M_w (the peak M_w of Figure 2.7) of detected VLFEs is smaller than 3.8 is larger than those in other regions, possibly because Hyuga-nada is at the edge of Japanese islands and the number of near stations is small.

Table 2.1. The number, Moment-density release rate, maximum Mw, and completeness Mw of VLFs at each area

Subduction zone	Area Name	Number	Mo-density release rate	Maximum Mw	Completeness Mw
Nankai Trough Deep VLFs	W Shikoku	788	$10^{5.6} - 10^{6.3}$	3.9	3.0
	E Shikoku	435	$10^{5.6} - 10^{5.7}$		
	Kii Pen.	681	$10^{5.6} - 10^{6.2}$		
	Tokai	204	$10^{5.3} - 10^{5.7}$		
Nankai Trough Shallow VLFs	Hyuga-nada	16,014	$10^{6.2} - 10^{8.7}$	4.8	3.8
	Off Muroto	1,217	$10^{5.3} - 10^{6.5}$	4.3	3.3
	Off S Kii	218	$10^{5.6} - 10^{6.4}$		
	Off SE Kii	2,216	$10^{6.8} - 10^{7.2}$		
Japan and Kuril Trenches VLFs	Off Ibaraki	2,911	$10^{5.3} - 10^{6.6}$	3.9	3.1
	Off Fukushima	373	$10^{5.5} - 10^{5.9}$		
	Off Miyagi	110	$10^{5.1} - 10^{5.6}$		
	Off Iwate	1,077	$10^{5.0} - 10^{6.4}$	4.2	3.4
	Off Aomori	602	$10^{5.3} - 10^{6.5}$		
	Off Tokachi	23,040	$10^{6.1} - 10^{7.9}$		

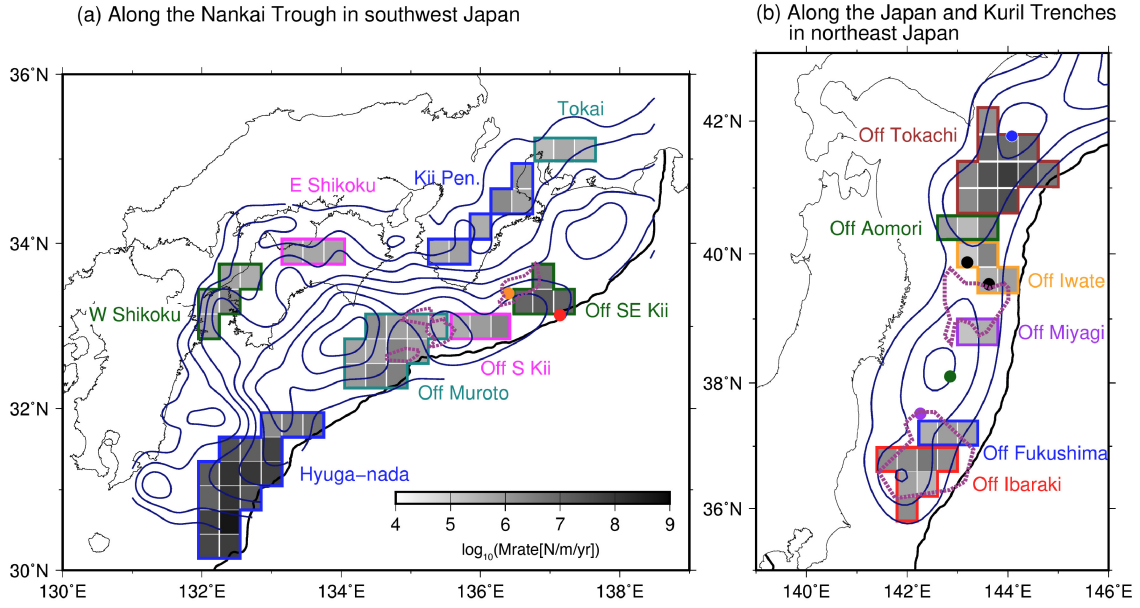


Figure 2.6. Moment-density release rate of VLFs (a) along the Nankai Trough in southwest Japan and (b) along the Japan and Kuril trenches in northeast Japan. Dark blue contours in Figures 2.6a and 2.6b show the slip-deficit rate distribution with a 10 mm/year interval (March 2005–February 2011; Noda et al., 2018) and that with a 30 mm/year interval (1996–2000 (before the 2003 Tokachi-Oki and the 2011 Tohoku earthquakes); Hashimoto et al., 2012), respectively. Dashed dark purple lines are low V_p areas shown in Yamamoto et al. (2017) and Zhao et al. (2011), respectively. Red and orange circles in Figure 2.6a represent the epicenters of the 2004 off the Kii Peninsula and the 2016 off the southeastern Mie Prefecture earthquakes, respectively. Blue, purple, and green circles in Figure 2.6b represent the epicenters of 2003 Tokachi-Oki, 2008 Fukushima-Oki and 2011 Tohoku earthquakes, respectively. Black circles in Figure 2.6b are the Tohoku earthquake aftershocks that activated VLFs off Iwate. The solid black lines are the same as those in Figure 1.3. The cumulative moments of each region were calculated by stacking moments of events of all grids contained in the region.

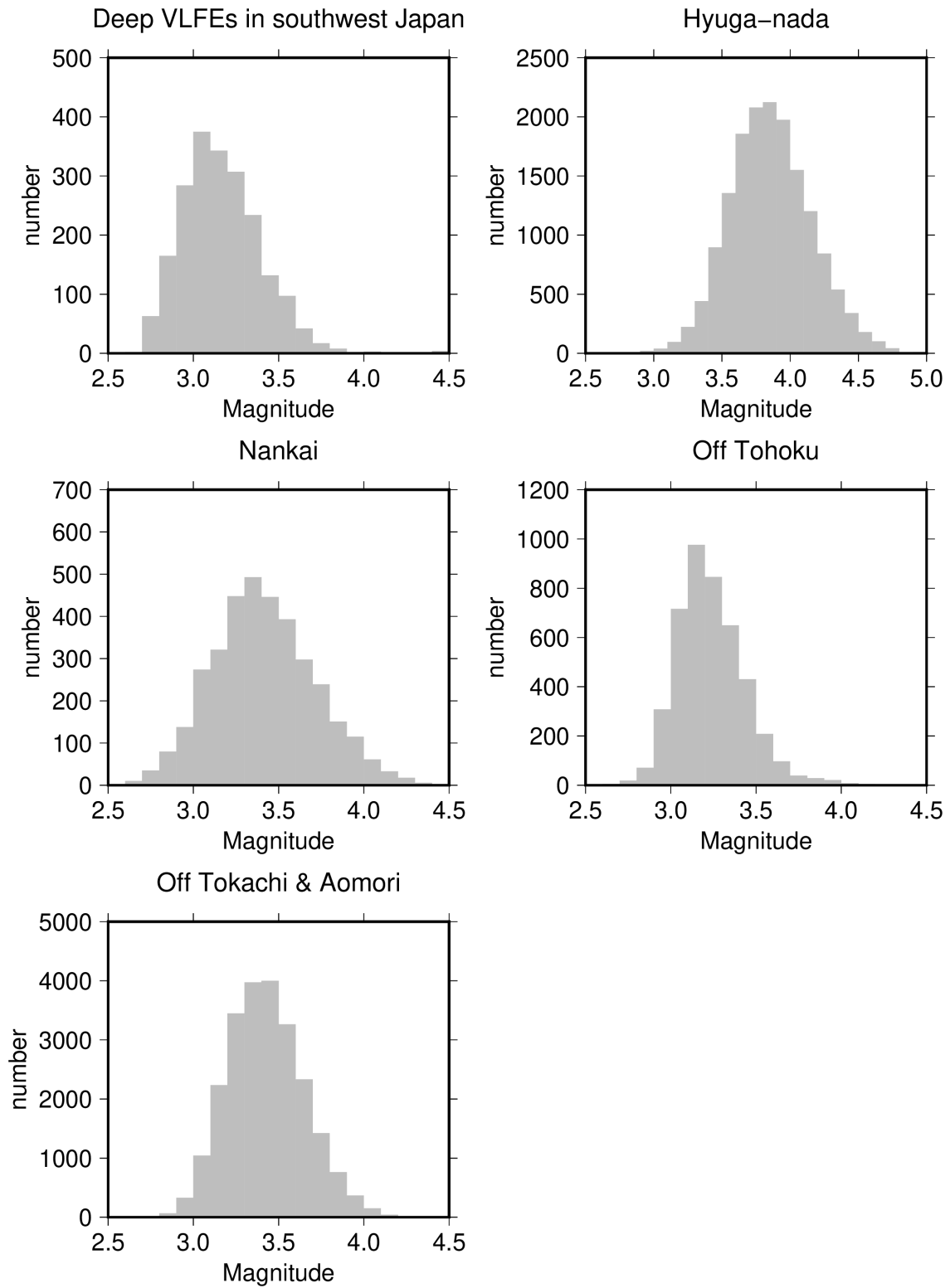


Figure 2.7. Histogram of magnitudes of VLFs detected in this study.

2.3.1. Correlation between the VLFE activity and interplate coupling

To compare the VLFE activity with the interplate coupling in both subduction zones, I determined the coupling ratio by dividing the slip-deficit rate of each grid by the maximum slip-deficit rate in each subduction zone, assuming that the interplate locking is 100% at the location of the maximum slip-deficit rate (Hashimoto et al., 2012; Noda et al., 2018). To compare the VLFE activity and slip-deficit rate both along the Nankai Trough and along the Japan Trenches, I used these two models because their inversion methods are similar. In addition, Noda et al. (2018) used offshore data and adopted the elastic-viscoelastic structures. The spatial variation in slip-deficit rates was derived from inversions of interseismic Global Navigation Satellite System (GNSS) displacement rate data. In this discussion, I consider the variation in the slip-deficit rate as that in the interplate coupling.

The strong spatial heterogeneity of offshore VLFE activity correlates well with the spatial distribution of the interplate coupling (Hashimoto et al., 2012; Noda et al., 2018) along the plate boundary (Figure 2.6). The regions with strong coupling (large slip-deficit rate) and those with VLFE activity are separated in both subduction zones. To compare the VLFE activity in preparation for the next megathrust earthquake with the coupling ratio, I use the moment-density release rate of VLFES along the Nankai Trough and VLFES off Tohoku (off Iwate, off Miyagi, off Fukushima, and off Ibaraki) only before the 2011 Tohoku earthquake for the comparison. Within megathrust earthquake (strong interplate coupling) areas, such as Nankai (off Cape Muroto, off the southern Kii, and off the southeastern Kii) and off Tohoku, the moment-density release rate of VLFES is low (Figures 2.8a).

The moment-density release rate of shallow VLFES and the coupling ratio are negatively correlated along the Nankai Trough (Figure 2.8a). The CC between the common logarithm of the moment-density release rate of shallow VLFES and the coupling ratio is -0.80. However, because offshore geodetic data are lacking in Hyuga-nada and Hyuga-nada is at the edge of the analysis area, the estimation error of slip-deficit rate in Hyuga-nada can be large. The CC between the common logarithm of the moment-density release rate of shallow VLFES and coupling ratio only in grids with estimation error is smaller than 15 mm/year in Nankai is -0.57 (Figure 2.8a). I also compared the moment-density release rate of shallow VLFES and slip-deficit rate by Agata (2020), which introduced the covariance components to avoid overfitting the non-uniformity of

geodetic data in the inversion method (Figure A3). The CC between the common logarithm of the moment-density release rate of shallow VLFs and the coupling ratio estimated from Agata (2020) is -0.69 (Figure A3). Therefore, there can be a negative correlation only in Nankai. This negative correlation suggests that the contribution to stress release by megathrust earthquakes is large and slow earthquakes release a small fraction in the strongly coupled areas. If the negative correlation between the coupling ratio and VLFE moment-density release rate can be extended to entire regions along the Nankai Trough, Hyuga-nada, where the moment-density release rate is large, is suggested to be a weak coupling area. The coupling ratio in Hyuga-nada is small (Figure 2.8a) although the estimation error can be large. If the interplate coupling is weak in Hyuga-nada, it is suggested that the accumulated stress may be released frequently by slow earthquakes in the weakly coupled areas.

In some areas off Tohoku, the interplate coupling is strong but the moment-density release rate is relatively large (Figure 2.8c). In 2008, Mw 6–7 interplate earthquakes occurred off Fukushima and off Ibaraki regions, which might have activated VLFs. The interplate slip rate estimated from repeating earthquakes also increased after these earthquakes (Nomura et al., 2017). Because of this triggering process by large earthquakes discussed in Section 2.4.1, the negative correlation between the interplate coupling ratio and VLFE activity may be unclear off Tohoku regions. In addition, there are no offshore geodetic data off Tohoku, therefore the estimation error of slip-deficit rate off Tohoku may be large.

The relationship between SSE activity and interplate coupling was discussed by geodetic studies. In Ecuador, megathrust earthquakes occur in strongly coupled areas, whereas SSEs release accumulated stress in weakly coupled areas in which no megathrust earthquakes have been recorded (Vaca et al., 2018). SSEs in the Cascadia subduction zone also occur in the area with weak interplate coupling (Michel et al., 2019). These tendencies can be the same as that in shallow VLFs along the Nankai Trough: accumulated stress can be frequently released by slow earthquakes in weakly coupled areas, whereas the proportion of slow earthquakes is relatively small in terms of stress release in strongly coupled areas. In other words, slow earthquake activity is probably related to the coupling ratio.

On the other hand, deep VLFs occur only in areas with weak interplate coupling, and the moment-density release rate and its variation are small (Figure 2.6a).

Thus, there are no meaningful spatial relationships between the moment-density release rate of deep VLFs and the coupling ratio (Figure 2.8b). In areas in which deep VLFs occur, the proportion of the release of the accumulated stress by deep VLFs may not be as large as that of shallow VLFs. The annual slip rate of short-term SSEs associated with ETS along the Nankai Trough was previously estimated to be 2–4 cm/year by Hirose & Obara (2006), which is approximately half of the convergence rate of the Philippine Sea Plate. The geodetically estimated weak coupling and small moment-density release rate of VLFs might be affected by such decoupling properties in deep slow earthquake source regions in brittle-ductile transition zone between strongly coupled and stable sliding zones.

Some geodetic studies discuss what percentage of the slip deficits is released by slow earthquakes. Most of the slip deficits beneath the Bungo channel are released by long-term SSEs (Noda et al., 2018), whereas the contribution of SSEs off the Kii to the release of slip deficits is 30–50% (Araki et al., 2017). VLFE activity reflects the occurrence SSEs (Ito et al., 2007). Ito et al. (2009) evaluated that the cumulative moments of deep VLFs are 0.1% of those of deep SSEs. If the relationship between VLFs and SSEs is similar in all regions along the Nankai Trough, the contribution of SSEs in Hyuga-nada to the release of slip deficits may be more than 30–50%.

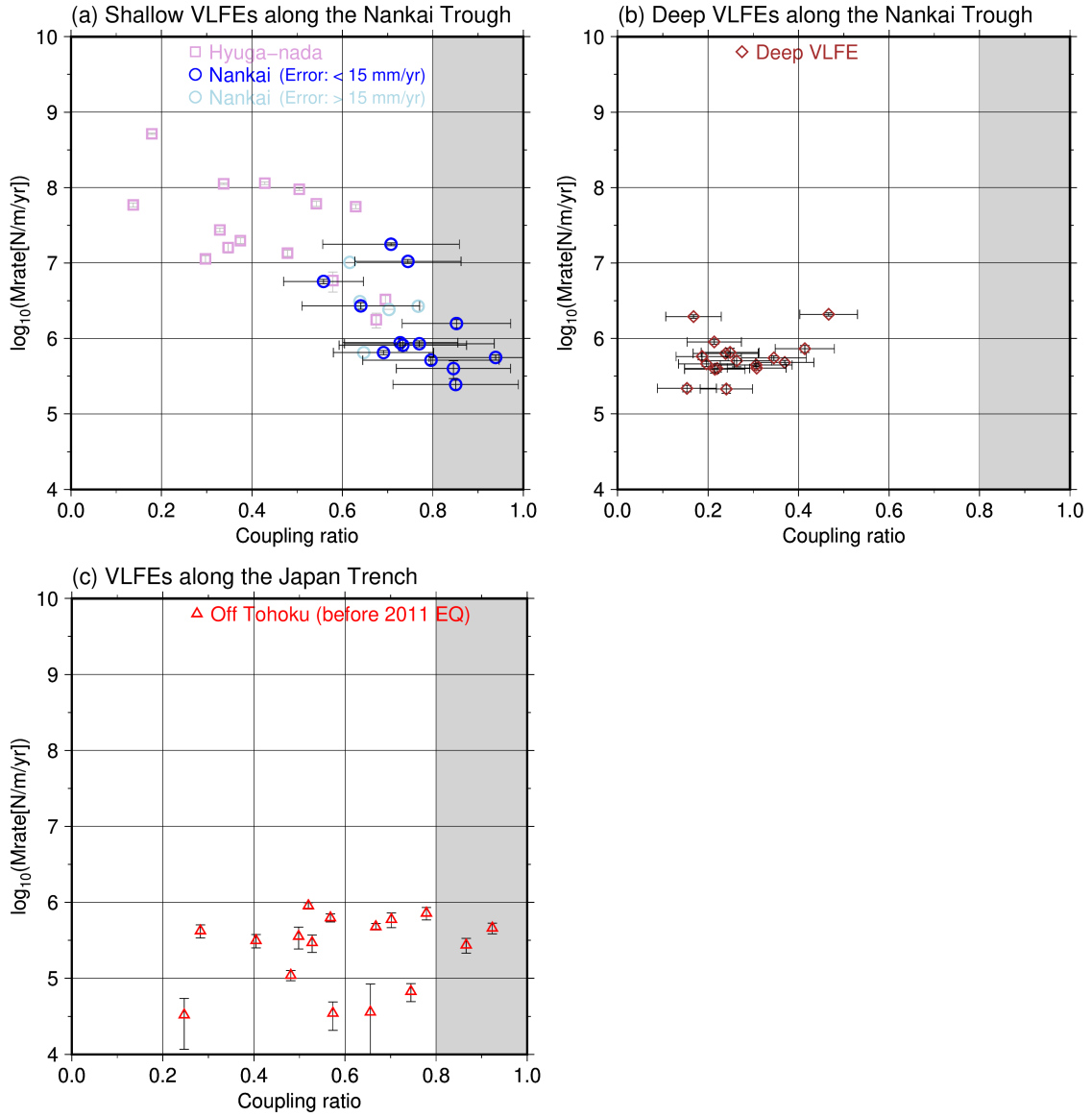


Figure 2.8. Relationship between the moment-density release rate and interplate coupling ratio. (a) Relationship between the logarithm of the cumulative moment of shallow VLFs along the Nankai Trough per year and per m^2 and coupling ratio estimated from the slip-deficit rate by Noda et al. (2018). Light symbols show grids in Hyuga-nada and those in Nankai with estimation errors with larger than 15 mm/yr are. Grey filling represents the large coupling ratio area. Errors of the cumulative moment in each grid were estimated by the nonparametric bootstrap method described in Section 2.2.3. (b) Same as (a) but for deep VLFs along the Nankai Trough. (c) Same as (a) but VLFs off Tohoku along the Japan Trench and the coupling ratio estimated from the slip deficit rate by Hashimoto et al. (2012).

2.3.2. Correlation between the VLFE activity and seismic velocity structure

Based on the comparison between shallow VLFE activity and seismic wave velocity variation along the Nankai Trough (Yamamoto et al., 2017), shallow VLFs are mainly distributed within low-velocity anomalies around the bottom of the overriding plate. Thus, fluids can potentially promote VLFE activity. This tendency is similar to that reported in previous studies (e.g., Kitajima & Saffer, 2012; Tonegawa et al., 2017). As for Japan and Kuril Trenches, there is a high P -wave velocity (V_P) area at the bottom of the hanging wall (Zhao et al., 2011). This high V_P area corresponds to the coseismic slip area of the 2011 Tohoku earthquake. On the other hand, low V_P areas can be observed north and south of the high V_P area (Zhao et al., 2011). These areas correspond to areas with VLFE activity, such as off Iwate, off Fukushima, and off Ibaraki regions. Within the largest coseismic slip area and on the plate boundary deeper than 35 km, V_P is high and there are few VLFs. Nishikawa et al. (2019) suggested that tremor activity is also rare in high V_P areas. Although the resolution of S -wave tomography is generally lower than that of P -wave, the distribution of low S -wave velocity areas is almost the same as that of low V_P areas (Huang & Zhao, 2013; Yamamoto et al., 2017).

The existence of low-velocity areas at shallower depths suggests a high pore fluid pressure (e.g., Kamei et al., 2012; Tonegawa et al., 2017). Akuhara et al. (2020) indicates that the depth of the area with high V_P/V_S ratio is consistent with that of shallow slow earthquakes off the southeastern Kii. Based on these observations, the decrease in the effective normal stress due to the high pore pressure reduces the frictional strength on the plate boundary and consequently promotes the generation of VLFs with a low stress drop (e.g., Ito & Obara, 2006; Saffer & Wallace, 2015). Deep LFEs are considered to be also promoted in the areas with much fluid on the plate boundary (e.g., Nakajima & Hasegawa, 2016). Off Tokachi and Aomori regions, VLFs actively occur but the V_P is high. In the region between the Japan and Kuril Trenches, regular earthquakes are rare. In addition, the afterslip of the 2003 Tokachi-Oki earthquake has continued in this region (e.g., Itoh et al., 2019; Nomura et al., 2017), indicating that there might be another factor activating VLFs.

2.3.3. Characteristics of areas with slow earthquake activity

VLFEs actively occur adjacent to large coseismic slip areas of megathrust earthquakes in both subduction zones of Japan. In the shallower part, the moment-density release rate of VLFEs and geodetically estimated coupling ratio on the plate boundary are negatively correlated (Figure 2.8a). Although there is a case of a large slip deficit area sticking out from a frictionally locked zone, the large slip deficit area is considered as frictionally locked (Herman et al., 2018; Lindsey et al., 2021). In strongly coupled areas, the interplate frictional strength can be high and high-speed ruptures occur. In addition, the large coseismic slip area of the 2011 Tohoku earthquake corresponds to the high V_p area (Zhao et al., 2011). The effective strength of the plate boundary may be high in such high-speed rupture areas, the slow earthquake activity rate is low. On the other hand, in weakly coupled areas, the accumulated stress is frequently released by slow earthquakes and megathrust earthquake nucleation cannot be favorably initiated.

Although there are a few exceptions, the shallow VLFE activity tends to be high in areas with relatively weak interplate coupling and low seismic velocities. In areas with weak interplate coupling, shallow VLFEs can be activated by the decrease in the effective normal stress due to the high pore fluid pressure. On the other hand, the variation in the moment-density release rate of deep VLFEs is smaller than that of shallow VLFEs. This suggests that the horizontal heterogeneity of the frictional properties is stronger in the shallower part of the plate boundary near the seismogenic zone than in the deeper part. The differences in thermal conditions between the deeper and shallower parts of the plate boundary (Saffer & Wallace, 2015) or the complex bathymetry of the plate interface in the shallower part (Okino et al., 1999), such as the existence of seamounts, may be the cause of strong heterogeneity of shallow slow earthquake activity. The heterogeneity of geometry in the shallower part can cause variation in effective stress. In addition, comparing the S -wave velocity in shallower and deeper parts along the Nankai Trough (shallower part: Tonegawa et al., 2017; deeper part: Nakajima & Hasegawa, 2016), the variation in the deviation from the average S -wave velocity in the shallower part ($\sim \pm 30\%$) is larger than that in the deeper part ($\sim \pm 9\%$). Therefore, the variation in the pore fluid pressure can be larger in the shallower part. In the shallower part at a low temperature, a large portion of fluids is released through compaction (Saffer & Tobin, 2011). The variation in the stress distribution derived from the complex geometry in the shallower part may cause the heterogeneity of the pore fluid pressure. The strong

heterogeneity in the shallower part may be attributed to the variations in pore fluid pressure or effective stress. Passarelli et al. (2021) indicated that shallow SSEs release larger seismic moments than deep SSEs. They suggested that the difference in deep and shallow SSE activity derives from the variation in frictional and rheological properties controlled by the temperature. Hutchison (2020) pointed out that physical complexities can control the distribution of slow earthquake activity; therefore, the physical complexity may be stronger in the shallower part than in the deeper part.

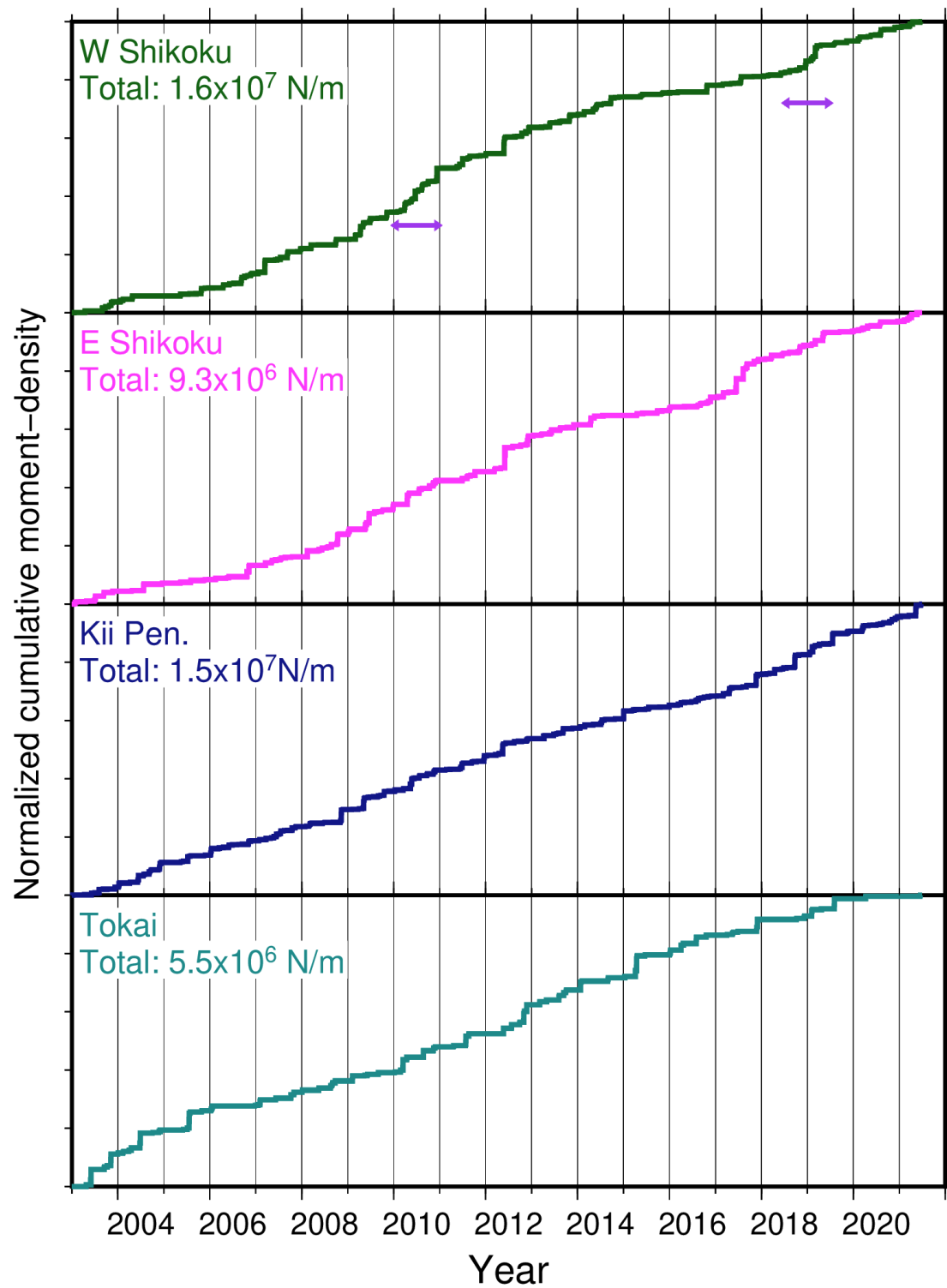
2.4. Temporal characteristics of VLFE activities

The number of deep VLFs detected in western Shikoku, eastern Shikoku, the Kii Peninsula, and Tokai is 788, 435, 681, and 204, respectively (Table 2.1; Figure A4a), whereas the number of shallow VLFs detected in Hyuga-nada, off Cape Muroto, off the southern Kii, and off the southeastern Kii regions is 16,014, 1,217, 218, and 2,216, respectively (Table 2.1; Figure A4b). The number of VLFs detected off Tokachi, off Aomori, off Iwate, off Miyagi, off Fukushima, and off Ibaraki is 2,911, 373, 110, 1,077, 602, and 23,040, respectively (Table 2.1; Figure A4c). The temporal change of cumulative moment calculated by the sum of seismic moments of each VLFE (details were described in Section 2.2.3) yielded results similar to the temporal change of the total number of VLFs (Figures 2.9 and A4). The cumulative number of VLFs at each grid is shown in Figure A5.

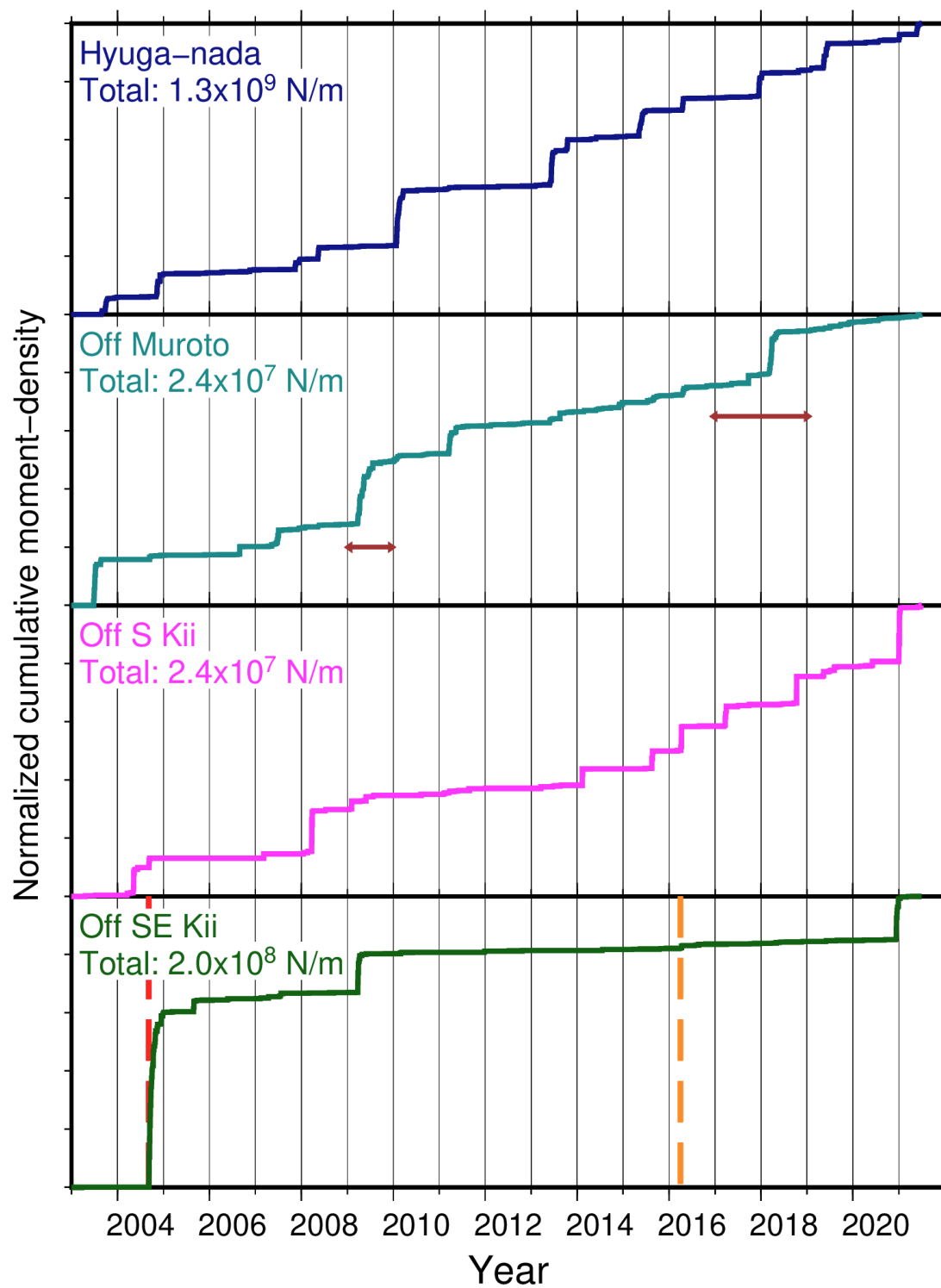
The cumulative number and moment of deep VLFs exhibit stepwise changes with an interval of several months accompanied by ETSSs, and the rapid increase in the cumulative moment of deep VLFs in western Shikoku in 2010 and 2019 can be modulated by long-term SSEs in the Bungo channel (e.g., Baba et al., 2018; Hirose & Obara, 2005). The rapid increases in the cumulative moment of shallow VLFs off Cape Muroto can be modulated by shallow SSEs off the Kii channel (Yokota & Ishikawa, 2020) in 2009 (Mw 6.2) and 2018 (Mw 6.6). The temporal correlation between seismic slow earthquake activity and geodetic data was also shown in Mexico (e.g., Frank & Brodsky, 2019) and in the Cascadia subduction zone (e.g., Rouet-Leduc et al., 2019). The intervals of VLFE activations are longer for shallow VLFs than for deep VLFs (Figures 2.9).

I categorized temporal evolutions of VLFE activities into three patterns: (i) activation after a large earthquake; (ii) quiescence after a large earthquake; (iii) repetition of swarm activities and quiescence (Figure 2.10; Table 2.2). In Sections 2.4.1 and 2.4.2, I discuss the pattern (i), (ii) and (iii), respectively.

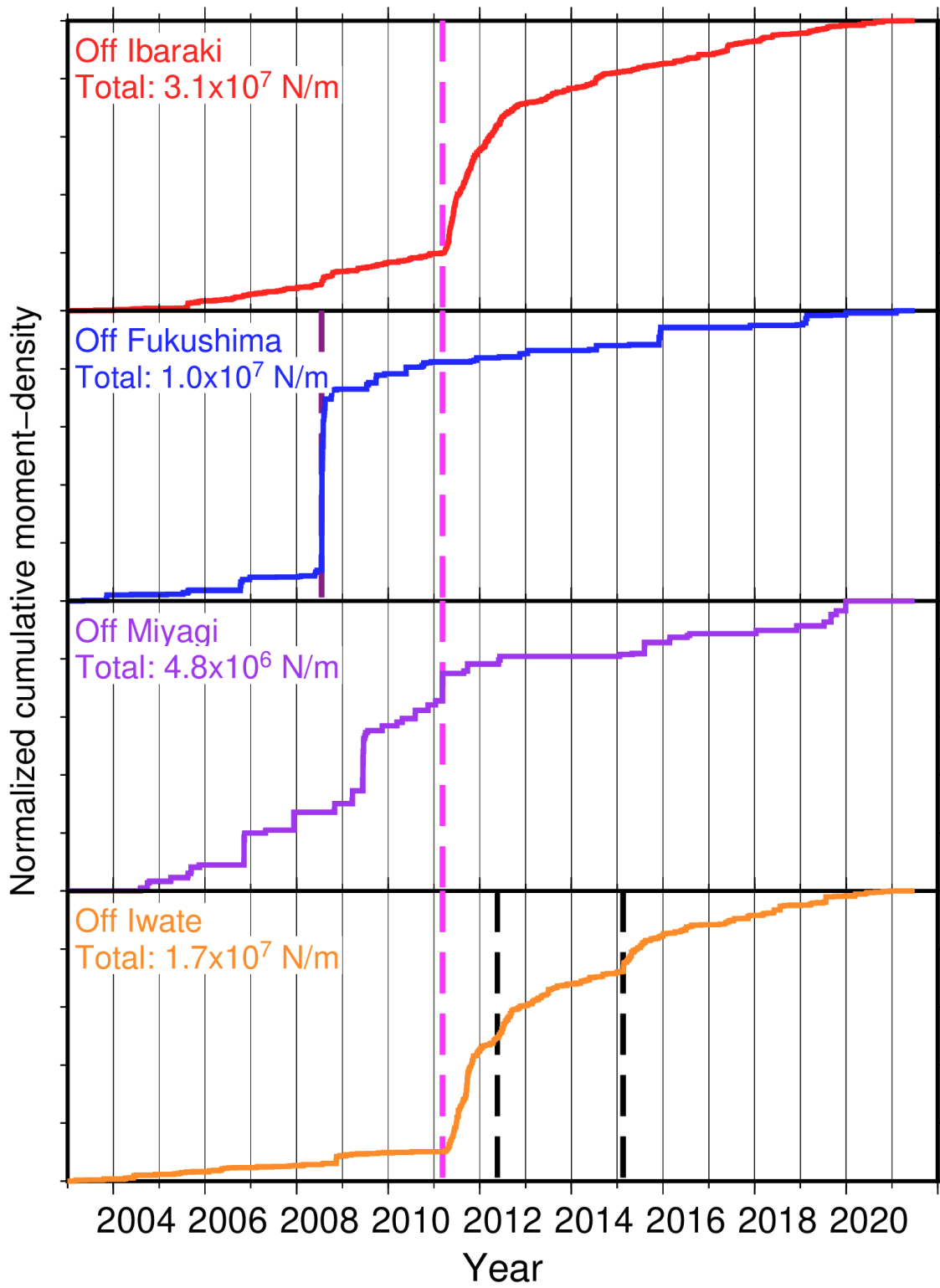
(a) Deep VLFES along the Nankai Trough



(b) Shallow VLFES along the Nankai Trough



(c) VLFEs along the Japan and Kuril Trenches



(c) continued

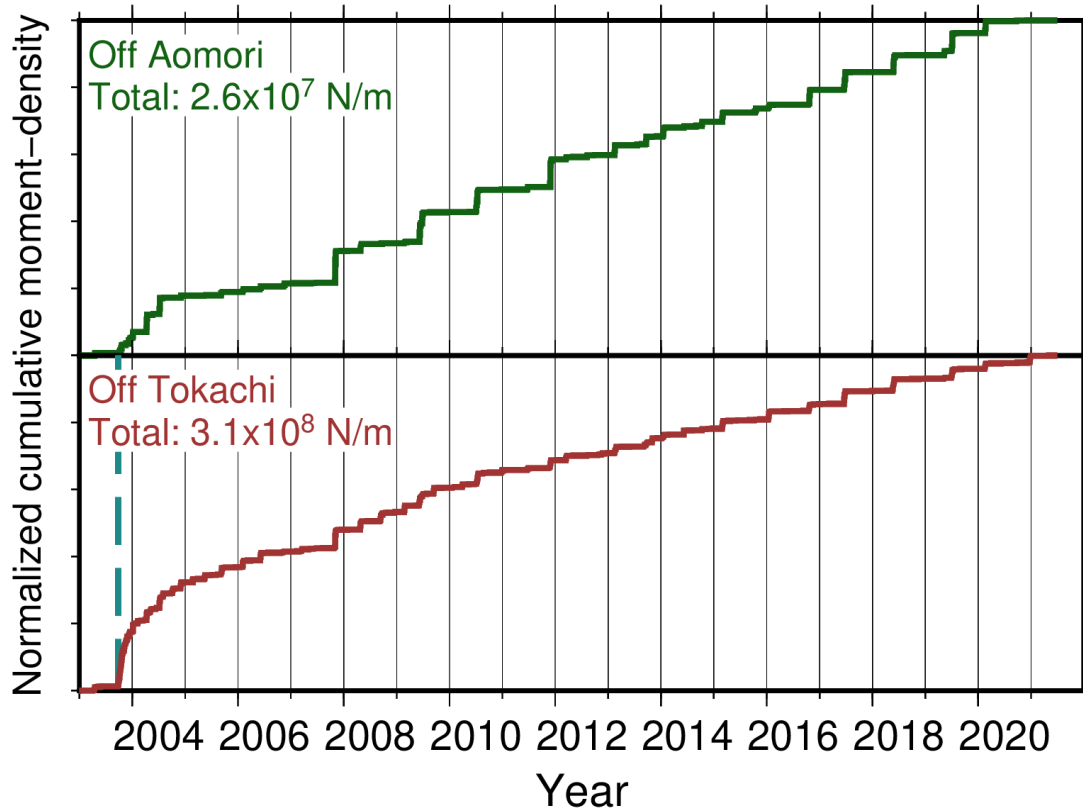


Figure 2.9. Cumulative moment density normalized by the total amount in the analysis period in (a) deep VLFs along the Nankai Trough in southwest Japan, (b) shallow VLFs along the Nankai Trough in southwest Japan, and (c) VLFs along the Japan and Kuril Trenches in northeast Japan. The cumulative moment densities of each region were calculated by dividing the cumulative moments by the area of the region. Horizontal purple and brown arrows in Figures 2.9a and 2.9b indicate the periods of SSEs in the Bungo channel (Ozawa, 2017) and off the Kii channel (Yokota & Ishikawa, 2020), respectively. Blue, red, purple, pink, orange, and black dashed vertical lines show the time of the following earthquakes: the 2003 Tokachi-Oki, the 2004 off the Kii Peninsula, the 2008 Fukushima-Oki, the 2011 Tohoku, the 2016 off southeastern Mie Prefecture, and the Tohoku earthquake aftershocks which activated VLFs off Iwate, respectively.

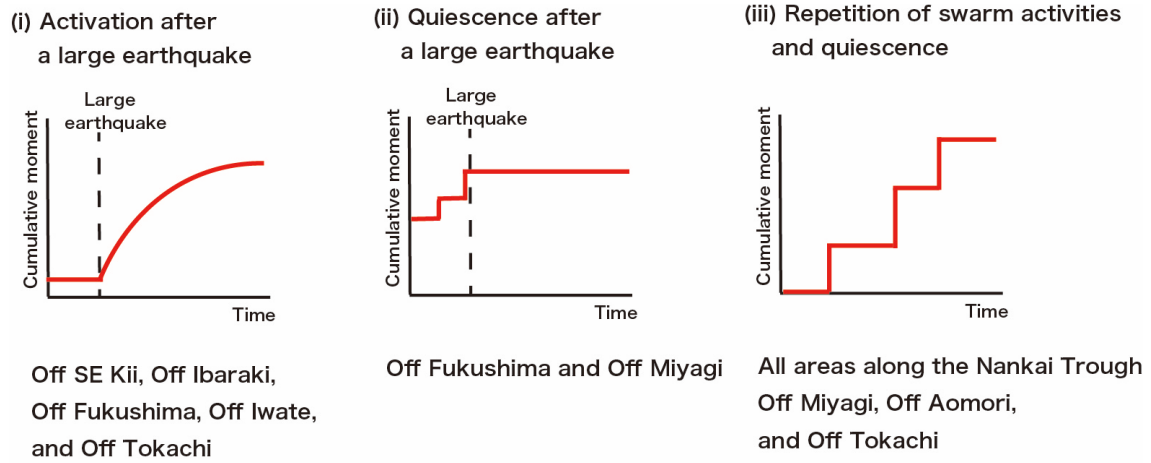


Figure 2.10. Temporal activity patterns of VLFs in Japan.

Table 2.2. Temporal activity patterns of VLFs in each area. (i), activation after a large earthquake; (ii), quiescence after a large earthquake; (iii), repetition of swarm activities and quiescence shown in Figure 2.10.

Subduction zone	Area Name	(i)	(ii)	(iii)
Nankai Trough Deep VLFs	W Shikoku			○
	E Shikoku			○
	Kii Pen.			○
	Tokai			○
Nankai Trough Shallow VLFs	Hyuga-nada			○
	Off Muroto			○
	Off S Kii			○
	Off SE Kii	○		○
Japan and Kuril Trenches VLFs	Off Ibaraki	○		
	Off Fukushima	○	○	
	Off Miyagi		○	○
	Off Iwate	○		
	Off Aomori			○
	Off Tokachi	○		○

2.4.1. Activation and quiescence after a large earthquake

The areas which showed increased VLFE activity after the 2003 Tokachi-Oki earthquake are consistent with the afterslip area of the earthquake estimated from the GNSS data (Figure 2.11; Uchida et al., 2009). Thus, it is considered that this increase is caused by the afterslip of the 2003 Tokachi-Oki earthquake, as indicated by Asano et al. (2008). The spatiotemporal consistency between afterslip distribution of the 2003 Tokachi-Oki earthquake and VLFE distribution off Tokachi suggests that VLFES can be modulated by afterslips, like by SSEs.

Significant increases in VLFE activity could be recognized off Iwate and Ibaraki (Figure 2.9c). These areas are outside the large coseismic slip area of the Tohoku earthquake identified by Iinuma et al. (2012; Figure 2.12), but inside or at the edge of the afterslip area identified by Ozawa et al. (2011; Figure 2.13a). As indicated by Matsuzawa et al. (2015), I interpret that those increases are caused by the afterslip of the Tohoku earthquake. However, VLFES off Fukushima and Miyagi were not activated after the Tohoku earthquake (Figure 2.9c). The off-Miyagi and off-Fukushima regions are within or near the largest coseismic slip area of the Tohoku earthquake (Figure 2.12). To interpret these results in more detail, I compare our results with repeating earthquakes and geodetic results.

Repeating earthquakes are considered to occur at small asperities on fault planes, which correlate with aseismic slips on the plate boundary (e.g., Nadeau & McEvilly, 1999; Uchida et al., 2003). Uchida & Matsuzawa (2013) investigated the evolution of the aseismic slips around the coseismic slip area of the Tohoku earthquake using the distribution of repeating earthquakes. They revealed that the slip rate in a large coseismic slip area of the Tohoku earthquake increased since 2008. This increase stopped entirely following the Tohoku earthquake, while clear postseismic slips appeared surrounding a large coseismic slip area (Figure 2.12). The slip rates estimated from repeating earthquakes off Iwate and off Ibaraki increased after the Tohoku earthquake, whereas those off Miyagi and off Fukushima decreased after the Tohoku earthquake. VLFE activity is, therefore, correlated with the repeating earthquake activity. Uchida and Matsuzawa (2013) as well as our results suggest that interplate aseismic slip stopped inside the large coseismic slip area after the Tohoku earthquake. In addition, there is an area within the large coseismic slip area where only a few VLFES and repeating earthquakes occurred both before and after the Tohoku earthquake (Figure 2.12). In this

area, I infer that the accumulated stress was released almost completely by the 2011 Tohoku earthquake, as suggested in previous studies (e.g., Hasegawa et al., 2011; Kato & Igarashi, 2012).

The off-Iwate, off-Miyagi, off-Fukushima, and off-Ibaraki regions are inside or at the edge of the afterslip area that was geodetically estimated by Ozawa et al. (2011; Figure 2.13a). Nevertheless, VLFs were activated only off Iwate and off Ibaraki after the Tohoku earthquake. According to Uchida and Matsuzawa (2013) and my results, the afterslip of the Tohoku earthquake occurred on a smaller scale outside a large coseismic slip area. The afterslip estimated by Inuma et al. (2016), in which onshore and seafloor geodetic data were used, is distributed outside the coseismic slip area of the Tohoku earthquake but does not contain the off-Iwate region unlike my result (Figure 2.13b). The possible cause of this difference is that seafloor geodetic data limited off Miyagi. VLFE and repeating earthquake activity may be useful to obtain the plate interface slip distribution at a higher spatial resolution.

Off Fukushima, a remarkable increase in VLFE activity started half a day after the 2008 Fukushima-Okai earthquake and lasted for two weeks (Figure 2.9c), probably caused by the afterslip of the 2008 Fukushima-Okai earthquake (Mw 6.9; The epicenter is shown in Figure 2.6b and 2.13). Off Iwate, the cumulative number of VLFs increased rapidly in the middle of 2012 and in early 2015 (Figure 2.9c). These increases were preceded by two aftershocks of the Tohoku earthquake with Mw 6.2 and 6.7 (Epicenters are shown in Figure 2.6b and 2.13). Along the Nankai Trough, the VLFE activity off the southeastern Kii in 2004 can be activated by the afterslip of an intraslab earthquake, the 2004 off the Kii Peninsula earthquake (Mw 7.4; the epicenter is shown in Figure 2.6a; Watanabe et al., 2018). An interplate earthquake, the 2016 off southeastern Mie Prefecture earthquake (Mw 6.0; Epicenters are shown in Figure 2.6a; Wallace et al., 2016) can also promote VLFE activity off the southeastern Kii approximately one week after the mainshock. These increases suggest that VLFs are sometimes activated by afterslips of interplate and intraslab earthquakes with Mw of 6–7. It should be noted, however, that VLFs are not always activated by an earthquake whose Mw is > 6. It is, therefore, possible that sizes of afterslips of regular earthquakes vary even though Mw of the earthquakes are comparable.

VLFE activities off Fukushima and Miyagi are composed of two activity patterns (Figure 2.10). Before the Tohoku earthquake, VLFs off Fukushima increased

after the 2008 Fukushima-Oki earthquake (pattern (i)) and VLFE activity off Miyagi represents episodic change (pattern (iii)). After the Tohoku earthquake, VLFEs off Fukushima and Miyagi decreased (pattern (ii)). In these two regions, the VLFE activity pattern was changed by the 2011 Tohoku earthquake. Shallow VLFE activity shows episodic change along the Nankai Trough last ~20 years. However, if a megathrust earthquake occurs along the Nankai Trough in the future, the shallow VLFE activity pattern may change. The regions off Cape Muroto and off the Kii Peninsula are near the strongly coupled areas; therefore, shallow VLFEs may decrease after the megathrust earthquake.

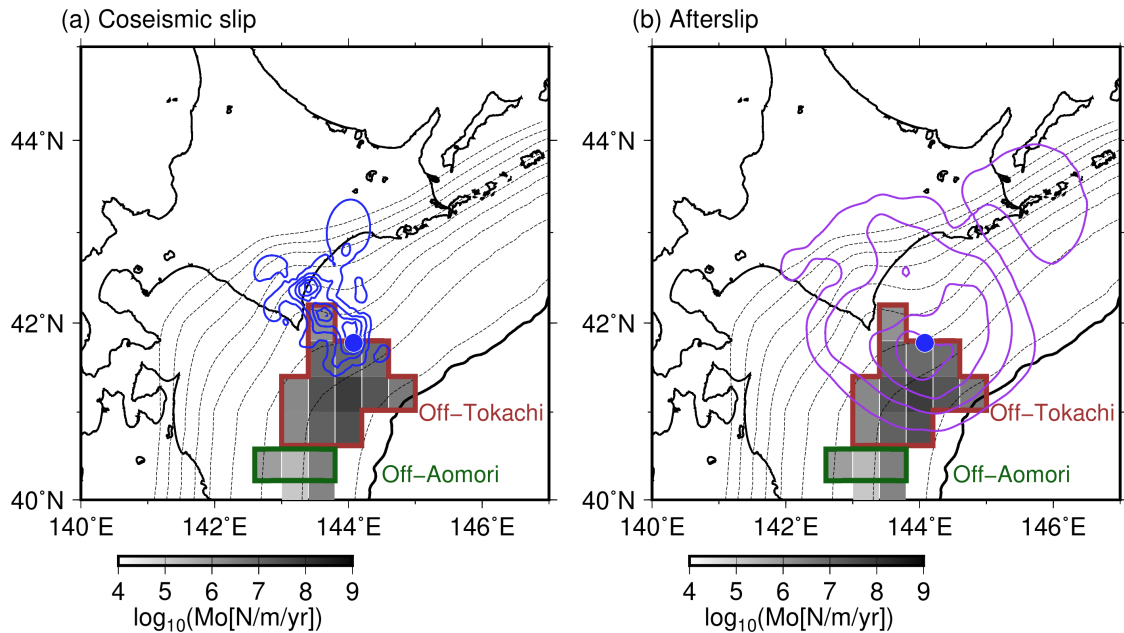


Figure 2.11. Comparison between the spatial distribution of VLFEs and (a) the coseismic slip and (b) the afterslip of the Tokachi-Oki earthquake, respectively. Blue contours in Figure 2.11a show the coseismic slip distribution of the Tokachi-Oki earthquake with a 1-m interval (Yagi, 2004). Blue circle represents the epicenter of the 2003 Tokachi-Oki earthquake. The purple contours in Figure 2.11b show the afterslip distribution of the Tokachi-Oki earthquake estimated from the GNSS data with a 0.2-m interval (Uchida et al., 2009). The analysis period of the afterslip is from September 26, 2003 to November 29, 2004. Polygons and gray scales are the same as displayed in Figure 2.6. Dotted contours and black lines are the same as displayed in Figure 1.3.

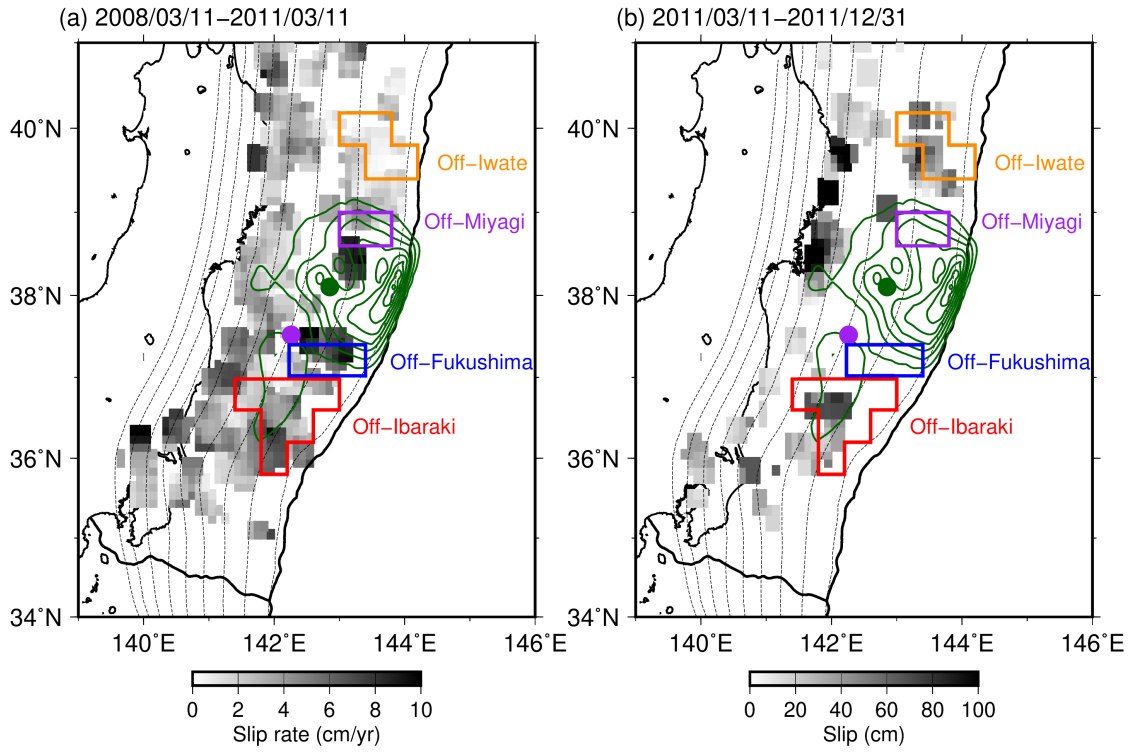


Figure 2.12. Comparison between the spatial distribution of VLFs and slip distributions off the Pacific coast of Tohoku estimated from repeating earthquakes: (a) from March 11, 2008 to March 11, 2011; and (b) from March 11 to December 31, 2011 (Uchida & Matsuzawa, 2013). Green contours show the coseismic slip distribution of the Tohoku earthquake with a 10-m interval (Inuma et al., 2012). Purple and green circles are the same as displayed in Figure 2.6b. Colored polygons are the same as displayed in Figure 2.6. Black lines and dotted contours are the same as displayed in Figure 1.3.

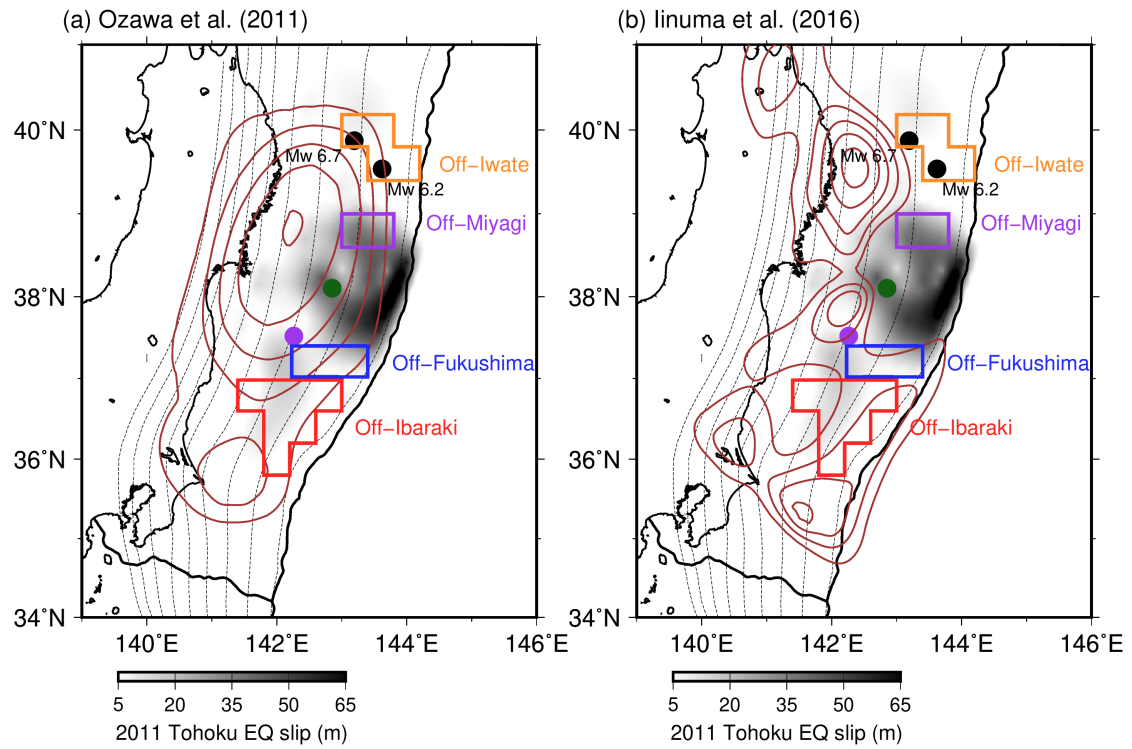


Figure 2.13. Comparison between the spatial distribution of VLFs and the geodetically estimated afterslip distribution of the Tohoku earthquake by (a) Ozawa et al. (2011) and (b) Inuma et al. (2016). The analysis period of the afterslip is (a) from March 12 to March 25, 2011 and (b) from April 23 to December 10, 2011. Brown contours show the afterslip distribution of the 2011 Tohoku earthquake drawn with a 0.2-m interval. Black circles are the Tohoku earthquake aftershocks that activated VLFs off Iwate. Purple and green circles are same as displayed in Figure 2.6b. Polygons are the same as displayed in Figure 2.6. Shadings, black lines, and dotted contours are the same as displayed in Figure 1.3.

2.4.2. Swarm activities of VLFs

To quantify the swarm activities of VLFs around Japan, I estimated the swarm ratio of VLF activity in each area and intervals of two successive swarms based on Kurihara & Obara (2021).

In each area, the expected interevent time was calculated by dividing the analysis period by the total number of VLFs. This value indicates the average interevent time from the former VLF. When 10 or more VLFs occur with shorter interevent times from the former VLFs, these 10 or more VLFs are considered as a swarm (Figure 2.14). I defined the swarm ratio in each area as the ratio of the number of VLFs which belong to a swarm (N^{Swarms}) to the number of total VLFs (N^{Total}) in each area;

$$Swarm\ ratio = \frac{N^{Swarms}}{N^{Total}}. \quad (2.4)$$

If the swarm ratio is large (swarm ratio > 0.6), the VLF activity is episodic, i.e., repetitions of swarm activities of many VLFs and quiet periods. If the swarm ratio is small, the VLF activity is continuous, or repetitions of swarm activities of a few VLFs and short quiet periods. After that, I evaluated the intervals of swarms with longer than 1 month at each area.

Generally, swarm ratios of shallow VLF activity are larger than those of deep VLFs (Figure 2.15). Especially, swarm ratios are very large (swarm ratio > 0.9) off Tokachi, off the southeastern Kii, and in Hyuga-nada. In these areas, almost all VLFs occur in periods of swarms. VLF activity is considered as a proxy of SSEs (e.g., Ito et al., 2007; Nakano et al., 2018); therefore, a VLF swarm can be a candidate of possible SSE. The smaller swarm ratios of deep VLF activities may indicate the occurrence of smaller SSEs more frequently in the deeper part than in the shallower part.

The intervals of swarms in shallow VLFs are very various (Figures 2.16 and 2.17). In Hyuga-nada, the median interval of swarms is ~8 months. On the other hand, intervals of swarms off the southeastern Kii, off the southern Kii, and off Cape Muroto are often longer than 1 year and reached ~7 years for the longest case. In deep VLF activity, the swarm ratio is relatively large in western Shikoku. The median interval of swarms is ~6 months, which is similar to the recurrence interval of ETS reported in previous studies (e.g., Obara et al., 2004; Sekine et al., 2010).

Liu & Rice (2005) simulated aseismic slips based on the rate and state friction law and suggested that the recurrence intervals of aseismic slips decrease with the

reduction of effective normal stress on the plate boundary. In addition, Audet & Bürgmann (2014) investigated the relationship between the recurrence intervals of slow earthquake (ETS) activities and the ratio of P -wave to S -wave velocities (V_P/V_S ratio) in the overriding plate in some subduction zones. They demonstrated a positive correlation between the recurrence interval of ETS activities and the V_P/V_S ratio. The small V_P/V_S ratio in the overriding plate indicates that the fluid does not infiltrate the overriding plate. Consequently, the fluid overpressure is facilitated on the plate boundary. Fluid overpressure causes the low effective normal stress; therefore, the recurrence intervals of ETS activities become shorter in the area with small V_P/V_S in the overriding plate.

Based on these previous studies, the variations in intervals of shallow VLFE swarms may reflect the spatial heterogeneities of the effective normal stress on the plate boundary. Along the Nankai Trough, the low V_S anomaly around the plate boundary is larger off the southeastern Kii and off Cape Muroto than off the southern Kii (e.g., Tonegawa et al., 2017; 2021); therefore, the effective normal stress on the plate boundary is expected to be lower off the southeastern Kii and off Cape Muroto than off the southern Kii. Larger median interval of VLFE swarms off the southern Kii than off the southeastern Kii and off Cape Muroto (Figure 2.17) is consistent with the interpretation that the variations in intervals of VLFE swarms may reflect the spatial heterogeneities of the effective normal stress.

Based on the differences in median intervals of swarms, the effective normal stress on the plate boundary may be higher off the southeastern Kii, off the southern Kii, and off Cape Muroto than in Hyuga-nada. The swarm ratios in the deep VLFE activities are generally smaller than those in the shallow VLFE activities; therefore, the effective normal stress on the plate boundary may be lower in the deeper part than in the shallower part. The more ductile condition and more fluid derived from basalt dehydration in the deeper part than in the shallower part may be related to the difference in the effective normal stress. In addition, the difference in other frictional parameters, such as a - b in the rate- and state-dependent friction law, may be a factor of the variation in swarm ratios.

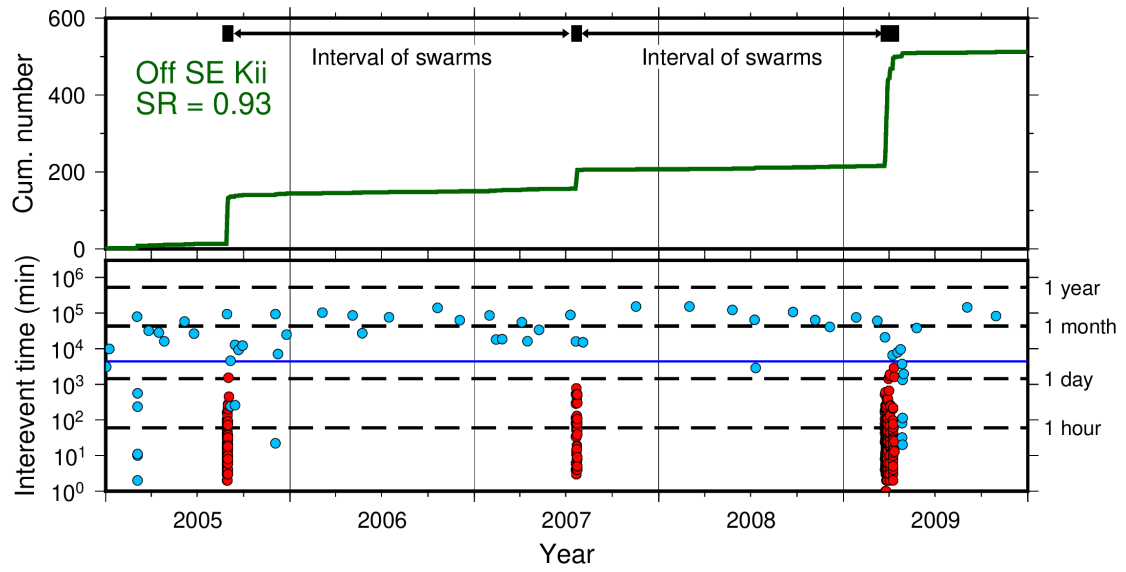
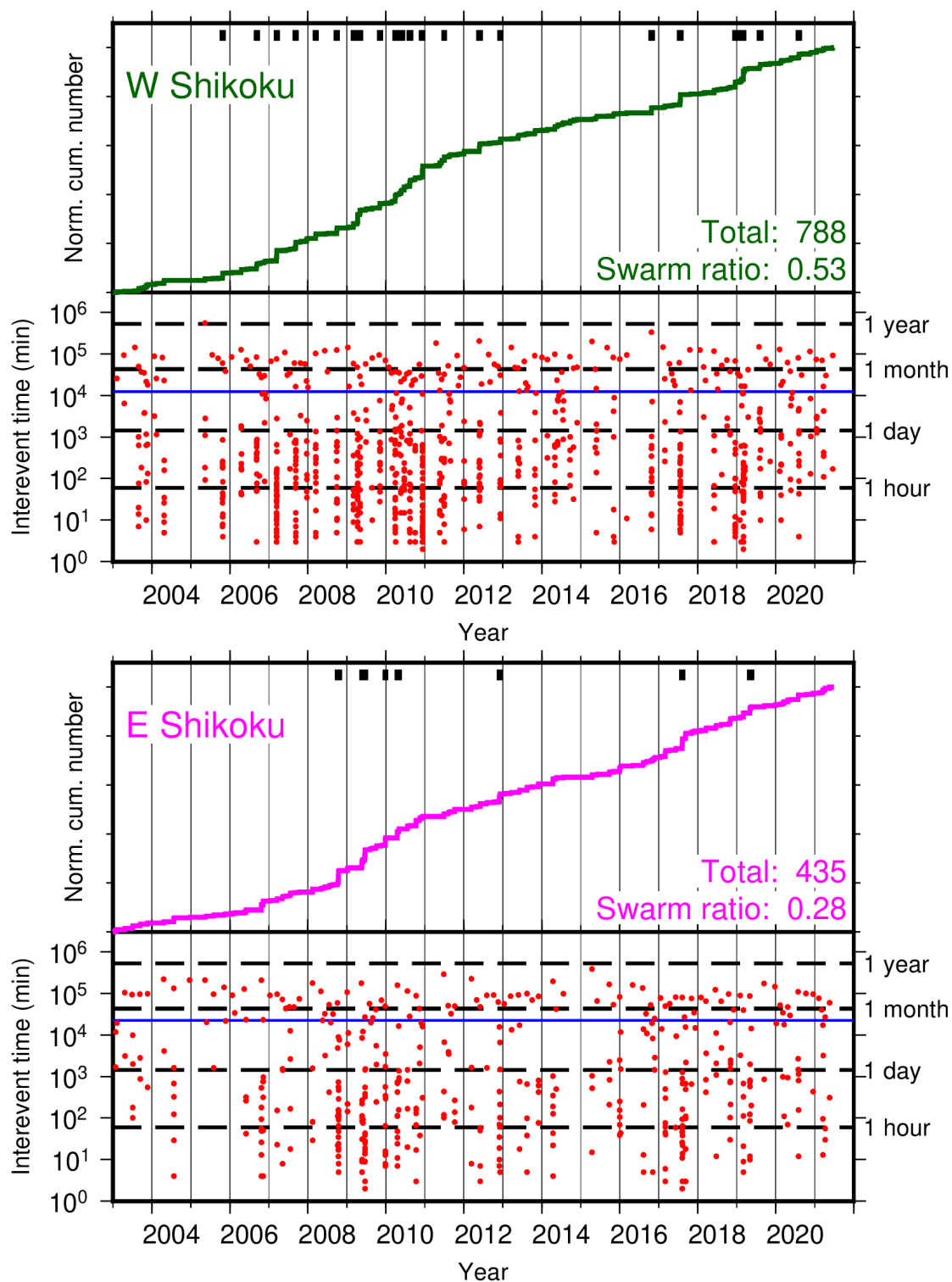
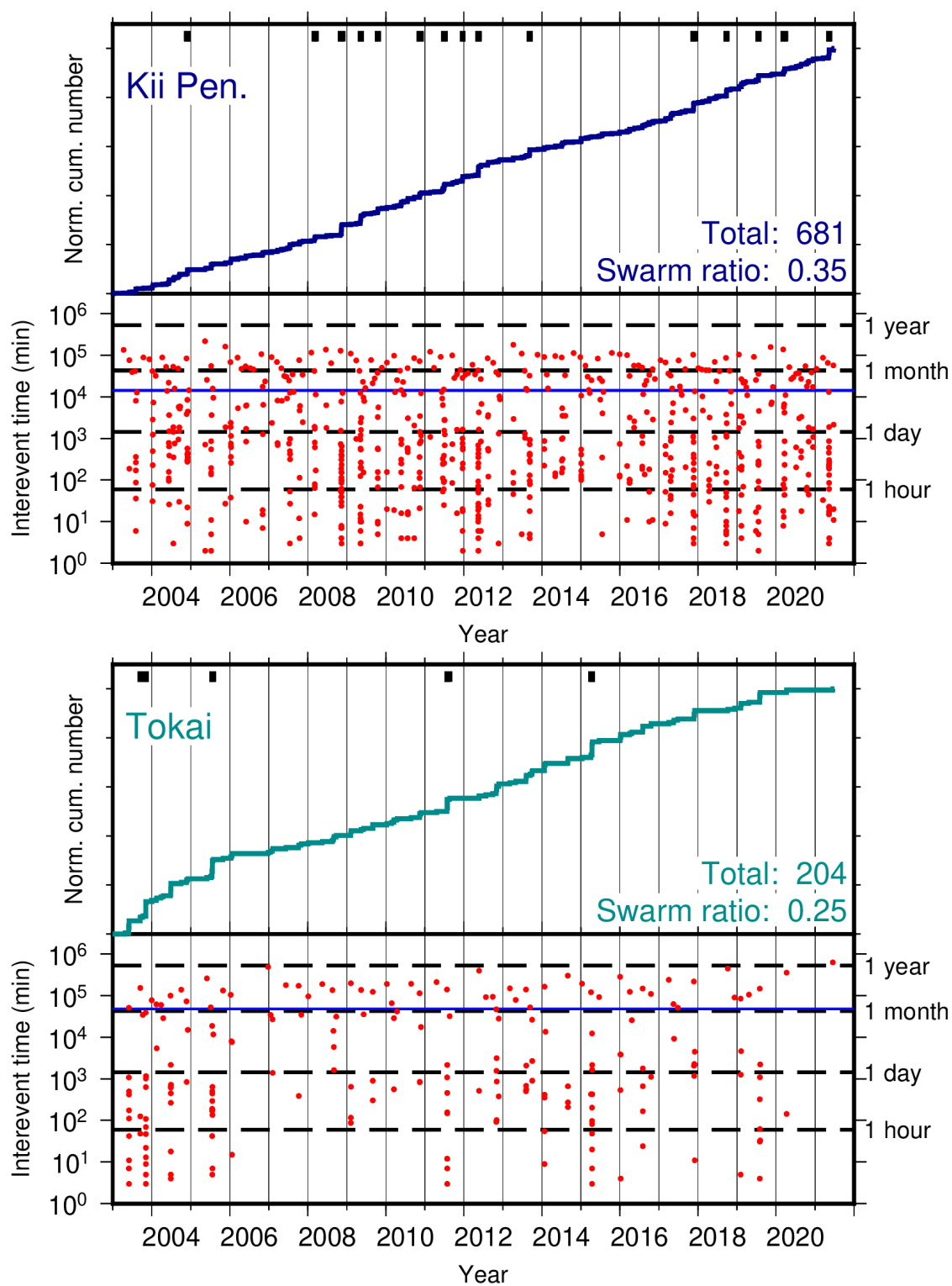


Figure 2.14. Example of a cumulative number of VLFs and temporal variation in interevent time from the former VLFE from 2005 to 2009 in Off SE Kii. Red and light blue circles show VLFs in a swarm and those not in a swarm, respectively. Blue line indicates the expected interevent time in Off southeastern Kii.

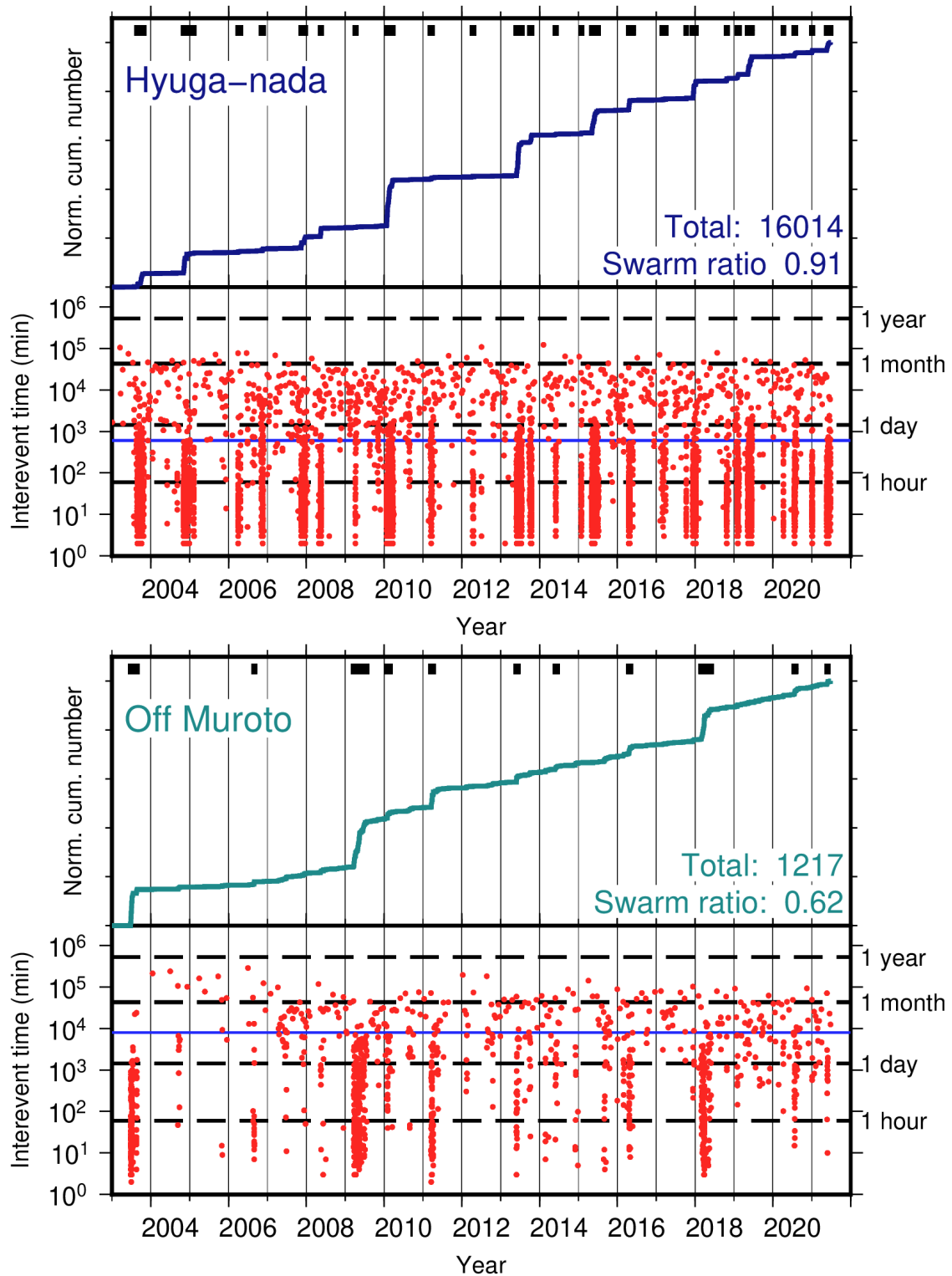
(a) Deep VLFEs along the Nankai Trough



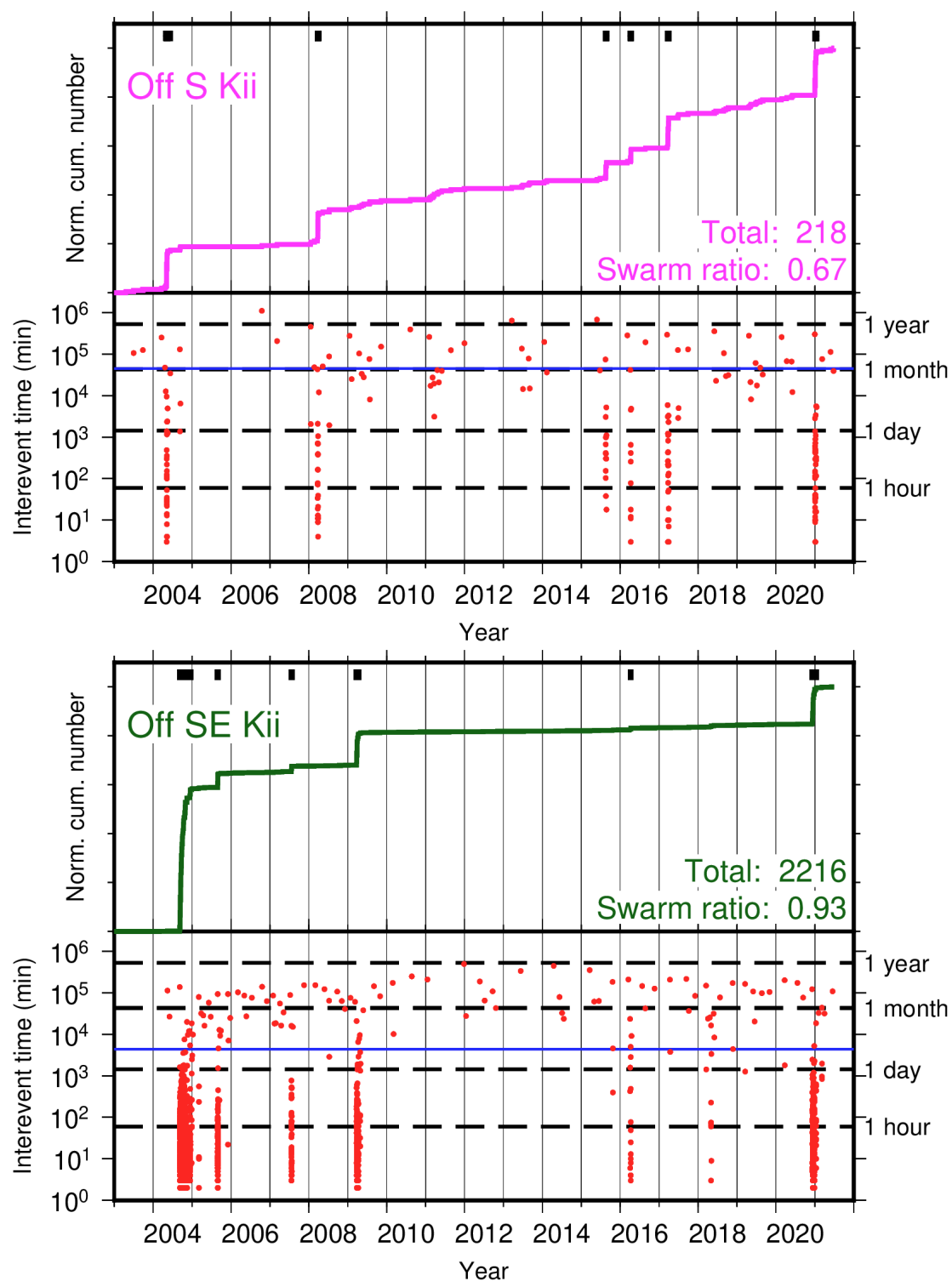
(a) continued



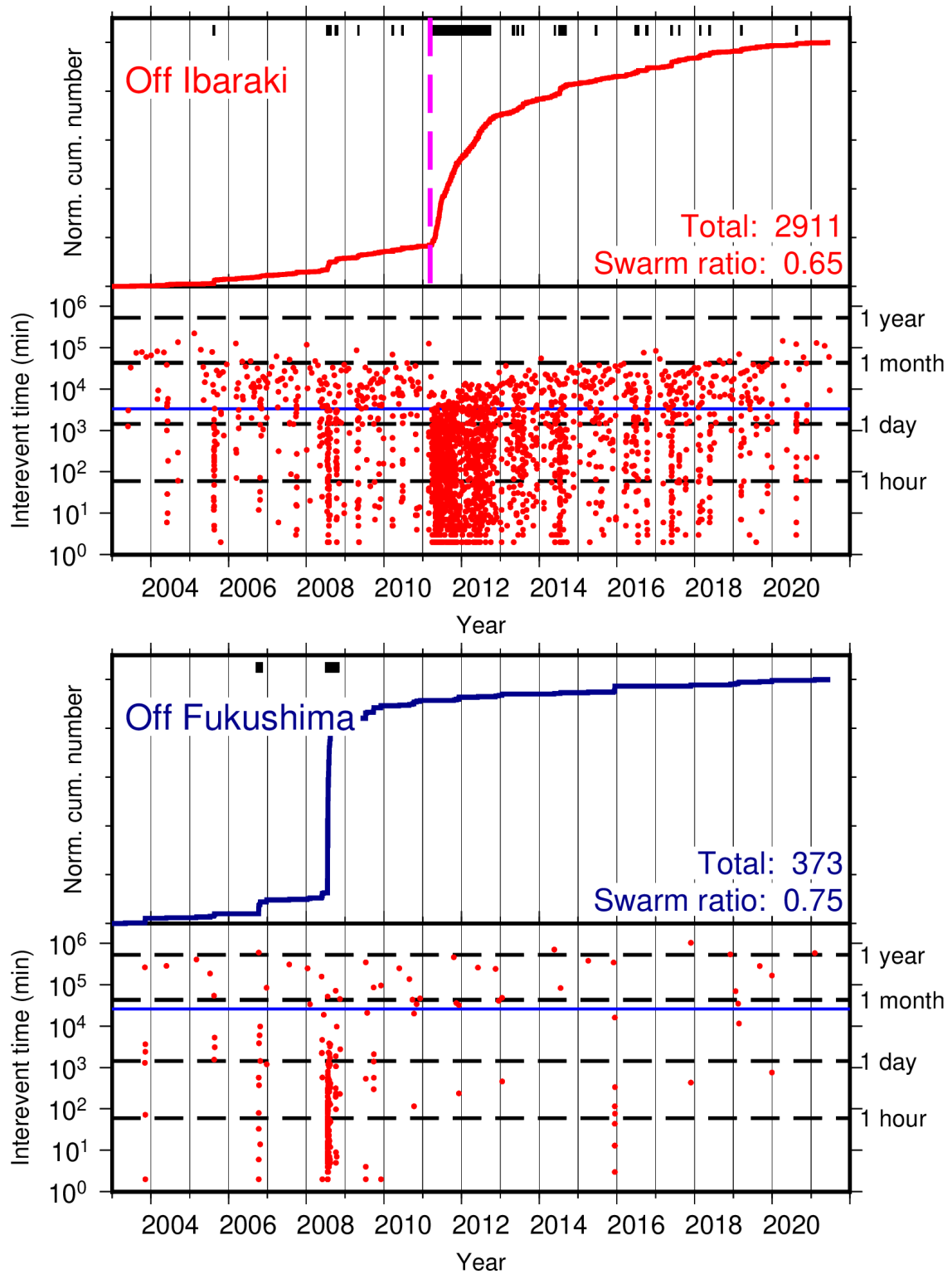
(b) Shallow VLFES along the Nankai Trough



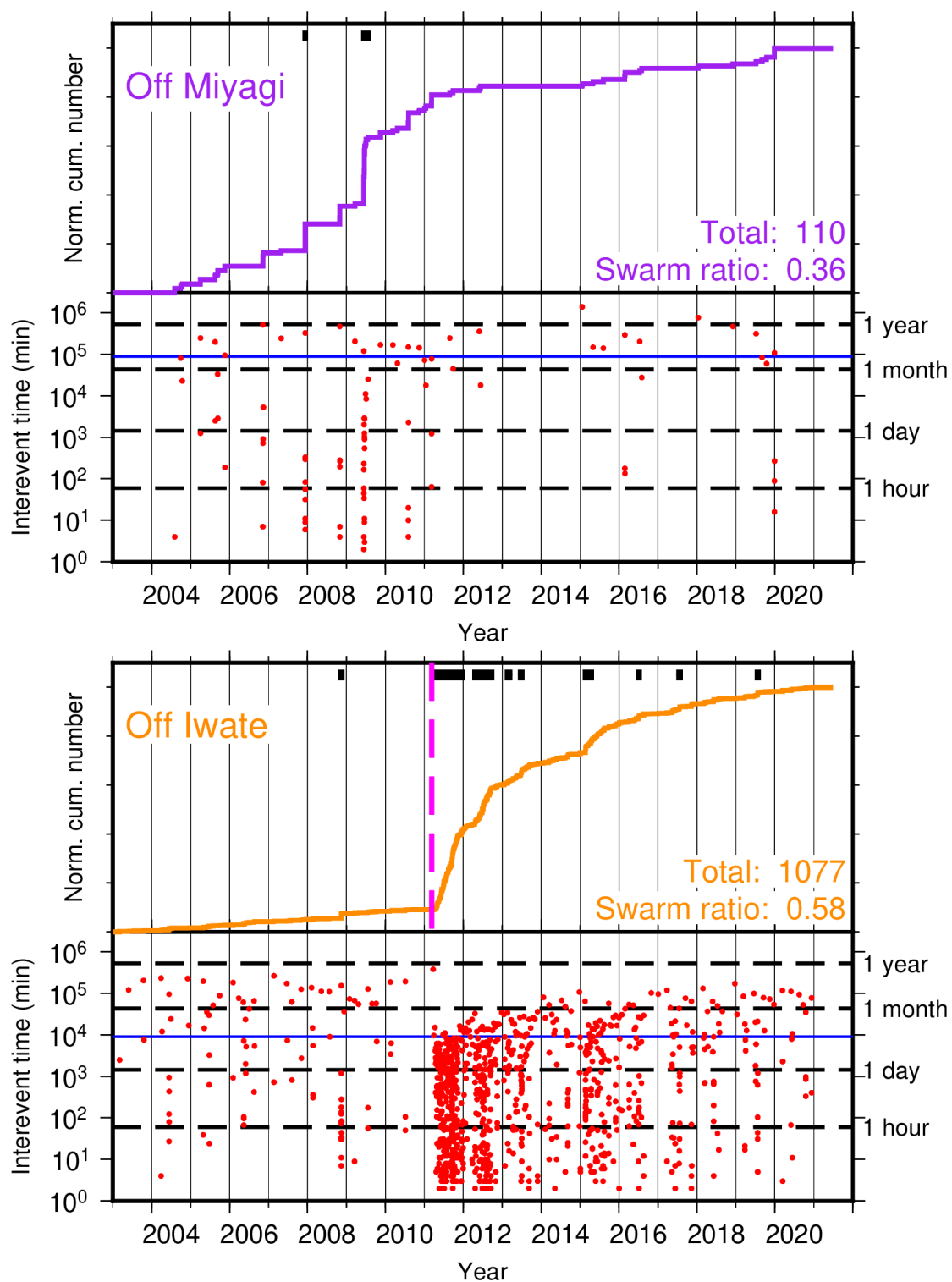
(b) continued



(c) VLFEs along the Japan and Kuril Trenches



(c) continued



(c) continued

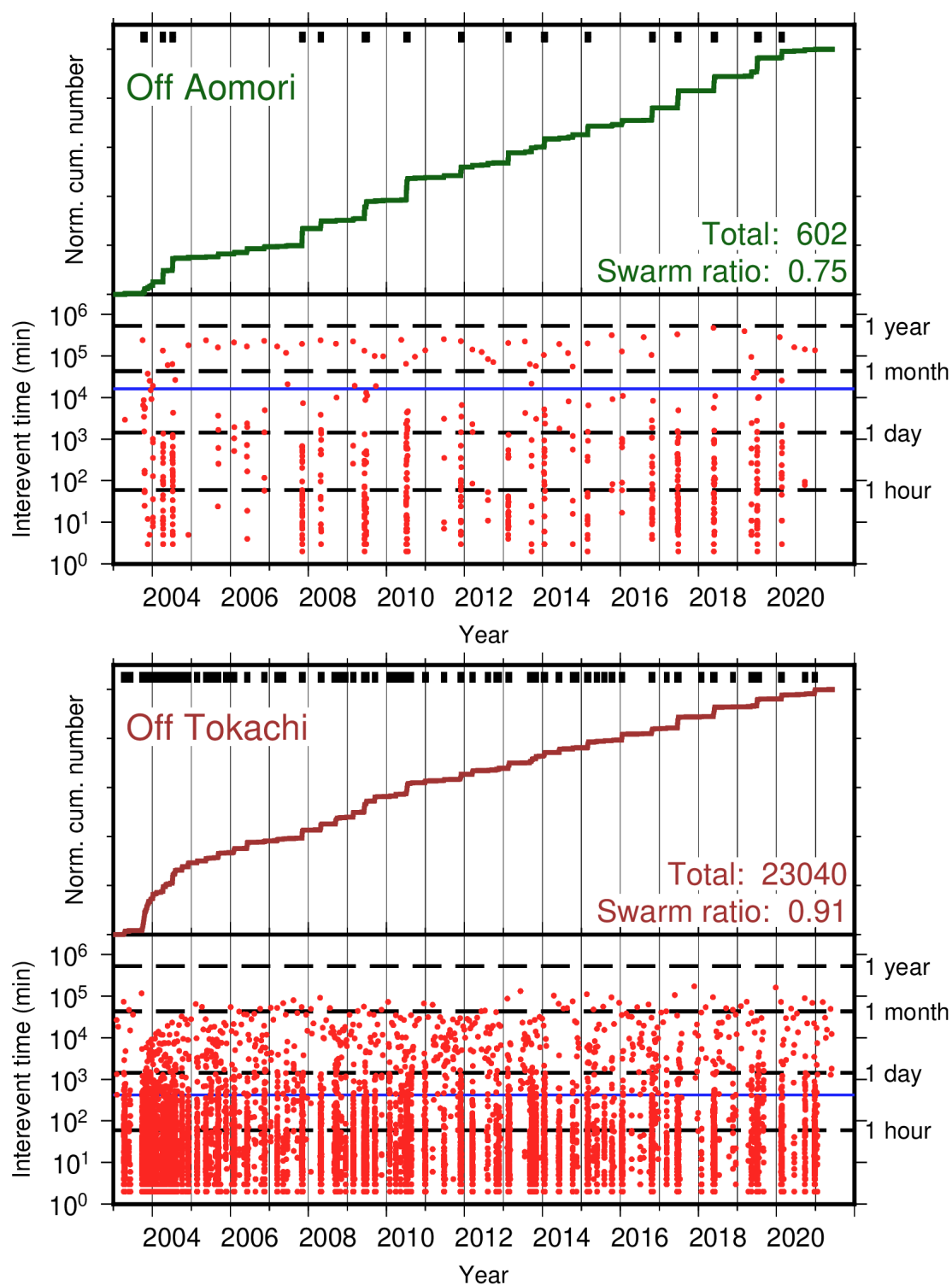
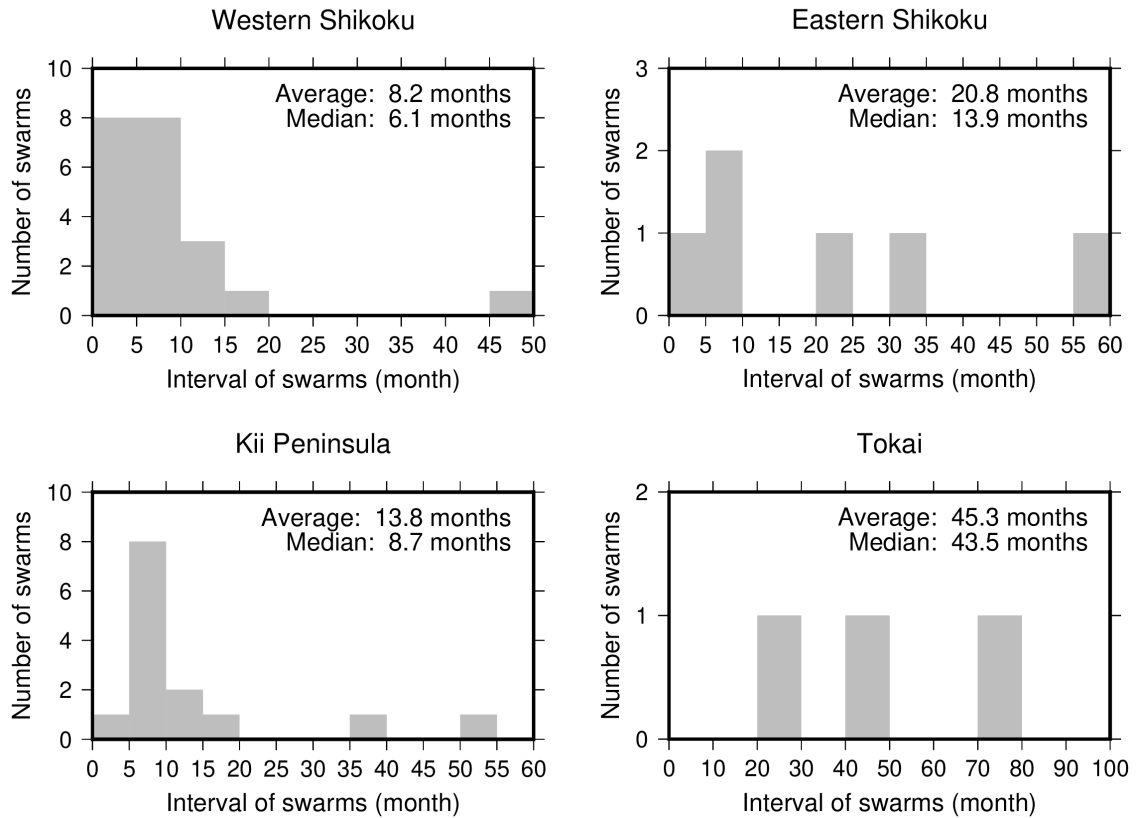
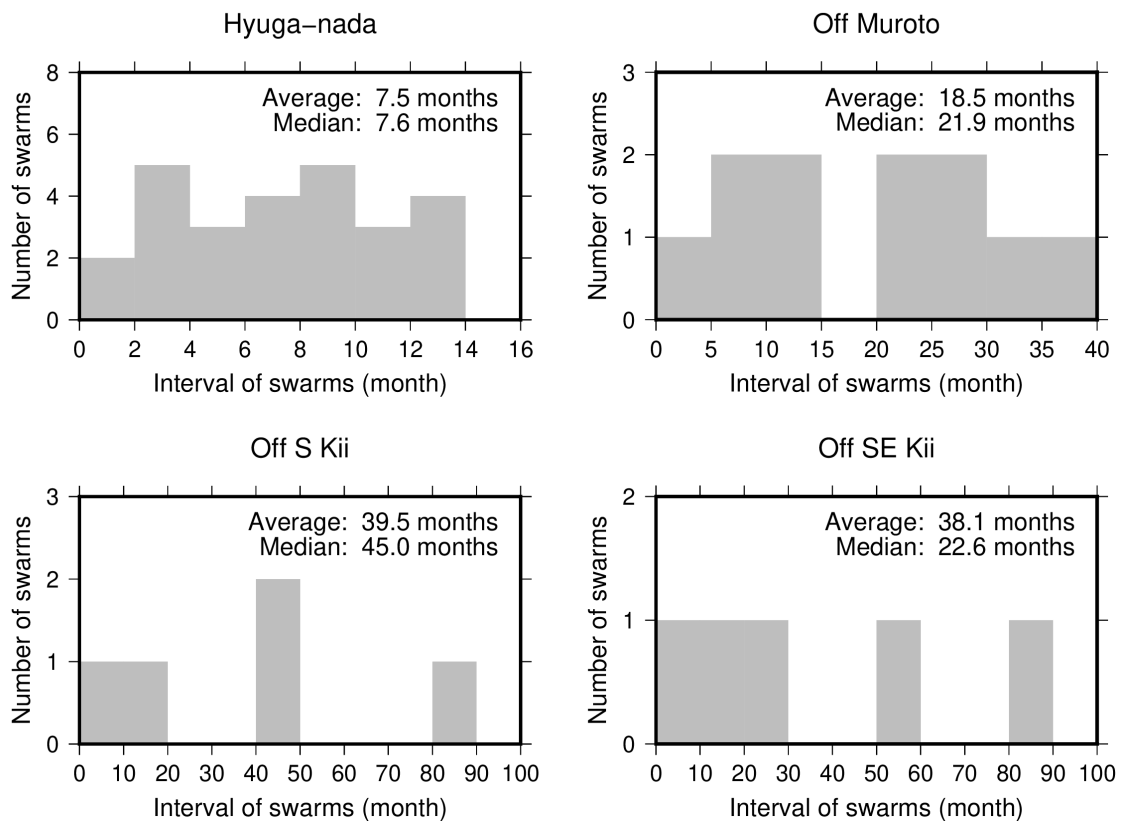


Figure 2.15. Cumulative number of VLFs and temporal variation in interevent time from the former VLFE in each area. Black bars show the periods of swarms. Blue line indicates the expected interevent time in each area.

(a) Deep VLFs in southwest Japan



(b) Shallow VLFs in southwest Japan



(c) VLFs along the Japan and Kuril Trenches

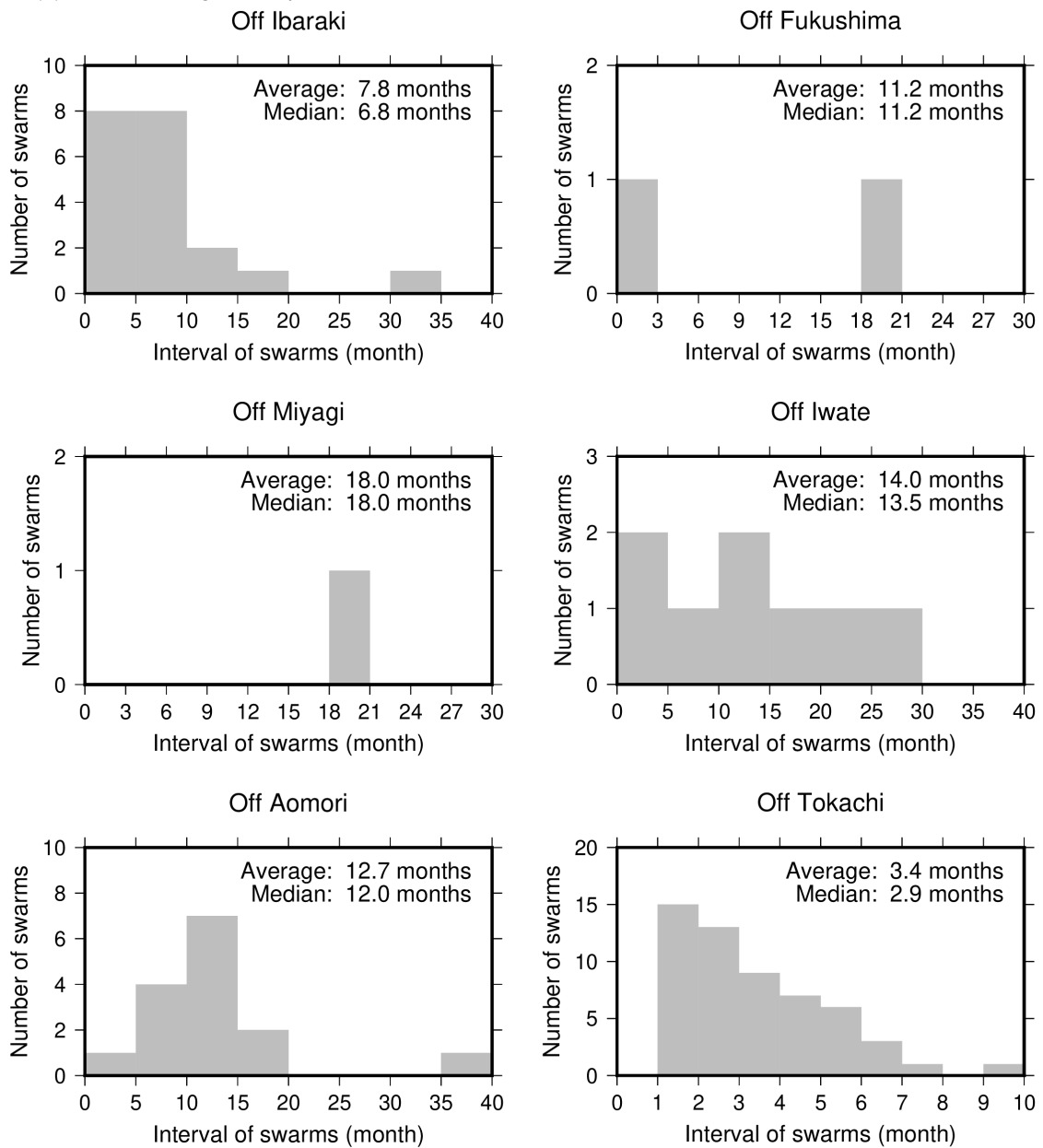


Figure 2.16. Histogram of intervals of successive swarms in each area.

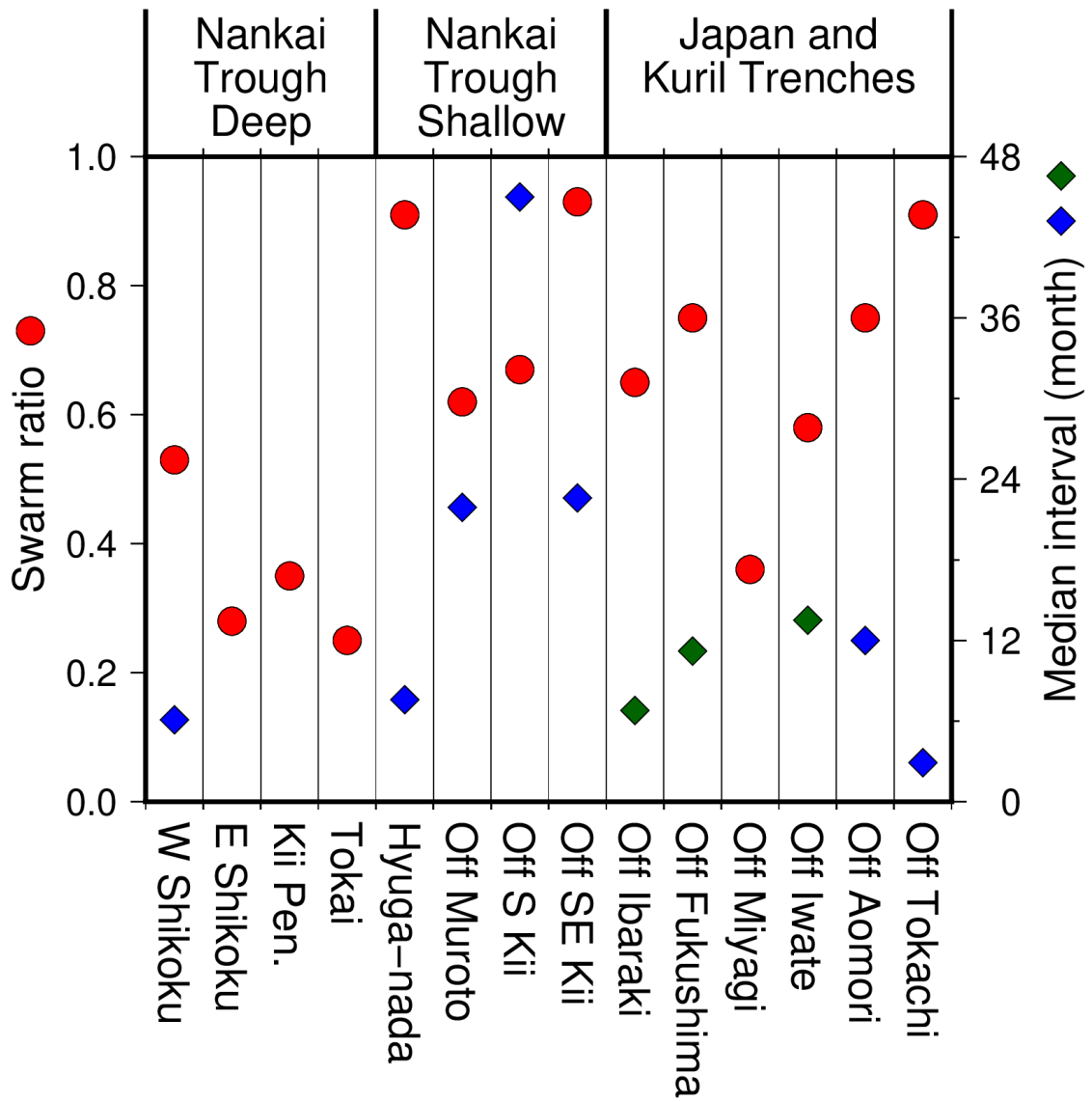


Figure 2.17. Temporal characteristics of VLFE activities. Red circles show the SRs in each area. Diamonds represent the medians of intervals of swarms where the SR is larger than 0.5. Most of VLFEs in the area with blue and green diamonds are in episodic swarm activities and after a large earthquake, respectively.

2.5. Summary of this chapter

In this chapter, to clarify the spatiotemporal characteristics of slow earthquake activity around Japan, I detected VLFs by the matched-filter technique and quantified spatiotemporal variations in VLFE activity around Japan by introducing moment-density release rate and the swarm ratio. The spatial heterogeneity in the moment-density release rate of VLFs (VLFE activity rate) is stronger in the shallower part than in the deeper part (Figure 2.18). Especially, VLFs are the most active in Hyuga-nada, the shallower part along the Nankai Trough. There is a negative correlation between shallow VLFE activity and interplate coupling in Nankai. This suggests that shallow VLFs are less active in the area near the strongly coupled areas. If the negative correlation is assumed in Hyuga-nada, it is suggested that the interplate coupling in Hyuga-nada is weak. Furthermore, VLFs tend to be active in regions with low seismic velocity anomalies, which can be considered as high pore fluid pressure condition. Thus, the fluid can be a potential for the activation of VLFs.

Temporal variations in VLFE activities are categorized into three patterns: activation after a large earthquake, quiescence after a large earthquake, and repetition of swarm activities and quiescence. Regarding the association with large earthquakes, VLFs outside a large coseismic slip area of the 2011 Tohoku earthquake increased rapidly, probably due to the afterslip of the Tohoku earthquake. In addition, VLFE activity often increases after large earthquakes with M_w of 6–8. These results suggest that VLFE activity reflects spatiotemporal evolution of the afterslip of large earthquakes. On the other hand, the VLFE activity was low after the Tohoku earthquake within the large coseismic slip area of the Tohoku earthquake. The relationship between VLFE activity and interplate coupling or afterslips of large earthquakes indicates that VLFE activity can be an indicator of stress state on the plate boundary.

To quantify the swarm activities of VLFs around Japan, I estimated swarm ratios of VLFE activity in each area and intervals of two successive swarms. Generally, swarm ratios of shallow VLFE activity are generally larger than those of deep VLFs; therefore, smaller SSEs occur more frequently in the deeper part than in the shallower part. The intervals of swarms in shallow VLFs are very various from 8 months (Hyuga-nada) to 2–4 years (off the southeastern Kii, off the southern Kii, and off Cape Muroto). Based on simulation or structural previous studies, the variations in intervals of shallow

VLFE swarms may reflect the spatial heterogeneities of the effective normal stress on the plate boundary.

In summary, the spatiotemporal variation in VLFE activity is larger in the shallower part than in the deeper part. This suggests that the spatiotemporal heterogeneity of frictional property on the plate boundary is large in the shallow part. In addition, Hyuga-nada is a characteristic region from the viewpoint of large moment-density release rate. To reveal the factors which control the variations in slow earthquake activity in more detail, I will investigate shallow VLFE activity in Hyuga-nada, where the moment-density release rate is the highest, at a high resolution.

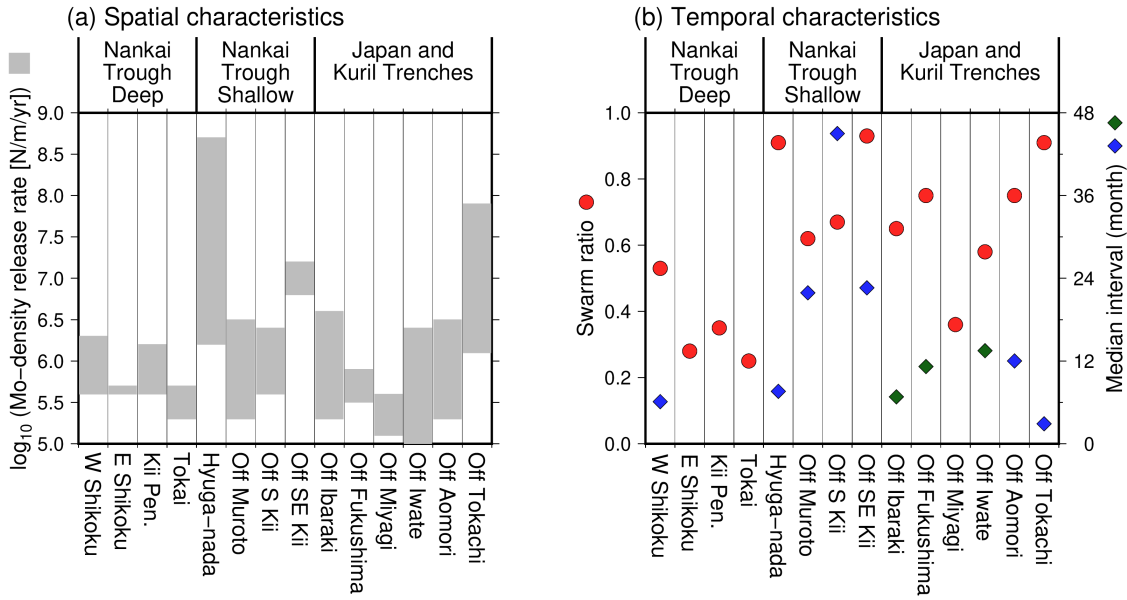


Figure 2.18. (a) Spatial and (b) temporal characteristics of VLFE activities. (a) The range of the moment-density release rate of VLFEs around Japan. (b) Same as Figure 2.17.

3. Spatial characteristics of slow earthquakes in Hyuga-nada on a local scale

3.1. Introduction

3.1.1. Tectonic setting in Hyuga-nada

As mentioned in Chapter 2, Hyuga-nada is the most active shallow slow earthquake region around Japan. In addition, the recurrence interval of VLFE swarms is shorter than other shallow slow earthquake regions along the Nankai Trough; therefore, the effective normal stress is inferred to be lower. However, the characteristics of slow earthquake activity have not been clarified on a local scale. The tectonic regime in Hyuga-nada is very characteristic; the Kyushu-Palau Ridge is subducted, and the trench axis bends around the subduction of the ridge (Figure 3.1). The age and temperature of the subducting plate changes at the ridge; the plate is older and colder from the south of the ridge (Yoshioka, 2007).

Yamashita et al. (2015) and Yamashita et al. (2021) detected shallow tremors and reported their migrations in Hyuga-nada utilizing temporal ocean bottom seismometers (OBSs) in 2013 and 2015, respectively (Figures 3.1b and c). In 2013, tremors migrated twice from 30.3° N to 31.7° N. The first and second migrations stopped exactly in, and at the edge of the subducted Kyushu-Palau Ridge, respectively (Yamashita et al., 2015). In 2015, tremors migrated from west to east in the north of 31° N and extended near the trench axis (Yamashita et al., 2021). Yamashita et al. (2015) suggested a spatiotemporal correlation between tremor and VLFE activity. Asano et al. (2015) reported the migration of shallow VLFs in Hyuga-nada that occurred in 2010 (Figure 3.1a). The spatial distribution of VLFs in 2010 contained both tremor distributions in 2013 and in 2015. VLFs first migrated from 30.5° N to 31.5° N and changed the direction of the migration at the subducted Kyushu-Palau Ridge. They migrated from west to east, north of 31° N and further extended near the trench axis. Then, VLFs returned from east to west, north of 31° N. Tonegawa et al. (2020) suggested that the depths of shallow VLFs near the subducted Kyushu-Palau Ridge are approximately 5 km different from the surrounding area.

Despite such shallow slow earthquake activity, no historical megathrust earthquakes with $M_w \geq 8$ exists, in contrast to other regions along the Nankai Trough and along the Japan Trench. In Hyuga-nada, repeating earthquakes, representing quasi-static slips on the plate boundary (e.g., Nadeau & McEvilly, 1999; Uchida et al., 2003), further

occur in the downdip of shallow slow earthquakes (e.g., Igarashi, 2020; Yamashita et al., 2012). The large moment-density release rate revealed by Chapter 2 and the occurrence of repeating earthquakes in Hyuga-nada suggest weak interplate coupling in this region. Such characteristic tectonic conditions in Hyuga-nada may have affected the slow earthquake activity; however, the factors leading to the difference in slow earthquake activity in Hyuga-nada and other shallow slow earthquake regions are unclear.

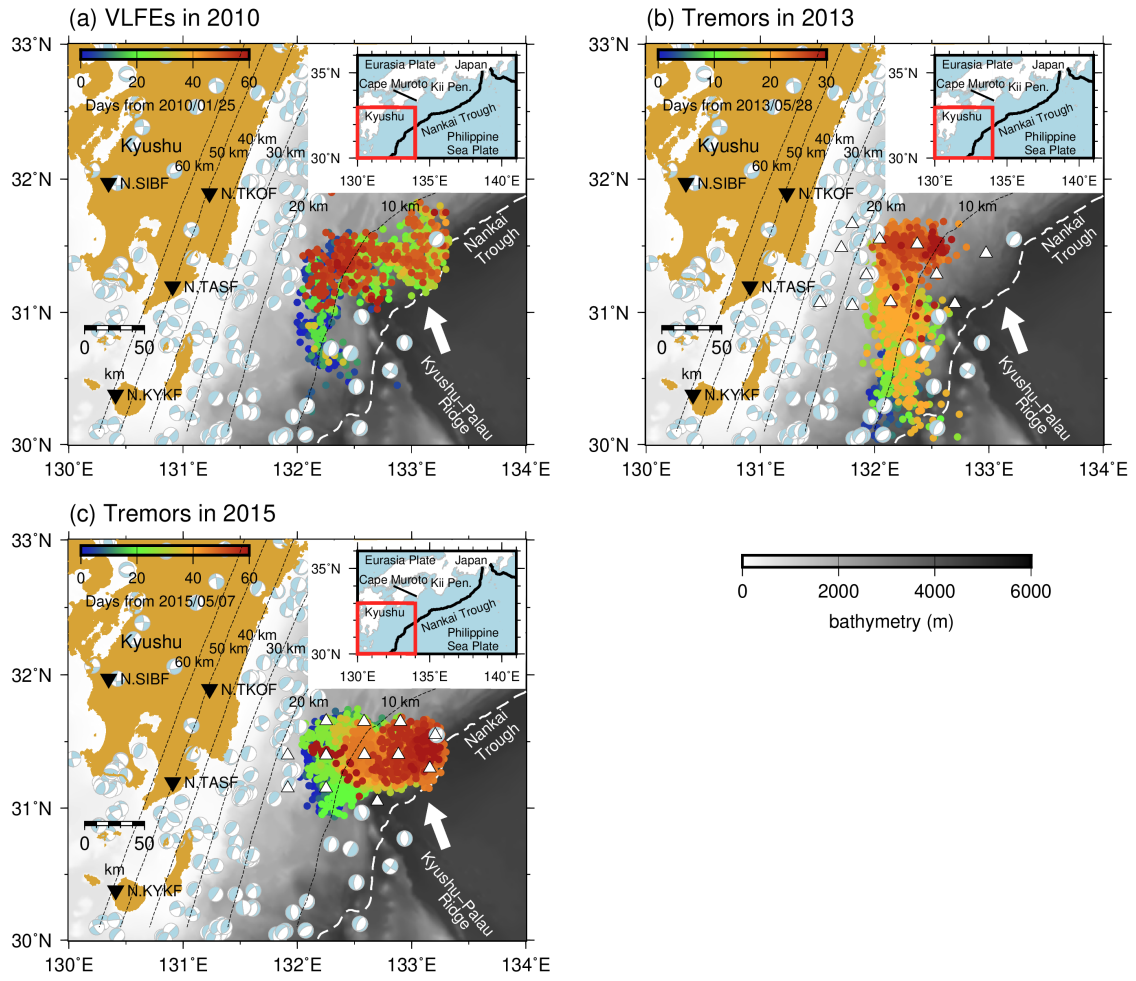


Figure 3.1. Map representing Hyuga-nada. Colored dots are epicenters of (a) shallow VLFEs in 2010 detected by Asano et al. (2015), (b) shallow tremors in 2013 detected by Yamashita et al. (2015), and (c) shallow tremors in 2015 detected by Yamashita et al. (2021). The colors of dots correspond to days from the first activity for each tremor. White triangles represent the locations of the OBSs utilized in the shallow tremor analysis. Inverted triangles exhibit the locations of the F-net stations utilized in the shallow VLFE analysis. Light blue beach balls show the focal mechanisms of regular earthquakes with $M_w > 3.5$ from 2010 to 2015 listed in F-net website (<https://www.fnet.bosai.go.jp/top.php?LANG=en>). White arrows indicate the direction of the motion of the Philippine Sea Plate relative to the Eurasia Plate (NUVEL-1A; (DeMets et al., 1994)). White dashed lines represent the trench axis. Background gray scale denotes the bathymetry (ETOPO1; Amante and Eakins, 2009). Dashed contours indicate the isodepth at the top of the Philippine Sea plate in intervals of 10 km (JIVSM; Koketsu et al., 2012). Black lines in the inset represent the boundaries between the plates.

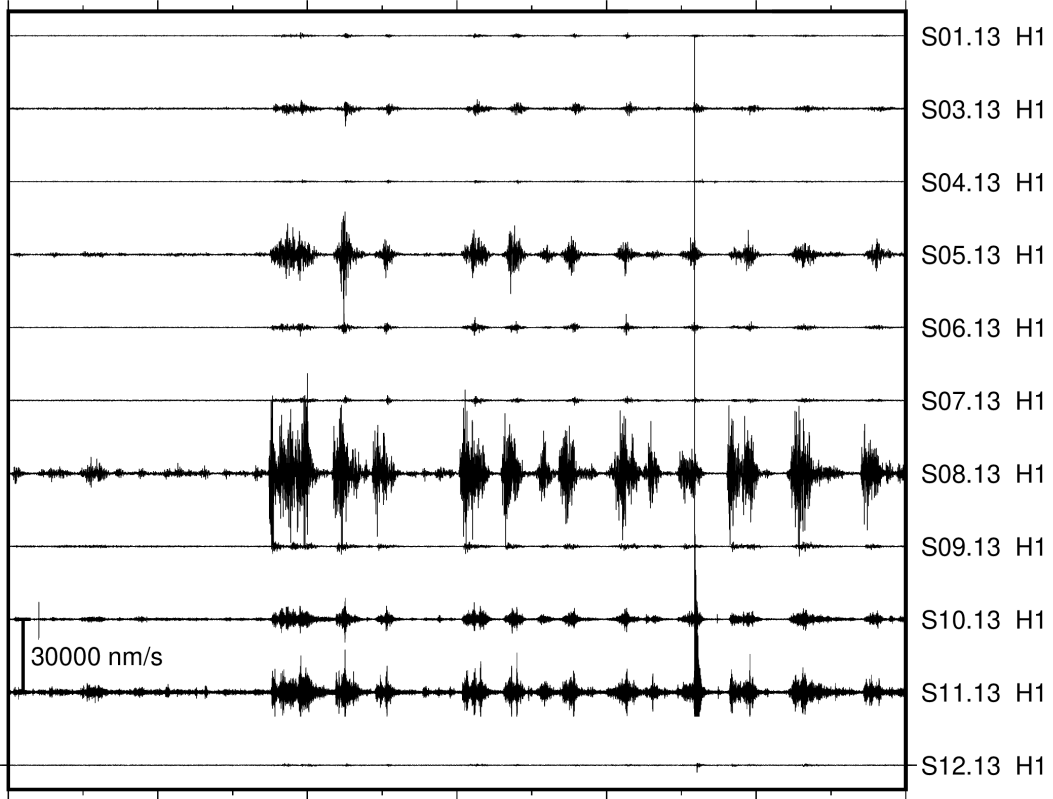
3.1.2. Purpose of this chapter

Hyuga-nada is a region exhibiting the maximum moment-density release rate of VLFs around Japan. In addition, the effective normal stress inferred from the interval of the VLF swarms may be lower in Hyuga-nada. As a factor of the spatial characteristics pertaining to shallow slow earthquakes in this region, the relationship with the development of low velocity areas or the low effective normal stress is suggested. In addition, the subducted Kyushu-Palau Ridge may affect the spatial variation in shallow slow earthquake activities, as suggested in other slow earthquake regions (e.g., Shiraishi et al., 2020; Sun et al., 2020; Todd et al., 2018; Toh et al., 2020).

Analyses of shallow slow earthquakes at a high resolution have become possible based on observations by ocean bottom seismometers (OBSs) in Hyuga-nada. Yabe & Ide (2014) estimated energy rates of tremors in southwest Japan, Cascadia, Mexico and Chile, and discussed their spatial variation, slow earthquake behavior, and variation of strength of tremor patches. In this chapter, to clarify the tectonic factors of slow earthquake activity, I estimated the energy rate functions of tremors and the moment rate functions of VLFs at a higher spatial resolution than the analysis in Chapter 2. The relationship between the subducted Kyushu-Palau Ridge and slow earthquake activity can be clarified by the distribution of energy and moment rate of slow earthquakes at a higher resolution.

Ide et al. (2008) demonstrated the seismic energy rates of slow earthquakes in 2–8 Hz are proportional to the seismic moment rates. They also reported that the ratio between energy rates of tremors to the moment rates, which is termed scaled energy, is constant and 4–5 orders smaller than those of regular earthquakes. Scaled energy of shallow slow earthquakes was estimated to be in the range of 10^{-10} – 10^{-8} off Cape Muroto off the Kii Peninsula, off Tohoku and off Tokachi (Yabe et al., 2019; Yabe, Baba, et al., 2021) by the ratio of the seismic energy rate of a tremor to the seismic moment rate of the corresponding VLF. Tremors and VLFs are temporally correlated also in Hyuga-nada (Figure 3.2). In addition, VLFs in Hyuga-nada are characteristic from the viewpoint of a large moment. Therefore, to reveal the differences in the characteristics of broadband slow earthquakes between Hyuga-nada and other slow earthquake regions, I evaluated the scaled energy of slow earthquakes in Hyuga-nada.

(a) 2–8 Hz OBS



(b) 0.02–0.05 Hz F-net

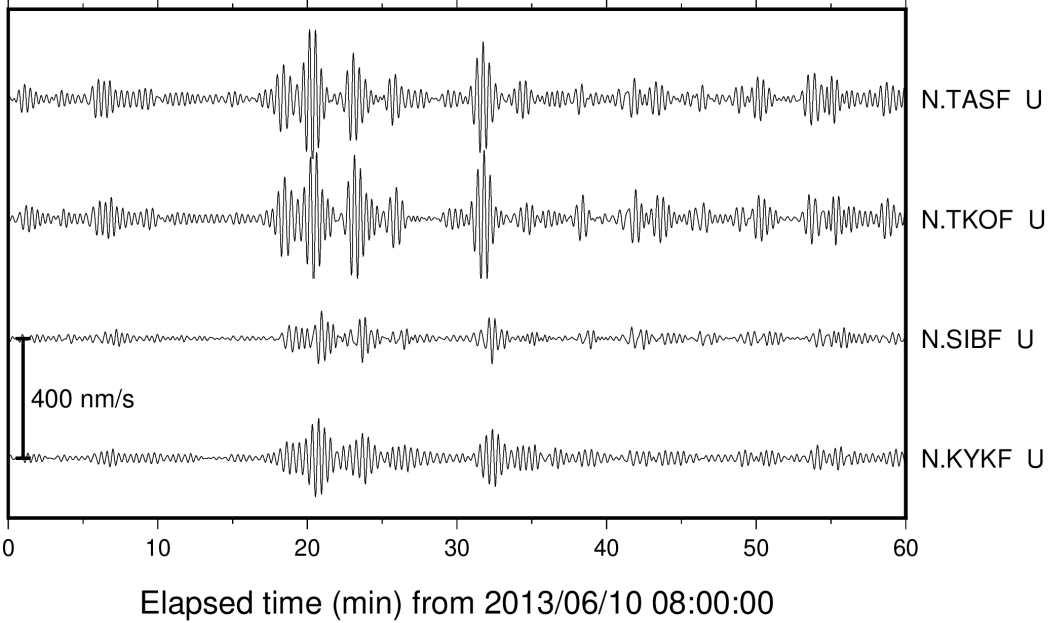


Figure 3.2. Example of one-hour records for (a) shallow tremors in a frequency range of 2–8 Hz at OBSs and (b) shallow VLFs in a frequency range of 0.02–0.05 Hz at F-net stations.

3.2. Data and method

3.2.1. Seismic energy rates of tremors

For the analysis of tremors, I used 1 Hz and 4.5 Hz short-period OBS records of temporal seismological observations in Hyuga-nada conducted by “Research project for compound disaster mitigation on the great earthquakes and tsunamis around the Nankai Trough region,” a project of the Ministry of Education, Culture, Sports, Science and Technology, Japan. 11 and 12 stations were incorporated from April 17 to July 4, 2013 (Yamashita et al., 2015), and from January 1, 2015, to January 1, 2016 (Yamashita et al., 2021), respectively.

The seismic energy rates of the tremors were evaluated following the method of Baba et al. (2021). After instrumental responses were removed, a bandpass filter was applied in a frequency range of 2–8 Hz and the vertical and horizontal components of root-mean-square velocity envelopes with a smoothing time window of 5 s was calculated. The envelopes were resampled at one sample per second. Examples of waveforms of a tremor in a frequency range of 2–8 Hz along with the envelopes obtained by the root-mean-square (RMS) of sums squared seismograms of two horizontal components are displayed in Figure 3.3.

I estimated the site amplification factors for each of vertical and horizontal components at each OBS relative to an F-net station, N.TASF, at 2–8 Hz, utilizing the relative *S*-wave coda amplitudes (e.g., Maeda & Obara, 2009; Phillips & Aki, 1986) of the regular earthquakes in Hyuga-nada. The coda amplitudes of local earthquakes in the same lapse time from the origin do not depend on the epicentral distance and the azimuth (e.g., Aki & Chouet, 1975); therefore, the ratio between coda amplitudes at the two stations depends on the relative site amplification. I implemented earthquakes at depths less than 100 km and magnitudes larger than 2.5 from the unified regular earthquake catalog of the Japan Meteorological Agency.

As the scattering loss parameter varies in the scaled of 100–150 km (Carcolé & Sato, 2010), the method based on coda waves cannot be applicable for stations far (> approximately 150 km) from the sources. However, OBSs near the trench axis are approximately 150 km away from the onland F-net stations, therefore, I classified these earthquakes into two groups. I used Group-1 earthquakes to estimate the site amplification of the reference OBS station relative to N.TASF. The reference OBS was the nearest OBS station from N.TASF for each observation period (S01.13 for the

observation in 2013 and NK1505 for the observation in 2015). The Group-1 earthquakes are thus those that occurred at hypocentral distances less than 150 km from both N.TASF and the nearest OBSs (in 2013, 19 earthquakes; in 2015, 88 earthquakes). To evaluate site amplification factors at all other OBS stations, I used the Group-2 earthquakes that occurred less than 150 km from all OBSs (in 2013, 13 earthquakes; in 2015, 61 earthquakes). Some earthquakes are classified into both Group-1 and Group-2.

If the characteristics of temporal coda-decay trends differ between used regular earthquakes, the estimated site amplification factors can be biased. To evaluate the consistency of temporal coda-decay trends, I estimated the coda Q value of the i -th regular earthquake of both Group-1 and Group-2 at the j -th station ($Q_{\text{Coda},ij}^{-1}$), utilizing the single scattering assumption (e.g., Carcolé & Sato, 2010; Jin & Aki, 2005):

$$P_{ij}(t) = C_{ij} e^{-Q_{\text{Coda},ij}^{-1} \pi f_c t} \quad (3.1)$$

where, $P_{ij}(t)$ is the temporal change in the coda amplitude (square root of the sum of amplitudes in three components) of the i -th regular earthquake at the j -th station, f_c is the central frequency (5 Hz in this study), and C_{ij} is a constant. I evaluated $Q_{\text{Coda},ij}^{-1}$ by solving formula (3.1) using the least-squares method in the time window of 70–110 s from the origin time of the regular earthquake. This is because a longer time window is required to evaluate the temporal changes of the coda-decay than the site amplification factors. If the median of the $Q_{\text{Coda},ij}^{-1}$ for all OBSs is not in the range of $10^{-2.8}$ – $10^{-2.45}$, the regular earthquake is discarded from this analysis. More than 90% of regular earthquakes remained. The remaining regular earthquakes are displayed in Figure 3.4.

I estimated the relative coda amplitude by the ratio of the average amplitudes in 80–100 s from the origin time at two stations. The site amplification factor at each OBS was calculated using the event-averaged coda amplitude ratio of each OBS to the reference F-net station, N.TASF. The coda amplitude ratio of the reference OBS to N.TASF and each OBS to the reference OBS was estimated using Group-1 and Group-2 earthquakes, respectively. In the following procedures, I utilized the RMS of sums of the squared three-component seismograms with a smoothing time window of 5 s after the site correction by implementing the site amplification factors displayed in Figure 3.5. By applying these site amplification factors to the tremor record, the amplitudes were normalized by the site condition at the reference onland station, N.TASF.

I estimated the quality factor of the apparent S -wave attenuation (Q_{app}) around OBS stations based on the coda-normalization method (e.g., Aki, 1980; Yoshimoto et al.,

1993) by incorporating the data pertaining to the Group-2 earthquakes. The distance between the hypocenter of the i -th earthquake and j -th station (L_{ij}) and the coda-normalized maximum S -wave amplitude of the i -th earthquake at the j -th station (A_{ij}) exhibit the following relationship (e.g., Takemura et al., 2017):

$$\ln(L_{ij}A_{ij}) = -\frac{\pi f_c Q_{\text{app}}^{-1}}{V_s} L_{ij} + C_i' \quad (3.2)$$

where, V_s is the S -wave velocity (assuming 3.5 km/s in this study), and C_i' is a constant. I evaluated Q_{app}^{-1} as $(1.7501 \pm 0.3035) \times 10^{-3}$, by solving equation (3.1) utilizing the least-squares method (Figure 3.6). As the path effects of the scattered wave field can be considered as a common parameter at all stations, the amplitudes of S -wave coda depend on the radiated source energy and site amplification factor. Thus, the attenuation curves of coda-normalized amplitudes can be simply described by equation (3.2). The scattering of the relationship between coda-normalized maximum S -wave amplitudes and hypocentral distance may be caused by the radiation pattern or the assumption that the amplitude of a seismic wave attenuates inversely proportional to the hypocentral distance.

I further calculated the energy rate functions of tremors detected by Yamashita et al. (2015; 2021) by implementing the site amplification factors and the Q_{app}^{-1} estimated by the above procedures. The energy rate function of a tremor ($E_j(t)$), estimated from the amplitudes of the j -th station, is calculated utilizing the following equation:

$$E_j(t) = 2\pi V_s r_j^2 \rho A_j'^2(t + t_j) \exp(2\pi f_c Q_{\text{app}}^{-1} t_j) \quad (3.3)$$

where, $A_j'(t)$ is the amplitude of envelopes after the site-correction at the j -th station, r_j is the hypocentral distance from the tremor source to the j -th station, t_j is the travel time from the tremor source to the j -th station, and ρ is the density (assuming 2,700 kg/m³ in this study). I used the epicenters of tremors located by Yamashita et al. (2015; 2021). Furthermore, the depth of tremors was set on the plate boundary of the JIVSM (Koketsu et al., 2012). For the calculation of the energy rate function, the time windows were set at 240 s, which started 60 s before the time window of the tremors set by Yamashita et al. (2015; 2021). I stacked the energy rate functions of a tremor for each station and estimated the average energy rate function, $E_{\text{ave}}(t)$, dividing by the number of stations. I calculated the CCs of the energy rate functions of all station pairs in Figure 3.7 and further utilized the stations whose CCs exceeded 0.6, with at least one other station when stacking the energy rate functions.

The seismic energy rate W of a tremor is calculated by the temporal average of $E_{ave}(t)$ in the time range from t_1 to t_2 :

$$W = \frac{1}{t_2 - t_1} \int_{t_1}^{t_2} E_{ave}(t) dt. \quad (3.4)$$

The integration range is the period when the values of $E_{ave}(t)$ exceeded 20% of the maximum value of $E_{ave}(t)$ (red line in the stacked energy rate function of Figure 3.7). The duration of a tremor is defined as $t_2 - t_1$.

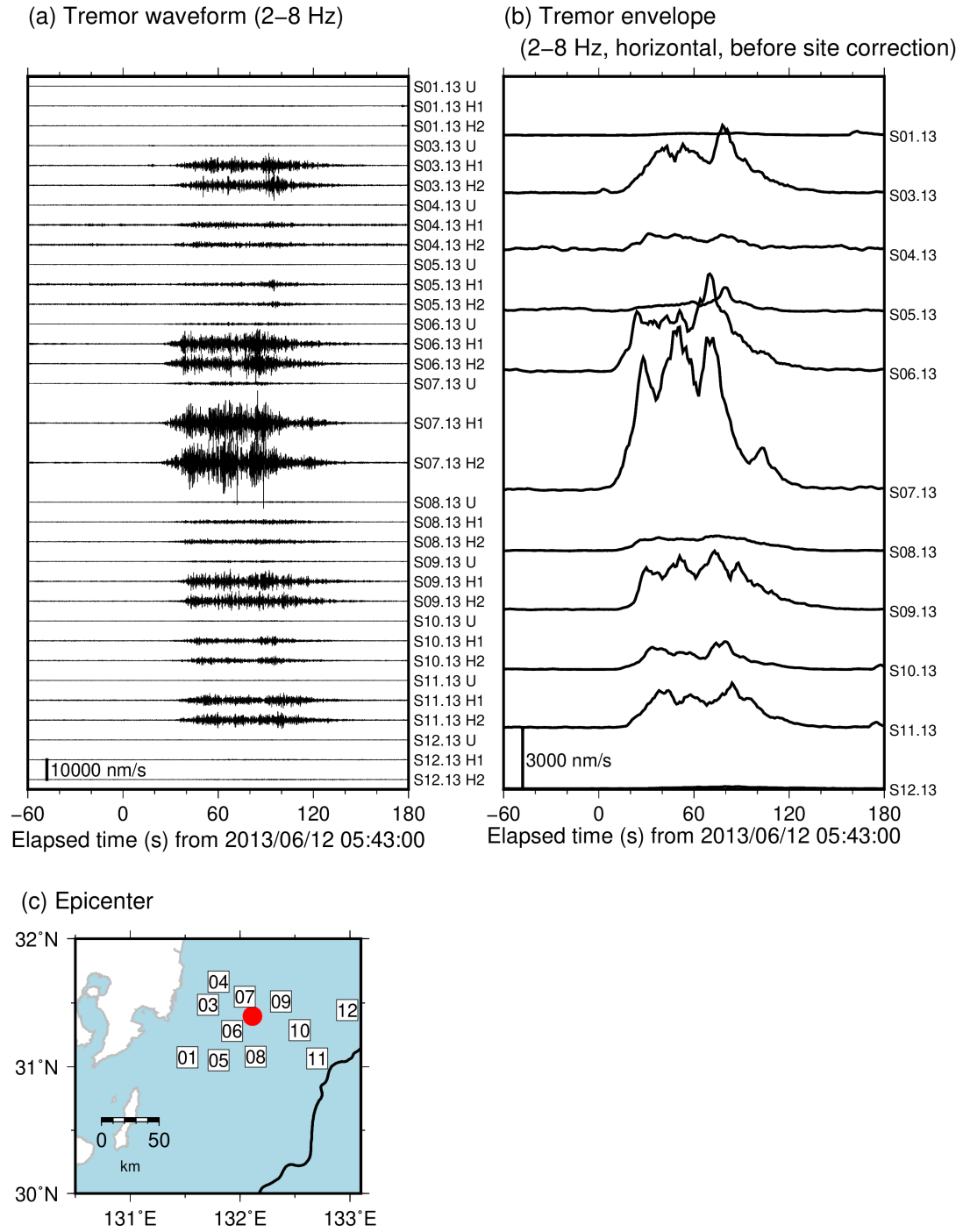


Figure 3.3. Example of (a) waveforms of a tremor in a frequency range of 2–8 Hz, and (b) envelopes obtained by the root-mean-square of sums squared seismograms of two horizontal components. Waveforms are displayed from 05:43:00 (JST, UTC+9), June 12, 2013. (c) Red circle depicts the epicenter of the tremor as displayed in in Figures 3.3a and b. Black line represents the trench axis. Squares are the same as displayed in Figure 3.1.

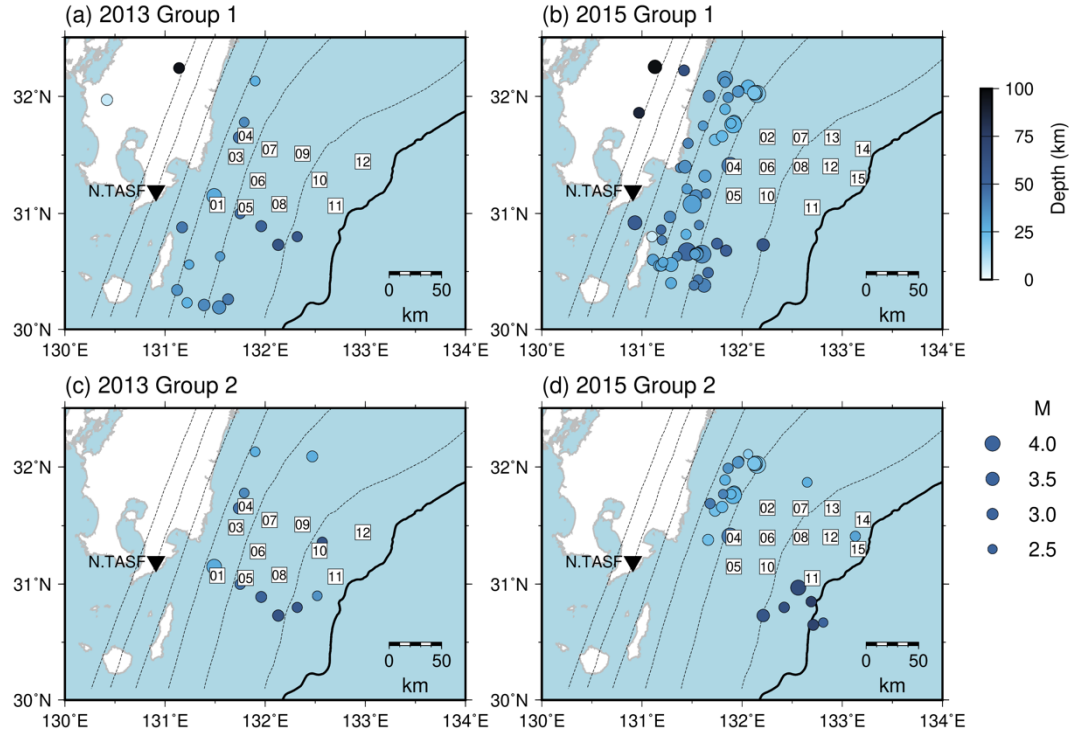


Figure 3.4. Distribution of earthquakes implement for the estimation of the site amplification factors and the apparent Q value. Inverted triangles display the locations of the F-net stations. Dashed contours indicate the isodepth of the top of the Philippine Sea plate (JIVSM; Koketsu et al., 2012). Black line represents the trench axis. Squares are the same as displayed in Figure 3.1.

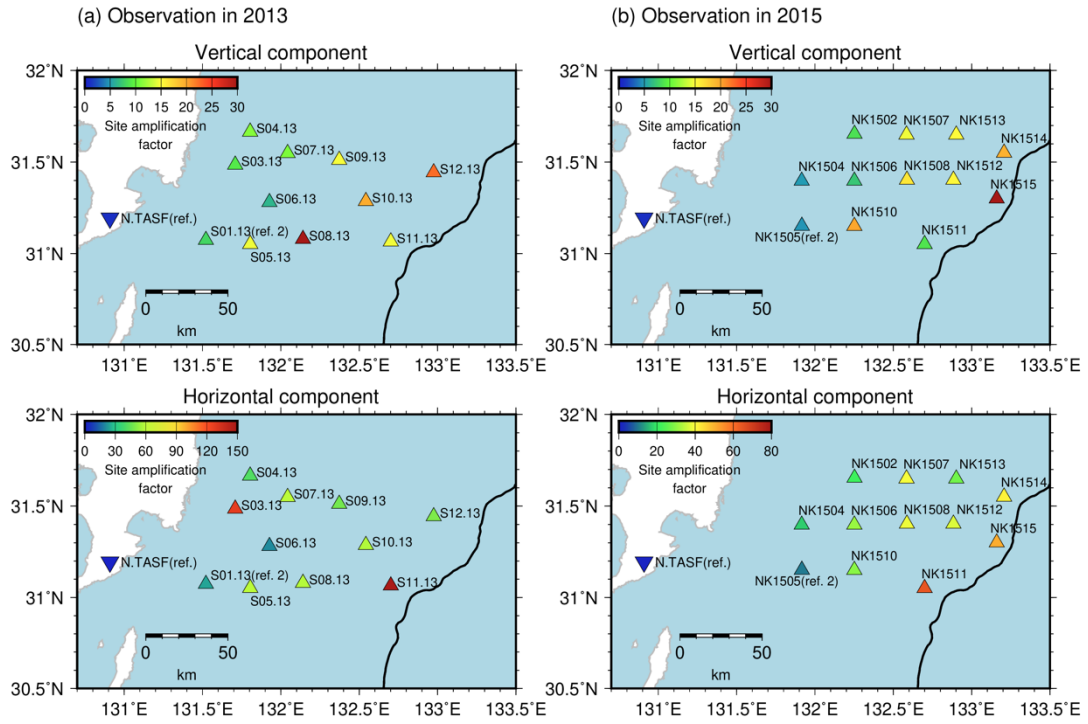


Figure 3.5. Site amplification factors relative to N.TASF based on the coda normalization method. Triangles represent the locations of OBSs. Inverted triangle indicates the location of the F-net station, N.TASF. S01.13 and NK1505 are utilized for the reference to evaluate site amplification factors at OBS stations in 2013 and in 2015, respectively. Black line is the same as displayed in Figure 3.3. Estimation error of site amplification factors is shown in Figure A6.

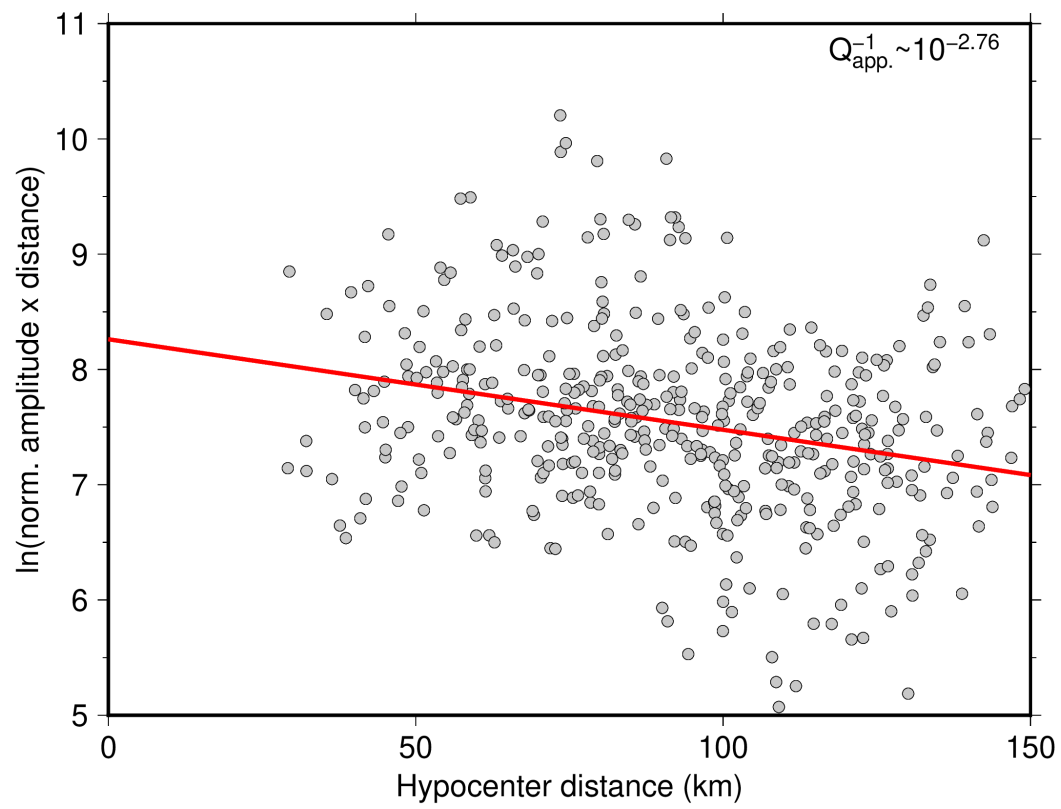
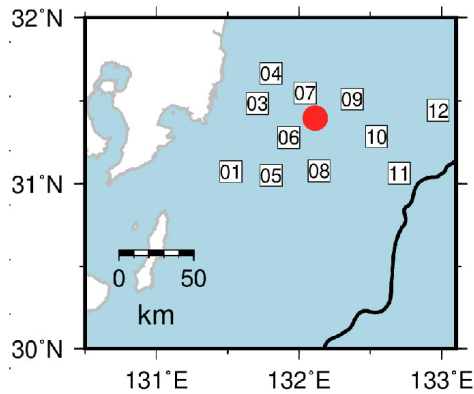
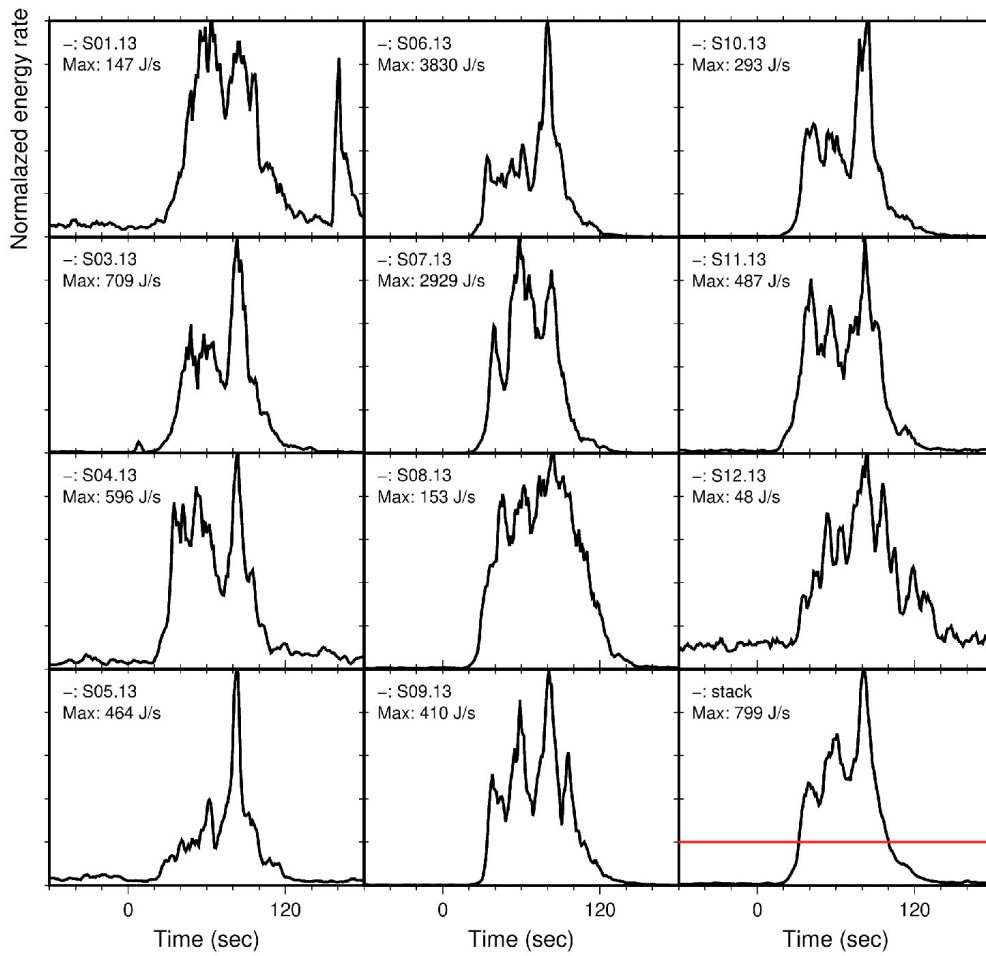


Figure 3.6. Relationship between logarithm of coda-normalized maximum S-wave amplitudes and hypocentral distances. Red line depicts the regression line using Equation (3.2).



2013/06/12

05:43:00

Total energy: 2.9×10^4 J

Duration: 69 s

Energy rate: 4.2×10^2 J/s

Figure 3.7. Temporal changes of energy rate functions of a tremor estimated at each OBS along with its stacked energy rate function. Red line of the stacked energy rate function indicates the threshold, which is set as 20% of the maximum value of the energy rate function. Red circle is the same as displayed in Figure 3.3. Squares and black line are the same as displayed in Figure 3.3.

3.2.2. Seismic moment rates of VLFs

I estimated the source durations and seismic moments of VLFs corresponding to the tremors in 2013 and 2015 detected by Yamashita et al. (2015; 2021), by comparing observed and synthetic waveforms following the procedure of Yabe, Baba, et al. (2021) and Baba et al. (2021). I additionally estimated the source durations and moment rates of VLFs in 2010, as detected by Asano et al. (2015) by implementing the same method. As long-period VLF signals are difficult to recognize in short-period OBS records, I utilized continuous seismograms at onland broadband F-net stations for the estimation. Before the analysis, I removed the instrumental responses, resampled at one sample per second, and applied a bandpass filter in a frequency range of 0.02–0.05 Hz.

To reduce the computational costs of calculating Green's functions, reciprocal calculations were conducted utilizing OpenSWPC (Maeda et al., 2017). I set source grids with an interval of 0.05° on the plate boundary of the area where tremors were detected (Figure 3.8a). The hypocenter of each VLF was supposed to be at the nearest grid from the hypocenter of the tremor located by Yamashita et al. (2015; 2021), or at the hypocenter of VLFs located by Asano et al. (2015). The JIVSM was implemented to calculate Green's functions. The minimum *S*-wave velocity was set to 1.5 km/s. The model includes the topography (ETOPO1; Amante & Eakins, 2009), air, and seawater layers. The default values of OpenSWPC were utilized for the density, seismic velocities, and quality factors in seawater and air. The model volume was discretized by a uniform grid of 0.2 km. The focal mechanisms were assumed to be consistent with the geometry of the plate boundary model of the JIVSM and the plate convergence direction of the plate motion model, NUVEL-1A (DeMets et al., 1994). By combining the assumed focal mechanisms and Green's functions, I prepared a series of synthetic velocity seismograms with triangle functions with source durations of 10–50 s.

The durations and origin times of VLFs were estimated by a grid search using the same method as described in Chapter 2. I calculated station- and component-averaged CCs between synthetic and observed waveforms in a time window of 150 s from the assumed origin time of a VLF. The origin time was searched in the range from 30 s before to 30 s after the start time of the duration range of the corresponding tremor estimated in Section 3.2.1 or the origin time of VLFs located by Asano et al. (2015). The source duration was searched in the range of 10–50 s. The fit between the observed and simulated Love waves was not sufficient than the Rayleigh wave. Thus it may be

inferred that the sedimentary structure of the JIVSM at very shallow (< 5 km) depths in Hyuga-nada is insufficient to simulate Love waves, which are sensitive to shallow structures. Therefore, I used only the vertical and radial components (Rayleigh waves) when calculating CCs between synthetic and observed waveforms. For the N.KYKF station, only the vertical component was utilized because the horizontal components were noisy. The combination of the source duration and the origin time, with the highest averaged CC in the grid search, was adopted. I calculated the relative amplitudes between synthetic and observed waveforms using the procedure described in Chapter 2, and further estimated the seismic moments of VLFEs using the estimated relative amplitudes. The events with averaged CCs between synthetic and observed waveforms smaller than 0.3 were discarded. The seismic moment rate of a VLFE was obtained by dividing the seismic moment by the source duration.

The moment and duration of an example in Figure 3.8 were 1.4×10^{15} Nm and 14 s, respectively. The observed waveforms of the example in Figure 3.8 were simulated well (CC = 0.64). Finally, the scaled energy was estimated by the ratio between the seismic energy rate of a tremor and the seismic moment rate of the accompanying VLFE. Finally, I estimated the scaled energy by the ratio between the seismic energy rate of a tremor and the seismic moment rate of the accompanying VLFE for activities in 2013 and 2015, in which the energy rate could be estimated from OBS records.

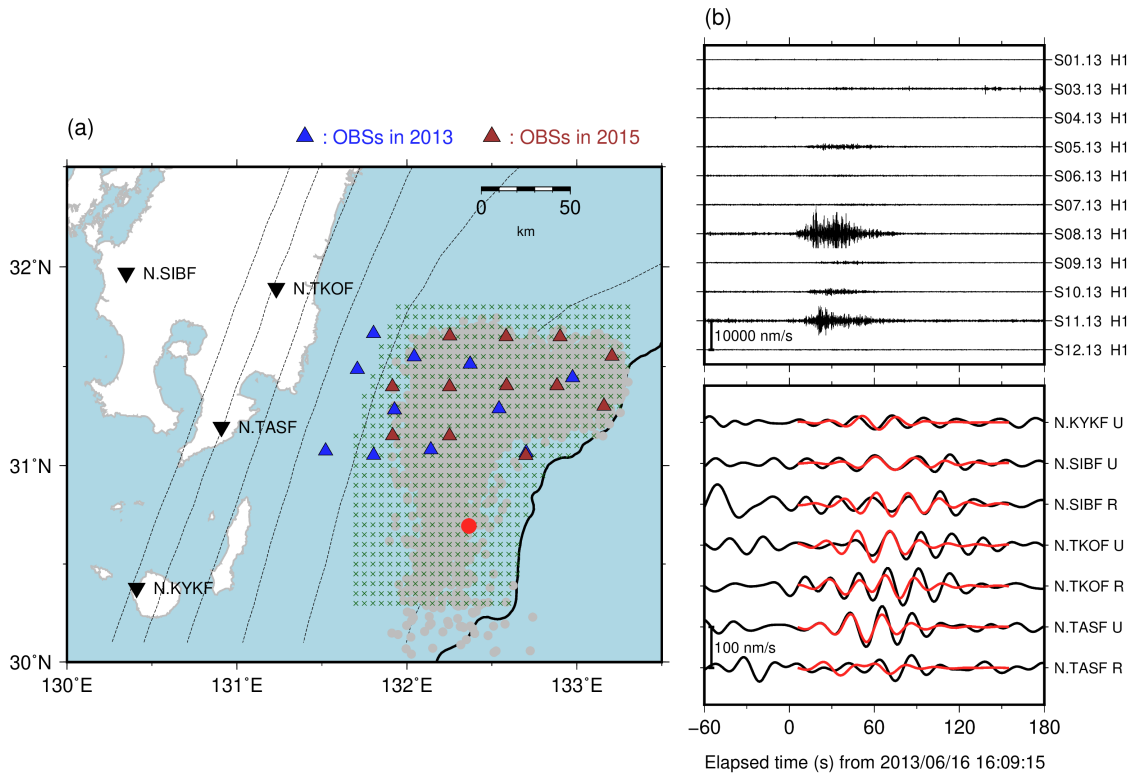


Figure 3.8. (a) VLFE source grids for the VLFE analysis. Green crosses indicate the locations of the VLFE source grids. Gray dots indicate the epicenters of tremors detected by Yamashita et al. (2015; 2021). Red circle indicates the epicenter of the tremor which corresponds to a VLFE displayed in Figure 3.8b. Blue and brown triangles depict the locations of OBSs in 2013 and 2015, respectively. Inverted triangles, black line, and dashed contours are the same as displayed in Figure 3.4. (b) An example of waveforms of a tremor in a frequency range of 2–8 Hz (top panel) and the accompanying VLFE in a frequency range of 0.02–0.05 Hz (bottom panel). Waveforms are depicted from 16:09:15 (JST, UTC+9), June 16, 2013. Black and red lines in the bottom panel are the observed and the synthetic waveforms, respectively.

3.3. Results

I estimated energy rates of 2,161 and 7,153 shallow tremors in 2013 and 2015, respectively. The dominant range of tremor energy rates is 10^1 – $10^{4.5}$ J/s with a spatial variation (Figure 3.9). Tremors with large energy rates ($> 10^3$ J/s) are concentrated from 30.6° N to 31.0° N, which is near the southern edge of the subducted Kyushu-Palau Ridge. In 2015, tremors with larger energy rates ($> 10^{3.5}$ J/s) occurred near the northeastern edge of the subducted Kyushu-Palau Ridge, toward the east of 132.4° E. Tremors in 2015 occurred in the inactive area of tremors in 2013.

Moment rates were also estimated for 1,297, 1,051, and 2,023 shallow VLFES in 2010, 2013, and 2015, respectively. The dominant range of the VLFE moment rates was 10^{13} – 10^{15} Nm/s (Figure 3.10). In the south of 31.0° N, VLFES with large moment rates ($> 10^{14}$ Nm/s) occurred in 2010 and 2013. In the north of 31.0° N, VLFES extended near the trench axis in 2010 and 2015. In particular, VLFES with large moment rates ($> 10^{14}$ Nm/s) in 2010 and 2015 are concentrated east of 132.4° E. In the west of 132.4° E and north of 31.0° N, the VLFE moment rates are relatively small.

The spatial variations in VLFE moment rates and tremor energy rates for each observation period were similar. Generally, the energy rates of tremors and moment rates of VLFES are larger outside the subducted ridge than inside the subducted ridge in 2010 and 2013, although there is an area with VLFES with large moment rates and tremors with large energy rates in the updip part inside the subducted Kyushu-Palau Ridge in 2015. For the west of 132.4° E, the depth of the area with small moment and energy rates seems to be deeper than that of the area with large moment and energy rates. However, the plate boundary model of JIVSM does not contain small-scale geometry, such as the subducted Kyushu-Palau Ridge, therefore, the actual depth of the plate boundary inside the subducted ridge can be shallower than the depth by JIVSM. Probably, the depths of these two areas cannot differ significantly. Thus, tremors and VLFES in 2010 and 2013 can migrate along the strike direction from south to north in the depth of ~ 10 km.

In Section 3.4, I mainly discuss regarding the spatial variation based on VLFE moment rates because VLFE analysis covers longer time periods than tremors due to the limitation of deployment of OBSs. As for the episodes in 2010 and 2013, when tremors and VLFES migrates along the strike direction from south to north, I defined the south of and inside the subducted ridge as the area with large and small moment rates in each episode, respectively (Figure 3.10ab).

The dominant range of the scaled energy was $10^{-12.5}$ – 10^{-10} both in 2013 and 2015 (Figure 3.11). The distribution of the scaled energy did not change spatially on the order scale. The dominant ranges of the scaled energies in 2013 and 2015 were similar (Figure A7). This suggests that the scaled energy does not change temporally, and the dominant range of scaled energy in Hyuga-nada is common for the entire Hyuga-nada region.

By considering the estimation error of site amplification factors, these factors can change from 0.5 to 1.5 times (Figure A6). The energy rate function is proportional to squared amplitude, therefore the estimated energy rate can change 0.44 to 4.0 times. In addition, considering the estimation error of the Q_{app}^{-1} (Figure 3.6), the energy rates can change from 0.67 to 1.5 times when the hypocentral distance is 150 km. Therefore, the uncertainty of energy rates of tremors can be ~ 0.3 to 6 times. Although the estimation errors of energy rates of tremors and scaled energy can be several times, the uncertainty may not be larger than an order of magnitude.

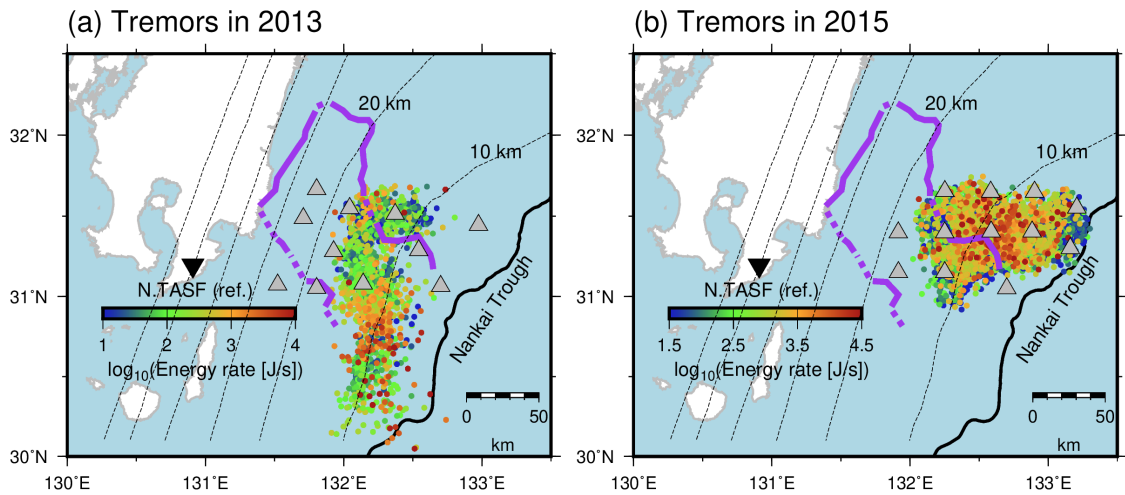


Figure 3.9. Spatial distribution of energy rates of shallow tremors (a) in 2013 and (b) in 2015. Purple lines represent the inferred subducted Kyushu-Palau Ridge (Yamamoto et al., 2013). Gray triangles depict the locations of OBSs. Inverted triangles, black line, and dashed contours are the same as displayed in Figure 3.4.

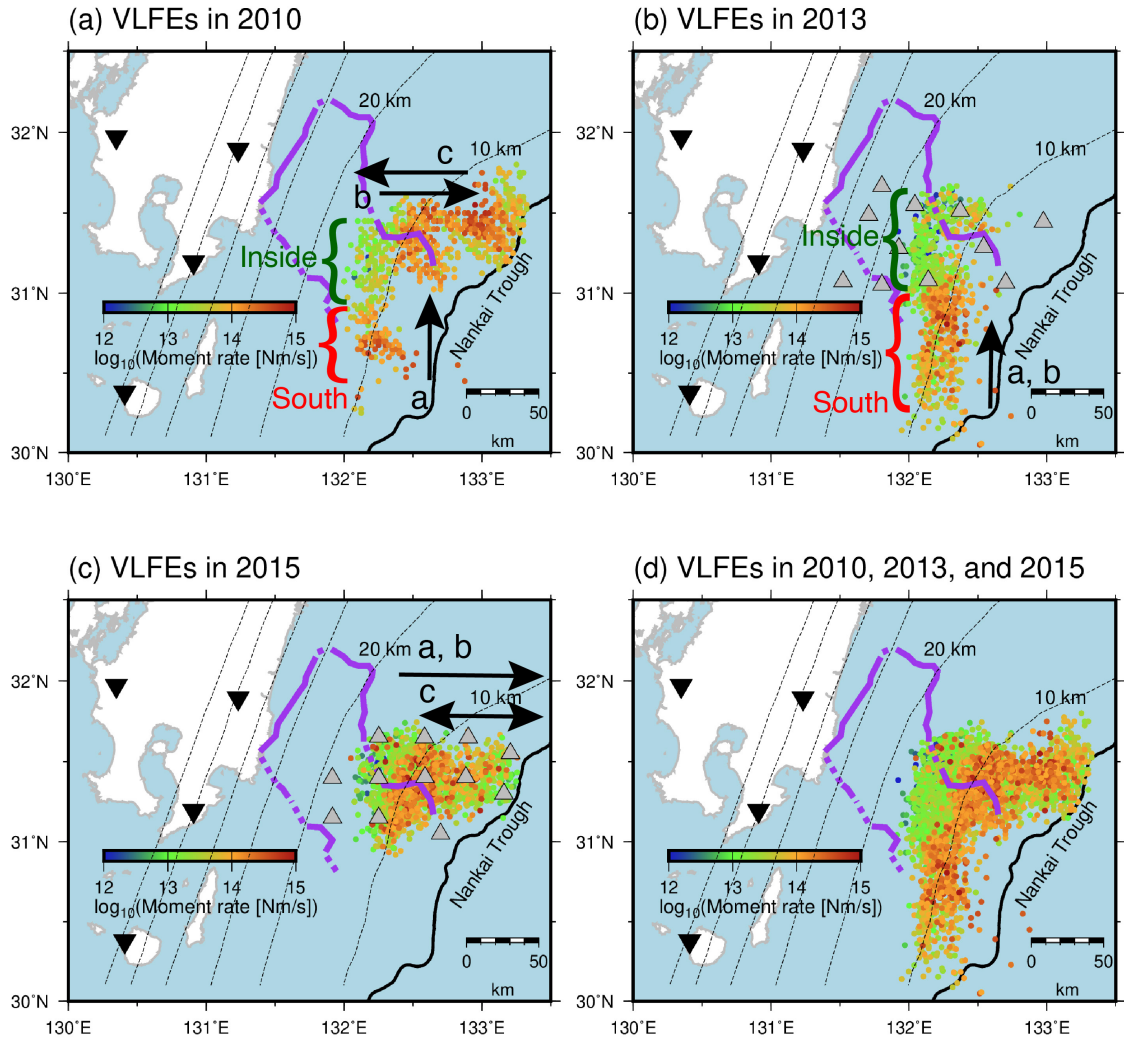


Figure 3.10. Spatial distribution of moment rates of shallow VLFs in (a) 2010, (b) 2013, (c) 2015, and (d) all analysis periods. Black arrows represent the directions of migrations. Purple lines are the same as in Figure 3.9. Gray triangles depict the locations of OBSs. Inverted triangles, black line, and dashed contours are the same as displayed in Figure 3.4. Green and red parentheses show the range of inside and south of the subducted ridge used in the along strike migration discussed in Section 3.4, respectively.

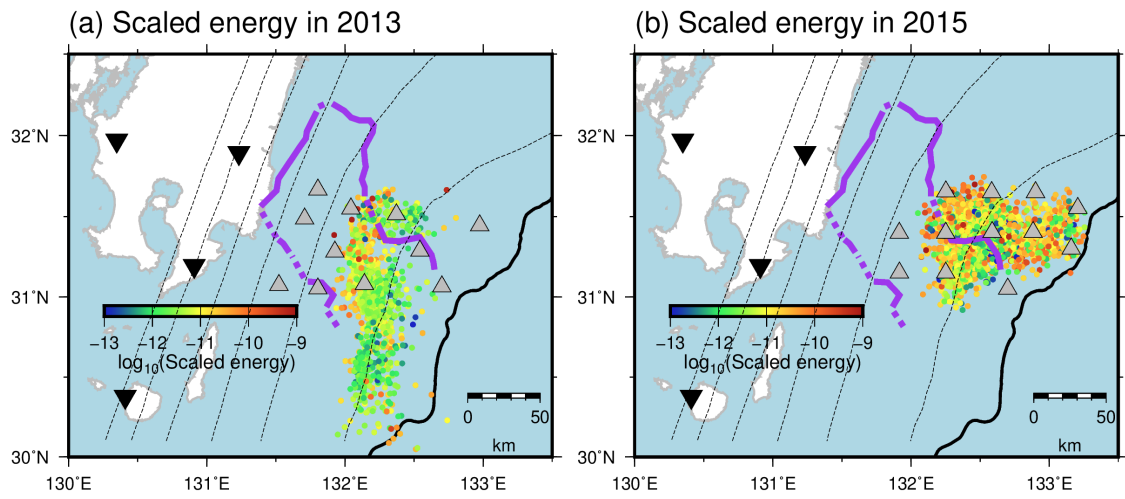


Figure 3.11. Spatial distribution of scaled energy of shallow slow earthquakes (a) in 2013 and (b) in 2015. Gray triangles depicted the locations of OBSs. Purple lines are the same as in Figure 3.9. Inverted triangles, black line, and dashed contours are the same as displayed in Figure 3.4.

3.4. Discussion

3.4.1. Relationship between slow and repeating earthquakes in Hyuga-nada

In the downdip of shallow tremors and VLFs, repeating earthquakes occur at depths of 15–30 km (Yamashita et al., 2012). They estimated the interplate slip rate from repeating earthquakes and demonstrated that the slip rate is higher in the south of the subducted Kyushu-Palau Ridge than inside the subducted ridge (Figure 3.12). The area with a large slip rate is considered as weak interplate coupling; therefore, Yamashita et al. (2012) interpreted that the interplate coupling is weaker in the south along the strike direction. The slip deficit rate estimated by Noda et al. (2018) is small in southern Hyuga-nada (Figure 2.6) although the resolution in Hyuga-nada is low; therefore, the inferred interplate coupling from Noda et al. (2018) is further weak in the south. The subducted ridge may affect the heterogeneity of the interplate coupling.

The cumulative moment of shallow VLFs in 2010 and 2013, the episodes with along-strike migrations, are smaller inside the subducted ridge than in the south of the subducted ridge (Figures 3.12a and b). The cumulative moment of shallow VLFs estimated in Chapter 2 exhibits a similar along-strike variation (Figure 3.12c). This tendency is similar to the slip rate estimated from the repeating earthquakes. Uchida et al. (2020) suggested an interaction between repeating earthquakes and shallow slow earthquakes along the Nankai Trough. If the tendency of the interplate coupling along the strike direction in the repeating earthquake area can be extended to the updip areas where shallow tremors and VLFs occur, the areas with large and small cumulative moments (i.e., south and inside of the subducted ridge) correspond to the areas with weak and strong interplate coupling, respectively. In Chapter 2, I suggest that shallow VLFs are active in areas with weak interplate coupling. This relationship can be observed not only on a regional scale around Japan, but also on a local scale in Hyuga-nada.

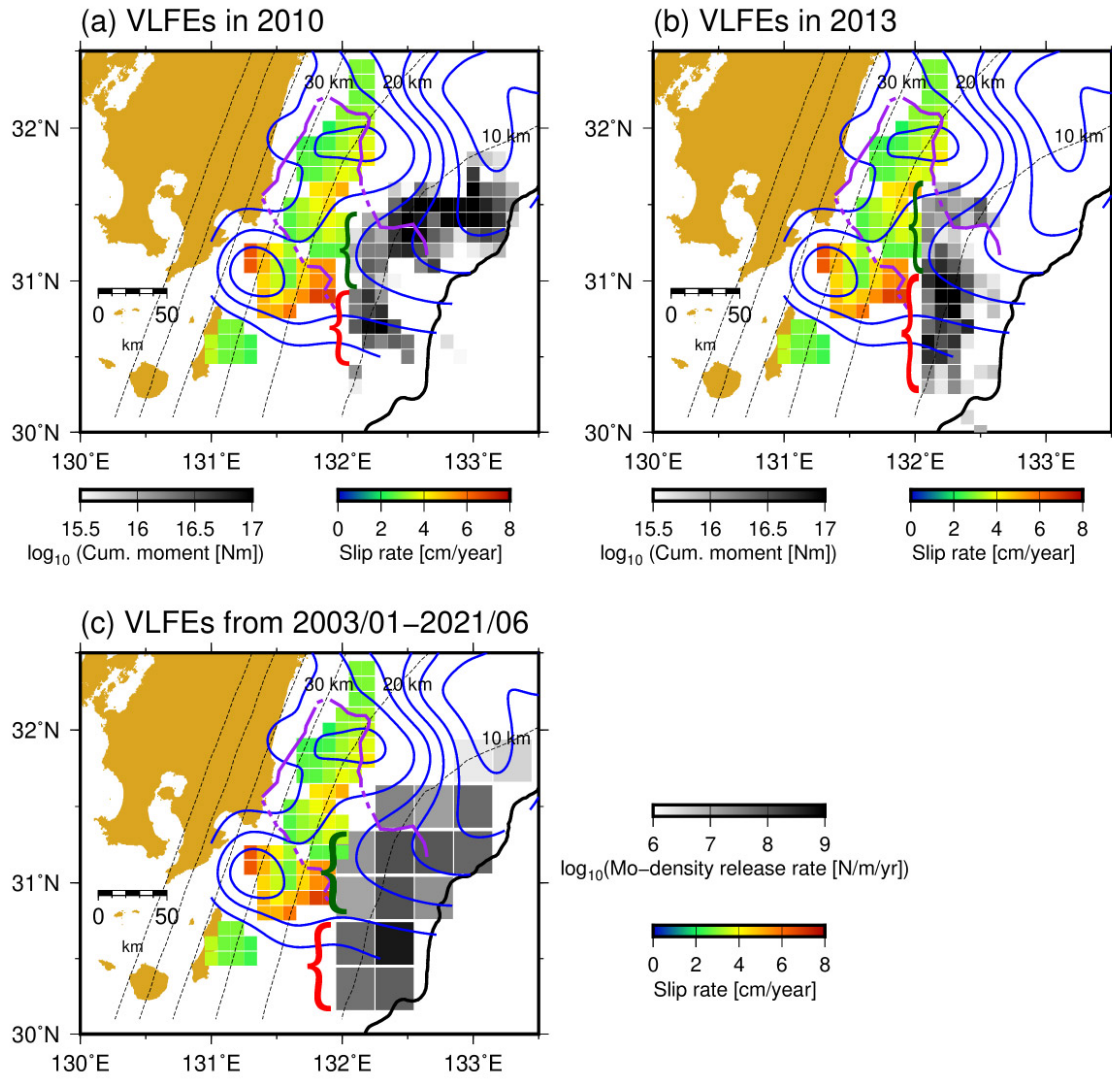


Figure 3.12. Relationship between slip rates estimated from repeating earthquakes (Yamashita et al., 2012) and shallow slow earthquakes. Gray scale in Figure 3.12a and 3.12b exhibits the cumulative moments of VLFs in 2013 and in 2015, respectively. Gray scale in Figure 3.12c represents moment-density release rate of VLFs estimated in Chapter 2. Color scale indicates the slip rate estimated from repeating earthquakes. Purple lines are the same as in Figure 3.9. Black line and dashed contours are the same as displayed in Figure 3.4. Green and red parentheses are the same as displayed in Figure 3.10.

3.4.2. Distribution of frictional properties inferred from physical models

Shallow tremor and VLFE episodes in 2010, 2013, and 2015 consisted of two or three migrations. I divided each episode in 2010 and 2015 into three migrations and the 2013 episode into two migrations (Figure 3.13). The 2010a, 2013a, and 2013b migrations are along the strike direction, whereas the 2010b, 2010c, 2015a, 2015b, and 2015c migrations are along the dip direction (Figure 3.10; Table 3.1).

The migrations along the strike direction in 2010 and 2013 consistently start south of the subducted Kyushu-Palau Ridge. Subsequently, tremors and VLFs migrate northward along a depth of ~ 10 km and enter the subducted ridge. After tremors and VLFs enter the area where the Kyushu-Palau Ridge is subducted (north of 31° N in Figure 3.13), their migration speed becomes slow, and the energy rates of tremors and moment rates of VLFs are small (indicated by arrows in Figures 3.13a, d, and e; Table 3.1). This tendency is consistent with the physical model of the ETS propagation by Ando et al. (2012). They assumed strong and weak brittle patches in the ductile background based on Newtonian rheology, which assumed that strength of the ductile background τ_v depends linearly on the slip velocity v :

$$\tau_v(v) = \eta_v v \quad (3.5)$$

where η_v is velocity strength coefficient. They also indicated that ETS starts migrating energetically in strong patch areas and decelerates with a parabolic spatiotemporal pattern as suggested by Ide (2010) in weak patch areas. They pointed out that the rheological heterogeneity on the plate boundary controls the ETS migration pattern. The main front of the along-strike migration of shallow slow earthquakes in Hyuga-nada can be explained well by the model of Ando et al. (2012). In Hyuga-nada, the south and inside of the subducted ridge correspond to a strong and weak patch area, respectively.

As indicated by Yamashita et al. (2015), rapid tremor reversals (RTRs; black dotted arrows in Figure 3.13d), which is the fast backward propagation of tremors (Houston et al., 2011), occurred in the migration of 2013a. When RTRs exit from the subducted ridge, the energy rates of tremors and moment rates of VLFs become large; therefore, these rates depend on the space.

I compared the shallow slow earthquake activity and P -wave velocity structure investigated in Nishizawa et al. (2009; Figure 3.14). I estimated the cumulative number and moment at each grid of $10 \text{ km} \times 10 \text{ km}$ along the profile of Nishizawa et al. (2009). The average moment of VLFs is small and large at distances of 0–30 km and 30–60 km

along the profile, respectively (Figure 3.14b). By comparing the grids with a large cumulative number of events (> 100 events), there are larger number of events, and the average moment of an event is smaller at a distance of 20–30 km, in contrast to a distance of 30–50 km (Figure 3.14c). More events with small moments occur in the northwestern part of the profile, whereas fewer events with large moments occur in the southeastern part, displaying larger cumulative moments. Based on the model of Ando et al. (2012), strong and weak patch areas correspond to the southeast and northwest of the 30 km point along the profile, respectively. A low seismic velocity anomaly is observed at a distance of 30–60 km, which corresponds to a strong patch area. The existence of low velocity anomalies can be considered to be a result of the high pore fluid pressure around the plate boundary.

Kano, Kato, et al. (2018) constructed a model of deep tremor patches in western Shikoku based on the model proposed by Ando et al. (2012). In the western part of western Shikoku in Chapter 2, which corresponds to a strong patch area, the fluid pressure on the plate boundary and the tidal sensitivity are lower than those in the central part of western Shikoku. Fluid dehydrated from the oceanic crust infiltrates the hanging wall, and the fluid pressure on the plate boundary in the western part was inferred to be lower than that in the central part. Thus, the effective normal stress is higher, and the strength of the patches is stronger in the western part than in the central part. As weak patches can be easily ruptured by external stress perturbations, the tidal sensitivity was observed to be high in the central part.

Based on the model of Kano, Kato, et al. (2018), I interpreted that a low velocity anomaly at a distance of 30–60 km exists in the hanging wall. The fluids released by the compaction of sediments, smectite-to-illite transition, or opal-to-quartz transition infiltrates the overriding plate at a distance of 30–60 km (e.g., Hyndman & Peacock, 2003; Katayama, 2016; Saffer & Wallace, 2015). Therefore, the fluid pressure on the plate boundary is lower and the effective normal stress is higher at a distance of 30–60 km (south of the subducted ridge), than at a distance of 0–30 km (inside the ridge). From the points of the number of events and the fluid pressure, the observation in Hyuga-nada is possibly consistent with the model of Kano, Kato, et al. (2018; Table 3.2). The recurrence interval of VLFE activity inside and in the south of the ridge estimated in Chapter 2 is 9.5 ± 1.2 and 11.0 ± 1.8 months, respectively (Figure 3.15). Based on simulation and structural studies, as in the case of Section 2.4.2, the longer recurrence

interval suggests higher effective normal stress. The recurrence intervals in two areas are not contradictory to the variation in effective normal stress inferred from the model by Kano, Kato, et al. (2018). However, the difference in the recurrence interval is not significant by considering the uncertainty.

Yamamoto et al. (2022) pointed out that the number of shallow VLFs is large, the moment of individual shallow VLFs is small, and migration velocity is slow in the eastern area, where the Paleo-Zenisu Ridge is subducted, as compared to the western area off the southeastern Kii. They suggested that the area with the subducted Paleo-Zenisu Ridge and in the west of the subducted ridge correspond to weak and strong patch areas, respectively. Furthermore, shallow VLFE activity off the southeastern Kii is explained by the model of Kano, Kato, et al. (2018). Based on shallow slow earthquake activity in Hyuga-nada and off the southeastern Kii, the area with a subducted ridge corresponds to a weak patch area in both regions.

At a distance of 20–30 km along the profile by Nishizawa et al. (2009), which is considered as a weak patch area, the depths of the layers of 4–5.5 km/s are shallower than the surrounding areas; therefore, there may be a subducted seamount (Figure 3.14a). The number of VLFs is smaller at a distance of 0–20 km (downdip of the inferred subducted seamount) than at a distance of 20–60 km (at the top or updip of the inferred subducted seamount). By using numerical simulations in the model with a subducted simple seamount, the updip of a subducted seamount corresponds to a stress shadow area, indicating a lower effective normal stress condition than the surrounding regions (Sun et al., 2020). Therefore, slow earthquake activity is promoted during the updip of the subducted seamount. Although the larger number of events at a distance of 20–60 km can be explained by Sun et al. (2020), the area at the distance of 0–20 km corresponds to the weak patch area based on the models of Ando et al. (2012) and Kano, Kato, et al. (2018), therefore the effective normal stress distributions inferred from the model of Sun et al. (2012) and the models of Ando et al. (2012) and Kano, Kato, et al. (2018) are not consistent. Although Sun et al. (2020) assumed a simple seamount, the geometry of the Kyushu-Palau Ridge can be more complex. In addition, the profile of Nishizawa et al. (2009) deviates from the along-dip direction. There is a possibility that the geometry of further downdip of the profile of Nishizawa et al. (2009) affects the effective normal stress at the distance of 0–20 km. The inconsistency may be caused by these factors.

Assuming a circular crack model, the seismic moment M_0 of an earthquake is given by (e.g., Kanamori & Anderson, 1975):

$$M_0 = \frac{16}{7} \Delta\tau r^3 \quad (3.6)$$

where, $\Delta\tau$ is the stress drop and r is the radius of the patch. In this section, this relationship is further assumed in VLFEs. The average moment of a VLFE in the south of the subducted ridge (strong patch area) and inside the ridge (weak patch area) is $\sim 2.4 \times 10^{15}$ Nm and $\sim 5.6 \times 10^{14}$ Nm, respectively. If the radius of patches r is assumed to be 5 km (e.g., Ohta & Ide, 2017), the stress drop of a VLFE in the south of the subducted ridge and inside the ridge is $\sim 8 \times 10^3$ Pa and $\sim 2 \times 10^3$ Pa, respectively.

Based on the model of Ando et al. (2012), which assumed Newtonian viscosity, the difference in the strength between strong and weak patches is represented by that in the stress drop. They suggested the important element to the parabolic migration pattern is sufficient difference in stress drop between strong and weak patches. Like Ando et al. (2012), I investigated which function is better for the fitting of the migration 2013a, exponential or parabolic. Although the start of migration is scattered, the migration pattern seems to be better fitted by a parabola ($t=D^{-1}x^2$; t is the elapsed time, x is the propagation distance, and D is the diffusion coefficient) (Figure 3.16). The diffusion coefficient D is $\sim 6 \times 10^4$ m²/s. Thus, the approximately four times difference in stress drop of strong and weak patches can be sufficient to generate the parabolic migration pattern and its pattern can be explained by the effect of Newtonian rheology in the ductile background. The relationship between D and velocity strength coefficient, η_v , is described by (Ando et al., 2012):

$$\eta_v = \frac{\mu \Delta\tau L}{2\pi\tau_e D} \quad (3.7)$$

where μ is the rigidity, L is the width of the strong patch, $\Delta\tau/\tau_e$ is the stress drop normalized by the strength excess. Ando et al. (2012) estimated η_v , as $\sim 10^{10}$ Pa s m⁻¹ from the observation of deep tremors in the Kii Peninsula. D and L of shallow slow earthquakes in Hyuga-nada is $\sim 6 \times 10^4$ m²/s and $\sim 8 \times 10^4$ m, respectively. Although these values are larger than those in the Kii Peninsula ($D \sim 0.5 \times 10^4$ m²/s and $L \sim 10^4$ m), if μ and $\Delta\tau/\tau_e$ are the same, the value of η_v is similar to that estimated by Ando et al. (2012) in the order scale.

Skarbek et al. (2012) modeled the features of interplate slips, such as high-speed slips, slow slips, and stable sliding, based on the rate- and state-dependent friction (RSF) law. They pointed out that the ratio of the length of the velocity-weakening materials to the total length (η) or frictional parameters can affect the features of slips on the fault. Based on the RSF law, the friction on the fault is given by (Dieterich, 1979):

$$\mu(V, \theta) = \mu_0 + a \ln\left(\frac{V}{V_0}\right) + b \ln\left(\frac{V_0 \theta}{D_c}\right) \quad (3.8)$$

where, a and b are frictional parameters, μ_0 is the friction coefficient at the reference velocity V_0 , θ is the state variable, V is the slip velocity, and D_c is the characteristic slip weakening distance. The state variable θ is described as follows:

$$\frac{d\theta}{dt} = -\frac{V\theta}{D_c} \ln\left(\frac{V\theta}{D_c}\right). \quad (3.9)$$

Skarbek et al. (2012) indicated that the migration speed of tremors is negatively correlated with η . They also suggested that the migration speed and stress drop $\Delta\tau$ are negatively correlated with a/b at velocity-weakening areas (i.e., $a/b < 1$) if η is constant.

In the south of the subducted ridge, the migration speed is faster than inside the ridge (Figures 3.13d and e). If the ratio of a to b is the same, the migration speed is fast when η is larger. Although Skarbek et al. (2012) assumed the migration speed along the dip direction, if this correlation is assumed in the along-strike migration, the ratio of the area of velocity-weakening materials to the total area may be larger in the south of the subducted ridge than inside the ridge.

Otherwise, the negative correlation between a/b at velocity-weakening areas and the migration speed by Skarbek et al. (2012) suggests that the absolute value of $a-b$ in a velocity-weakening material may be large in the south of the subducted ridge. As described above, the stress drop of VLFs may be large in the south of the subducted ridge. The negative correlation between a/b in the velocity-weakening areas and $\Delta\tau$ also indicates that the absolute value of $a-b$ ($a-b < 0$) in the velocity-weakening material may be large in the south of the subducted ridge. The heterogeneity of slow earthquake activity can be controlled by various factors, such as the effective normal stress, η , or $a-b$ (Table 3.3).

Inside the subducted ridge, the strength of the patches can be weaker although the interplate coupling is suggested to be stronger than that in the south of the ridge as discussed in Section 3.4.1. Inside the ridge, interplate regular earthquakes occur closely

downdip to the slow earthquake area (Figure 3.1). On the other hand, the area with interplate regular earthquakes is apart from the slow earthquake area in the south of the ridge. Therefore, some portion of the accumulated stress in the slow earthquake area may be released by adjacent regular earthquakes inside the ridge. On the other hand, most of the accumulated stress may be released by slow earthquakes in the south of the ridge. Regular earthquake patches are stronger than strong slow earthquake patches in the south of the ridge. Inside the ridge, regular earthquake patches and weak slow earthquake patches may be close, therefore interplate coupling may be stronger on a large scale (Figure 3.17).

The number of tremors is small in the distance of 0–20 km, downdip of a subducted seamount, along the profile of Nishizawa et al. (2009) (Figure 3.14). This area is immediately adjacent to the regular earthquake area, therefore the effective normal stress in this area may be higher as inferred from the model by Sun et al. (2020), and the portion of accumulated stress released by regular earthquakes may be larger.

However, the estimation error of slip deficit rate estimated by Noda et al. (2018) can be large in Hyuga-nada due to the lack of offshore data. In addition, repeating earthquake area is downdip of the slow earthquake area, therefore the tendency of interplate coupling in slow earthquake area may be different from that in repeating earthquake area. Due to these factors, the possibility that the interplate coupling inside the ridge is not stronger than that in the south of the ridge cannot be denied. To reveal the variation in the interplate coupling, stress release by regular and slow earthquakes, and strength of their patches in more detail, seismic and geodetic observations with a higher resolution by using offshore data are necessary.

There are various directions for along-dip migrations. 2010b, 2015a, and 2015b migrations were eastward, whereas the 2010c migration was westward (Figures 3.13b, f, and g; Table 3.1). The 2015c migration was bilateral (Figure 3.13c). In the migrations of 2010b, 2010c, and 2015c, the migration speed is slow in the east of 133.0°E compared to west of 133.0°E regardless of the direction of migrations. Based on Kano, Kato, et al. (2018), the strength of the patch may be weak in the east of 133.0°E. However, the difference in energy and moment rates between the east and west of 133.0°E is unclear. The area in the east of 133.0°E is near the trench axis, thus this area is far from onshore F-net stations and at the edge of the OBS network. Therefore, the uncertainty of hypocenter of tremors and VLFs may be large. To discuss the difference in energy and

moment rate in this area, analysis with an offshore network in more episodes is necessary in future works.

Table 3.1. Characteristics of migrations in Hyuga-nada.

Migration direction			Parabolic migration pattern	Start energetically
2010a	Along-strike	South to north	○	○
2010b	Along-dip	Downdip to updip	○	○
2010c	Along-dip	Updip to downdip	×	×
2013a	Along-strike	South to north	○	○
2013b	Along-strike	South to north	○	○
2015a	Along-dip	Downdip to updip	×	○
2015b	Along-dip	Downdip to updip	×	×
2015c	Along-dip	Bilateral	×	×

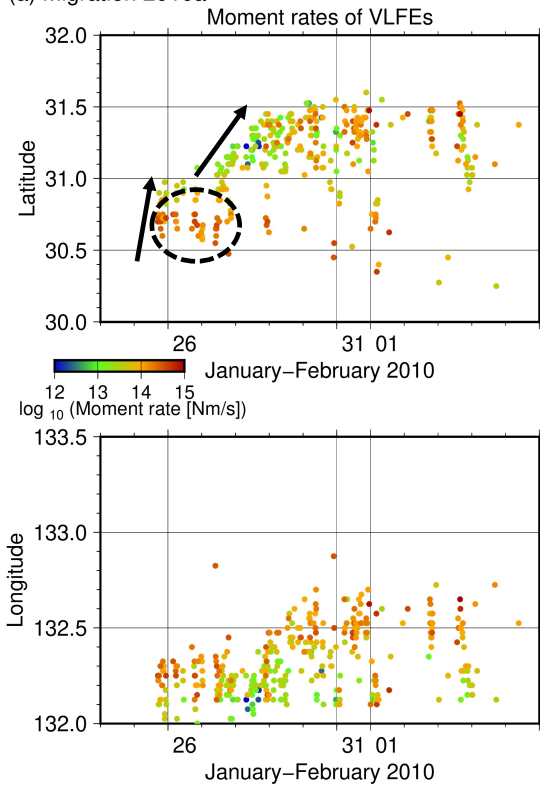
Table 3.2. Difference in strong and weak patch areas based on the model by Ando et al. (2012) and Kano, Kato, et al. (2018).

	Strong patch area	Weak patch area	Observation in Hyuga-nada
	(South of the subducted ridge)	(Inside the subducted ridge)	
This study (Hyuga-nada)			
Kano, Kato, et al. (2018; W. Shikoku)	Western part	Central part	
Migration speed	Fast	Slow	○
Energy or moment	Large	Small	○
Pore pressure on the plate boundary	Low	High	○
Tidal sensitivity	Low	High	
Number of events	Small	Large	○

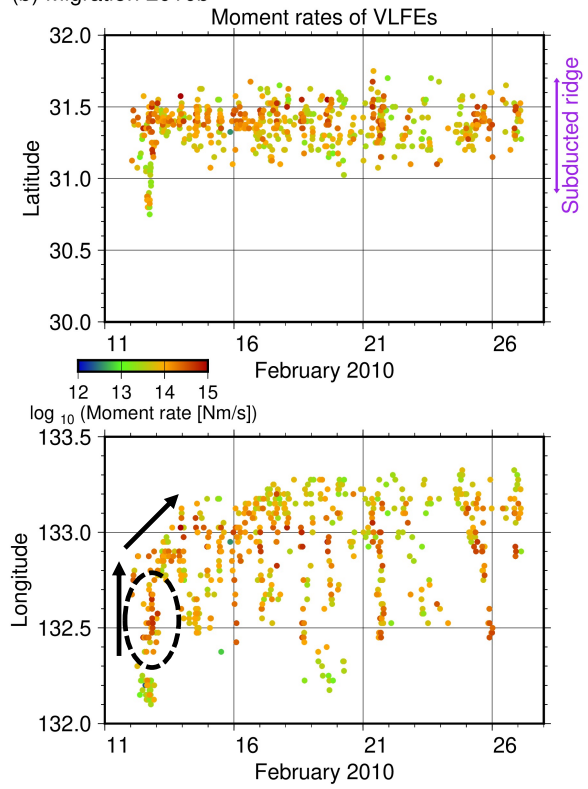
Table 3.3. Difference of slow earthquake activity between south of the subducted ridge and inside of the subducted ridge at a depth of ~ 10 km, and inferences from the observations of slow and repeating earthquakes and physical models.

		South of the subducted ridge	Inside the subducted ridge (depth: ~ 10 km)
Observation	Moment rate and energy		
	rate of an event	Large	Small
	Total moment	Large	Small
	Migration speed	Fast	Slow
	Low velocity area	○ (overriding plate?)	
	Number of events	Small	Large
Inference from repeating earthquakes	Interplate coupling	Weak	Strong
	Patch strength	Strong	Weak
Inference from physical models	Pore pressure on the plate boundary	Low	High
	Effective normal stress	High	Low
	Stress drop	Large	Small
	Radius of a patch	Large	Small
	The ratio of velocity- weakening materials	Large	Small
	a - b at brittle patches	Small	Large

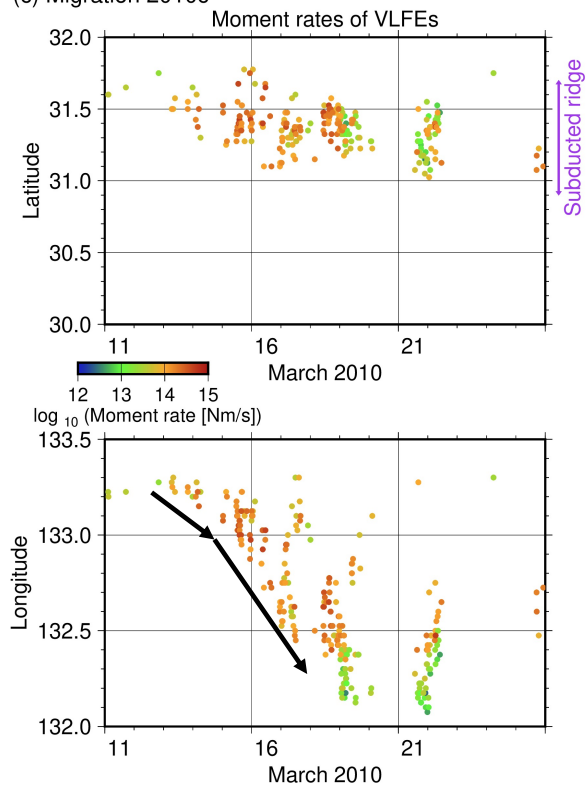
(a) Migration 2010a



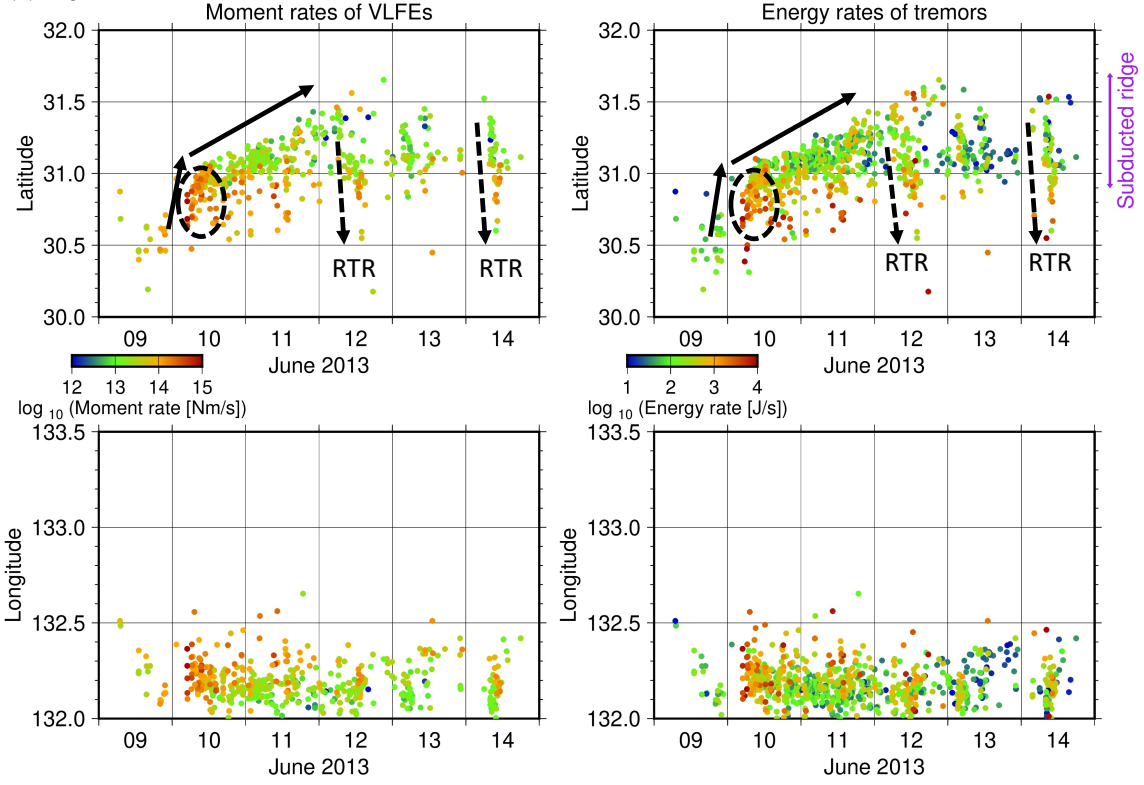
(b) Migration 2010b



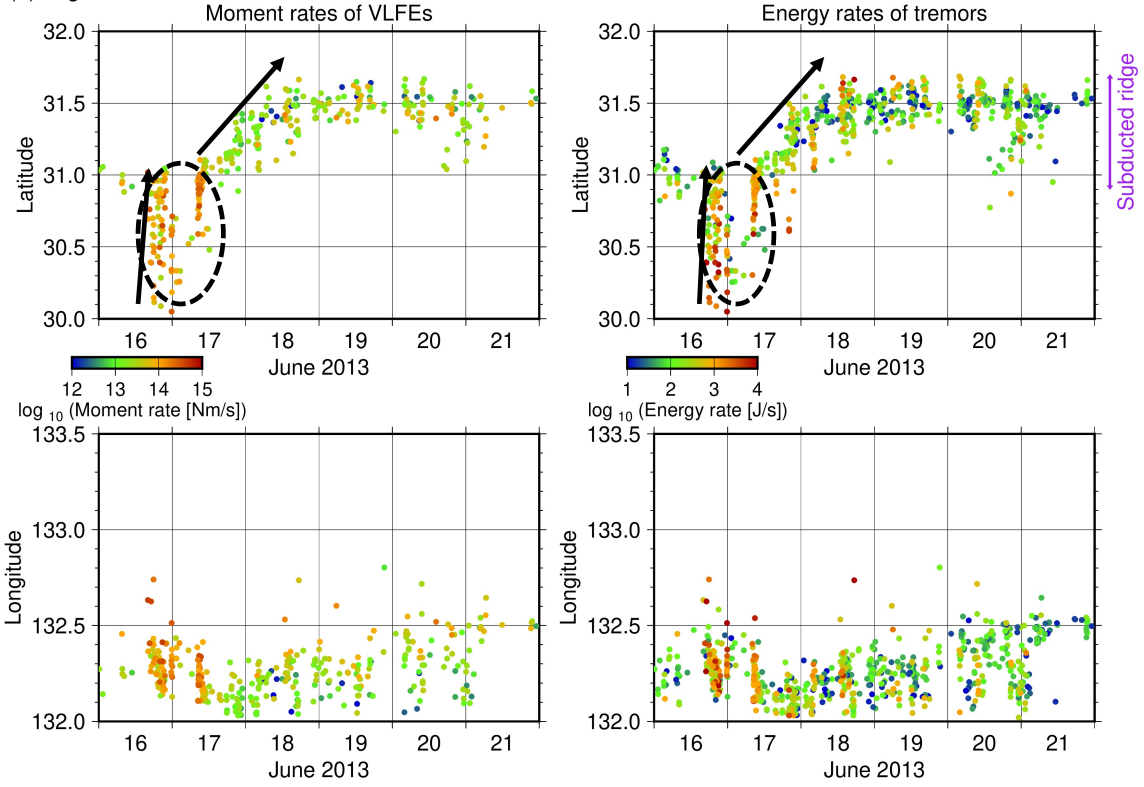
(c) Migration 2010c



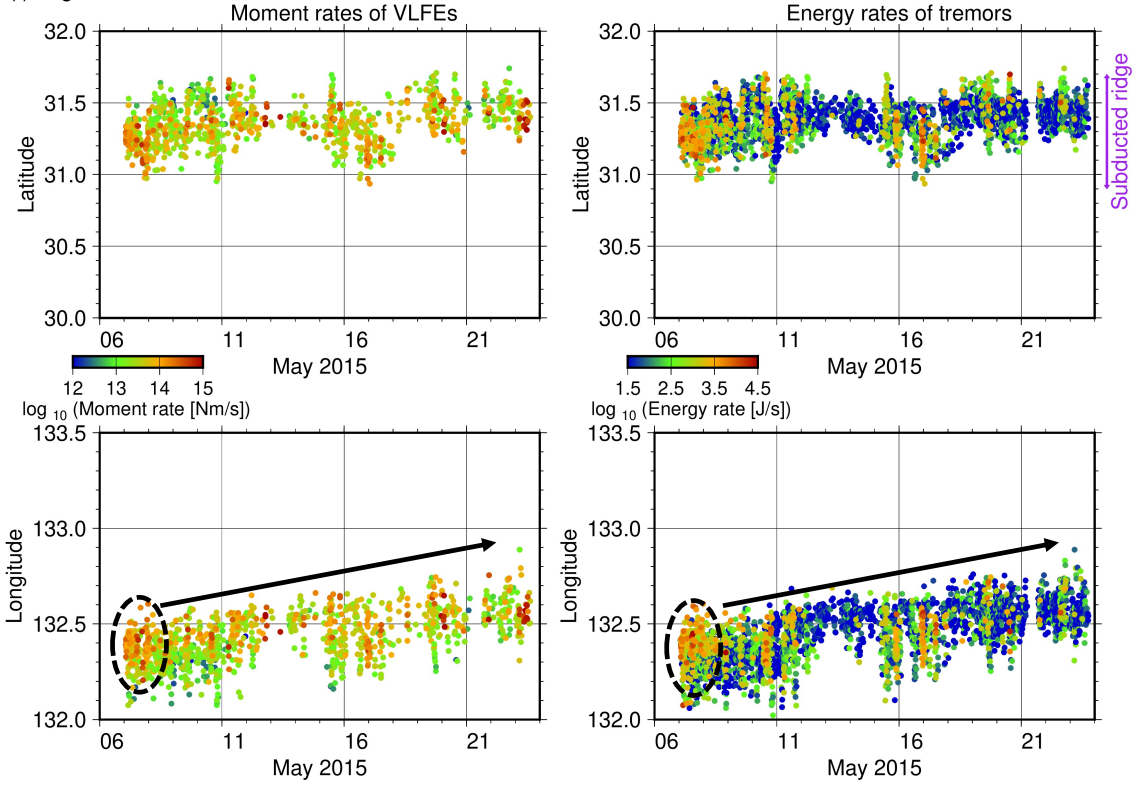
(d) Migration 2013a



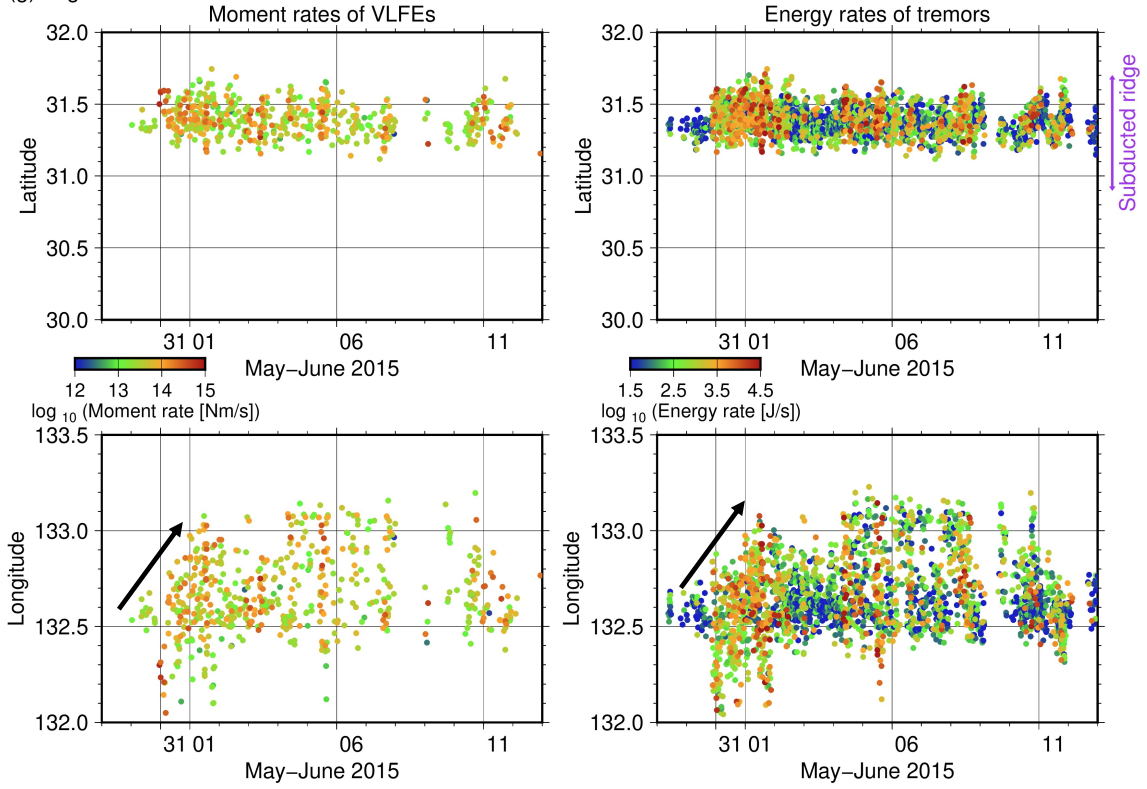
(e) Migration 2013b



(f) Migration 2015a



(g) Migration 2015b



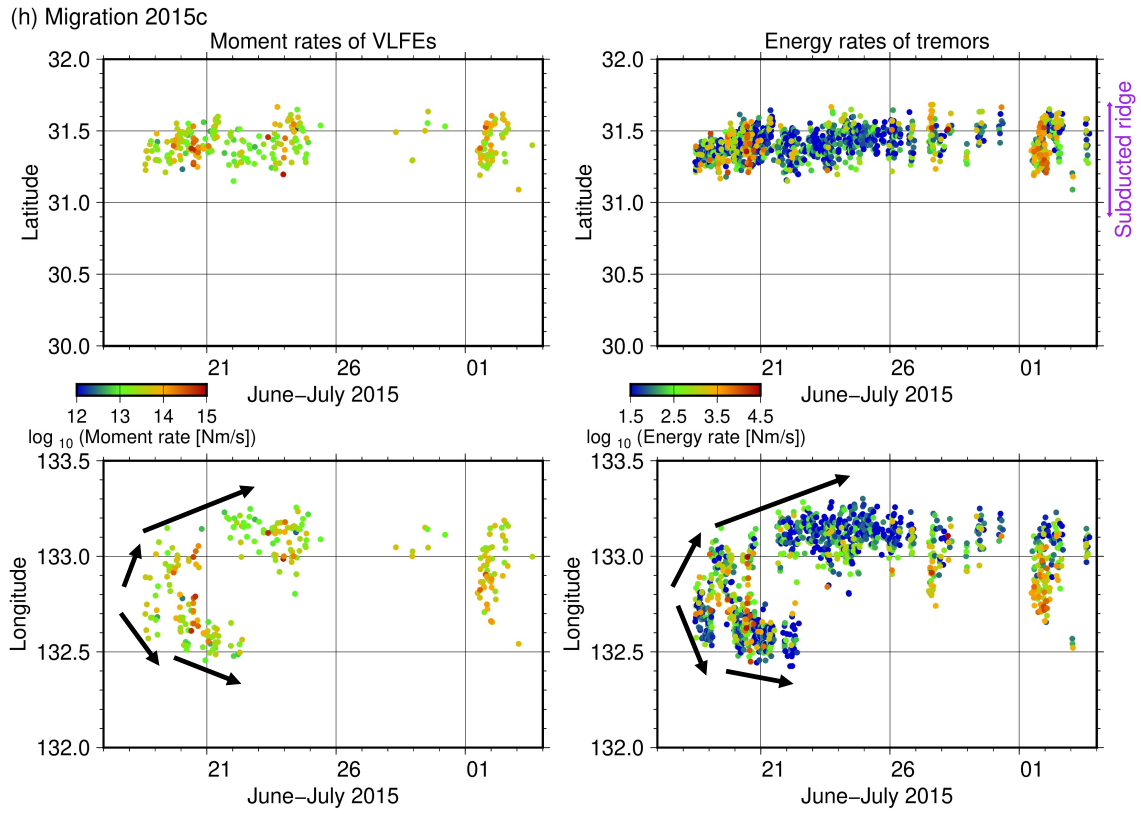


Figure 3.13. Spatiotemporal distributions of moment rates of VLFs and energy rates of tremors in the directions along the N-S and E-W sections for each migration. Black arrows and circles indicate the direction of migrations and the events when a migration starts with large energy rate or moment rate. Black dotted arrows in Figure 3.13d represents the RTR.

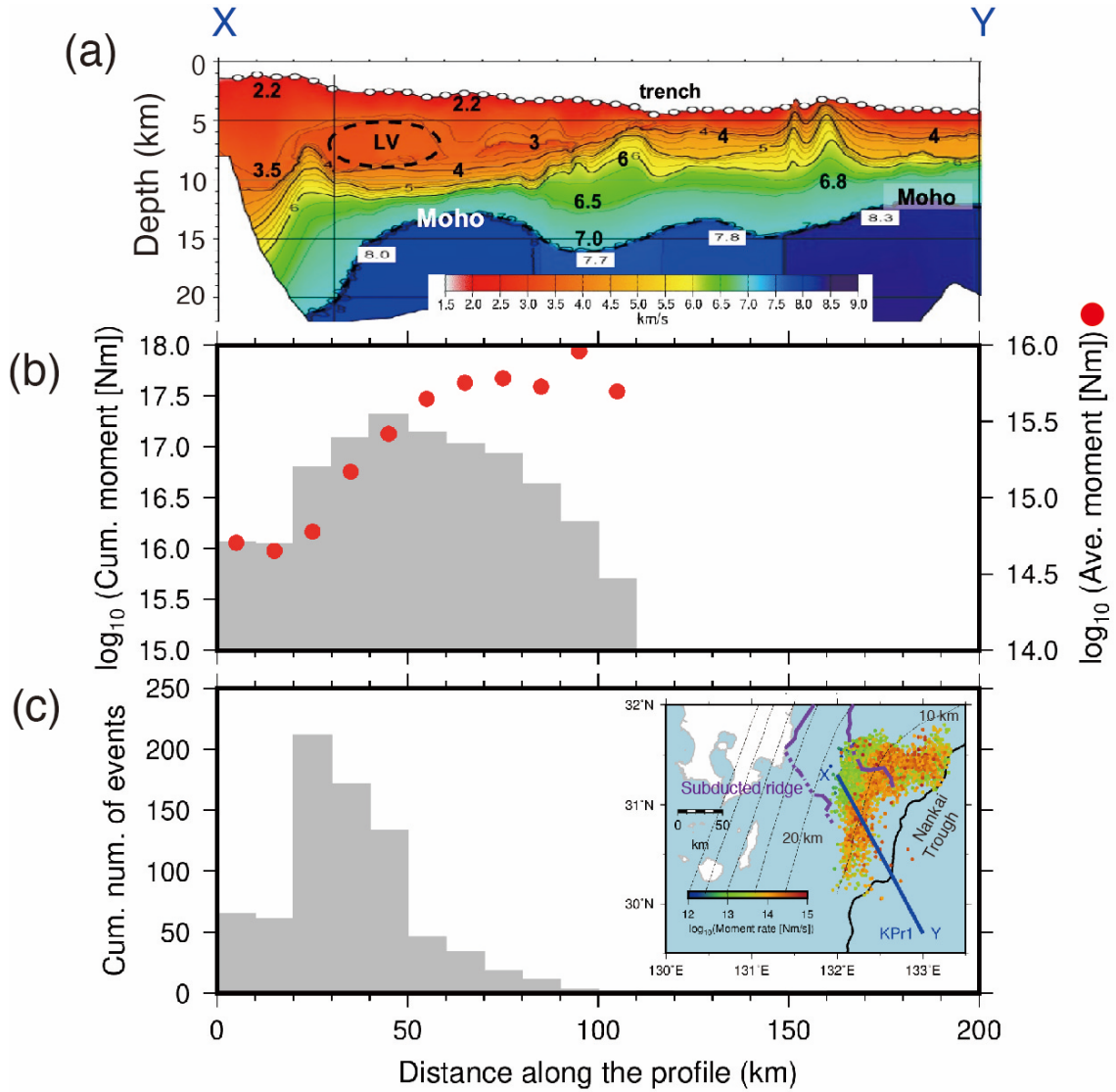


Figure 3.14. (a) *P*-wave structure model along the profile (Nishizawa et al., 2009), (b) histogram of cumulative moment and average moment of VLFs, and (c) number of shallow VLFs at each grid of 10 km \times 10 km in the horizontal directions. Grids are set along the profile and the profile penetrates the center of the ordered grids. The red circles in Figure 3.14b display the average moment of VLFs at each grid. The profile is indicated by a blue line in the map in Figure 3.14c. Purple contour, black line, and dashed contours in the map are the same as displayed in Figure 3.9.

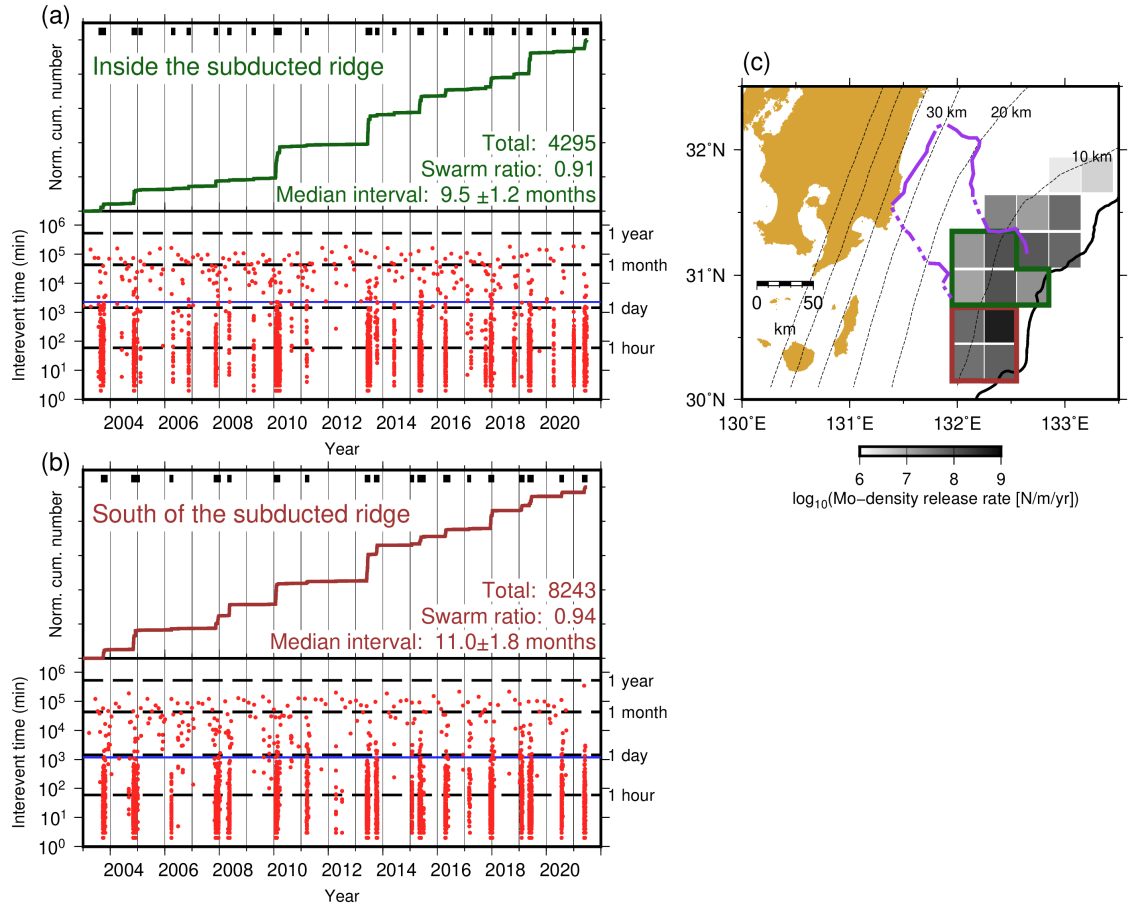


Figure 3.15. Cumulative number of VLFs and temporal variation in interevent time from the former VLFE (a) inside (surrounded by green polygon in Figure 3.15c) and (b) in the south (surrounded by brown square in Figure 3.15c) of the subducted ridge, respectively. Black bars indicate the periods of swarms. Blue line indicates the expected interevent time in each area. The error of median interval is estimated by the standard deviations of the 500 bootstrap samples. (c) The area of The Gray scale represents moment-density release rate of VLFs estimated in Chapter 2. Purple lines are the same as in Figure 3.9. Black line and dashed contours are the same as displayed in Figure 3.4.

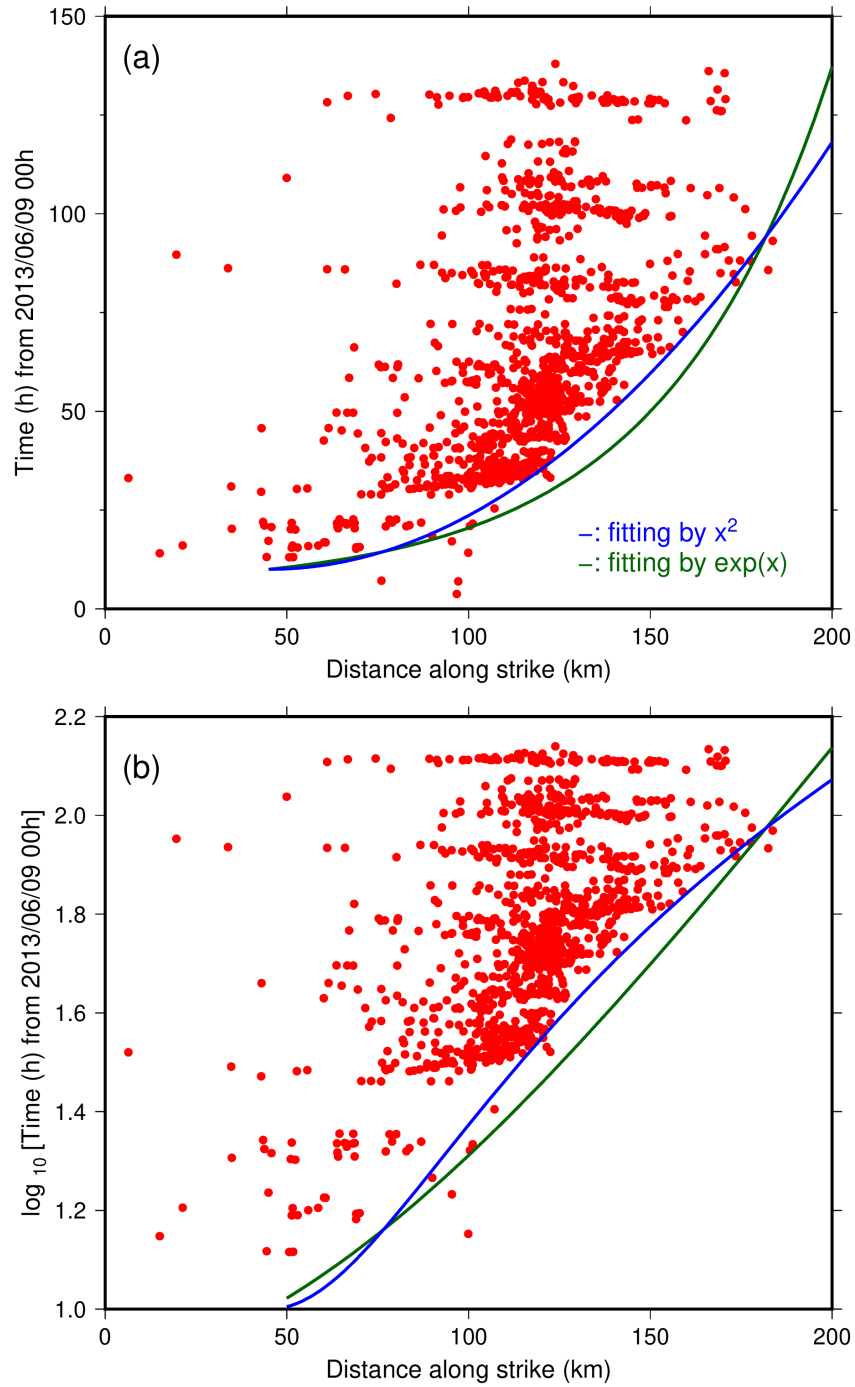


Figure 3.16. (a) Spatiotemporal distribution of tremor migration in the episode of 2013a. Vertical and horizontal axis shows the elapsed time from 2013/06/09 00:00:00 JST, and Distance along the strike (N-S) from 30.0°N, respectively. Blue and green lines indicate the parabolic and exponential curves, respectively. (b) Same as (a) but the vertical axis is log-scale.

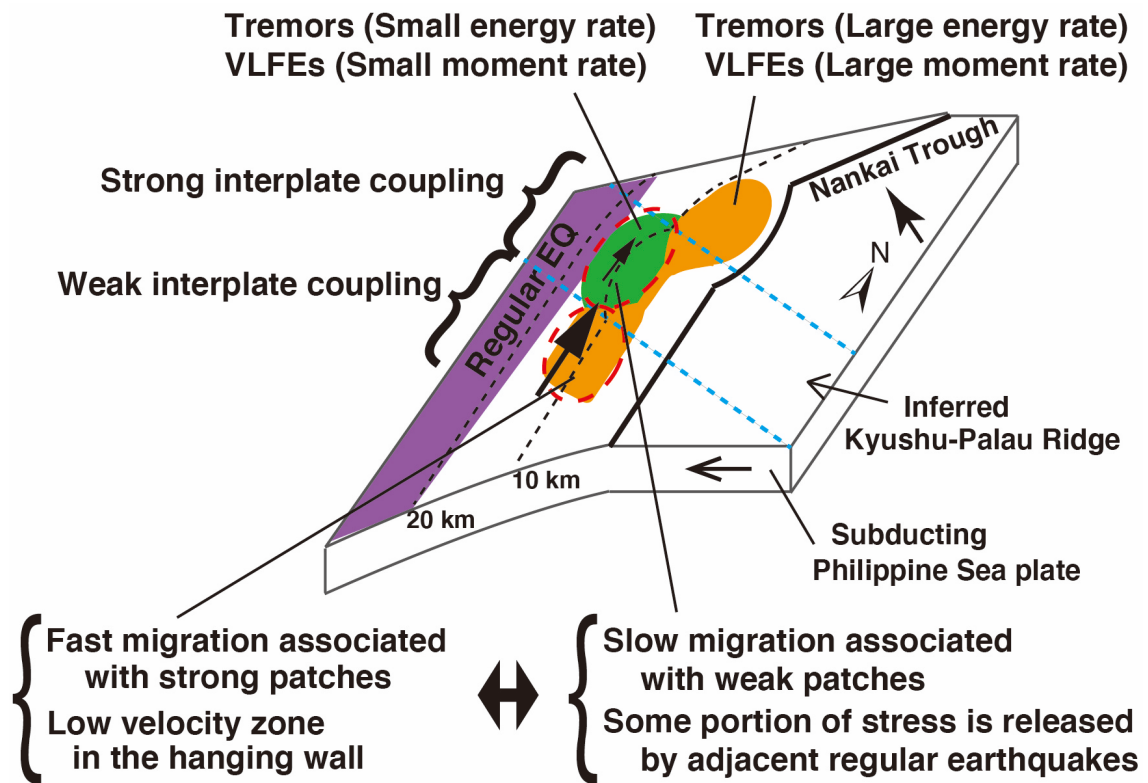


Figure 3.17. Schematic illustration showing the interpretation of distributions of slow earthquakes and Kyushu-Palau Ridge.

3.4.3. Scaled energy of shallow slow earthquakes in Hyuga-nada compared with other slow earthquake regions

The dominant range of energy rates of shallow tremors in Hyuga-nada (10^1 – $10^{4.5}$ J/s) is similar to or smaller than that of the other shallow slow earthquake regions, which predominantly ranges from 10^3 to 10^5 J/s (Yabe et al., 2019; Yabe, Baba, et al., 2021). In contrast, the dominant range of moment rates of shallow VLFs in Hyuga-nada (10^{13} – 10^{15} Nm/s) is larger than that of other shallow slow earthquake regions, where the moment rates of shallow VLFs are distributed in the dominant range of 10^{12} – 10^{14} Nm/s (Nakano et al., 2018; Takemura, Matsuzawa, et al., 2019; Yabe, Baba, et al., 2021). The scaled energy of shallow slow earthquakes in Hyuga-nada is $10^{-12.5}$ – 10^{-10} , which is one to three orders smaller than that of shallow slow earthquakes in other regions along the Nankai Trough except Hyuga-nada (10^{-10} – 10^{-8} ; Yabe et al., 2019; Yabe, Baba, et al., 2021), along the Japan Trench (10^{-10} – 10^{-9} ; Yabe, Baba, et al., 2021), and in Costa Rica (10^{-9} – 10^{-8} ; Baba et al., 2021), or that of deep slow earthquakes in southwest Japan, Cascadia, and Mexico ($10^{-9.5}$ – 10^{-9} ; Ide, 2016; Ide & Maury, 2018; Ide & Yabe, 2014; Figure 3.18).

The difference in scaled energy of slow earthquakes between Hyuga-nada and other regions is a difference in relative intensity between high-frequency (2–8 Hz) and low-frequency (0.02–0.05 Hz) radiation during the rupture of slow earthquakes. Numerical studies (Dunham et al., 2011) and spectral analysis of kinematic fault models of regular earthquakes (e.g., Graves & Pitarka, 2016; Mai & Beroza, 2002) suggested that the complicated slip history and the relative intensity between low- and high-frequency ranges in observed seismograms are controlled by fault zone heterogeneities (e.g., fault roughness or scattering of seismic waves). According to these studies and our results, I consider that the spectral feature of fault zone heterogeneity for shallow slow earthquakes in Hyuga-nada is different from other slow earthquake regions. Seafloor explorations and detailed geophysical surveys in the future may contribute toward the investigation of the difference between scaled energies of shallow slow earthquakes.

Ide (2008) and Ide & Maury (2018) discussed the theoretical relationship between seismic energy and seismic moment of slow earthquakes by the Brownian slow earthquake model. In their model, the characteristic size of the slip area S is described by:

$$S = Cr^2 \quad (3.10)$$

where r is a random variable and C is a constant. The temporal change of r is described by:

$$dr = -\alpha r dt + \sigma dB \quad (3.11)$$

where α is the characteristic frequency, dB is the random variable of Gaussian distribution with the mean 0 and the variance 1, σ is the fluctuation magnitude. Ide & Maury (2018) discussed that the energy rate divided by the square of the moment rate depends on α :

$$\frac{E[E_{rate}]}{E[M_{rate}]^2} = \frac{4\alpha}{5\pi\rho V_s^5 \Delta t} \quad (3.12)$$

where ρ is the density, V_s is the S -wave velocity, and Δt is the time steps of the stochastic process. $E[E_{rate}]$ and $E[M_{rate}]$ indicates the long-term averages of energy rates and moment rates, respectively.

The energy rate divided by the square of the moment rate estimated from seismic signals is in the range of 10^{-26} – 10^{-23} in Hyuga-nada. This value is estimated as 10^{-22} – 10^{-20} by stacked very low frequency signals in deep southwest Japan, Cascadia, and Mexico (Ide & Maury, 2018). Off the Kii Peninsula, this value estimated from the energy rates of tremors and moment rates of VLEFs by Yabe et al. (2019) is also 10^{-22} – 10^{-20} . Therefore, there is a one to six orders difference between the ratio in Hyuga-nada and in other slow earthquake regions. If ρ , V_s , and Δt are the same as the assumption in Ide & Maury (2018), the range of α^{-1} , which represents the characteristic time, is 300–300000 s in Hyuga-nada, whereas 0.3–30 s in other slow earthquake regions. The range of α^{-1} of SSE scale in deep southwest Japan, Cascadia, and Mexico evaluated in Ide & Maury (2018) is 75–300 s. Thus, the range of α^{-1} in Hyuga-nada is longer than that in other slow earthquake regions. However, the uncertainty of the energy rates is nearly one order (see Section 3.3). If the uncertainty with one order is considered, the lower limit of α^{-1} in Hyuga-nada is comparable to that in other regions. Although the range of scaled energy in Hyuga-nada is smaller than that in other slow earthquake regions, the Brownian slow earthquake model cannot be denied by considering the uncertainty of the estimated energy rate in Hyuga-nada.

Although there is a possibility that events with small maximum amplitude and long duration due to the large α^{-1} were not detected in Hyuga-nada, I will discuss the relationship between amplitudes and durations of tremors based on the Brownian slow earthquake model. The model by Ide (2008) explained the observation that the relationship between cumulative duration and reduced displacement of deep tremors in southwest Japan can be explained by an exponential law (Watanabe et al., 2007). Cumulative duration is the duration when the reduced amplitude is larger than an

amplitude threshold. The reduced amplitude u is defined by (Ide, 2008; Watanabe et al., 2007):

$$u = \frac{Ad}{2\sqrt{2}} \quad (3.13)$$

where, A is root-mean-square displacement with 6 s time window in a frequency range of 2–8 Hz and d is the distance between tremor source to the station. I investigated the relationship between cumulative duration and reduced displacement of shallow tremors in Hyuga-nada (Figure 3.19). The relationship seems to be better explained by an exponential law than a power law like Ide (2008) and Watanabe et al. (2007). Possibly, the relationship between cumulative duration and reduced displacement is explained by the model by Ide (2008) as for the detected events in Hyuga-nada.

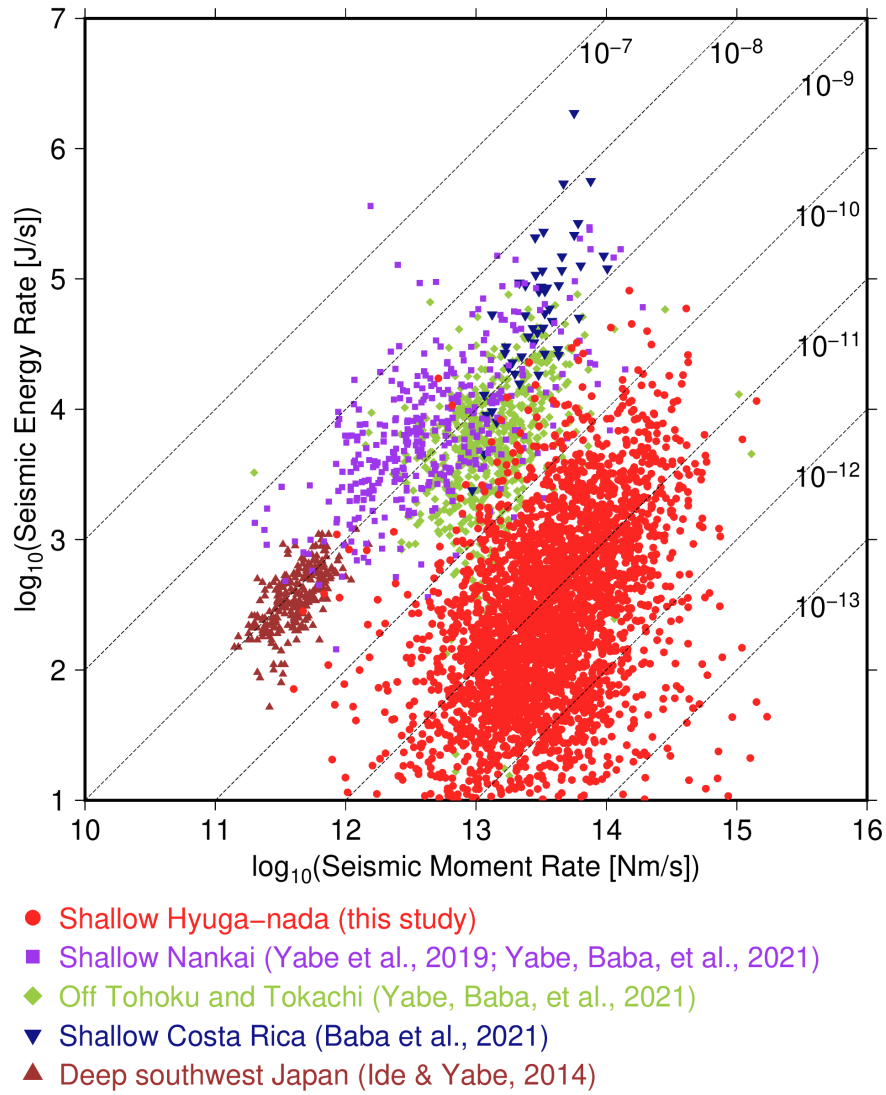


Figure 3.18. Relationship between seismic moment rates of VLFs and seismic moment rates of tremors. Red circles, purple squares, green diamonds, dark blue inverted triangles, and dark blue triangles indicate the relationships between seismic moment rates of VLFs and seismic moment rates of tremors in shallow Hyuga-nada (this study), shallow Nankai except Hyuga-nada (Yabe et al., 2019; Yabe, Baba, et al., 2021), off Tohoku and Tokachi (Yabe, Baba, et al., 2021), shallow Costa Rica (Baba et al., 2021), and deep slow earthquakes (Ide and Yabe, 2014; Ide, 2016; Ide and Maury, 2018). Dashed lines represent scaled energies of 10^{-7} , 10^{-8} , 10^{-9} , 10^{-10} , 10^{-11} , and 10^{-12} . It is noted that scaled energies of shallow slow earthquakes were estimated for individual events, whereas those of deep slow earthquakes were estimated for stacked events.

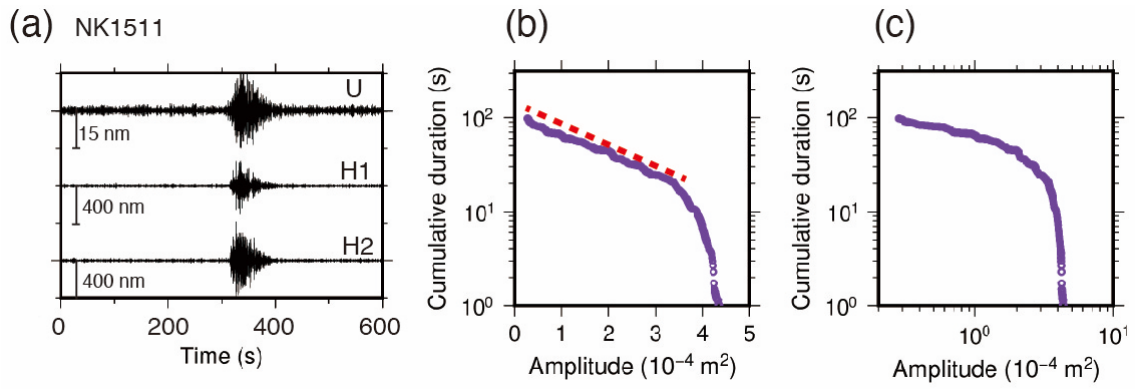


Figure 3.19. (a) Waveform of a tremor located at 132.3752°E, 31.2186°N by Yamashita et al. (2021) in a frequency range of 2–8 Hz. Horizontal axis is the elapsed time from 2015/05/07, 02:00:00JST. (b) Example of a comparison between reduced amplitude threshold and cumulative duration of a tremor of Figure 3.19a shown by a log-linear plot. (c) Same as (b) but shown by a log-log plot.

3.5. Summary of this chapter

To investigate the spatial variation in shallow slow earthquakes in Hyuga-nada at a higher resolution than in Chapter 2, and further reveal the factors that control the spatial variation in slow earthquake activity, I estimated the energy rates of shallow tremors, moment rates of shallow VLFs, and scaled energy of shallow slow earthquakes in Hyuga-nada. The dominant ranges of energy rates of tremors, moment rates of VLFs, and scaled energy are 10^1 – $10^{4.5}$ J/s, 10^{13} – 10^{15} Nm/s, $10^{-12.5}$ – 10^{-10} , respectively. The scaled energy of slow earthquakes in Hyuga-nada is 1–3 orders smaller than that of other slow earthquake regions; therefore, the characteristics of the fault zone of slow earthquakes may be different in Hyuga-nada from other slow earthquake regions. Based on the model by Ide & Maury (2008) and Ide (2008), the difference in scaled energy may be attributed to the characteristic frequency α .

The energy rates of tremors and moment rates of VLFs are larger outside the subducted ridge than inside the ridge, although there is an area with larger events in the updip part of the inside of the subducted ridge in 2015. The cumulative moment of the VLFs exhibits the same tendency. Although the interplate coupling in Hyuga-nada is generally weaker than in other slow earthquake regions (Chapter 2), there is a heterogeneity of interplate coupling at the local scale of Hyuga-nada. The interplate coupling inferred from slip rates by repeating earthquakes is weak and strong in the south and inside the subducted ridge, respectively; therefore, a negative correlation exists between shallow slow earthquake activity and interplate coupling in Hyuga-nada. This tendency is the same as observed in the regional analysis around Japan, as demonstrated in Chapter 2.

The migration of tremors and VLFs along the strike direction at a depth of ~ 10 km starts in the south of the subducted ridge with events of larger energy and moment rates. After entering the area of the subducted ridge, the migration speed slows, and the energy rates of tremors and moment rates of VLFs were observed to be small (Figure 3.17). This tendency is consistent with the model of Ando et al. (2012) and observations by Kano, Kato, et al. (2018). Based on their model, the south of the subducted ridge and inside the ridge corresponds to strong and weak patch areas, respectively, and the observed low velocity anomaly may exist above the strong patch area. In the strong patch area, the fluids infiltrate the overriding plate, and the fluid pressure on the plate boundary is lower; therefore, the effective normal stress is higher than in the weak patch area. The

tremor migration pattern in 2013 can be fitted by a parabolic function. If a circular crack model is assumed, the stress drop of VLFs in the south (strong patch) of and inside (weak patch) the subducted ridge is $\sim 8 \times 10^3$ Pa and $\sim 2 \times 10^3$ Pa, respectively. The approximately four times difference in stress drop of strong and weak patches can be sufficient to generate parabolic migration pattern and the migration pattern can be explained by the effect of Newtonian rheology in the ductile background (Ando et al., 2012).

Although the interplate coupling is suggested to be stronger inside the ridge, the strength of the patches inferred from the model by Ando et al. (2012) can be weaker. Interplate regular earthquakes occur close to the slow earthquake area inside the subducted ridge, whereas the area with interplate regular earthquakes is apart from the slow earthquake area in the south of the ridge. I interpreted that some portion of the accumulated stress in the slow earthquake area may be released by adjacent regular earthquakes inside the ridge, thus the interplate coupling inside the ridge is stronger. On the other hand, most of the accumulated stress is released by slow earthquakes in the south of the ridge, where the interplate coupling is suggested to be weaker.

3.6. Extension of discussion in Hyuga-nada to the other slow earthquake regions around Japan

Based on the observations and inference of shallow slow earthquakes in Hyuga-nada, weak patches with low effective normal stress exists in strongly coupled regions on a regional scale. In contrast, strong patches with a high effective normal stress exists in weakly coupled regions. The former and latter are inside and south of the subducted ridge, respectively. The cumulative moment released by the VLFs was larger in the latter.

In Nankai (off Cape Muroto, off the southern Kii, and off the southeastern Kii), the number of events is smaller than in Hyuga-nada. In addition, based on the intervals of successive swarms, the effective normal stress on the plate boundary may be lower in Hyuga-nada than in Nankai (Section 2.4.2). These characteristics suggest that the strength of patches in Nankai is stronger than that in Hyuga-nada (Table 3.4). In contrast, the moment rate of a VLF is larger in Hyuga-nada than in Nankai. As the scaled energy is quite different in the two regions, the energy of a tremor is similar or slightly smaller in Hyuga-nada than in Nankai. The difference in scaled energy may be related to the variation in a - b . Hence, it is difficult to clarify whether the strength of patches in Nankai is stronger than in Hyuga-nada.

By comparing the slow earthquake activity off Tokachi and along the Nankai Trough, the interval of swarms of VLFs off Tokachi is shorter than in Nankai and in Hyuga-nada; therefore, the effective normal stress off Tokachi may be lower. The number of VLFs off Tokachi is similar to that in Hyuga-nada and larger than that in Nankai. The moment rate is similar to that in Nankai and smaller than that in Hyuga-nada (Table 3.4). Based on these results, the strength of the patches off Tokachi may be weaker than those in Nankai and Hyuga-nada. However, the 2003 Tokachi-Oki earthquake occurred in the first year of the analysis period, and many VLFs can be promoted by the afterslip of the earthquake. Most VLFs off Tohoku can also be activated by the afterslip of the 2011 Tohoku earthquake. Thus, it is difficult to compare slow earthquake activity along the Japan and Kuril Trenches and along the Nankai Trough.

Table 3.4. Comparison of shallow slow earthquake activity around Japan. The median interval of swarms and expected effective normal stress does not defined off Tohoku because most of VLFEs off Tohoku is promoted by the afterslip of the 2011 Tohoku earthquake.

	Hyuga-nada	Nankai	Off Tohoku	Off Tokachi
Moment rate of a VLFE (Nm/s)	$10^{13} - 10^{15}$	$10^{12} - 10^{14}$	$10^{12.5} - 10^{13}$	$10^{12.5} - 10^{14}$
Energy rate of a tremor (J/s)	$10^1 - 10^{4.5}$	$10^3 - 10^5$	$10^{2.5} - 10^{4.5}$	$10^{2.5} - 10^5$
Scaled energy	$10^{-12.5} - 10^{-10}$	$10^{-10} - 10^{-8}$	$10^{-10} - 10^{-9}$	$10^{-10} - 10^{-9}$
Mo-density release rate of VLFEs (N/m/year)	$10^6 - 10^{8.5}$	$10^{5.5} - 10^7$	$10^5 - 10^{6.5}$	$10^{5.5} - 10^{7.5}$
Interplate coupling	Weak	Strong	Strong	Strong
Number of events	Large	Medium	Small	Large
Median interval of VLFE swarms	8 months	2-4 years	-	3 months
Expected effective normal stress	Medium	High	-	Low

4. Conclusions

In this study, I aim to reveal the factors that control the spatiotemporal variations in slow earthquake activity on the plate boundary. For this purpose, the spatiotemporal characteristics of VLFE activity around Japan was investigated on a regional scale in Chapter 2. I detected VLFES and quantified their spatiotemporal distribution by introducing moment-density release rate and swarm ratio around Japan (Figure 4.1). This is the first study that quantified spatiotemporal variation in VLFE activity around Japanese islands by a uniform method. The spatiotemporal variation in slow earthquake activity was more heterogeneous in the shallower part than in the deeper part. In space, the heterogeneity of the moment-density release rate of VLFES is much stronger in the shallower part, which can be related to interplate coupling. Generally, shallow VLFE activity is low in strongly coupled areas. Furthermore, VLFES are often active in low seismic velocity anomalies that may be developed by fluids. Thus, fluids can potentially activate VLFES.

Temporal variations in VLFE activities are categorized into three patterns: activation after a large earthquake, quiescence after a large earthquake, and repetition of swarm activities and quiescence. VLFES often increase after large earthquakes around their coseismic slip areas; therefore, VLFE activity reflects the spatiotemporal evolution of the afterslip of large earthquakes. The relationship between VLFE activity and interplate coupling or afterslips of large earthquakes indicates that VLFE activity can be an indicator of the stress state on the plate boundary. For the repetition of swarm activities and quiescence, the swarm ratio is generally larger than that of deep VLFES, and the intervals of swarms in shallow VLFES vary from 8 months to 4 years (Figure 4.1). Based on previous simulation or structural studies, the variations in the intervals of VLFE swarms may be related to the spatial heterogeneities of the effective normal stress on the plate boundary.

In Chapter 2, the VLFE activity in Hyuga-nada is notably active. To reveal the factors that control the spatial variation in slow earthquake activity in Hyuga-nada, a detailed analysis was conducted, as described in Chapter 3. The spatial variation in shallow slow earthquakes was investigated in Hyuga-nada at a higher resolution than described in Chapter 2. Generally, energy rates of tremors and moment rates of VLFES are larger outside the subducted ridge than inside the ridge. The scaled energy of slow earthquakes in Hyuga-nada is one to three orders smaller than that of other slow

earthquake regions (Figure 4.1). Based on the model by Ide (2008) and Ide & Maury (2018), the difference in characteristic frequency may be the factor of the difference in the scaled energy. The negative correlation between interplate coupling and VLFE activity can be further observed inside the Hyuga-nada region, although interplate coupling in Hyuga-nada is suggested to be generally weaker than in other slow earthquake regions. The migration of tremors and VLFs in the along-strike direction starts in the south of the ridge with large energy rates and moment rates and slows after entering the area of the subducted ridge. This tendency is explained by the models of Ando et al. (2012) and Kano, Kato, et al. (2018). Based on their model, the south of the subducted ridge and the inside of the ridge corresponds to strong and weak patches, respectively. In the strong patch area, the fluids infiltrate the overriding plate, and the fluid pressure on the plate boundary is lower; therefore, the effective normal stress is higher than in the weak patch area. By assuming the circular crack model, the stress drop of VLFs in strong and weak patch areas is evaluated as $\sim 8 \times 10^3$ Pa and $\sim 2 \times 10^3$ Pa, respectively. The approximately four times difference in stress drop between strong and weak patches along the strike direction in Hyuga-nada is sufficient to generate parabolic migration pattern, which is modeled by the effect of Newtonian rheology in the ductile background. Inside the ridge, the strength of the patches is suggested to be weaker although the interplate coupling is inferred to be stronger than in the south of the subducted ridge. Some portions of the accumulated stress of the slow earthquake area inside the ridge may be released by adjacent interplate regular earthquakes. In Chapter 3, I revealed the spatial distribution of sizes of tremors and VLFs in Hyuga-nada, suggested that the heterogeneity of stress drop of VLFs is significant enough to cause the parabolic migration pattern, and discussed the variation in the style of stress release on the plate boundary.

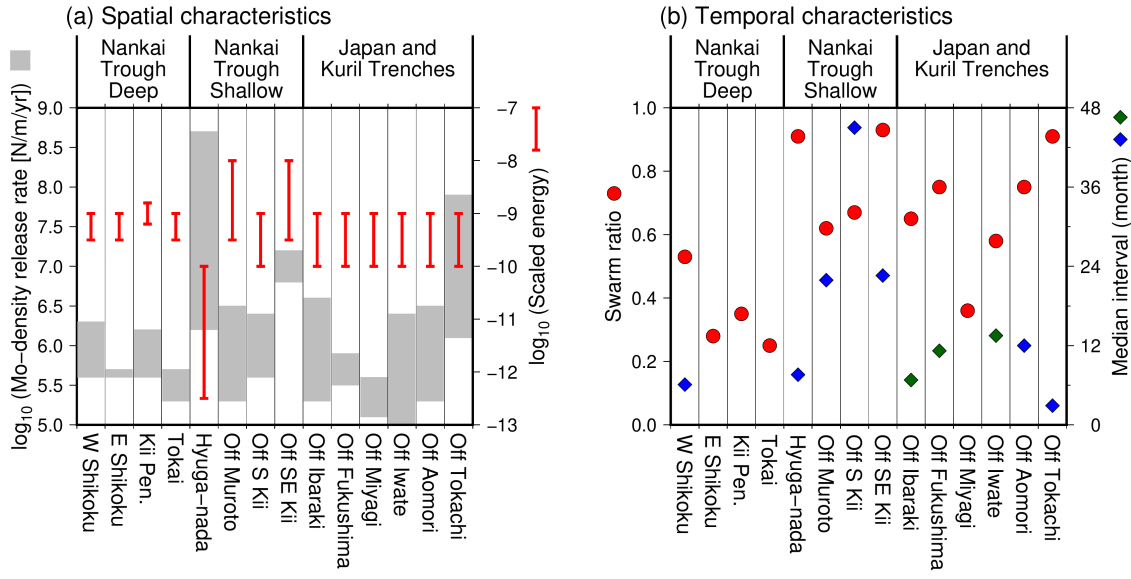


Figure 4.1. (a) Spatial and (b) temporal characteristics of VLFE activities. (a) The range of moment-density release rate of VLFEs and scaled energy of slow earthquakes around Japan. The ranges of slow earthquakes except Hyuga-nada is referred from Ide and Yabe (2014: deep slow earthquakes), Yabe et al. (2019: off the southeastern Kii), and Yabe, Baba, et al. (2021: slow earthquakes in northeast Japan, off the southern Kii, and off Cape Muroto). (b) Same as Figure 2.17.

5. Future works

Ide (2010) demonstrated that tremor activity is modulated by tidal stress. Kano, Kato, et al. (2018) suggested a relationship between the strength of deep tremor patches and tidal sensitivity along the Nankai Trough. The relationship between slow earthquake activity and tidal sensitivity should be investigated in slow earthquake regions. However, tremors of the migration fronts are less sensitive to tidal stress (Houston, 2015; Yabe et al., 2015); therefore, tremor catalogs with a higher resolution are necessary to define the events of the migration front. To compare the relationship between the strength of slow earthquake patches and the tidal sensitivity in various slow earthquake regions, the catalogs of slow earthquakes with a higher resolution and with many episodes are needed.

In Hyuga-nada, an offshore network of seismometers, Nankai Trough Seafloor Observation Network for Earthquakes and Tsunamis, will be deployed in the future. Although the energy rates of shallow tremors in only two tremor episodes were evaluated in this study, monitoring of shallow slow earthquake activity will be possible using the N-net. The location and estimation of energy of tremors in many tremor episodes may provide new insights into the shallow tremor activity in Hyuga-nada.

Finally, I propose explorations in offshore slow earthquake regions in more detail. Audet and Bürgmann (2014) suggested a positive correlation between the V_p/V_s ratio in the hanging wall and the recurrence intervals of ETSSs. To investigate this relationship in various offshore slow earthquake regions, an investigation of the seismic velocity structure (especially V_s and V_p/V_s ratio) is required in offshore regions. In addition, to clarify the cause of the difference in the scaled energy between Hyuga-nada and other slow earthquake regions, the investigation of the heterogeneity of the plate boundary in these regions may be helpful. This is because the difference in fault roughness may be related to the variation in the scaled energy. Heterogeneity may be revealed by explorations of the topography of the seafloor near the trench axis.

Acknowledgments

First, I would like to express my best appreciation to my supervisor, Professor Kazushige Obara for his constant advice, various support, and discussions for the six years of my study. I would like to express my deepest appreciation to Assistant Professors Shunsuke Takemura and Akiko Takeo for discussions and comments which occurred every week. Additionally, I would like to express my gratitude to Professor Takuto Maeda, Professor Geoffrey A. Abers, Professor Masanao Shinohara, Dr. Takanori Matsuzawa, Dr. Akemi Noda, Dr. Ryo Kurihara, Assistant Professor Yusuke Yamashita, Assistant Professor Masayuki Kano, Dr. Suguru Yabe, and Dr. Yusaku Tanaka for helpful discussions. I would like to thank the thesis committee (Associate Professor Ryosuke Ando, Professor Aitaro Kato, Professor Satoshi Ide, Associate Professor Asuka Yamaguchi, and Professor Shoichi Yoshioka) for reviewing this thesis. The members of the Obara laboratory and the seismogenic zone physical properties and structure seminar provided me with a lot of constructive comments. I appreciate all the professors, researchers, staffs, and students at the University of Tokyo.

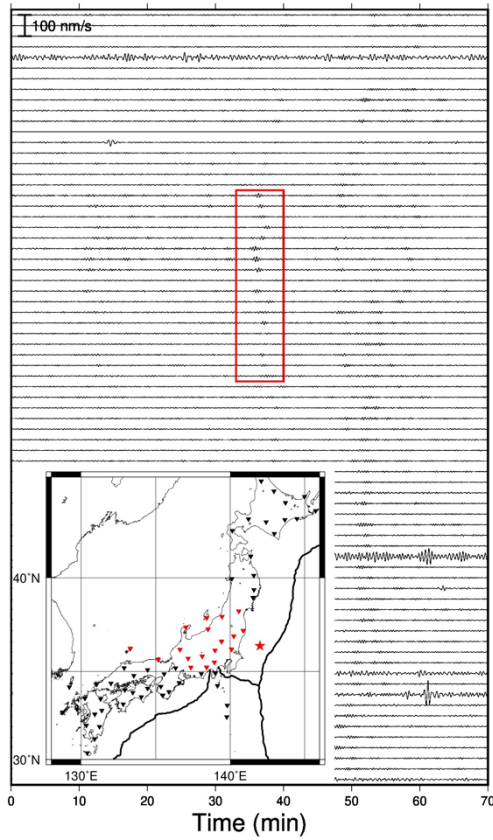
I would like to thank Associate Professor Naoki Uchida, Dr. Takeshi Iinuma, and Dr. Shinzaburo Ozawa for providing the distribution of interplate slip data off the Pacific coasts of Hokkaido and Tohoku, the coseismic slip and afterslip distribution data of the Tohoku earthquake, and the afterslip distribution data of the Tohoku earthquake, respectively. I would also like to thank Associate Professor Chihiro Hashimoto, Dr. Akemi Noda, Dr. Ryoichiro Agata for providing the slip-deficit rate distributions. I duly appreciate Dr. Nishizawa for providing the distribution of seismic velocity structures along the profiles in Hyuga-nada. I also appreciate Assistant Professor Yusuke Yamashita for providing the catalog of shallow tremors and repeating earthquakes in Hyuga-nada; and Dr. Youichi Asano for providing the catalog of VLFs in Hyuga-nada.

The coseismic slip data of the 1944 Tonankai earthquake by Kikuchi et al. (2003), the 1946 Nankai earthquake by Tanioka and Satake (2001), and the 2003 Tokachi-Oki earthquake by Yagi (2004) were obtained from the Finite-Source Rupture Model Database (Mai & Thingbaijam, 2014; <http://equake-rc.info/SRCMOD/>). The VLFE catalog detected by Matsuzawa et al. (2015) and Takemura, Matsuzawa, et al. (2019), the tremor catalog detected by Obara et al. (2010), and the SSE catalog detected by Takagi et al. (2019) were obtained from the Slow Earthquake Database (Kano, Aso, et al., 2018; <http://www-solid.eps.s.u-tokyo.ac.jp/~sloweql/>). Generic mapping tools

(Wessel et al., 2013) and the Seismic Analysis Code (Helfrich et al., 2013) were used to prepare the figures and process seismograms, respectively. The temporal seismological observations in Hyuga-nada were conducted as part of "Research project for compound disaster mitigation on the great earthquakes and tsunamis around the Nankai Trough region," a project of Ministry of Education, Culture, Sports, Science and Technology. F-net broadband seismograms (<http://www.fnet.bosai.go.jp>) from the National Research Institute for Earth and Disaster Resilience (2019) were used. OpenSWPC code Version 5.0.2 (Maeda et al., 2017) was utilized for the numerical simulations. Numerical simulations were conducted using the Fujitsu PRIMERGY CX600M1/CX1640M1 (Oakforest-PACS) at the Information Technology Center, the University of Tokyo. This study was supported by ERI JURP 2021-S-B102, providing computational resources for calculating synthetic waveforms. I used the earthquake catalog of the United States Geological Survey (<https://earthquake.usgs.gov>) and the Japan Meteorological Agency (<http://www.jma.go.jp>). This research was supported by JSPS KAKENHI Grant Number JP16H06473 in Scientific Research on Innovative Areas "Science of Slow Earthquakes," and Grant Number JP17H05414, and JSPS Research Fellowship DC1 (JP19J20760).

Appendix

(a)



(b)

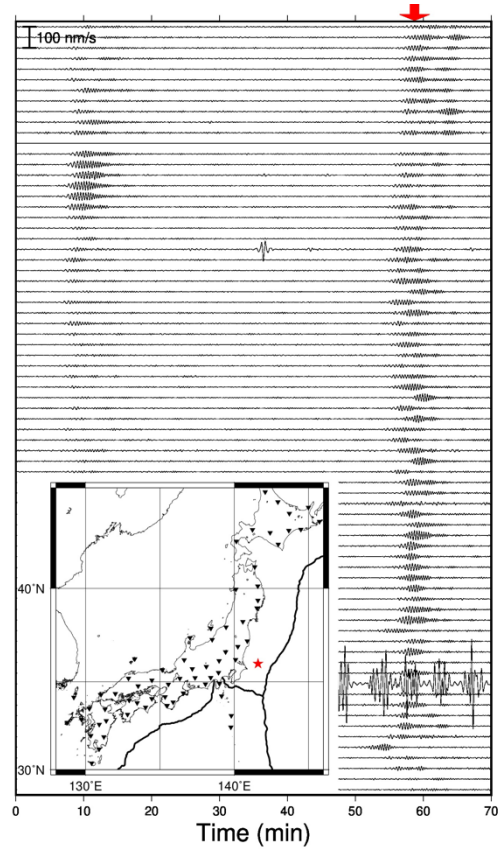


Figure A1. (a) Example of waveforms of a VLFE at 142.0°E and 36.4°N for an event with a time of origin 1:34:44 JST on June 17, 2011. Data were filtered with a frequency range of 0.02–0.05 Hz. The red box shows the VLFE signals. The horizontal axis shows the elapsed time from 1:00:00 JST. Waveforms are plotted from north to south in vertical components. The black inverted triangles and black lines in the inset are the same as in Figure 1.3. The red inverted triangles show the location of F-net stations whose waveforms are shown in the red box. The red star shows the virtual source where the VLFE was detected. (b) Example of waveforms with false detection by teleseismic events at 141.6°E and 36.0°N detected at 10:56:52 JST on May 21, 2017 and filtered with a frequency range of 0.02–0.05 Hz. The red arrow shows the detected teleseismic event signals. The waveform order is the same as displayed in Figure 2.6a. Inverted triangles and black lines in the inset are the same as displayed in Figure 1.3. The red star shows a falsely located source due to a teleseismic event.

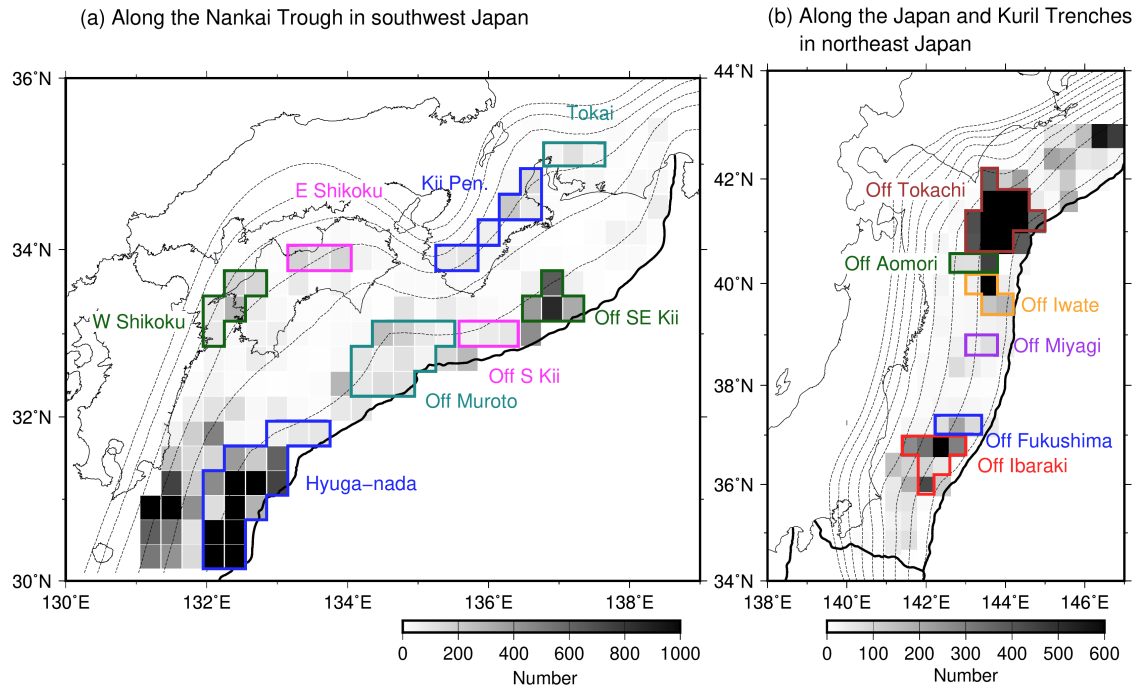


Figure A2. Distribution of number of VLFs (a) along the Nankai Trough in southwest Japan and (b) along the Japan and Kuril trenches in northeast Japan. Dashed contours indicate the isodepths of the top of (a) the Philippine Sea plate (Koketsu et al., 2012) and (b) the Pacific plate with a 10-km interval (along the Japan Trench: Nakajima and Hasegawa, 2006; Nakajima et al., 2009; along the Kuril Trench: Kita et al., 2010). The black lines in Figures 1.3a and 1.3b represent Nankai Trough and Japan and Kuril Trenches, respectively.

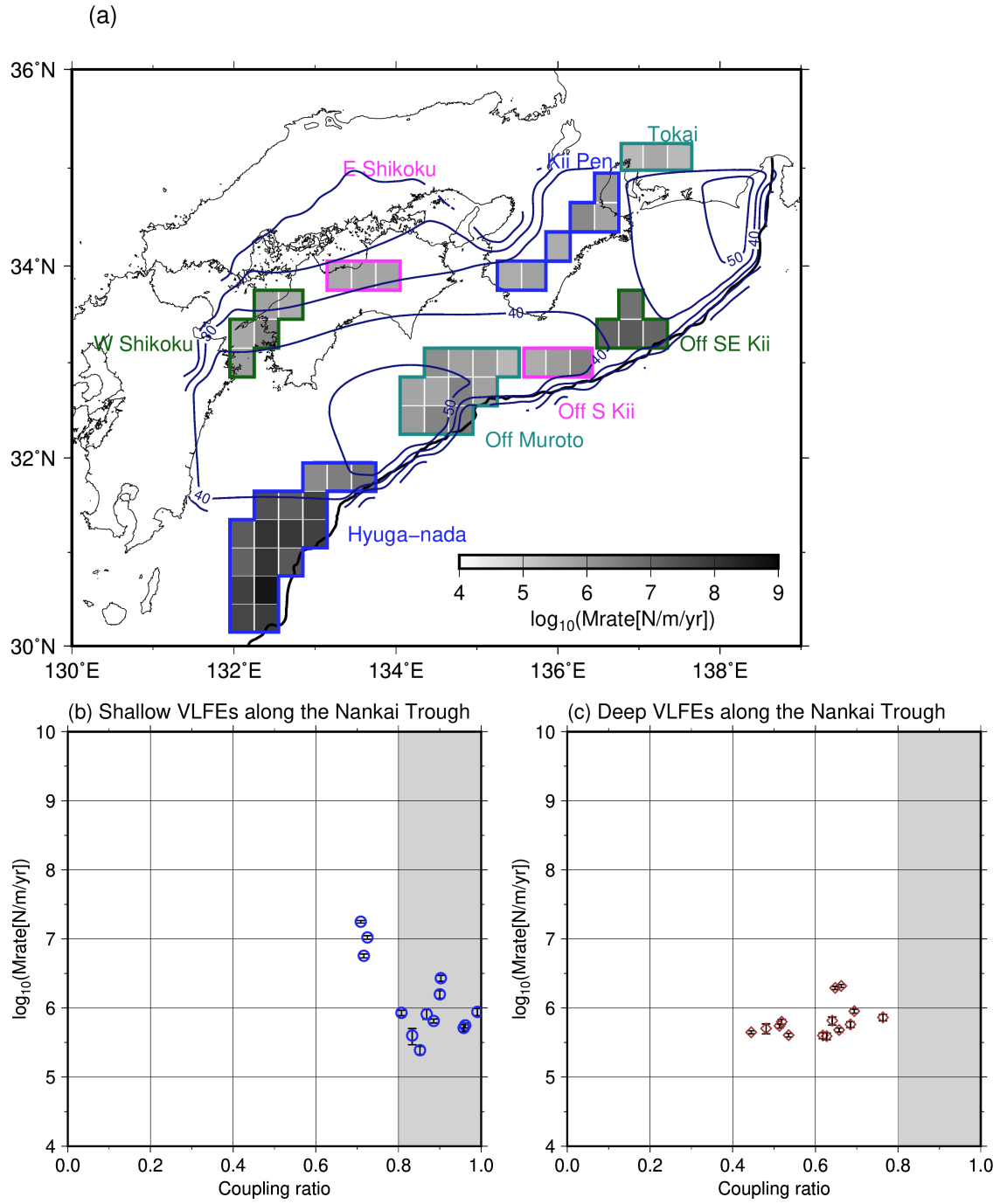
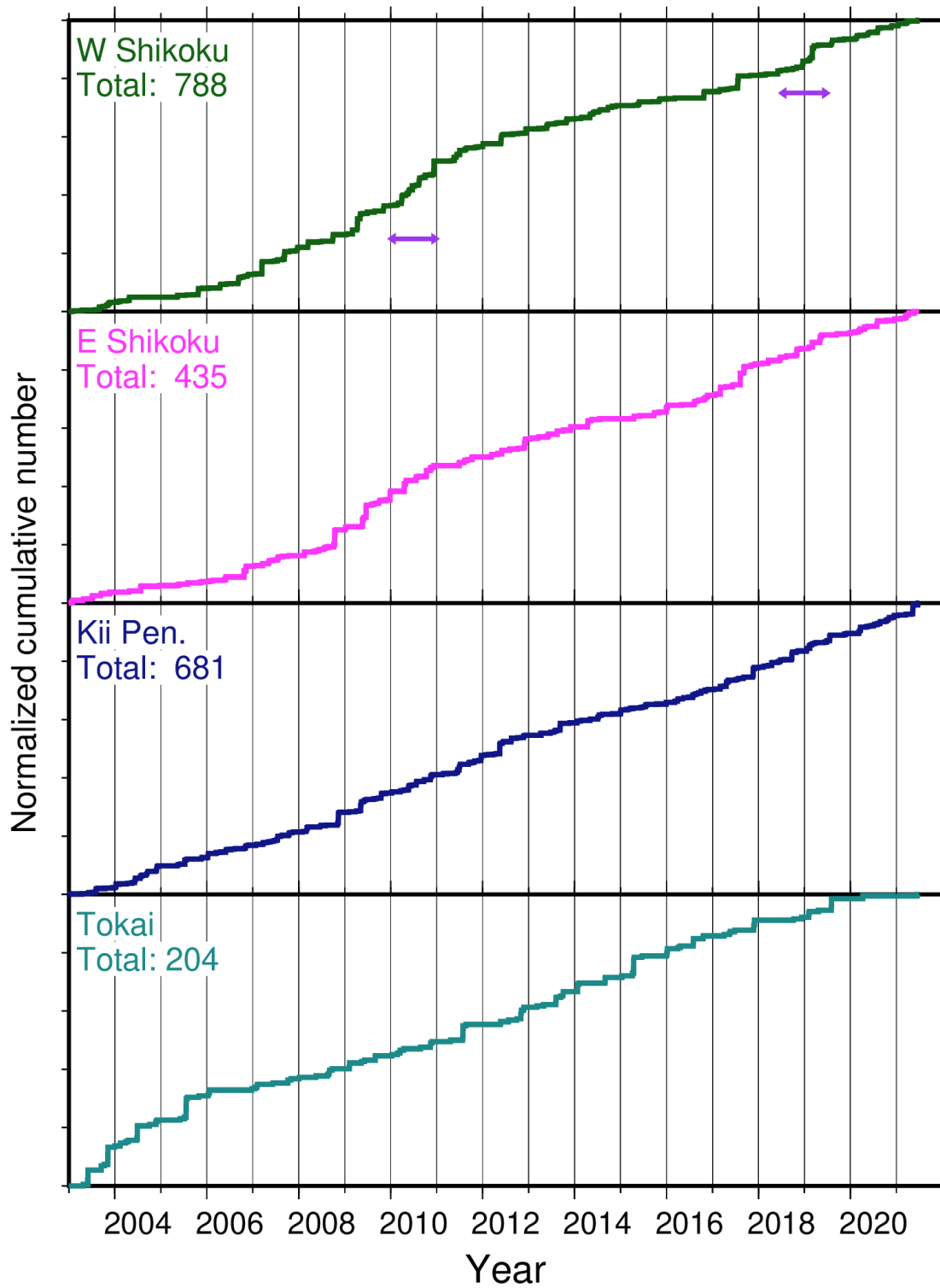
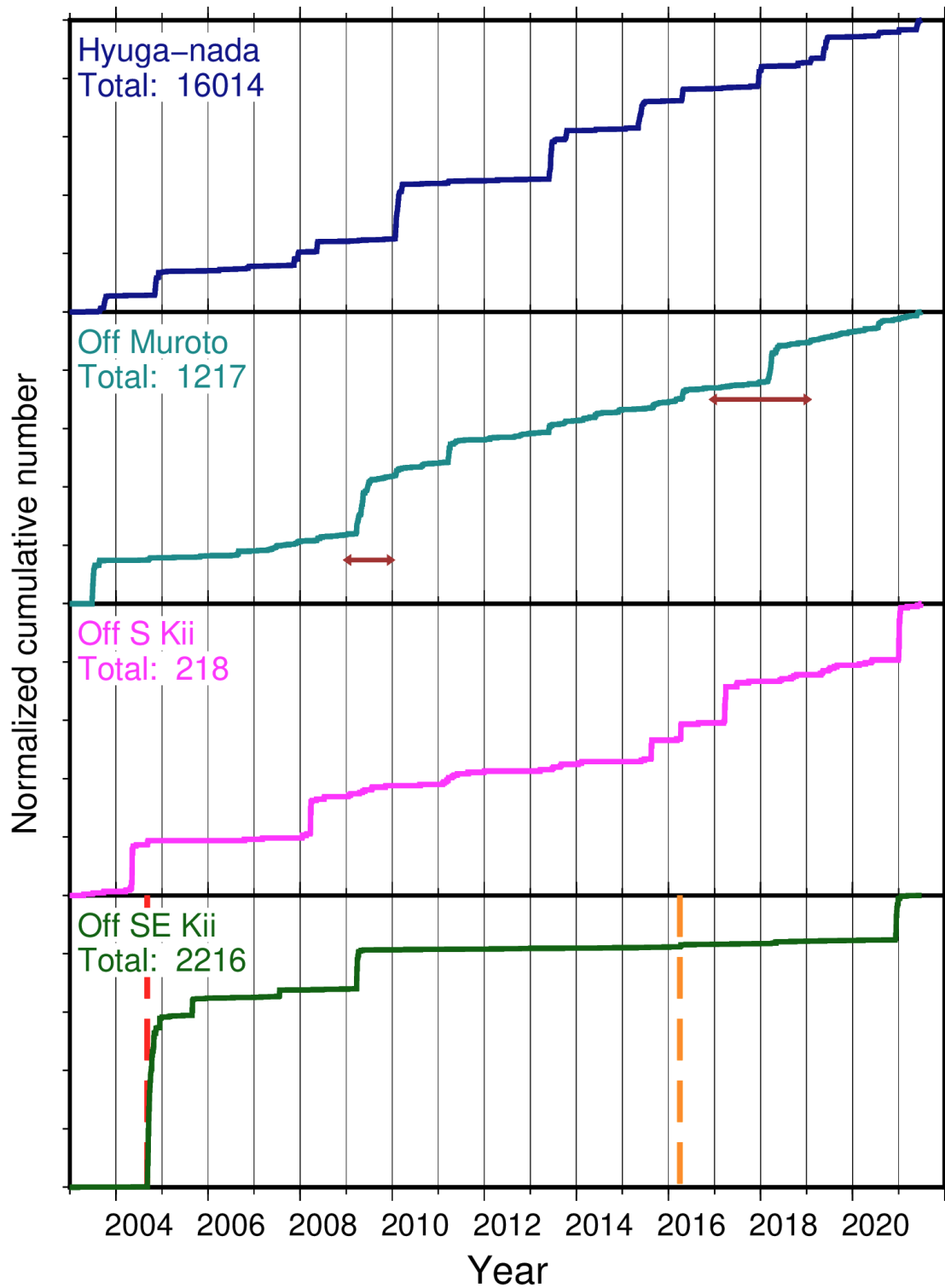


Figure A3. (a) Same as Figure 2.6a but the slip-deficit rate distribution estimated by Agata (2020) with a 10 mm/year interval (analysis period: 2005-2009). (b) Same as Figure 2.8a but the coupling ratio estimated from the slip-deficit rate by Agata (2020). (c) Same as Figure 2.8b but the coupling ratio estimated from the slip-deficit rate by Agata (2020).

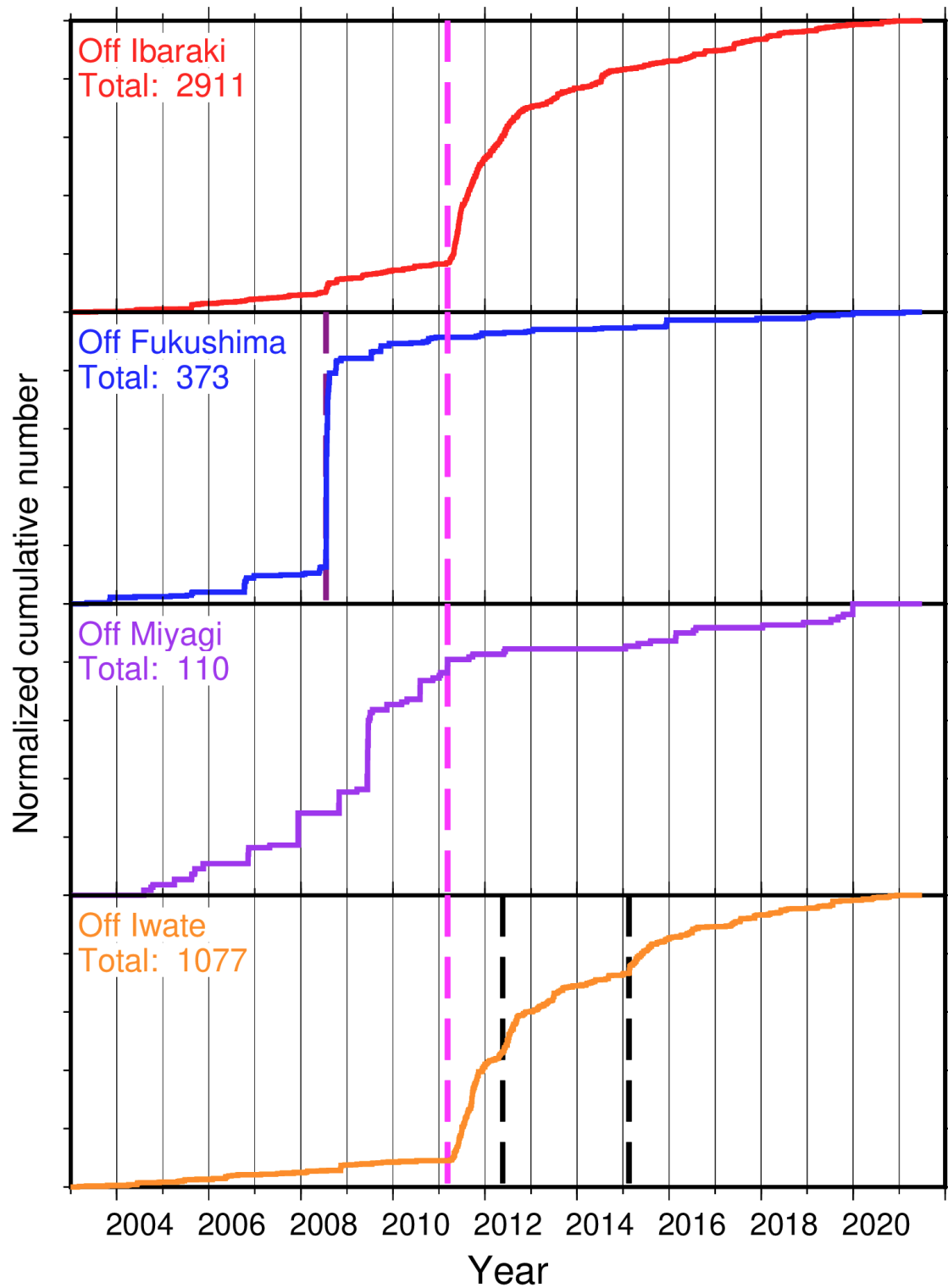
(a) Deep VLFES along the Nankai Trough



(b) Shallow VLFES along the Nankai Trough



(c) VLFEs along the Japan and Kuril Trenches



(c) continued

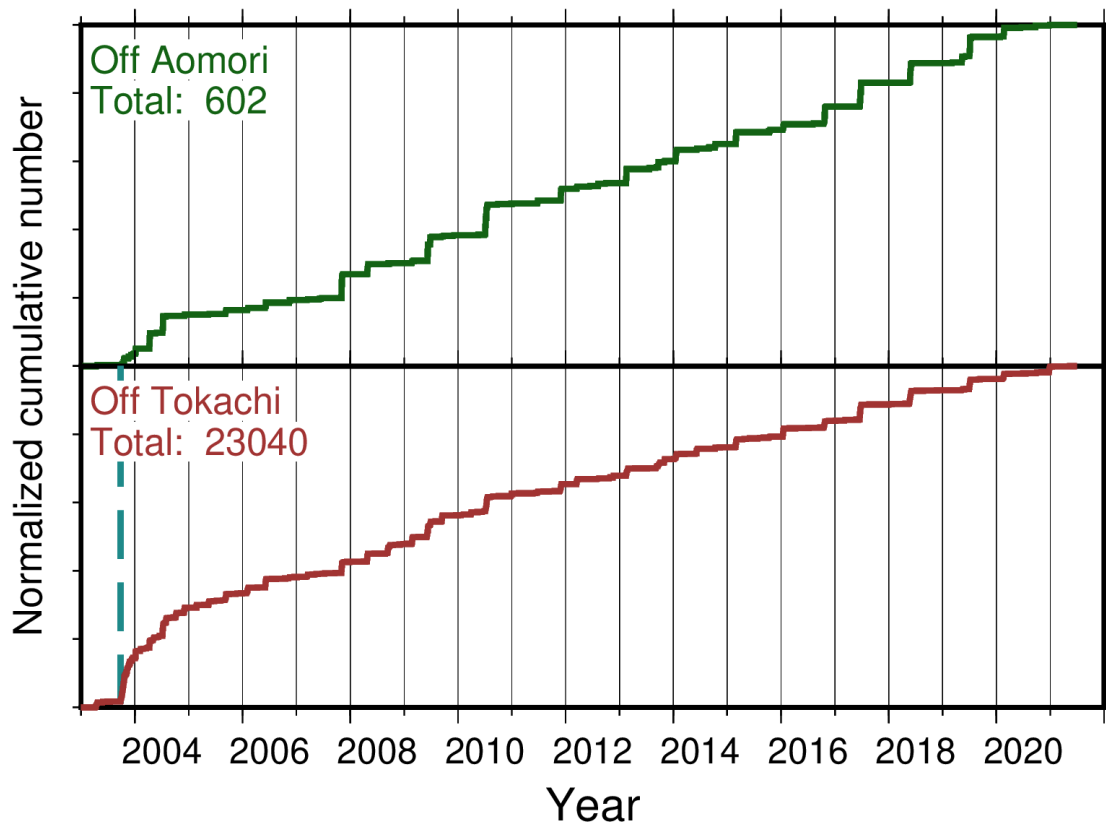
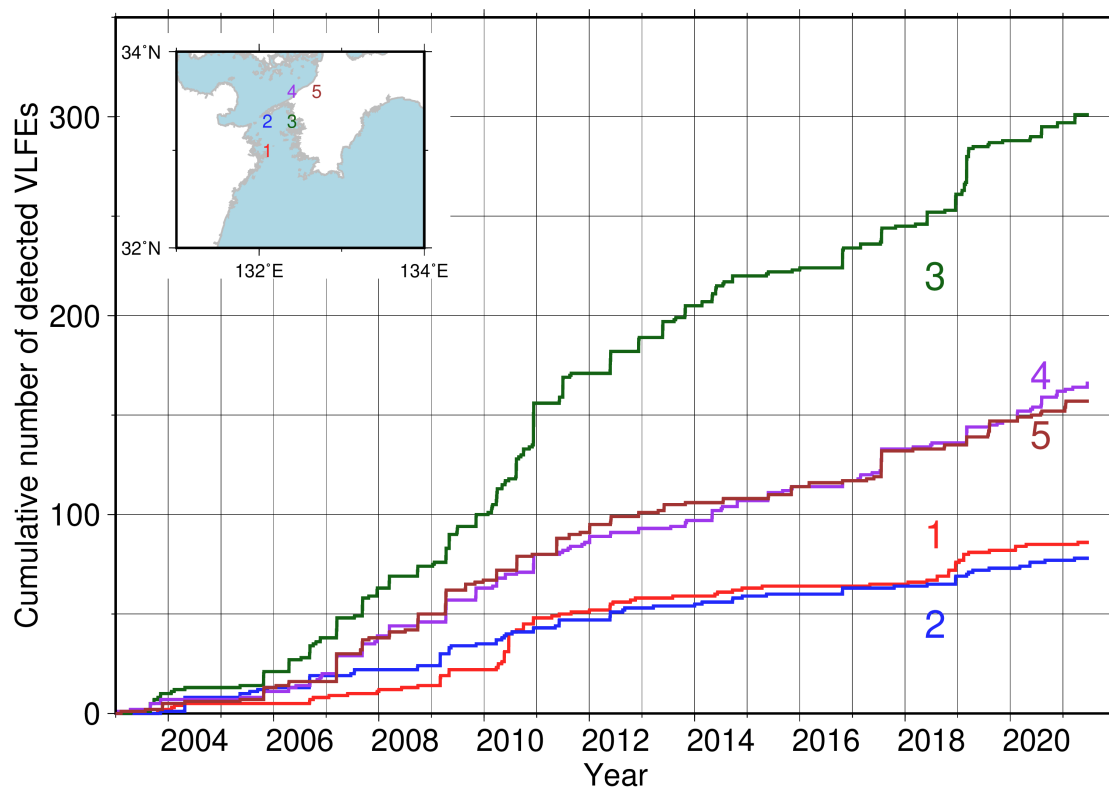
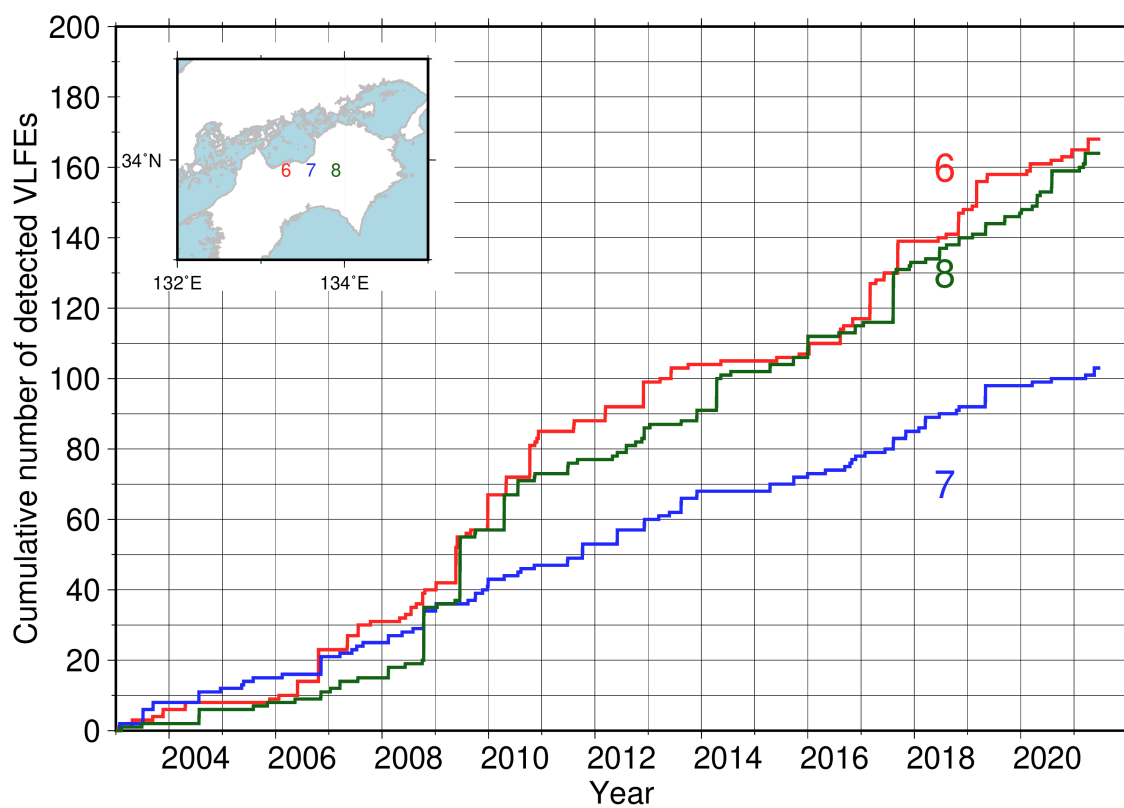


Figure A4. Cumulative number normalized by the total amount in the analysis period in (a) deep VLFs along the Nankai Trough in southwest Japan, (b) shallow VLFs along the Nankai Trough in southwest Japan, and (c) shallow VLFs along the Japan and Kuril trenches in northeast Japan. Horizontal purple and brown arrows in Figures 2c and 2d indicate the periods of SSEs in the Bungo channel (Ozawa, 2017) and off the Kii channel (Yokota & Ishikawa, 2020), respectively. Blue, red, purple, pink, orange, and black dashed vertical lines show the time of the following earthquakes: the 2003 Tokachi-Oki, the 2004 off the Kii Peninsula, the 2008 Fukushima-Oki, the 2011 Tohoku, the 2016 off southeastern Mie Prefecture, and the Tohoku earthquake aftershocks which activated VLFs off Iwate respectively.

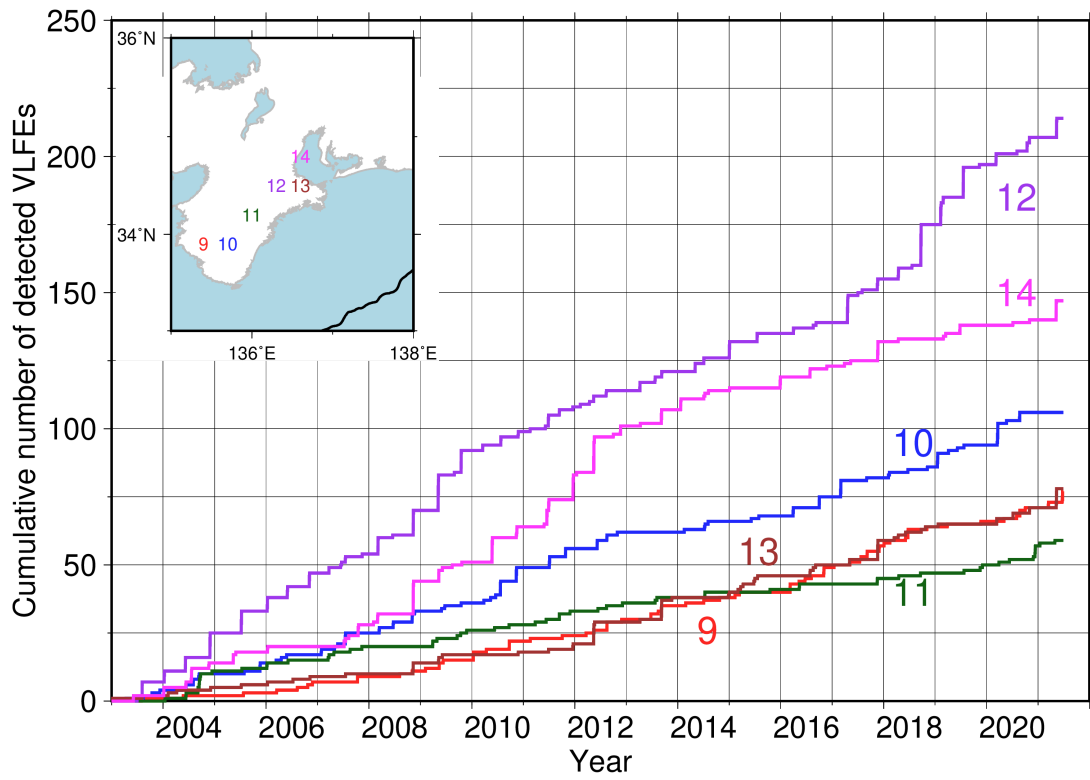
(a) Deep VLFs in Western Shikoku



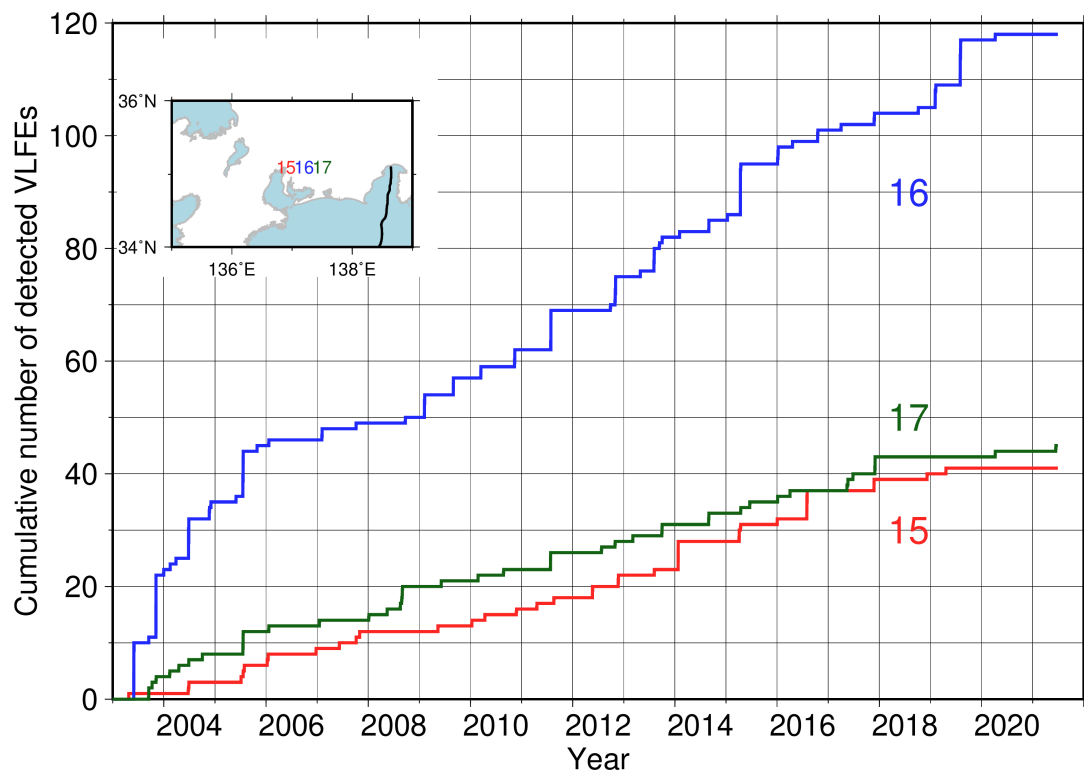
(b) Deep VLFs in Eastern Shikoku



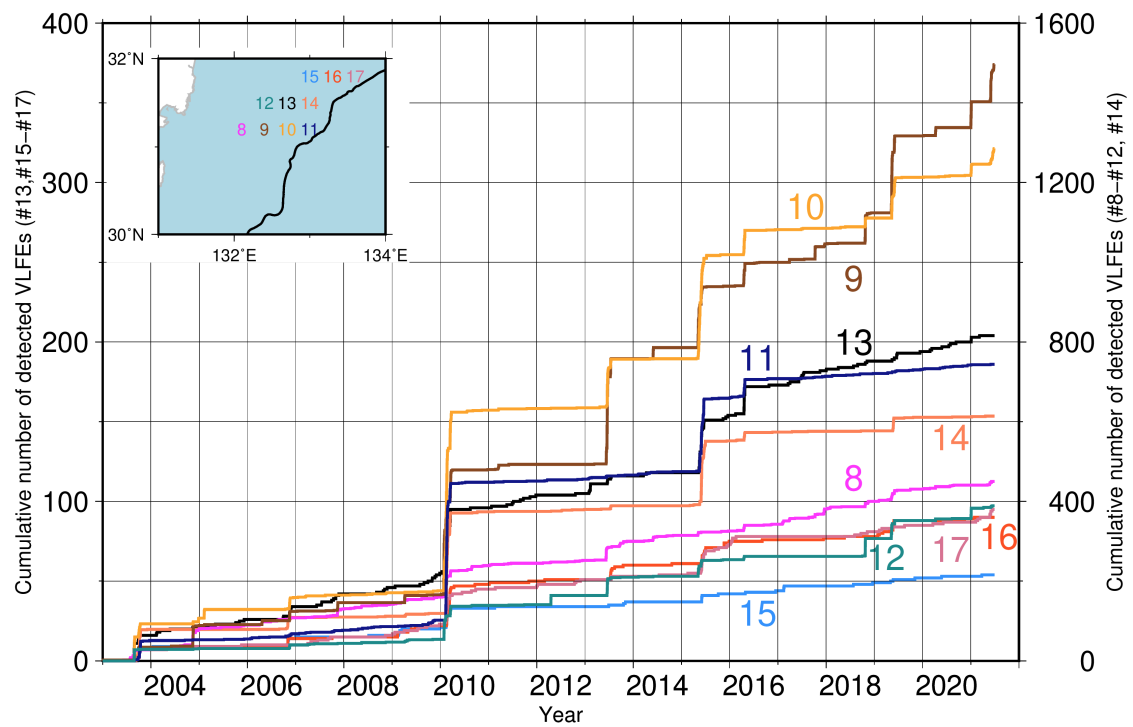
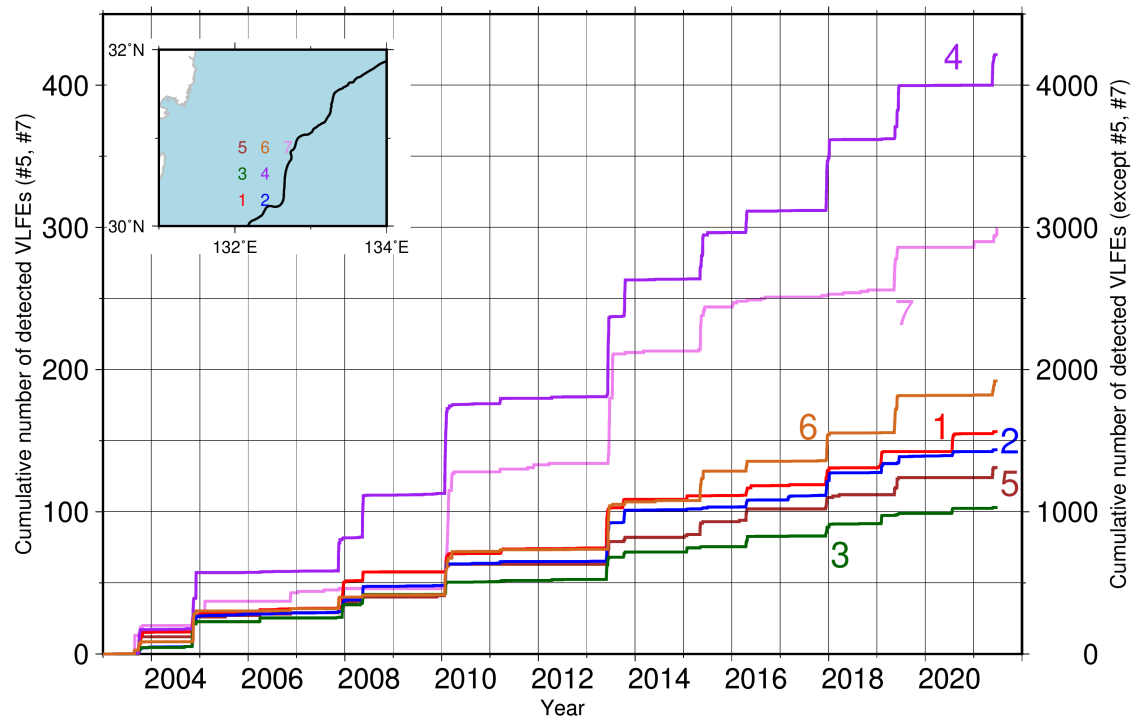
(c) Deep VLFs in Kii Peninsula



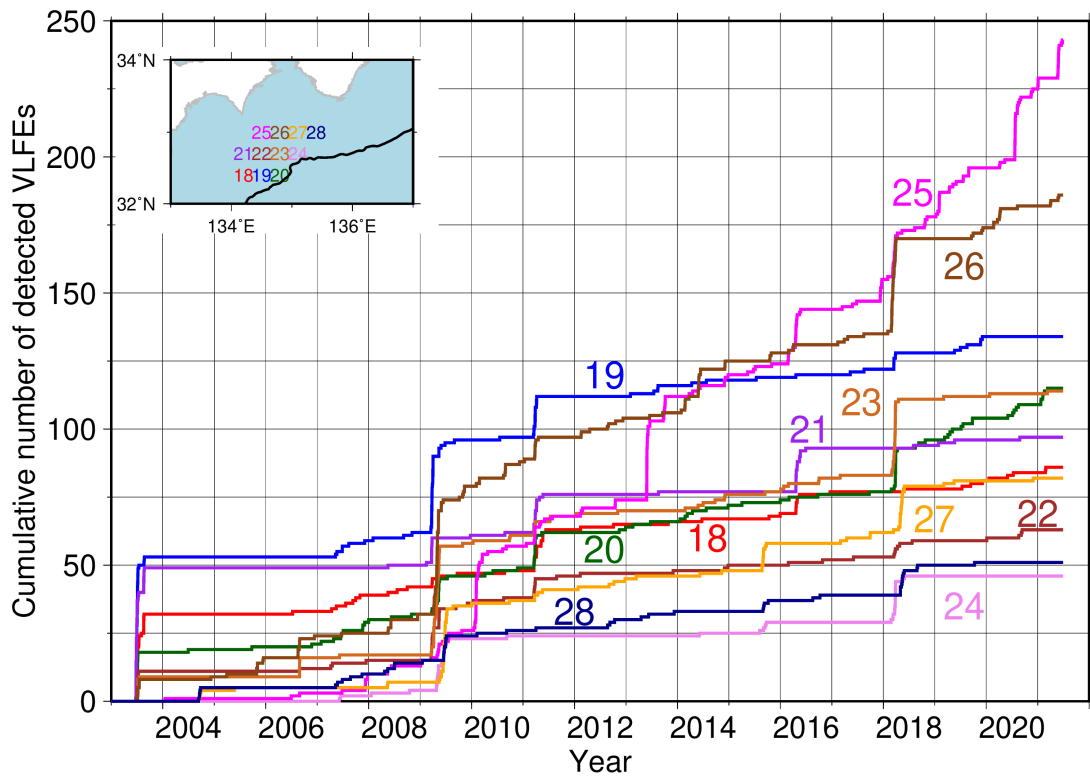
(d) Deep VLFs in Tokai



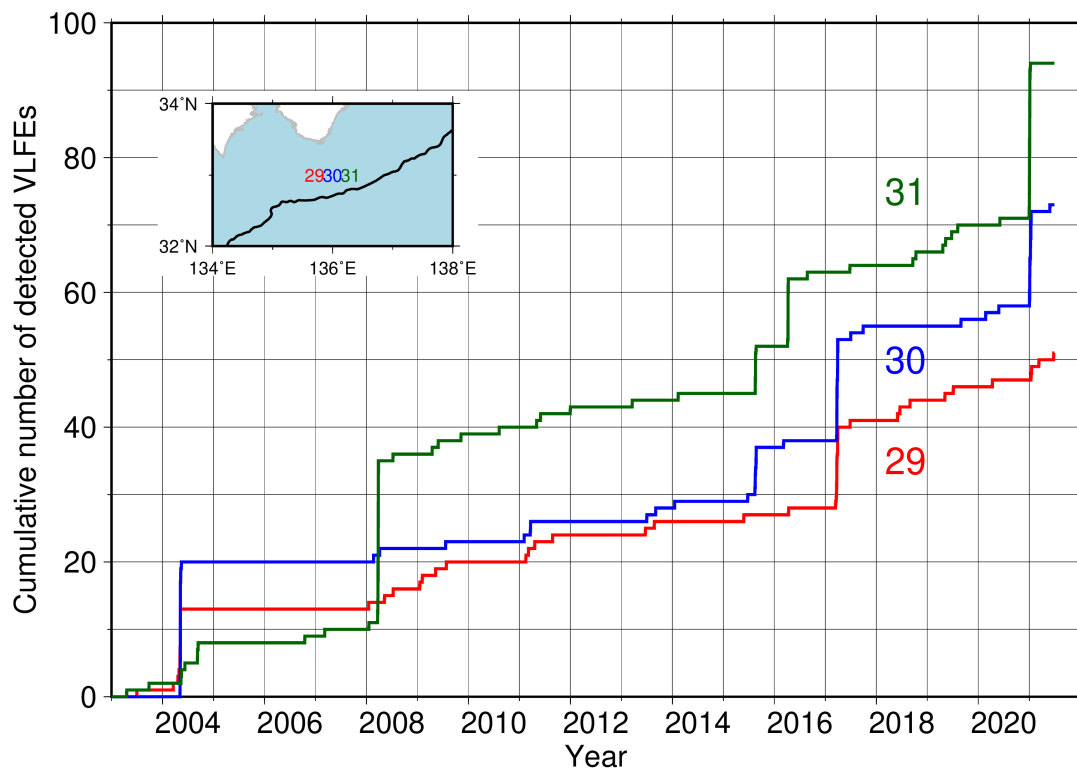
(e) Shallow VLFs in Hyuga-nada



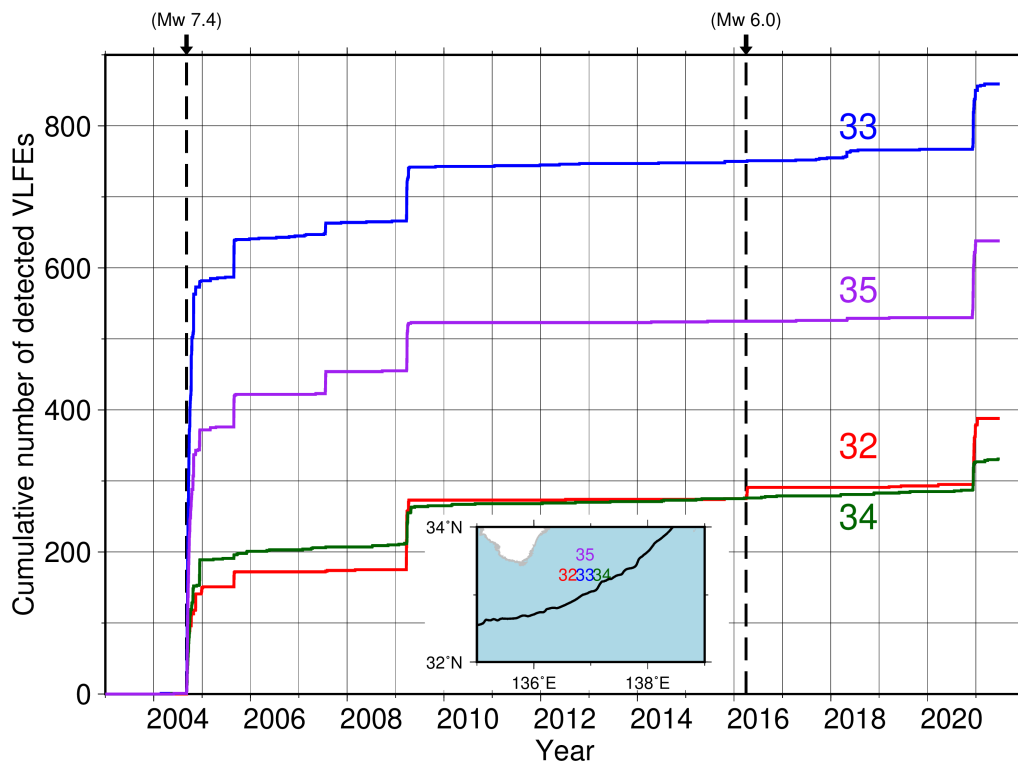
(f) Shallow VLFs off Cape Muroto



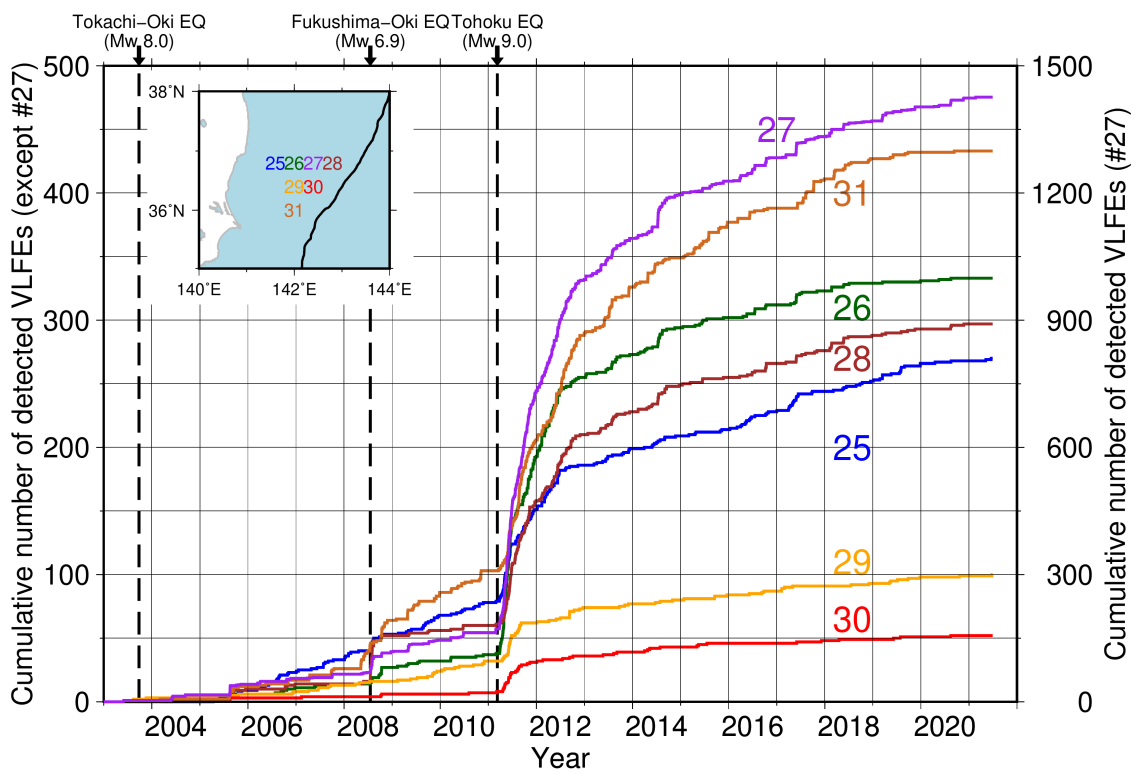
(g) Shallow VLFs off southern Kii



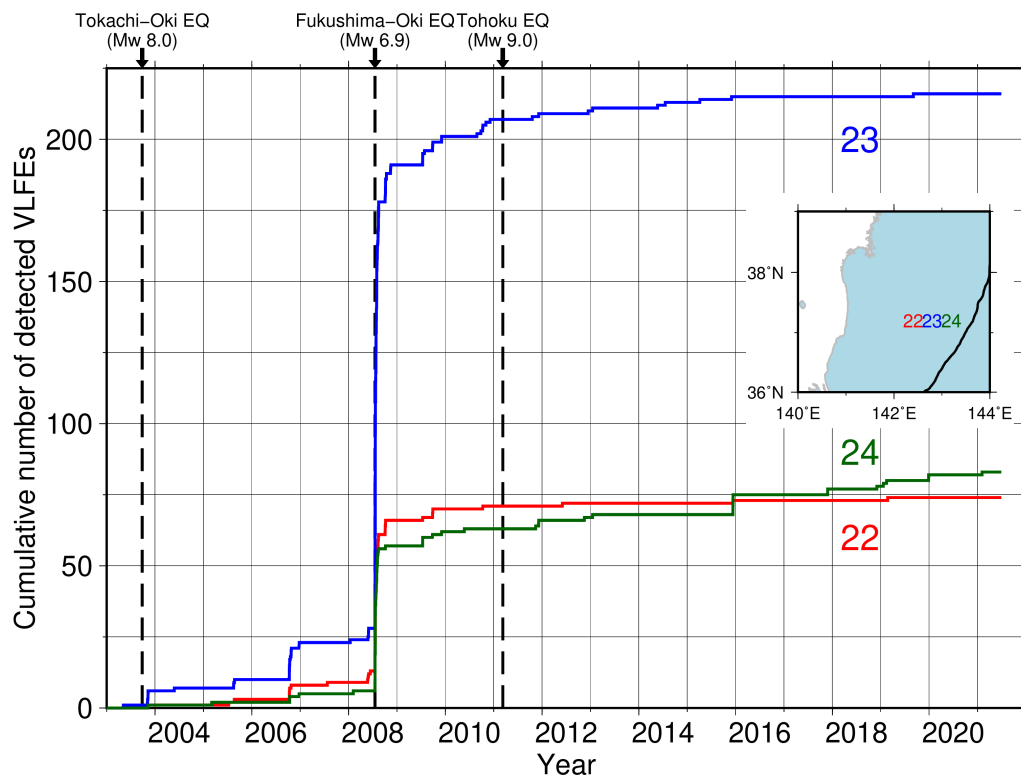
(h) Shallow VLFs off southeastern Kii



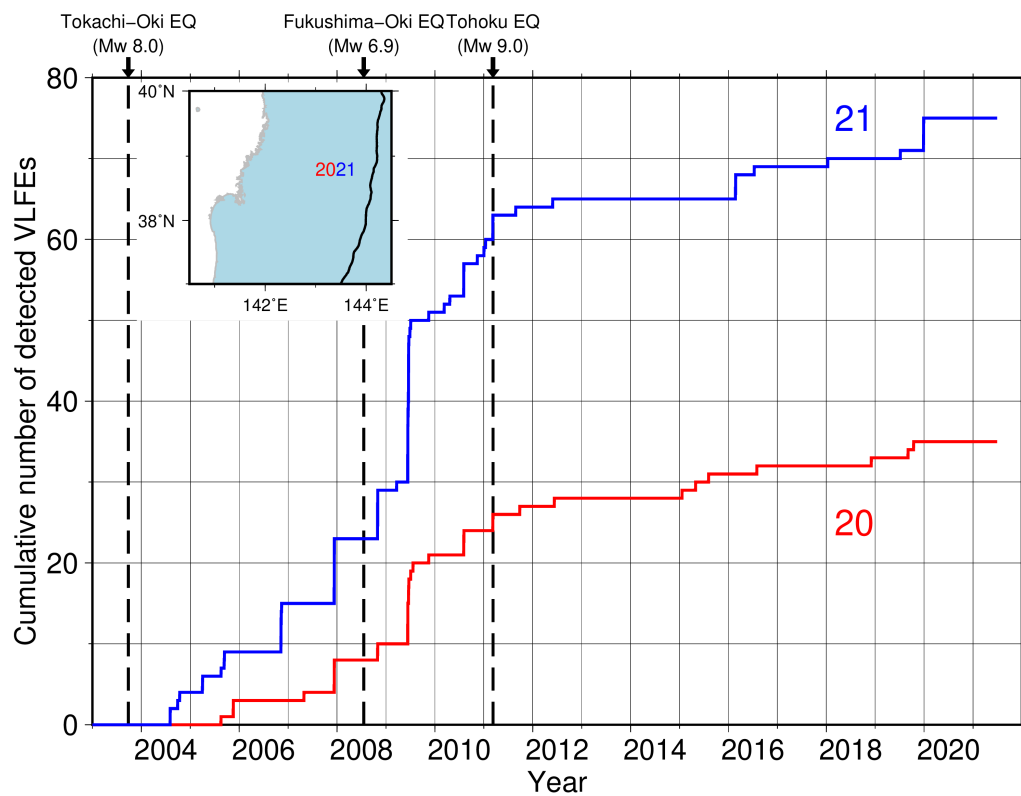
(i) VLFs off Ibaraki



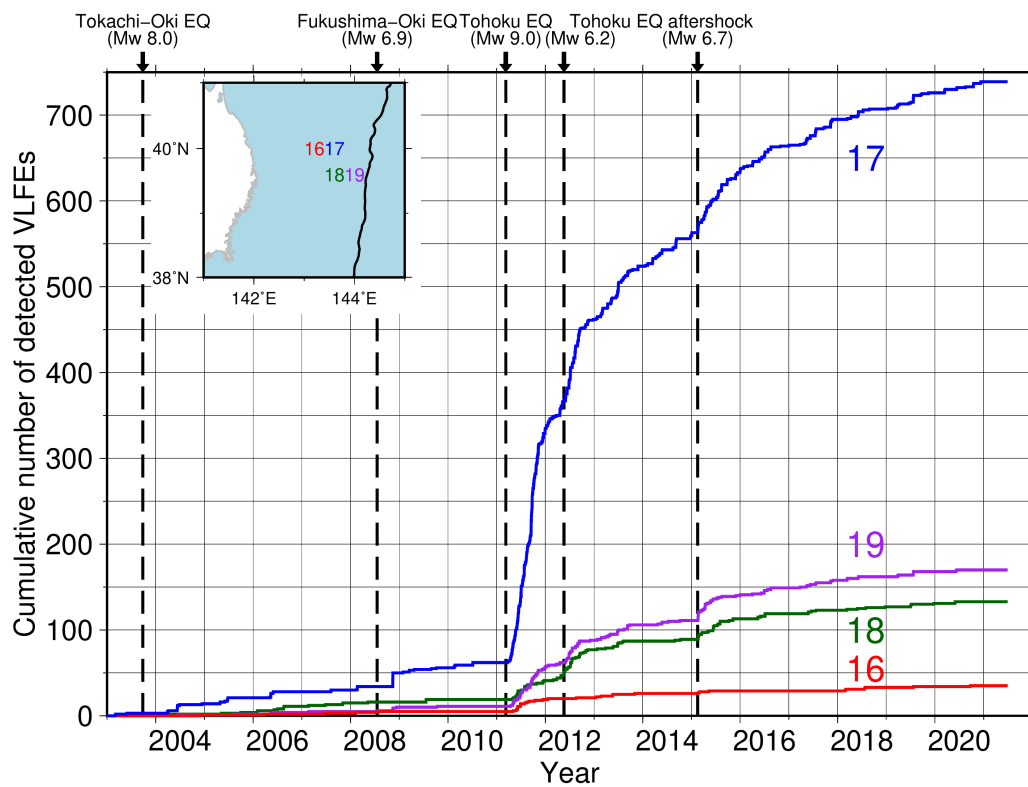
(j) VLFs off Fukushima



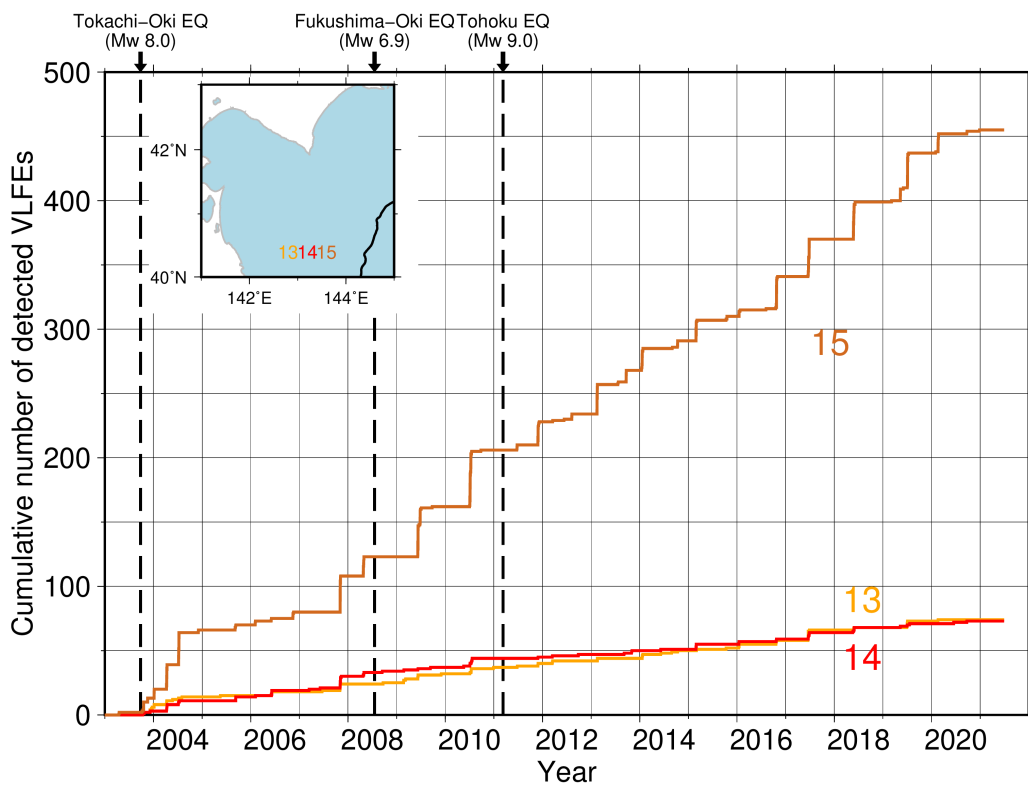
(k) VLFs off Miyagi



(l) VLFs off Iwate



(m) VLFs off Aomori



(n) VLFs off Tokachi

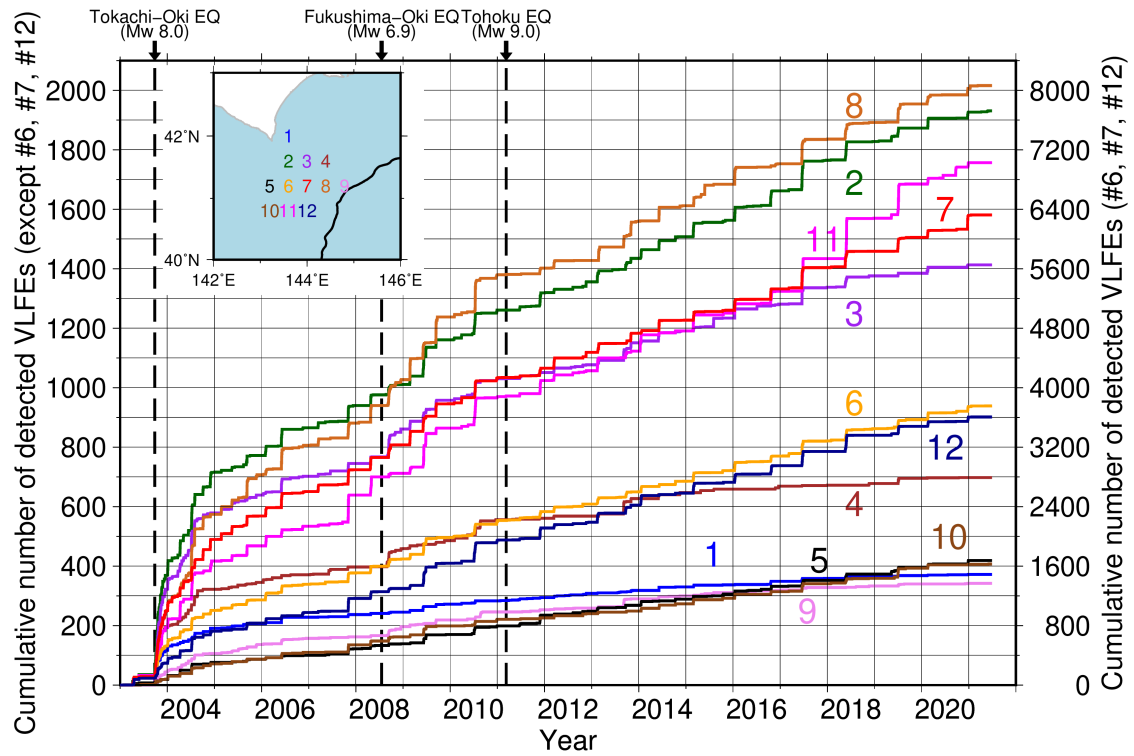


Figure A5. Cumulative number of VLFs at each source grid from January 2003 to June 2021. Dashed vertical lines in Figures A4i–n show the times of the 2003 Tokachi-Oki earthquake, the 2008 Fukushima-Oki earthquake, and the Tohoku earthquake, respectively. Dashed vertical lines for 2004 and 2016 in Figure A4h represent times of earthquakes which activated VLFs off southeastern Kii. Dashed vertical lines for 2012 and 2015 in Figure A4l indicate the times of the Tohoku earthquake aftershocks which activated VLFs off Iwate.

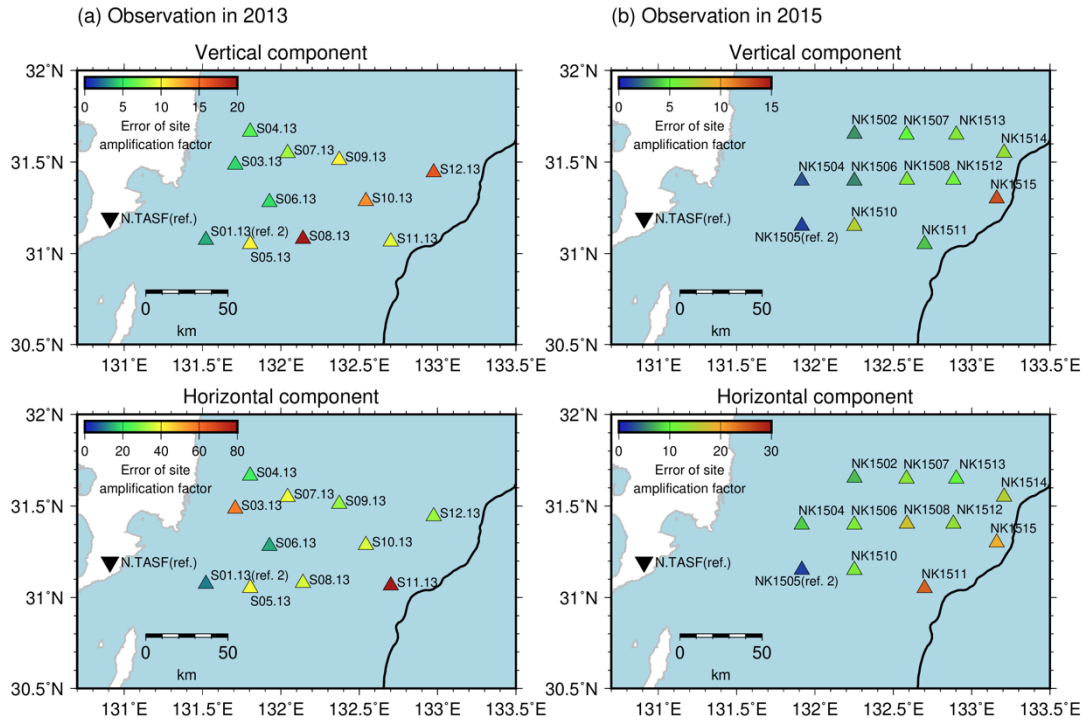


Figure. A6. Same as Figure 3.5 but the estimation errors (standard deviation) of site amplification factors at each station.

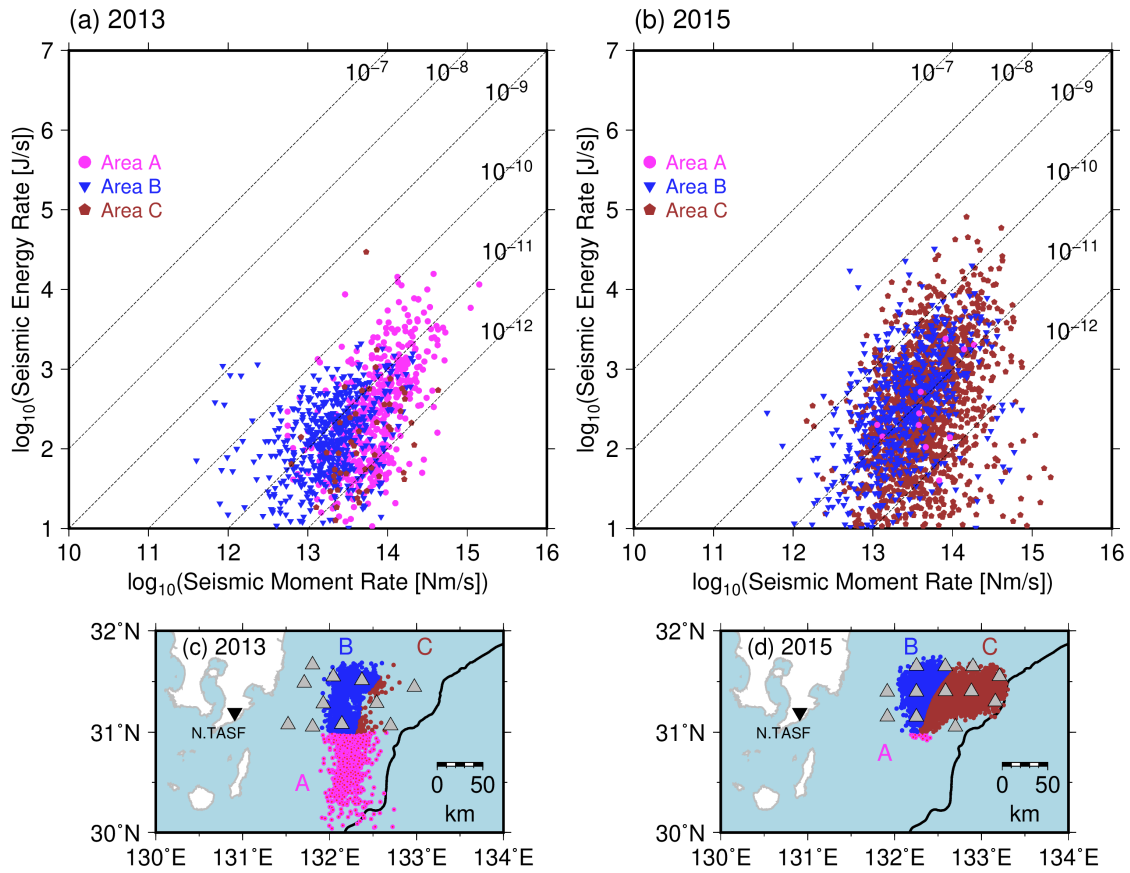


Figure A7. Relationship between seismic moment rates of VLFs and seismic moment rates of shallow tremors at each area in Hyuga-nada (a) in 2013 and (b) in 2015. Area A, events in the south of 31.0° (occurred only in 2013); Area B, events in the north of 31.0° and the depth of the plate interface is deeper than 10 km (occurred both in 2013 and 2015); and Area C, events in the north of 31.0° and depth of the plate interface is shallower than 10 km (occurred mainly in 2015). Epicenters of shallow tremors at each area (c) in 2013 and (d) in 2015. Shallow tremors in Area A, B, and C are depicted by magenta, blue, and brown dots, respectively. Gray triangles display the locations of OBSs. Black inverted triangles indicates the location of an F-net station, N.TASF. Black lines show the Nankai Trough.

References

- Agata, R. (2020). Introduction of covariance components in slip inversion of geodetic data following a non-uniform spatial distribution and application to slip deficit rate estimation in the Nankai Trough subduction zone. *Geophysical Journal International*, 221(3), 1832–1844. <https://doi.org/10.1093/gji/ggaa116>
- Aki, K. (1980). Attenuation of shear-waves in the lithosphere for frequencies from 0.05 to 25 Hz. *Physics of the Earth and Planetary Interiors*, 21(1), 50–60. [https://doi.org/10.1016/0031-9201\(80\)90019-9](https://doi.org/10.1016/0031-9201(80)90019-9)
- Aki, K., & Chouet, B. (1975). Origin of coda waves: Source, attenuation, and scattering effects. *Journal of Geophysical Research*, 80(23), 3322–3342. <https://doi.org/10.1029/JB080i023p03322>
- Akuhara, T., Tsuji, T., & Tonegawa, T. (2020). Overpressured underthrust sediment in the Nankai Trough forearc inferred from transdimensional inversion of high-frequency teleseismic waveforms. *Geophysical Research Letters*. <https://doi.org/10.1029/2020GL088280>
- Amante, C., & Eakins, B.W. (2009). ETOPO1 1 Arc-Minute Global Relief Model: Procedures, Data Sources and Analysis. NOAA Technical Memorandum NESDIS NGDC-24. <https://doi.org/10.7289/V5C8276M>
- Ando, R., Takeda, N., & Yamashita, T. (2012). Propagation dynamics of seismic and aseismic slip governed by fault heterogeneity and Newtonian rheology. *Journal of Geophysical Research B: Solid Earth*, 117(11). <https://doi.org/10.1029/2012JB009532>
- Annoura, S., Obara, K., & Maeda, T. (2016). Total energy of deep low-frequency tremor in the Nankai subduction zone, southwest Japan. *Geophysical Research Letters*, 43(6), 2562–2567. <https://doi.org/10.1002/2016GL067780>
- Aoi, S., Asano, Y., Kunugi, T., Kimura, T., Uehira, K., Takahashi, N., Ueda, H., Shiomi, K., Matsumoto, T., & Fujiwara, H. (2020). MOWLAS: NIED observation network for earthquake, tsunami and volcano. *Earth, Planets and Space*, 72(1). <https://doi.org/10.1186/s40623-020-01250-x>
- Araki, E., Saffer, D. M., Kopf, A. J., Wallace, L. M., Kimura, T., Machida, Y., Ide, S., Davis, E., & IODP Expedition 365 shipboard scientists. (2017). Recurring and triggered slow-slip events near the trench at the Nankai Trough subduction

- megathrust. *Science*, 356(6343), 1157–1160.
<https://doi.org/10.1126/science.aan3120>
- Arisa, D., & Heki, K. (2017). Space geodetic observations of repeating slow slip events beneath the Bonin Islands. *Geophysical Journal International*, 210(3), 1494–1502.
<https://doi.org/10.1093/gji/ggx258>
- Asano, Y., Obara, K., & Ito, Y. (2008). Spatiotemporal distribution of very-low frequency earthquakes in Tokachi-oki near the junction of the Kuril and Japan trenches revealed by using array signal processing. *Earth, Planets and Space*, 60(8), 871–875.
<https://doi.org/10.1186/BF03352839>
- Asano, Y., Obara, K., Matsuzawa, T., Hirose, H., & Ito, Y. (2015). Possible shallow slow slip events in Hyuga-nada, Nankai subduction zone, inferred from migration of very low frequency earthquakes. *Geophysical Research Letters*, 42(2), 331–338.
<https://doi.org/10.1002/2014GL062165>
- Audet, P., & Bürgmann, R. (2014). Possible control of subduction zone slow-earthquake periodicity by silica enrichment. *Nature*, 510(7505), 389–392.
<https://doi.org/10.1038/nature13391>
- Baba, S., Takeo, A., Obara, K., Kato, A., Maeda, T., & Matsuzawa, T. (2018). Temporal Activity Modulation of Deep Very Low Frequency Earthquakes in Shikoku, Southwest Japan. *Geophysical Research Letters*, 45(2), 733–738.
<https://doi.org/10.1002/2017GL076122>
- Baba, S., Obara, K., Takemura, S., Takeo, A., & Abers, G. A. (2021). Shallow Slow Earthquake Episodes Near the Trench Axis Off Costa Rica. *Journal of Geophysical Research: Solid Earth*. <https://doi.org/10.1029/2021JB021706>
- Beroza, G. C., & Ide, S. (2011). Slow Earthquakes and Nonvolcanic Tremor. *Annual Review of Earth and Planetary Sciences*, 39(1), 271–296.
<https://doi.org/10.1146/annurev-earth-040809-152531>
- Carcolé, E., & Sato, H. (2010). Spatial distribution of scattering loss and intrinsic absorption of short-period S waves in the lithosphere of Japan on the basis of the Multiple Lapse Time Window Analysis of Hi-net data. *Geophysical Journal International*, 180(1), 268–290. <https://doi.org/10.1111/j.1365-246X.2009.04394.x>
- Coffin, M.F., Gahagan, L.M., & Lawver, L.A. (1998). Present-day Plate Boundary Digital Data Compilation. *University of Texas Institute for Geophysics Technical Report*, 174, 5.

- DeMets, C., Gordon, R. G., Argus, D. F., & Stein, S. (1994). Effect of recent revisions to the geomagnetic reversal time scale on estimates of current plate motions. *Geophysical Research Letters*, 21(20), 2191–2194. <https://doi.org/10.1029/94GL02118>
- Dieterich, J. H. (1979). Modeling of rock friction 1. Experimental results and constitutive equations. In *Journal of Geophysical Research: Solid Earth* (Vol. 84, pp. 2161–2168). Blackwell Publishing Ltd. <https://doi.org/10.1029/JB084iB05p02161>
- Dragert, H., Wang, K., James, T. S. (2001). A Silent Slip Event on the Deeper Cascadia Subduction Interface. *Science*, 292(5521), 1525–1528. <https://doi.org/10.1126/science.1060152>
- Dunham, E. M., Belanger, D., Cong, L., & Kozdon, J. E. (2011). Earthquake ruptures with strongly rate-weakening friction and off-fault plasticity, part 2: Nonplanar faults. *Bulletin of the Seismological Society of America*, 101(5), 2308–2322. <https://doi.org/10.1785/0120100076>
- Frank, W. B., & Brodsky, E. E. (2019). Daily measurement of slow slip from low-frequency earthquakes is consistent with ordinary earthquake scaling. *Science Advances*, 5(10), 1–7. <https://doi.org/10.1126/sciadv.aaw9386>
- Fukao, Y., Kubota, T., Sugioka, H., Ito, A., Tonegawa, T., Shiobara, H., Yamashita, M., & Saito, T. (2021). Detection of “Rapid” Aseismic Slip at the Izu-Bonin Trench. *Journal of Geophysical Research: Solid Earth*, 126(9). <https://doi.org/10.1029/2021JB022132>
- Furumura, T., Hayakawa, T., Nakamura, M., Koketsu, K., & Baba, T. (2008). Development of long-period ground motions from the Nankai trough, Japan, earthquakes: Observations and computer simulation of the 1944 Tonankai (Mw 8.1) and the 2004 SE Off-Kii Peninsula (Mw 7.4) earthquakes. *Pure and Applied Geophysics*, 165(3–4), 585–607. <https://doi.org/10.1007/s00024-008-0318-8>
- Ghosh, A., Huesca-Pérez, E., Brodsky, E., & Ito, Y. (2015). Very low frequency earthquakes in Cascadia migrate with tremor. *Geophysical Research Letters*, 42(9), 3228–3232. <https://doi.org/10.1002/2015GL063286>
- Graves, R., & Pitarka, A. (2016). Kinematic ground-motion simulations on rough faults including effects of 3D stochastic velocity perturbations. *Bulletin of the Seismological Society of America*, 106(5), 2136–2153. <https://doi.org/10.1785/0120160088>

- Hanks, T. C., & Kanamori, H. (1979). A moment magnitude scale. In *Journal of Geophysical Research B: Solid Earth* (Vol. 84, pp. 2348–2350). <https://doi.org/10.1029/JB084iB05p02348>
- Harris, R., Yamano, M., Kinoshita, M., Spinelli, G., Hamamoto, H., & Ashi, J. (2013). A synthesis of heat flow determinations and thermal modeling along the Nankai Trough, Japan. *Journal of Geophysical Research: Solid Earth*, 118(6), 2687–2702. <https://doi.org/10.1002/jgrb.50230>
- Hasegawa, A., Yoshida, K., & Okada, T. (2011). Nearly complete stress drop in the 2011 Mw 9.0 off the Pacific coast of Tohoku Earthquake. *Earth, Planets and Space*, 63(7), 703–707. <https://doi.org/10.5047/eps.2011.06.007>
- Hashimoto, C., Noda, A., & Matsu'ura, M. (2012). The M w 9.0 northeast Japan earthquake: Total rupture of a basement asperity. *Geophysical Journal International*, 189(1), 1–5. <https://doi.org/10.1111/j.1365-246X.2011.05368.x>
- Hasselmann, K. (1963). A statistical analysis of the generation of microseisms. *Reviews of Geophysics*, 1(2), 177–210. <https://doi.org/10.1029/RG001i002p00177>
- Heki, K., & Kataoka, T. (2008). On the biannually repeating slow-slip events at the Ryukyu Trench, southwestern Japan. *Journal of Geophysical Research: Solid Earth*, 113(11). <https://doi.org/10.1029/2008JB005739>
- Helffrich, G., Wookey, J., & Bastow, I. (2013). *The Seismic Analysis Code*. Cambridge: Cambridge University Press. <https://doi.org/10.1017/CBO9781139547260>
- Herman, M. W., Furlong, K. P., & Govers, R. (2018). The Accumulation of Slip Deficit in Subduction Zones in the Absence of Mechanical Coupling: Implications for the Behavior of Megathrust Earthquakes. *Journal of Geophysical Research: Solid Earth*, 123(9), 8260–8278. <https://doi.org/10.1029/2018JB016336>
- Hirose, H., Asano, Y., Obara, K., Kimura, T., Matsuzawa, T., Tanaka, S., & Maeda, T. (2010). Slow earthquakes linked along dip in the Nankai subduction zone. *Science*, 330(6010), 1502. <https://doi.org/10.1126/Science.1197102>
- Hirose, H., & Obara, K. (2005). Repeating short- and long-term slow slip events with deep tremor activity around the Bungo channel region, southwest Japan. *Earth, Planets and Space*, 57(10), 961–972. <https://doi.org/10.1186/BF03351875>
- Hirose, H., & Obara, K. (2006). Short-term slow slip and correlated tremor episodes in the Tokai region, central Japan. *Geophysical Research Letters*, 33(17), 1–5. <https://doi.org/10.1029/2006GL026579>

- Hirose, H., Hirahara, K., Kimata, F., Fujii, N., & Miyazaki, S. (1999). A slow thrust slip event following the two 1996 Hyuganada earthquakes beneath the Bungo Channel, southwest Japan. *Geophysical Research Letters*, 26(21), 3237–3240. <https://doi.org/10.1029/1999GL010999>
- Houston, H. (2015). Low friction and fault weakening revealed by rising sensitivity of tremor to tidal stress. *Nature Geoscience*, 8(5), 409–415. <https://doi.org/10.1038/ngeo2419>
- Houston, H., Delbridge, B. G., Wech, A. G., & Creager, K. C. (2011). Rapid tremor reversals in Cascadia generated by a weakened plate interface. *Nature Geoscience*, 4(6), 404–409. <https://doi.org/10.1038/ngeo1157>
- Huang, Z., & Zhao, D. (2013). Mechanism of the 2011 tohoku-oki earthquake (Mw 9.0) and tsunami: Insight from seismic tomography. *Journal of Asian Earth Sciences*, 70–71(1), 160–168. <https://doi.org/10.1016/j.jseaes.2013.03.010>
- Hutchison, A. A. (2020). Interepisodic Tremor and Slip Event Episodes of Quasi-spatiotemporally Discrete Tremor and Very Low Frequency Earthquakes in Cascadia Suggestive of a Connective Underlying, Heterogeneous Process. *Geophysical Research Letters*, 47(3), 1–7. <https://doi.org/10.1029/2019GL086798>
- Hutchison, A. A., & Ghosh, A. (2019). Repeating VLFs During ETS Events in Cascadia Track Slow Slip and Continue Throughout Inter-ETS Period. *Journal of Geophysical Research: Solid Earth*, 124(1), 554–565. <https://doi.org/10.1029/2018JB016138>
- Hyndman, R. D., & Peacock, S. M. (2003). Serpentinization of the forearc mantle. *Earth and Planetary Science Letters*, 212(3–4), 417–432. [https://doi.org/10.1016/S0012-821X\(03\)00263-2](https://doi.org/10.1016/S0012-821X(03)00263-2)
- Ide, S. (2008). A Brownian walk model for slow earthquakes. *Geophysical Research Letters*, 35(17), 3–7. <https://doi.org/10.1029/2008GL034821>
- Ide, S. (2010). Striations, duration, migration and tidal response in deep tremor. *Nature*, 466(7304), 356–359. <https://doi.org/10.1038/nature09251>
- Ide, S. (2012). Variety and spatial heterogeneity of tectonic tremor worldwide. *Journal of Geophysical Research: Solid Earth*, 117(3), 1–18. <https://doi.org/10.1029/2011JB008840>

- Ide, S. (2016). Characteristics of slow earthquakes in the very low frequency band: Application to the Cascadia subduction zone. *Journal of Geophysical Research: Solid Earth*, 121(8), 5942–5952. <https://doi.org/10.1002/2016JB013085>
- Ide, S., & Maury, J. (2018). Seismic Moment, Seismic Energy, and Source Duration of Slow Earthquakes: Application of Brownian slow earthquake model to three major subduction zones. *Geophysical Research Letters*, 45(7), 3059–3067. <https://doi.org/10.1002/2018GL077461>
- Ide, S., & Yabe, S. (2014). Universality of slow earthquakes in the very low frequency band. *Geophysical Research Letters*, 41(8), 2786–2793. <https://doi.org/10.1002/2014GL059712>
- Ide, S., Beroza, G. C., Shelly, D. R., & Uchide, T. (2007). A scaling law for slow earthquakes. *Nature*, 447(7140), 76–79. <https://doi.org/10.1038/nature05780>
- Ide, S., Imanishi, K., Yoshida, Y., Beroza, G. C., & Shelly, D. R. (2008). Bridging the gap between seismically and geodetically detected slow earthquakes. *Geophysical Research Letters*, 35(10), 2–7. <https://doi.org/10.1029/2008GL034014>
- Idehara, K., Yabe, S., & Ide, S. (2014). Regional and global variations in the temporal clustering of tectonic tremor activity New Perspective of Subduction Zone Earthquake. *Earth, Planets and Space*, 66(1). <https://doi.org/10.1186/1880-5981-66-66>
- Igarashi, T. (2020). Catalog of small repeating earthquakes for the Japanese Islands. *Earth, Planets and Space*, 72(1). <https://doi.org/10.1186/s40623-020-01205-2>
- Iinuma, T., Hino, R., Kido, M., Inazu, D., Osada, Y., Ito, Y., Ohzono, M., Tsushima, H., Suzuki, S., Fujimoto, H., & Miura, S. (2012). Coseismic slip distribution of the 2011 off the Pacific Coast of Tohoku Earthquake (M9.0) refined by means of seafloor geodetic data. *Journal of Geophysical Research: Solid Earth*, 117(7), 1–18. <https://doi.org/10.1029/2012JB009186>
- Iinuma, T., Hino, R., Uchida, N., Nakamura, W., Kido, M., Osada, Y., & Miura, S. (2016). Seafloor observations indicate spatial separation of coseismic and postseismic slips in the 2011 Tohoku earthquake. *Nature Communications*, 7, 1–9. <https://doi.org/10.1038/ncomms13506>
- Ito, Y., Obara, K., Shiomi, K., Sekine, S., & Hirose, H. (2007). Slow Earthquakes Coincident with Episodic Tremors and Slow Slip Events. *Science*, 315(5811), 503–506. <https://doi.org/10.1126/science.1134454>

- Ito, Y., & Obara, K. (2006). Very low frequency earthquakes within accretionary prisms are very low stress-drop earthquakes. *Geophysical Research Letters*, 33(9), 1–4. <https://doi.org/10.1029/2006GL025883>
- Ito, Y., Obara, K., Matsuzawa, T., & Maeda, T. (2009). Very low frequency earthquakes related to small asperities on the plate boundary interface at the locked to aseismic transition. *Journal of Geophysical Research: Solid Earth*, 114(11), 1–16. <https://doi.org/10.1029/2008JB006036>
- Ito, Y., Hino, R., Kido, M., Fujimoto, H., Osada, Y., Inazu, D., Ohta, Y., Iinuma, T., Ohzono, M., Miura, S., Mishina, M., Suzuki, K., Tsuji, T., & Ashi, J. (2013). Episodic slow slip events in the Japan subduction zone before the 2011 Tohoku-Oki earthquake. *Tectonophysics*, 600, 14–26. <https://doi.org/10.1016/j.tecto.2012.08.022>
- Itoh, Y., Nishimura, T., Ariyoshi, K., & Matsumoto, H. (2019). Interplate Slip Following the 2003 Tokachi-oki Earthquake From Ocean Bottom Pressure Gauge and Land GNSS Data. *Journal of Geophysical Research: Solid Earth*, 124(4), 4205–4230. <https://doi.org/10.1029/2018JB016328>
- Jin, A., & Aki, K. (2005). High-resolution maps of Coda Q in Japan and their interpretation by the brittle-ductile interaction hypothesis. *Earth, Planets and Space*, 57(5), 403–409. <https://doi.org/10.1186/BF03351825>
- Kamei, R., Pratt, R. G., & Tsuji, T. (2012). Waveform tomography imaging of a megasplay fault system in the seismogenic Nankai subduction zone. *Earth and Planetary Science Letters*, 317–318, 343–353. <https://doi.org/10.1016/j.epsl.2011.10.042>
- Kanamori, H., & Anderson, D. L. (1975). Theoretical basis of some empirical relations in seismology. *Bulletin of the Seismological Society of America* (Vol. 65). Retrieved from <http://pubs.geoscienceworld.org/ssa/bssa/article-pdf/65/5/1073/5320189/bssa0650051073.pdf>
- Kaneko, L., Ide, S., & Nakano, M. (2018). Slow Earthquakes in the Microseism Frequency Band (0.1–1.0 Hz) off Kii Peninsula, Japan. *Geophysical Research Letters*, 45(6), 2618–2624. <https://doi.org/10.1002/2017GL076773>
- Kano, M., Aso, N., Matsuzawa, T., Ide, S., Annoura, S., Arai, R., Baba, S., Bostock, M., Chao, K., Heki, K., Itaba, S., Ito, Y., Kamaya, N., Maeda, T., Maury, J., Nakamura, M., Nishimura, T., Obana, K., Ohta, K., Poiata, N., Rousset, B., Sugioka, H., Takagi,

- R., Takahashi, T., Takeo, A., Tu, Y., Uchida, N., Yamashita, Y., & Obara, K. (2018). Development of a Slow Earthquake Database. *Seismological Research Letters*, 89(4), 1566–1575. <https://doi.org/10.1785/0220180021>
- Kano, M., Kato, A., Ando, R., & Obara, K. (2018). Strength of tremor patches along deep transition zone of a megathrust. *Scientific Reports*, 8(1). <https://doi.org/10.1038/s41598-018-22048-8>
- Katayama, I. (2016). Water Circulation System at Subduction Zones. *Bulletin of the Volcanological Society of Japan*, 61, 69-77. https://doi.org/10.18940/kazan.61.1_69 (in Japanese)
- Kato, A., Obara, K., Igarashi, T., Tsuruoka, H., Nakagawa, S., & Hirata, N. (2012). Propagation of Slow Slip Leading Up to the 2011 Mw 9.0 Tohoku-Oki Earthquake. *Science*, 335(6069), 705–708. <https://doi.org/10.1126/science.1215141>
- Kato, A., & Igarashi, T. (2012). Regional extent of the large coseismic slip zone of the 2011 Mw 9.0 Tohoku-Oki earthquake delineated by on-fault aftershocks. *Geophysical Research Letters*, 39(15), 2–7. <https://doi.org/10.1029/2012GL052220>
- Kato, A., & Nakagawa, S. (2014). Multiple slow-slip events during a foreshock sequence of the 2014 Iquique, Chile Mw 8.1 earthquake. *Geophysical Research Letters*, 41, 6413–6419. <https://doi.org/10.1002/2014GL061184>. Received
- Katsumata, A., & Kamaya, N. (2003). Low-frequency continuous tremor around the Moho discontinuity away from volcanoes in the southwest Japan. *Geophysical Research Letters*, 30(1), 1-4. <https://doi.org/10.1029/2002GL0159812>
- Kikuchi, M., Nakamura, M., & Yoshikawa, K. (2003). Source rupture processes of the 1944 Tonankai earthquake and the 1945 Mikawa earthquake derived from low-gain seismograms. *Earth, Planets and Space*, 55(4), 159–172. <https://doi.org/10.1186/BF03351745>
- Kimura, G., Hina, S., Hamada, Y., Kameda, J., Tsuji, T., Kinoshita, M., & Yamaguchi, A. (2012). Runaway slip to the trench due to rupture of highly pressurized megathrust beneath the middle trench slope: The tsunamigenesis of the 2011 Tohoku earthquake off the east coast of northern Japan. *Earth and Planetary Science Letters*, 339–340, 32–45. <https://doi.org/10.1016/j.epsl.2012.04.002>
- Kita, S., Okada, T., Hasegawa, A., Nakajima, J., & Matsuzawa, T. (2010). Anomalous deepening of a seismic belt in the upper-plane of the double seismic zone in the Pacific slab beneath the Hokkaido corner: Possible evidence for thermal shielding

- caused by subducted forearc crust materials. *Earth and Planetary Science Letters*, 290(3–4), 415–426. <https://doi.org/10.1016/j.epsl.2009.12.038>
- Kitajima, H., & Saffer, D. M. (2012). Elevated pore pressure and anomalously low stress in regions of low frequency earthquakes along the Nankai Trough subduction megathrust. *Geophysical Research Letters*, 39(23), 1–5. <https://doi.org/10.1029/2012GL053793>
- Kobayashi, A., & Tsuyuki, T. (2019). Long-term slow slip event detected beneath the Shima Peninsula, central Japan, from GNSS data. *Earth, Planets and Space*, 71(1), 1–7. <https://doi.org/10.1186/s40623-019-1037-3>
- Koketsu, K., Miyake, H., Suzuki, H. (2012). Japan Integrated Velocity Structure Model Version 1. In: Proceedings of the 15th World Conference on Earthquake Engineering, Lisbon, Portugal, 24-28 September, Paper 1773.
- Kurihara, R., & Obara, K. (2021). Spatiotemporal Characteristics of Relocated Deep Low-Frequency Earthquakes Beneath 52 Volcanic Regions in Japan Over an Analysis Period of 14 Years and 9 Months. *Journal of Geophysical Research: Solid Earth*, 126(10). <https://doi.org/10.1029/2021jb022173>
- Lindsey, E. O., Mallick, R., Hubbard, J. A., Bradley, K. E., Almeida, R. v., Moore, J. D. P., Bürgmann, R., & Hill, E. M. (2021). Slip rate deficit and earthquake potential on shallow megathrusts. *Nature Geoscience*, 14(5), 321–326. <https://doi.org/10.1038/s41561-021-00736-x>
- Liu, Y., & Rice, J. R. (2005). Aseismic slip transients emerge spontaneously in three-dimensional rate and state modeling of subduction earthquake sequences. *Journal of Geophysical Research: Solid Earth*, 110(8), 1–14. <https://doi.org/10.1029/2004JB003424>
- Maeda, T., & Obara, K. (2009). Spatiotemporal distribution of seismic energy radiation from low-frequency tremor in western Shikoku, Japan. *Journal of Geophysical Research: Solid Earth*, 114(10). <https://doi.org/10.1029/2008JB006043>
- Maeda, T., Takemura, S., & Furumura, T. (2017). OpenSWPC: An open-source integrated parallel simulation code for modeling seismic wave propagation in 3D heterogeneous viscoelastic media 4. Seismology. *Earth, Planets and Space*, 69(1). <https://doi.org/10.1186/s40623-017-0687-2>

- Mai, P. M., & Beroza, G. C. (2002). A spatial random field model to characterize complexity in earthquake slip. *Journal of Geophysical Research: Solid Earth*, 107(B11), ESE 10-1-ESE 10-21. <https://doi.org/10.1029/2001jb000588>
- Mai, P. M., & Thingbaijam, K. K. S. (2014). SRCMOD: An online database of finite-fault rupture models. *Seismological Research Letters*, 85(6), 1348–1357. <https://doi.org/10.1785/0220140077>
- Masuda, K., Ide, S., Ohta, K., & Matsuzawa, T. (2020). Bridging the gap between low-frequency and very-low-frequency earthquakes. *Earth, Planets and Space*, 72(1). <https://doi.org/10.1186/s40623-020-01172-8>
- Matsuzawa, T., Asano, Y., & Obara, K. (2015). Very low frequency earthquakes off the Pacific coast of Tohoku, Japan. *Geophysical Research Letters*, 42(11), 4318–4325. <https://doi.org/10.1002/2015GL063959>
- Michel, S., Gualandi, A., & Avouac, J. P. (2019). Similar scaling laws for earthquakes and Cascadia slow-slip events. *Nature*, 574(7779), 522–526. <https://doi.org/10.1038/s41586-019-1673-6>
- Nadeau, R. M., & Dolenc, D. (2005). Nonvolcanic tremors deep beneath the San Andreas Fault. *Science*, 307(5708), 389. <https://doi.org/10.1126/science.1107142>
- Nadeau, R. M., & McEvilly, T. V. (1999). Fault Slip Rates at Depth from Recurrence Intervals of Repeating Microearthquakes. *Science*, 285(5428), 718–721. <https://doi.org/10.1126/science.285.5428.718>
- Nakajima, J., & Hasegawa, A. (2006). Anomalous low-velocity zone and linear alignment of seismicity along it in the subducted Pacific slab beneath Kanto, Japan: Reactivation of subducted fracture zone? *Geophysical Research Letters*, 33(16). <https://doi.org/10.1029/2006GL026773>
- Nakajima, J., & Hasegawa, A. (2016). Tremor activity inhibited by well-drained conditions above a megathrust. *Nature Communications*, 7(May), 1–7. <https://doi.org/10.1038/ncomms13863>
- Nakajima, J., Hirose, F., & Hasegawa, A. (2009). Seismotectonics beneath the 144okyo metropolitan area, Japan: Effect of slab-slab contact and overlap on seismicity. *Journal of Geophysical Research: Solid Earth*, 114(8). <https://doi.org/10.1029/2008JB006101>

- Nakamura, M. (2017). Distribution of low-frequency earthquakes accompanying the very low frequency earthquakes along the Ryukyu Trench 4. *Seismology. Earth, Planets and Space*, 69(1). <https://doi.org/10.1186/s40623-017-0632-4>
- Nakamura, M., & Sunagawa, N. (2015). Activation of very low frequency earthquakes by slow slip events in the Ryukyu Trench. *Geophysical Research Letters*, 42(4), 1076–1082. <https://doi.org/10.1002/2014GL062929>
- Nakano, M., Hori, T., Araki, E., Kodaira, S., & Ide, S. (2018). Shallow very-low-frequency earthquakes accompany slow slip events in the Nankai subduction zone /704/2151/210 /704/2151/508 article. *Nature Communications*, 9(1). <https://doi.org/10.1038/s41467-018-03431-5>
- National Research Institute for Earth Science and Disaster Resilience. (2019). NIED F-net. <https://doi.org/10.17598/NIED.0005>
- Nishikawa, T., Matsuzawa, T., Ohta, K., Uchida, N., Nishimura, T., & Ide, S. (2019). The slow earthquake spectrum in the Japan Trench illuminated by the S-net seafloor observatories. *Science*, 365(6455), 808–813. <https://doi.org/10.1126/science.aax5618>
- Nishimura, T., Matsuzawa, T., & Obara, K. (2013). Detection of short-term slow slip events along the Nankai Trough, southwest Japan, using GNSS data. *Journal of Geophysical Research: Solid Earth*, 118(6), 3112–3125. <https://doi.org/10.1002/jgrb.50222>
- Nishizawa, A., Kaneda, K., & Oikawa, M. (2009). Seismic structure of the northern end of the Ryukyu Trench subduction zone, southeast of Kyushu, Japan. *Earth, Planets and Space*, 61(8), e37–e40. <https://doi.org/10.1186/bf03352942>
- Noda, A., Saito, T., & Fukuyama, E. (2018). Slip-Deficit Rate Distribution Along the Nankai Trough, Southwest Japan, With Elastic Lithosphere and Viscoelastic Asthenosphere. *Journal of Geophysical Research: Solid Earth*, 123(9), 8125–8142. <https://doi.org/10.1029/2018JB015515>
- Nomura, S., Ogata, Y., Uchida, N., & Matsu'ura, M. (2017). Spatiotemporal variations of interplate slip rates in northeast Japan inverted from recurrence intervals of repeating earthquakes. *Geophysical Journal International*, 208(1), 468–481. <https://doi.org/10.1093/gji/ggw395>
- Obara, K. (2002). Nonvolcanic Deep Tremor Associated with Subduction in Southwest Japan. *Science*, 296(5573), 1679–1681. <https://doi.org/10.1126/science.1070378>

- Obara, K. (2020). Characteristic activities of slow earthquakes in Japan. *Proceedings of the Japan Academy. Series B, Physical and Biological Sciences*, 96(7), 297–315. <https://doi.org/10.2183/pjab.96.022>
- Obara, K., & Ito, Y. (2005). Very low frequency earthquakes excited by the 2004 off Kii peninsula earthquakes: A dynamic deformation process in the large accretionary prism. *Earth, Planets and Space*, 57(4), 321–326. <https://doi.org/10.1186/BF03352570>
- Obara, K., & Kato, A. (2016). Connecting slow earthquakes to huge earthquakes. *Science*, 353(6296), 253–257. <https://doi.org/10.1126/science.aaf1512>
- Obara, K., Hirose, H., Yamamizu, F., & Kasahara, K. (2004). Episodic slow slip events accompanied by non-volcanic tremors in southwest Japan subduction zone. *Geophysical Research Letters*, 31(23), 1–4. <https://doi.org/10.1029/2004GL020848>
- Obara, K., Tanaka, S., Maeda, T., & Matsuzawa, T. (2010). Depth-dependent activity of non-volcanic tremor in southwest Japan. *Geophysical Research Letters*, 37, L13306. <https://doi.org/10.1029/2010GL043679>
- Ohta, K., & Ide, S. (2017). Resolving the Detailed Spatiotemporal Slip Evolution of Deep Tremor in Western Japan. *Journal of Geophysical Research: Solid Earth*, 122(12), 10,009–10,036. <https://doi.org/10.1002/2017JB014494>
- Okada, Y., Kasahara, K., Hori, S., Obara, K., Sekiguchi, S., Fujiwara, H., & Yamamoto, A. (2004). Recent progress of seismic observation networks in Japan. *Journal of Physics: Conference Series*, 56(8), 15–18. <https://doi.org/10.1088/1742-6596/433/1/012039>
- Okino, K., Ohara, Y., Kasuga, S., & Kato, Y. (1999). The Philippine Sea: New survey results reveal the structure and the history of the marginal basins. *Geophysical Research Letters*, 26(15), 2287–2290. <https://doi.org/10.1029/1999GL900537>
- Ozawa, S. (2017). Long-term slow slip events along the Nankai trough subduction zone after the 2011 Tohoku earthquake in Japan. *Earth, Planets and Space*, 69(1). <https://doi.org/10.1186/s40623-017-0640-4>
- Ozawa, S., Nishimura, T., Suito, H., Kobayashi, T., Tobita, M., & Imakiire, T. (2011). Coseismic and postseismic slip of the 2011 magnitude-9 Tohoku-Oki earthquake. *Nature*, 475(7356), 373–377. <https://doi.org/10.1038/nature10227>

- Passarelli, L., Selvadurai, P. A., Rivalta, E., & Jónsson, S. (2021). *The source scaling and seismic productivity of slow slip transients. Science Advances* (Vol. 7). Retrieved from <http://advances.sciencemag.org/>
- Phillips, W. S., & Aki, K. (1986). Site amplification of coda waves from local earthquakes in central California. *Bulletin of the Seismological Society of America*, 76(3), 627–648.
- Rogers, G., & Dragert, H. (2003). Episodic Tremor and Slip on the Cascadia Subduction Zone: The Chatter of Silent Slip. *Science*, 300(5627), 1942–1943. <https://doi.org/10.1126/science.1084783>
- Rouet-Leduc, B., Hulbert, C., & Johnson, P. A. (2019). Continuous chatter of the Cascadia subduction zone revealed by machine learning. *Nature Geoscience*, 12(1), 75–79. <https://doi.org/10.1038/s41561-018-0274-6>
- Ruiz, S., Metois, M., Fuenzalida, A., Ruiz, J., Leyton, F., Grandin, R., Vigny, C., Madariaga, R., & Campos, J. (2014) Intense foreshocks and a slow slip event preceded the 2014 Iquique M_w 8.1 earthquake. *Science*, 345, 6201. <https://doi.org/10.1126/science.1256074>
- Saffer, D. M., & Tobin, H. J. (2011). Hydrogeology and mechanics of subduction zone forearcs: Fluid flow and pore pressure. *Annual Review of Earth and Planetary Sciences*, 39, 157–186. <https://doi.org/10.1146/annurev-earth-040610-133408>
- Saffer, D. M., & Wallace, L. M. (2015). The frictional, hydrologic, metamorphic and thermal habitat of shallow slow earthquakes. *Nature Geoscience*, 8(8), 594–600. <https://doi.org/10.1038/ngeo2490>
- Sekine, S., Hirose, H., & Obara, K. (2010). Along-strike variations in short-term slow slip events in the southwest Japan subduction zone. *Journal of Geophysical Research: Solid Earth*, 115(9). <https://doi.org/10.1029/2008JB006059>
- Shelly, D. R., Beroza, G. C., & Ide, S. (2007). Non-volcanic tremor and low-frequency earthquake swarms. *Nature*, 446(7133), 305–307. <https://doi.org/10.1038/nature05666>
- Shiraishi, K., Yamada, Y., Nakano, M., Kinoshita, M., & Kimura, G. (2020). Three-dimensional topographic relief of the oceanic crust may control the occurrence of shallow very-low-frequency earthquakes in the Nankai Trough off Kumano. *Earth, Planets and Space*, 72(1). <https://doi.org/10.1186/s40623-020-01204-3>

- Skarbek, R. M., Rempel, A. W., & Schmidt, D. A. (2012). Geologic heterogeneity can produce aseismic slip transients. *Geophysical Research Letters*, 39(21). <https://doi.org/10.1029/2012GL053762>
- Sugioka, H., Okamoto, T., Nakamura, T., Ishihara, Y., Ito, A., Obana, K., Kinoshita, M., Nakahigashi, K., Shinohara, M., & Fukao, Y. (2012). Tsunamigenic potential of the shallow subduction plate boundary inferred from slow seismic slip. *Nature Geoscience*, 5(6), 414–418. <https://doi.org/10.1038/ngeo1466>
- Sun, T., Saffer, D., & Ellis, S. (2020). Mechanical and hydrological effects of seamount subduction on megathrust stress and slip. *Nature Geoscience*, 13(3), 249–255. <https://doi.org/10.1038/s41561-020-0542-0>
- Syracuse, E. M., van Keken, P. E., & Abers, G. A. (2010). The global range of subduction zone thermal models. *Physics of the Earth and Planetary Interiors*, 183(1–2), 73–90. <https://doi.org/10.1016/j.pepi.2010.02.004>
- Takagi, R., Obara, K., & Maeda, T. (2016). Slow slip event within a gap between tremor and locked zones in the Nankai subduction zone. *Geophysical Research Letters*, 43(3), 1066–1074. <https://doi.org/10.1002/2015GL066987>
- Takagi, R., Uchida, N., & Obara, K. (2019). Along-Strike Variation and Migration of Long-Term Slow Slip Events in the Western Nankai Subduction Zone, Japan. *Journal of Geophysical Research: Solid Earth*, (Figure 1), 3853–3880. <https://doi.org/10.1029/2018JB016738>
- Takemura, S., Kobayashi, M., & Yoshimoto, K. (2017). High-frequency seismic wave propagation within the heterogeneous crust: Effects of seismic scattering and intrinsic attenuation on ground motion modelling. *Geophysical Journal International*, 210(3), 1806–1822. <https://doi.org/10.1093/gji/ggx269>
- Takemura, S., Noda, A., Kubota, T., Asano, Y., Matsuzawa, T., & Shiomi, K. (2019). Migrations and Clusters of Shallow Very Low Frequency Earthquakes in the Regions Surrounding Shear Stress Accumulation Peaks Along the Nankai Trough. *Geophysical Research Letters*, 46(21), 11830–11840. <https://doi.org/10.1029/2019GL084666>
- Takemura, S., Kubo, H., Tonegawa, T., Saito, T., & Shiomi, K. (2019). Modeling of Long-Period Ground Motions in the Nankai Subduction Zone: Model Simulation Using the Accretionary Prism Derived from Oceanfloor Local S-Wave Velocity

- Structures. *Pure and Applied Geophysics*, 176(2), 627–647. <https://doi.org/10.1007/s00024-018-2013-8>
- Takemura, S., Matsuzawa, T., Noda, A., Tonegawa, T., Asano, Y., Kimura, T., & Shiomi, K. (2019). Structural Characteristics of the Nankai Trough Shallow Plate Boundary Inferred From Shallow Very Low Frequency Earthquakes. *Geophysical Research Letters*, 46(8), 4192–4201. <https://doi.org/10.1029/2019GL082448>
- Tanaka, S., Matsuzawa, T., & Asano, Y. (2019). Shallow Low-Frequency Tremor in the Northern Japan Trench Subduction Zone. *Geophysical Research Letters*, 2019GL082817. <https://doi.org/10.1029/2019GL082817>
- Tanioka, Y., & Satake, K. (2001). Coseismic slip distribution of the 1946 Nankai earthquake and aseismic slips caused by the earthquake. *Earth, Planets and Space*, 53(4), 235–241. <https://doi.org/10.1186/BF03352380>
- Tichelaar, B. W., & Ruff, L. J. (1989). How good are our best models? Jackknifing, bootstrapping, and earthquake depth. *Eos, Transactions American Geophysical Union*, 70(20), 593. <https://doi.org/10.1029/89EO00156>
- Todd, E. K., Schwartz, S. Y., Mochizuki, K., Wallace, L. M., Sheehan, A. F., Webb, S. C., Williams, C. A., Nakai, J., Yancey, J., Fry, B., Henrys, S., & Ito, Y. (2018). Earthquakes and Tremor Linked to Seamount Subduction During Shallow Slow Slip at the Hikurangi Margin, New Zealand. *Journal of Geophysical Research: Solid Earth*, 123(8), 6769–6783. <https://doi.org/10.1029/2018JB016136>
- Toh, A., Chen, W. J., Takeuchi, N., Dreger, D. S., Chi, W. C., & Ide, S. (2020). Influence of a Subducted Oceanic Ridge on the Distribution of Shallow VLFs in the Nankai Trough as Revealed by Moment Tensor Inversion and Cluster Analysis. *Geophysical Research Letters*, 47(15). <https://doi.org/10.1029/2020GL087244>
- Tonegawa, T., Araki, E., Kimura, T., Nakamura, T., Nakano, M., & Suzuki, K. (2017). Sporadic low-velocity volumes spatially correlate with shallow very low frequency earthquake clusters. *Nature Communications*, 8(1), 2048. <https://doi.org/10.1038/s41467-017-02276-8>
- Tonegawa, T., Takemura, T., Yabe, S., & Yomogida, K. (2021). Fluid migration before and during slow earthquakes in the shallow Nankai subduction zone. *Earth and Space Science Open Archive*. <https://doi.org/10.1002/essoar.10508646.1>
- Tonegawa, T., Yamashita, Y., Takahashi, T., Shinohara, M., Ishihara, Y., Kodaira, S., & Kaneda, Y. (2020). Spatial relationship between shallow very low frequency

- earthquakes and the subducted Kyushu-Palau Ridge in the Hyuga-nada region of the Nankai subduction zone. *Geophysical Journal International*, 1542–1554. <https://doi.org/10.1093/gji/ggaa264>
- Tu, Y., & Heki, K. (2017). Decadal Modulation of Repeating Slow Slip Event Activity in the Southwestern Ryukyu Arc Possibly Driven by Rifting Episodes at the Okinawa Trough. *Geophysical Research Letters*, 44(18), 9308–9313. <https://doi.org/10.1002/2017GL074455>
- Uchida, N., & Matsuzawa, T. (2013). Pre- and postseismic slow slip surrounding the 2011 Tohoku-oki earthquake rupture. *Earth and Planetary Science Letters*, 374, 81–91. <https://doi.org/10.1016/j.epsl.2013.05.021>
- Uchida, N., Matsuzawa, T., Hasegawa, A., & Igarashi, T. (2003). Interplate quasi-static slip off Sanriku, NE Japan, estimated from repeating earthquakes. *Geophysical Research Letters*, 30(15). <https://doi.org/10.1029/2003GL017452>
- Uchida, N., Yui, S., Miura, S., Matsuzawa, T., Hasegawa, A., Motoya, Y., & Kasahara, M. (2009). Quasi-static slip on the plate boundary associated with the 2003 M8.0 Tokachi-oki and 2004 M7.1 off-Kushiro earthquakes, Japan. *Gondwana Research*, 16(3–4), 527–533. <https://doi.org/10.1016/j.gr.2009.04.002>
- Uchida, N., Takagi, R., Asano, Y., & Obara, K. (2020). Migration of shallow and deep slow earthquakes toward the locked segment of the Nankai megathrust. *Earth and Planetary Science Letters*, 531. <https://doi.org/10.1016/j.epsl.2019.115986>
- Vaca, S., Vallée, M., Nocquet, J. M., Battaglia, J., & Régnier, M. (2018). Recurrent slow slip events as a barrier to the northward rupture propagation of the 2016 Pedernales earthquake (Central Ecuador). *Tectonophysics*, 724–725, 80–92. <https://doi.org/10.1016/j.tecto.2017.12.012>
- Wallace, L. M., Araki, E., Saffer, D., Wang, X., Roesner, A., Kopf, A., Nakanishi, A., Power, W., Kobayashi, R., Kinoshita, C., Toczko, S., Kimura, T., Machida, Y., & Carr, S. (2016). Near-field observations of an offshore Mw 6.0 earthquake from an integrated seafloor and subseafloor monitoring network at the Nankai Trough, southwest Japan. *Journal of Geophysical Research: Solid Earth*, 121(11), 8338–8351. <https://doi.org/10.1002/2016JB013417>
- Watanabe, S. I., Bock, Y., Melgar, D., & Tadokoro, K. (2018). Tsunami Scenarios Based on Interseismic Models Along the Nankai Trough, Japan, From Seafloor and

- Onshore Geodesy. *Journal of Geophysical Research: Solid Earth*, 123(3), 2448–2461. <https://doi.org/10.1002/2017JB014799>
- Watanabe, T., Hiramatsu, Y., & Obara, K. (2007). Scaling relationship between the duration and the amplitude of non-volcanic deep low-frequency tremors. *Geophysical Research Letters*, 34(7). <https://doi.org/10.1029/2007GL029391>
- Wessel, P., Smith, W. H. F., Scharroo, R., Luis, J., & Wobbe, F. (2013). Generic mapping tools: Improved version released. *Eos, Transactions American Geophysical Union*, 94(45), 409–410. <https://doi.org/10.1002/2013EO450001>
- Yabe, S., & Ide, S. (2014). Spatial distribution of seismic energy rate of tectonic tremors in subduction zones. *Journal of Geophysical Research: Solid Earth*, 119(11), 8171–8185. <https://doi.org/10.1002/2014JB011383>
- Yabe, S., Tanaka, Y., Houston, H., & Ide, S. (2015). Tidal sensitivity of tectonic tremors in Nankai and Cascadia subduction zones. *Journal of Geophysical Research: Solid Earth*, 120(11), 7587–7605. <https://doi.org/10.1002/2015JB012250>
- Yabe, S., Tonegawa, T., & Nakano, M. (2019). Scaled Energy Estimation for Shallow Slow Earthquakes. *Journal of Geophysical Research: Solid Earth*, 124(2), 1507–1519. <https://doi.org/10.1029/2018JB016815>
- Yabe, S., Baba, S., Tonegawa, T., Nakano, M., & Takemura, S. (2021). Seismic energy radiation and along-strike heterogeneities of shallow tectonic tremors at the Nankai Trough and Japan Trench. *Tectonophysics*, 800, 228714. <https://doi.org/10.1016/j.tecto.2020.228714>
- Yagi, Y. (2004). Source rupture process of the 2003 Tokachi-oki earthquake determined by joint inversion of teleseismic body wave and strong ground motion data. *Earth, Planets and Space*, 56(3), 311–316. <https://doi.org/10.1186/BF03353057>
- Yamamoto, Y., Obana, K., Takahashi, T., Nakanishi, A., Kodaira, S., & Kaneda, Y. (2013). Imaging of the subducted kyushu-palau ridge in the hyuga-nada region, western nankai trough subduction zone. *Tectonophysics*, 589, 90–102. <https://doi.org/10.1016/j.tecto.2012.12.028>
- Yamamoto, Y., Takahashi, T., Kaiho, Y., Obana, K., Nakanishi, A., Kodaira, S., & Kaneda, Y. (2017). Seismic structure off the Kii Peninsula, Japan, deduced from passive- and active-source seismographic data. *Earth and Planetary Science Letters*, 461, 163–175. <https://doi.org/10.1016/j.epsl.2017.01.003>

- Yamamoto, Y., Ariyoshi, K., Yada, S., Nakano, M., & Hori, T. (2022). Spatio-temporal distribution of shallow very-low-frequency earthquakes between December 2020 and January 2021 in Kumano-nada, Nankai subduction zone, detected by a permanent seafloor seismic network. *Earth, Planets and Space*, 74(1), 14. <https://doi.org/10.1186/s40623-022-01573-x>
- Yamashita, Y., Asano, Y., Shimizu, H., Uchida, K., Hirano, S., Umakoshi, K., Miyamachi, H., Nakamoto, M., Fukui, M., Kamizono, M., Kanehara, H., Yamada, T., Shinohara, M., & Obara, K. (2015). Migrating tremor off southern Kyushu as evidence for slow slip of a shallow subduction interface. *Science*, 348(6235), 676–679. <https://doi.org/10.1126/science.aaa4242>
- Yamashita, Y., Shimizu, H., & Goto, K. (2012). Small repeating earthquake activity, interplate quasi-static slip, and interplate coupling in the Hyuga-nada, southwestern Japan subduction zone. *Geophysical Research Letters*, 39(8). <https://doi.org/10.1029/2012GL051476>
- Yamashita, Y., Shinohara, M., & Yamada, T. (2021). Shallow tectonic tremor activities in Hyuga-nada, Nankai subduction zone, based on long-term broadband ocean bottom seismic observations. *Earth, Planets and Space*, 73(1), 196. <https://doi.org/10.1186/s40623-021-01533-x>
- Yokota, Y., & Ishikawa, T. (2020). Shallow slow slip events along the Nankai Trough detected by GNSS-A. *Science Advances*, 6(3), 1–12. <https://doi.org/10.1126/sciadv.aay5786>
- Yoshimoto, K., Sato, H., & Ohtake, M. (1993). Frequency-Dependent Attenuation of P and S Waves In the Kanto Area, Japan, Based On the Coda-Normalization Method. *Geophysical Journal International*, 114(1), 165–174. <https://doi.org/10.1111/j.1365-246X.1993.tb01476.x>
- Yoshioka, S. (2007). Difference in the maximum magnitude of interplate earthquakes off Shikoku and in the Hyuganada region, southwest Japan, inferred from the temperature distribution obtained from numerical modeling. - The proposed Hyuganada triangle -. *Earth and Planetary Science Letters*, 263(3–4), 309–322. <https://doi.org/10.1016/j.epsl.2007.08.025>
- Zhao, D., Huang, Z., Umino, N., Hasegawa, A., & Kanamori, H. (2011). Structural heterogeneity in the megathrust zone and mechanism of the 2011 Tohoku-oki

earthquake (Mw 9.0). *Geophysical Research Letters*, 38(17), 5–9.
<https://doi.org/10.1029/2011GL048408>